Role of cellular sorting nexins during infections with the human pathogen *Chlamydia trachomatis*

Inaugural-Dissertation

to obtain the academic degree
Doctor rerum naturalium (Dr. rer. nat.)

submitted to the Department of Biology, Chemistry, Pharmacy
of Freie Universität Berlin

by
Laura Rose

Berlin
2019

Diese Arbeit wurde von Januar 2015 bis September 2019 im Fachgebiet "Sexuell übertragbare bakterielle Krankheitserreger" am Robert Koch-Institut, Berlin unter der Leitung und Betreuung von Dr. Dagmar Heuer angefertigt.

This work was realised from January 2015 until September 2019 in the Unit "Sexually Transmitted Bacterial Pathogens" at the Robert Koch Institute, Berlin and was supervised by Dr. Dagmar Heuer.

First Reviewer: Dr. Dagmar Heuer
Second Reviewer: Prof. Dr. Helge Ewers

Date of thesis defense: 02 July 2020

Zusammenfassung

Chlamydia trachomatis ist ein intrazelluläres bakterielles Pathogen, das sich in einem Membran-gebundenen Kompartiment, der Inklusion, befindet und sich dort repliziert. Während des Entwicklungszyklus inseriert *C. trachomatis* Inklusionsmembranproteine in die Inklusionsmembran. Außerdem rekrutiert *C. trachomatis* selektiv Lipide und Proteine der Wirtszelle. Unter den rekrutierten Proteinen befinden sich auch Sorting Nexin Proteine des humanen Retromers. Das SNX-BAR Retromer ist ein Multi-Protein Komplex, der aus zwei Subkomplexen besteht, einem Trimer aus VPS Proteinen und einem Dimer aus SNX-BAR Proteinen. SNX-BAR Proteine besitzen eine PX- und eine BAR-Domäne. Zum mittleren Infektionszeitpunkt lokalisierten SNX Proteine um die Inklusion herum, wohingegen VPS35 angrenzend zur Inklusion im Cytosol lokalisierte. Darüber hinaus beobachteten wir tubulär-ähnliche Strukturen, die scheinbar von der Inklusion ausgehen. Diese Strukturen sind sowohl positiv für die bakteriellen Inklusionsmembranproteine IncA und IncE als auch für die zellulären Proteine SNX1, 2, 5 und 6. Wenig ist jedoch über die Mechanismen und die Funktion der SNX-BAR Rekrutierung bekannt. Um die räumlich-zeitlichen Dynamiken der SNX Rekrutierung zu untersuchen, analysierten wir die Lokalisierung der SNX-BAR Proteine, VPS35 und des Retromer Transportproteins CI-MPR in einem Zeitverlauf. 8 h nach der Infektion akkumulierten die SNX-BAR Proteine und VPS35 in räumlicher Nähe zu *C. trachomatis*, was auf eine Umlagerung der Retromer-Komponenten während der frühen Infektion hindeutet. Die Lokalisierung von CI-MPR war durch die Infektion mit *C. trachomatis* nicht verändert. Knockout von SNX5 und SNX6 resultierte in einem verminderten Transport von *C. trachomatis* zum MTOC. Zum mittleren Infektionszeitpunkt ist die chlamydiale Inklusion mit SNX-BAR Proteinen dekoriert, aber nicht mit VPS35. Die funktionalen Domänen der SNX-BAR Proteine wiesen ein unterschiedliches Lokalisierungsmuster auf: Während von SNX5 und SNX6 die PX-Domäne zur Inklusion rekrutiert wurde, war es für SNX1 und SNX2 die BAR-Domäne, die an der Inklusion lokalisierte. Funktionale Analysen der SNX Proteine mittels Knockout-Zelllinien zeigten eine jeweils erhöhte chlamydiale Primärinfektion und Genomkopienanzahl sowie einen Anstieg infektiöser Partikel in SNX5/SNX6 Knockout-Zellen. Dies deutet darauf hin, dass SNX5/SNX6 die Infektion beeinträchtigen. Schließlich identifizierten wir mit Hilfe einer Distanz-abhängigen Biotinylierung zelluläre Proteine, die mit SNX1 assoziiert sind. Bei dieser Methode wird eine promiskuitive Biotin-Ligase durch Fusion an SNX1 zu einem bestimmten subzellulären Ort gesteuert. Die anschließende nLC-MS/MS Analyse der affinitätsaufgereinigten biotinylierten Proteine assoziiert mit SNX1 identifizierte IncE, SNX5 und SNX6, die eine Interaktion mit SNX1 schlussfolgern lassen. Weiterhin wurde RPL13a der großen ribosomalen Untereinheit identifiziert. Zu mittleren Infektionszeitpunkten lokalisierte RPL13a an der Inklusion, was auf eine spezifische Rekrutierung schließen lässt. Eine Depletion von RPL13a resultierte in einer erhöhten Genomkopienanzahl und einem Anstieg der infektiösen Partikel. Zudem waren die

Expressionslevel bakterieller Proteine und die Größe der Inklusionen erhöht. Da bestimmte ribosomale Proteine in Zusammenhang mit Ribosomenheterogenität stehen, untersuchten wir die Hypothese, dass *C. trachomatis* ribosomale Proteine wie RPL13a zweckentfremdet, um den zellulären Translationsprozess zu regulieren. Während die Absorptionsprofile der Proteine keine Unterschiede zwischen infizierten und uninfizierten Zellen zeigten, unterschieden sich die ribosomalen Absorptionsprofile. Dies lässt auf eine mögliche heterogene ribosomale RNA Komposition schließen.

Zusammenfassend verdeutlichen unsere Daten, wie *C. trachomatis* durch die Rekrutierung von SNX Proteinen des humanen Retromers in zelluläre Transportwege eingreift. Darüber hinaus könnte die Rekrutierung von RPL13a zu der Inklusion ein interessantes Beispiel zur Einflussnahme in zelluläre Translationsprozesse darstellen.

Abstract

Chlamydia trachomatis is an intracellular bacterial pathogen that resides and replicates within a membrane-bound compartment, termed ‚inclusion'. During the developmental cycle, *C. trachomatis* inserts inclusion membrane proteins into the inclusion membrane. In addition, *C. trachomatis* selectively recruits host cellular lipids and proteins. Among those proteins are sorting nexins (SNX) of the human retromer. The SNX-BAR retromer is a multi-protein complex comprising two subcomplexes, a trimer of VPS proteins and a dimer of a PX and a BAR-domain bearing SNX proteins. SNX proteins localised on the inclusion in a rim-like pattern at mid-infection whereas VPS35 localised adjacent to the inclusion. Moreover, we observed tubular-like structures emanating from the inclusion. These structures are positive for bacterial Inc proteins IncA, IncE as well as host cellular SNX1, 2, 5 and 6. However, little is known about the mechanism and functional consequences of SNX-BAR recruitment. To unravel spatio-temporal dynamics of SNX recruitment, we analysed the localisation of SNX-BAR proteins, VPS35 and one of retromer's cargo CI-MPR over time. At 8 h p.i., SNX-BAR proteins and VPS35 accumulated proximally to *C. trachomatis* at the MTOC indicating a rearrangement of retromer components at the early infection stage while the localisation of CI-MPR was not affected. Knockout of both, SNX5 and SNX6 resulted in reduced trafficking of *C. trachomatis* towards the MTOC. At mid-infection stage, the chlamydial inclusion is decorated with SNX-BAR proteins but not with VPS35. The functional domains of SNX-BAR fusion proteins revealed a different localisation pattern: While the PX domain of SNX5 and SNX6 localised on the inclusion, the opposite was true for SNX1 and SNX2 whose BAR domains localised on the inclusion. Functional analyses of SNX proteins using knockout cell lines revealed increased chlamydial primary infection, genome copy number and infectious progeny formation in SNX5/SNX6 knockout cells suggesting that SNX5/SNX6 restrict *C. trachomatis* at mid-infection stage. Finally, we identified host-cellular proteins associated with SNX1 by using a proximity-dependent biotinylation assay (BioID) in which a promiscuous biotin ligase is targeted to a definite subcellular location by fusion to SNX1 as SNX1 was recruited to the inclusion. Subsequent nLC-MS/MS analysis of affinity-captured biotinylated proteins close to SNX1 identified IncE, SNX5 and SNX6 suggesting interaction of these proteins with SNX1 at the cytosolic site of the inclusion. Furthermore, we identified RPL13a of the large ribosomal subunit. At mid-infection time points, RPL13a localised on the inclusion suggesting specific recruitment. Depletion of RPL13a resulted in increased genome copy number and infectious progeny formation. In addition, bacterial protein levels were elevated and the inclusion enlarged. As some ribosomal proteins are involved in ribosome heterogeneity, we considered the hypothesis that *C. trachomatis* co-opts ribosomal proteins such as RPL13a to regulate the host cellular translation machinery. While proteins exhibited similar absorption profiles of *C. trachomatis* and

uninfected cells, ribosomal absorption profiles differed suggesting possible heterogeneous ribosome RNA composition.

Taken together, these data highlight how *C. trachomatis* interfere with host cellular trafficking pathways by recruiting SNX proteins of the human retromer. Moreover, the recruitment of RPL13a to the inclusion may exhibit an interesting example of *C. trachomatis* interfering in the translation machinery of the host cell.

Table of Contents

1 Introduction

1.1 *Chlamydia*

The phylum *Chlamydia*e comprises the order *Chlamydiales* whose members are strict obligate intracellular pathogens residing in a membrane-bound vacuole, termed ‘inclusion’. Species of *Chlamydia*e depend on eukaryotic host cells to fulfil their unique biphasic developmental cycle (Collingro et al. 2011; Nunes and Gomes 2014). *Chlamydiales* encompasses the three major families *Chlamydiaceae*, *Simkaniacaeae* and *Waddliaceae* and the family *Parachlamydiaceae* that displays a *Chlamydia*-like developmental cycle (Collingro et al. 2011; Greub and Raoult 2002). The ability to adapt to various niches made *Chlamydiaceae* successful pathogens that infect numerous host organisms (Bachmann, Polkinghorne, and Timms 2014; Nunes and Gomes 2014). With a reduced genome of about 1 Mb, *Chlamydiaceae* developed several specialised mechanisms for their interplay with the host cell (Moulder 1991; Stephens et al. 1998; Bastidas et al. 2013; Elwell, Mirrashidi, and Engel 2016).

*Chlamydia*e were first discovered by Halberstädter and Prowazek in 1907 who analysed inclusion bodies (Halberstädter 1907a, 1907b). Before the trachoma causing agent was identified as bacteria in 1960, *Chlamydia*e have been classified as protozoa and later as a virus (Moulder 1966; Schwartz 1966; Schachter 1978; Wang 1999).

The order *Chlamydiales* causes acute and, if left untreated, chronic diseases in both, animals and humans. In animals, *Chlamydia* spp. cause pulmonary infections, conjunctivitis and urogenital tract infections causing considerable impact on farming. In humans, *Chlamydia* spp. are responsible for a variety of infections ranging from ocular and pulmonary infections to urogenital infections (Bachmann, Polkinghorne, and Timms 2014). Currently, there are 11 described species of *Chlamydia* whereby *Chlamydia trachomatis* and *Chlamydia pneumonia* are among the best characterised bacterial pathogens (Bachmann, Polkinghorne, and Timms 2014; Collingro et al. 2011). Human urogenital *Chlamydia trachomatis* infections are a public health concern as *C. trachomatis* is the most prevalent bacterial, sexually transmitted infection worldwide (World Health Organization 2010; World Health Organization 2012).

1.1.1 Taxonomy

Chlamydiaceae were initially described based on the displayed phenotype including morphology, replication, structure and chemical composition (Moulder 1966). In 1998, the first genome sequence of *C. trachomatis* was published opening the way for molecular-based taxonomic classification analysis. Due to systematic differential clustering of 16S rRNA gene sequence data analysis, Everett and colleagues proposed a reclassification of groups in the order *Chlamydiales* and introduced two genera *Chlamydia* and *Chlamydophila* involving nine species (Everett, Bush, and Andersen 1999; Bush and Everett 2001). However, this concept was discussed controversially and was largely rejected by the scientific community as the

separation of strains was considered as not being robust and lacking other consistent biological markers (Schachter et al. 2001; Stephens et al. 2009). In addition, comparative whole-genome analysis considering protein distribution, *Chlamydia*-specific indels (insertions/deletions) and a common chlamydial plasmid found in both genera (*Chlamydia* and *Chlamydophila*) argued against the classification proposed by Everett et al. (Griffiths, Ventresca, and Gupta 2006; Gupta and Griffiths 2006). According to Stephens et al., the proposal by Everett and colleagues neglected i) common clustering, ii) highly conserved 16S rRNA gene sequence similarity of ≥ 96% and iii) shared fundamental and classically defined phenotypic characteristics among chlamydial species (Stephens et al. 2009). As a consequence, the chlamydial taxonomy was revised resulting in a reunited *Chlamydiaceae* tree made up of one genus '*Chlamydia*' that comprises nine species (Stephens et al. 2009). Most recently, Sachse et al. extended the discussion thereby supporting the arguments by Stephens et al. Accordingly, Sachse et al. proposed a classification of eleven currently recognised *Chlamydiaceae* species enclosed in a single genus '*Chlamydia'* (Sachse et al. 2015).

This thesis refers to the classification proposed by Stephens et al. and Sachse et al. although the agreement on the final taxonomic classification remains to be resolved (Figure 1). The history of chlamydial taxonomy was reviewed in detail by Longbottom and Coulter (Longbottom and Coulter 2003).

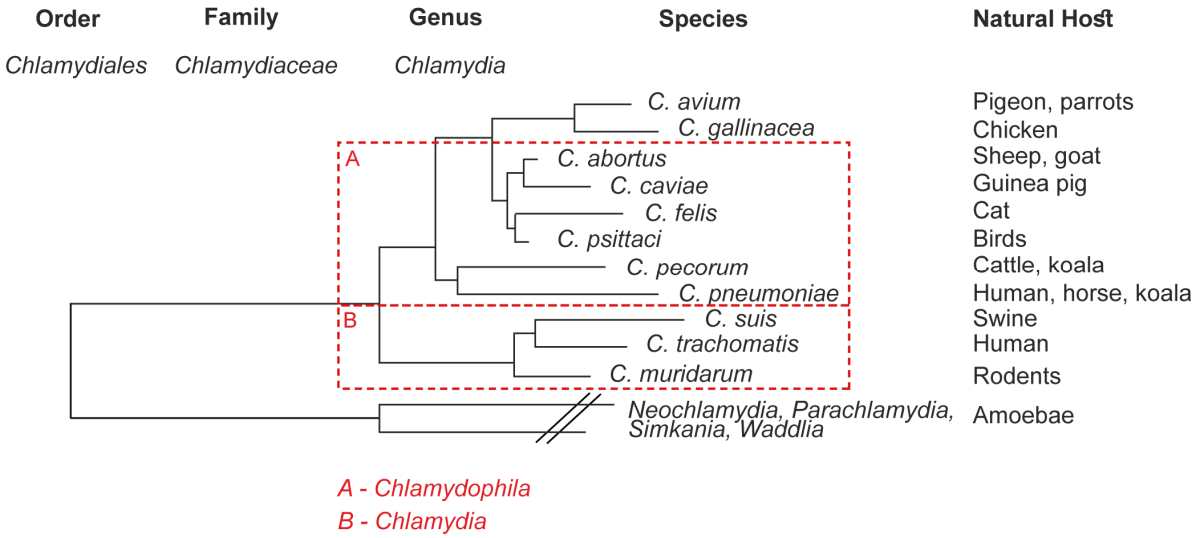

Figure 1: Taxonomy of the order *Chlamydiales*.
Taxonomic classification of the order *Chlamydiales* as proposed by Stephens et al. 2009 and Sachse et al 2015 based on almost complete 16S rRNA genes. Classification includes species of the described species of the family *Chlamydiaceae* and the recently proposed new species *C. avium* and *C. gallinaceae*. Natural hosts are assigned for each species. Dashed boxes surround the two genera proposed by Everett et al. Adapted from Sachse et al. 2015 and doctoral thesis from Sophia Edelmann 2016 (Edelmann 2016).

1.1.2 *C. trachomatis* infections: Clinical manifestations and host immune responses

Chlamydial infections cause severe diseases in both, animals and humans. This thesis focusses on *C. trachomatis* as this human pathogen is of significant worldwide public health concern causing hundreds of millions of cases of human genital tract or ocular diseases (Abdelsamed, Peters, and Byrne 2013). Depending on the virulence and tissue tropism as well as clinical manifestations, *C. trachomatis* is categorised into three biovars: systematic lymphogranuloma venereum (LGV), genital and ocular biovars (Figure 2). Moreover, biovars are subdivided into serovars depending on the major outer membrane protein (MOMP) (Abdelsamed, Peters, and Byrne 2013).

LGV and genital serovars are sexually or perinatally transmitted causing diseases on a global scale in both, men and women (Geisler 2010; Malhotra et al. 2013; World Health Organization 2010). Serovars D - K infect epithelial cells of the genital tract causing urethritis, cervicitis and endometritis in women (Fisher 1993; Malhotra et al. 2013). If left untreated, infections lead to serious complications including pelvic inflammatory disease (PID), ectopic pregnancy or infertility (Peeling and Brunham 1996; Mpiga and Ravaoarinoro 2006; Geisler et al. 2013). In addition, these serovars cause urethritis in men and if left untreated, infections are associated with epididymitis and proctitis (Geisler et al. 2013; Malhotra et al. 2013; World Health Organization 2010). However, asymptomatic infections or infections with few symptoms occur in about 70% of infections in women and 50% of infections in men (Bebear and de Barbeyrac 2009; Monden and Kumon 2009). LGV serovars infect macrophages wherefrom LGV disseminate to lymph nodes causing systemic diseases (Schachter 1999; Abdelsamed, Peters, and Byrne 2013). *C. trachomatis* genital serovars are the most prevalent sexually transmitted bacterial infection worldwide with approximately 100 million new infections that occur each year, exhibiting a global estimated prevalence of 4.2% in 2012 (World Health Organization 2012; Newman et al. 2015). In Germany, the prevalence of sexually transmitted *C. trachomatis* is currently estimated at about 4-5% of sexually active women and men (Koch-Institute 2013). Ocular serovars A - C infect conjunctival epithelial cells through transmission by smear-infection or flies and can lead to severe sequelae including blindness (Solomon, Foster, and Mabey 2006; Mpiga and Ravaoarinoro 2006; Abdelsamed, Peters, and Byrne 2013). Trachoma is the major cause of preventable blindness with approximately 1.3 million people suffering blindness from trachoma (Resnikoff et al. 2004). It affects poorer communities living in rural areas where health care is limited or unavailable (Solomon, Foster, and Mabey 2006).

C. trachomatis infections are diagnosed by cell culture, antigen-based methods (e.g. DFA, EIA) and molecular methods (e.g. hybrid capture, NAATs) and commonly treated with antibiotics such as cyclins (doxycycline and tetracycline), macrolides (erythromycin and azithromycin) and quinolones (ofloxacin and levofloxacin) (Mpiga and Ravaoarinoro 2006; Bebear and de Barbeyrac 2009; Centers for Disease Control and Prevention 2010).

In humans, *C. psittaci* infections cause respiratory psittacosis, also known as ornithosis. Symptoms resemble those of influenza. Towards the end of the first week of the disease, the symptoms resemble those of pneumonia (Rohde et al. 2010).

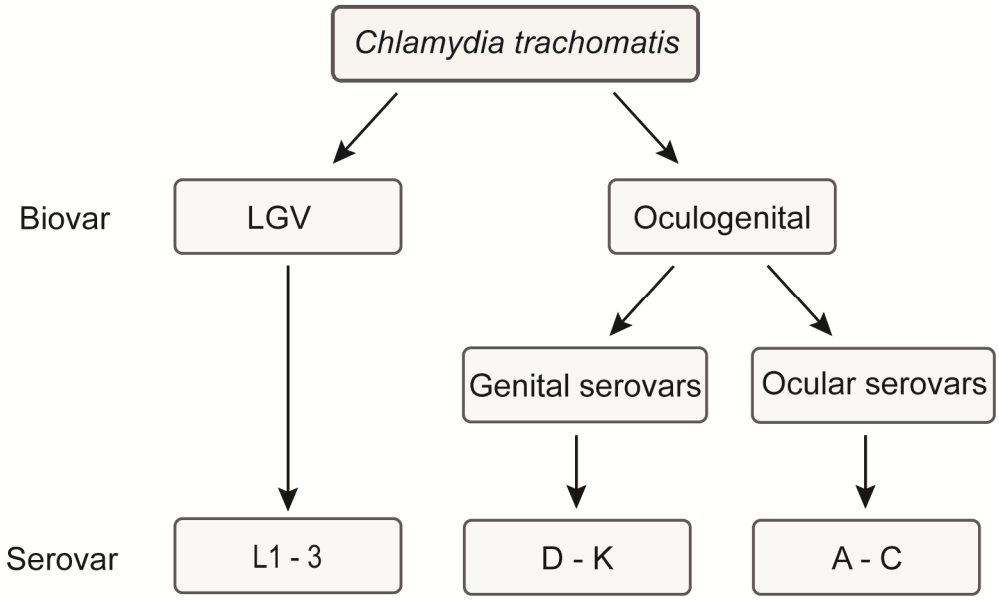

Figure 2. Classification of *C. trachomatis* based on tissue tropism and serotype.
C. trachomatis is divided into LGV and oculogenital biovars. Biovars are further subdivided into serovars. LGV biovars are sexually transmitted (serovars L1 – L3). Oculogenital biovars include sexually transmittable genital serovars (serovars D – K) and ocular serovars that are transmitted by smear-infection (serovars A-C). LGV: lymphogranuloma venereum. Adapted from Abdelsamed, Peters, and Byrne 2013.

Infection with *Chlamydia* spp. stimulates both, the human innate and adaptive immune system (Brunham and Rey-Ladino 2005; Hafner, Beagley, and Timms 2008). *Chlamydia* spp. are detected by host cell membranous pattern recognition receptors (RPPs) that recognise chlamydial lipopolysaccharide (LPS) and chlamydial heat shock protein (Hsp60) (Bastidas et al. 2013). Toll-like receptors (TLRs) are crucial PRRs at the surface of primarily dendritic cells and macrophages to induce innate and adaptive immune responses. In addition, cytosolic PRRs recognise pathogen-associated molecular pattern (PAMP) such as peptidoglycans and outer membrane proteins (MOMP, OmcA, OmcB and other) (Hatch 1996; Wang et al. 2010). Upon infection with *Chlamydia* spp., various pro-inflammatory cytokines (chemokines, interleukins, interferons, colony-stimulating factor, tumour necrosis factor) are produced by epithelial cells which trigger inflammation and promote recruitment of further immune cells such as dendritic cells, neutrophils and leukocytes (Brunham and Rey-Ladino 2005; Vasilevsky et al. 2014). However, *Chlamydia* spp. have evolved strategies to subvert host-innate immune responses, for instance by interfering with the NF-κB signalling pathway (Cocchiaro and Valdivia 2009; Bastidas et al. 2013). NF-κB is a transcription factor that is released through sequestration of IκB upon stimulation of PRRs and subsequently translocates into the nucleus where it activates NF-κB target gene expression (e.g. numerous cytokines, immunoreceptors). *Chlamydia* spp.

block degradation of retention factor IκB and translocation of NF-κB into the nucleus or blocks activation of NF-κB through proteolysis of one of NF-κB's subunits (Cocchiaro and Valdivia 2009; Bastidas et al. 2013). Moreover, *Chlamydia* spp. limit the recognition of PAMPs by reorganising actin and intermediate filaments, peripherally of the inclusion since disruption of these cytoskeleton elements eventuates in increase of IL-8 transcription (Kumar and Valdivia 2008b). Besides, *Chlamydia* spp. may promote chlamydial protease-like factor (CPAF)-dependent degradation of IFNγ induced MCH class I and II transcriptional gene regulators (RFX5 and USF-1) resulting in limited presentation of chlamydial antigens by MCH class I and II (Zhong, Fan, and Liu 1999; Zhong et al. 2000).

1.1.3 The developmental cycle: exceptional and adapted to the host

Shared by all species of *Chlamydiaceae*, *Chlamydia* spp. display a unique, biphasic developmental cycle that involves two distinct morphological and functional forms: the elementary bodies and the reticulate bodies (Abdelrahman and Belland 2005; Bastidas et al. 2013; Elwell, Mirrashidi, and Engel 2016). Elementary bodies (EBs) are 0.3 µm in diameter, infectious and low in metabolic activity. In addition, EBs are resistant to osmotic and physical stress by their spore-like cell wall in adaptation to their extracellular survival. The DNA of EBs is condensed (Hatch, Allan, and Pearce 1984; Nelson 2012; Barry, Hayes, and Hackstadt 1992; Perara, Ganem, and Engel 1992). In contrast, reticulate bodies (RBs) are 1 µm in diameter, non-infectious but metabolically active and specialised to nutrient acquisition and replication (Moulder 1991).

EB surface molecules that function as adhesins attach to epithelial host cell receptors such as cell surface heparan-like glycosaminoglycans (Dautry-Varsat, Balana, and Wyplosz 2004; Dautry-Varsat, Subtil, and Hackstadt 2005). Glycosaminoglycan, MOMP, OmcB and PmpD have been discussed as adhesins (Su et al. 1996; Menozzi et al. 2002; Wehrl et al. 2004; Fadel and Eley 2007). Internalisation of EBs into the host cell is facilitated by endocytosis that involves invagination of the plasma membrane (PM), budding and scission of vesicles and fusion of membrane-coated vesicles with endosomes allowing to enter the endolysosomal membrane system (Smythe and Ayscough 2006). The entry process is accompanied by association of bacteria to host cellular PM lipid microdomains or 'rafts' and rearrangement of the actin cytoskeleton (Carabeo et al. 2002; Subtil and Dautry-Varsat 2004; Dautry-Varsat, Balana, and Wyplosz 2004; Dautry-Varsat, Subtil, and Hackstadt 2005; Cocchiaro and Valdivia 2009). Entry of bacteria in a raft-dependent pathway is assumed to prevent fusion with the endocytic degradative pathway (Duncan, Shin, and Abraham 2002). During the early infection stage, the internalised endocytic compartment is rapidly remodelled to a membrane-bound vacuole, termed 'inclusion' allowing to establish interaction with the host cell and nutrient acquisition but to avoid fusion with lysosomal compartments (Wyrick 2000; Bastidas et al. 2013; Elwell, Mirrashidi, and Engel 2016; Banhart et al. 2017). Furthermore, the inclusion is dynein-dependently translocated to the microtubule-organising centre (MTOC) where *Chlamydia* spp.

establises their niche (Grieshaber, Grieshaber, and Hackstadt 2003). Inside the inclusion, EBs differentiate into RBs (Wyrick 2000). Around the mid-infection stage, the inclusion expands as RBs replicate by binary fission (Lee et al. 2018). The DNA of RBs is decondensed enabling transcription and replication (Grieshaber et al. 2004). In parallel, the inclusion extensively interacts with the host cell (Bastidas et al. 2013; Elwell, Mirrashidi, and Engel 2016; Banhart et al. 2017). Midway through the developmental cycle, RBs asynchronously redifferentiate into EBs (Wyrick 2000; Bastidas et al. 2013; Elwell, Mirrashidi, and Engel 2016; Banhart et al. 2017). During mid and late infection stages, the integrity of the inclusion is stabilised by a surrounding dynamic actin and intermediate filaments scaffold (Kumar and Valdivia 2008a, 2008b). Eventually, newly formed EBs are released by cell lysis or extrusion to initiate new infection rounds (Wyrick 2000; Bastidas et al. 2013; Elwell, Mirrashidi, and Engel 2016; Banhart et al. 2017; Hybiske and Stephens 2007; Zuck et al. 2016). Depending on the serovar, the developmental cycle lasts between 48 to 72 h p.i. (Figure 3).

Apart from the acute infection, certain *Chlamydia* species have been shown to enter a reversible persistent state in response to stress such as antibiotic treatment, nutrient starvation or host immune factor IFNy (Beatty, Morrison, and Byrne 1994; Mpiga and Ravaoarinoro 2006; Hogan et al. 2004). Persistence is defined as a long-term association and in terms of chlamydial infections, it is considered as continued occurrence of *Chlamydia* spp. but with an altered developmental cycle (Beatty, Morrison, and Byrne 1994). Thereby, RB maturation is delayed and RB to EB redifferentiation is arrested or yet inhibited resulting in arrested/decelerated growth which correlates with a lessened metabolic activity leading to reduced progeny formation (Beatty, Morrison, and Byrne 1994). In addition, RBs transition into enlarged, aberrant bodies (ABs) (Beatty, Morrison, and Byrne 1994; Wyrick 2000; Mpiga and Ravaoarinoro 2006). Removal of persistence stimulating factors allow *Chlamydia* spp. to revert to acute infection exhibiting recovery of RBs to acute infection form and growth and re-differentiation to EBs (Beatty, Morrison, and Byrne 1994; Wyrick 2000; Mpiga and Ravaoarinoro 2006).

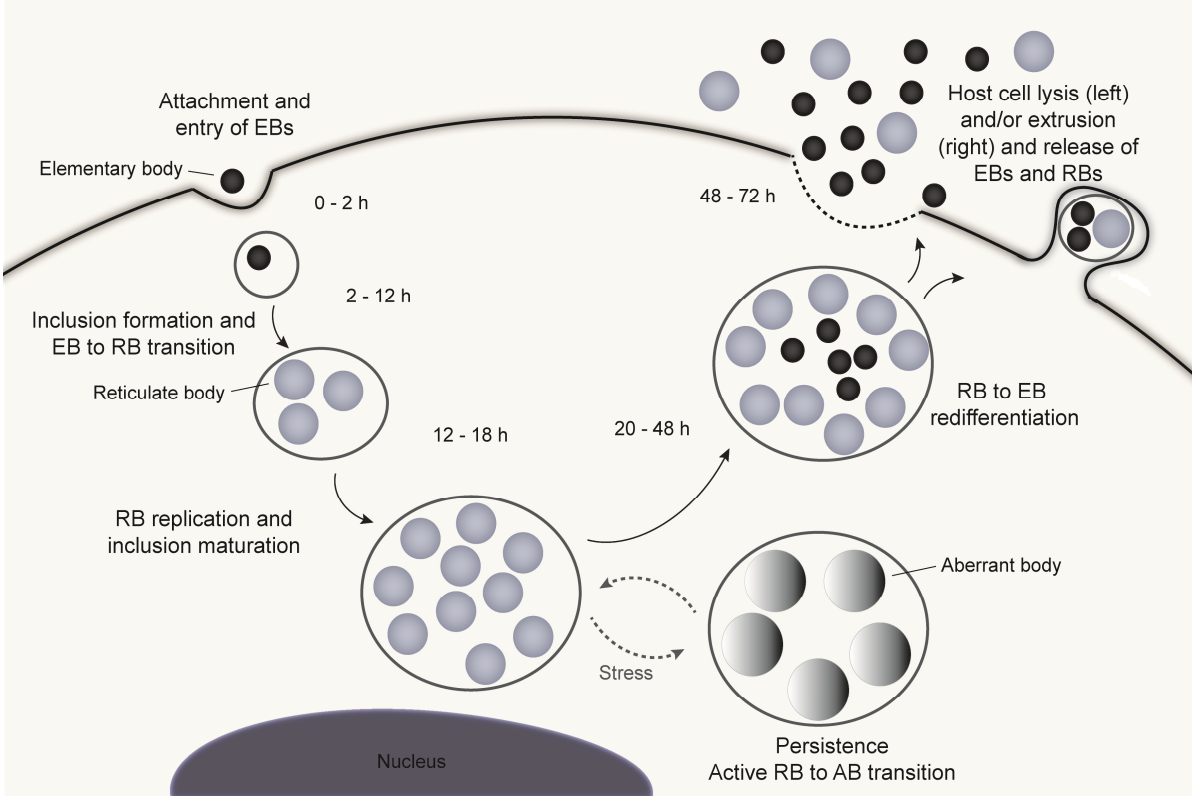

Figure 3. Developmental cycle of *Chlamydia* spp.
Following entry of *Chlamydia* spp. into the host cell, EBs differentiate into RBs. In acute infections during mid-infection, the inclusion expands as RBs replicate by binary fission. Midway through the developmental cycle, RBs asynchronously redifferentiate into EBs which are eventually released by cell lysis or extrusion ready to infect surrounding cells. Under physiologically relevant stress conditions, *C. trachomatis* enters a reversible persistent state in which *C. trachomatis* exhibits an altered developmental cycle. EB: elementary body; RB: reticulate body; AB: aberrant body.

1.2 Creating unique niches within the host cellular endomembrane system

1.2.1 The eukaryotic endomembrane system

The eukaryotic endomembrane system encompasses a series of membrane-bound organelles that together shape a functional unit either by direct connections of the organelles or by an exchange of material through vesicular transport (Figure 4) (Casem 2016). The nuclear membrane, endoplasmic reticulum (ER), Golgi apparatus (GA), lysosomes, vesicles, endosomes, plasma membrane (PM) and several intermediate compartments form the endomembrane system which is subdivided in two systems: the secretory and the endolysosomal (also known as endosomal-lysosomal or endocytic) transport system (Casem 2016). Both trafficking pathways are governed by a unifying principle: transport of membrane and soluble proteins (= cargo proteins, cargoes) from one membrane-bound compartment to another via vesicular intermediates (transport vesicles). Transport vesicles bud from a donor and fuse with an acceptor compartment thereby delivering transported cargoes (Bonifacino and Glick 2004; Burd 2011; Lodish 2008). Importantly, giving the fact that trafficking of cargoes in transport vesicles occurs by budding and fusion of vesicles, the same face of the membrane remains oriented toward the cytosol. Thus, a cargo protein moves from one organelle to

another without being translocated across a membrane (Lodish 2008). The secretory system on the one hand, includes the ER, Golgi cisternae (*cis, media, trans*), *trans*-Golgi network (TGN), various types of secretory vesicles and the PM (Bonifacino and Rojas 2006). It describes a trafficking pathway in which newly synthesised proteins that are destined for secretion into the extracellular space, to the PM or for residence within organelles of the endomembrane system (e.g. secretory vesicles, endosomes), move from the ER via the GA to their final destinations. Newly synthesised proteins are translocated into the ER, properly folded and post-translationally modified and then progressed to the GA via transport vesicles that fuse with each other to form *cis*-Golgi cisternae (Griffiths and Simons 1986; Lodish 2008). These transport vesicles are in turn part of the anterograde (forward-moving) transport pathway as secreted proteins move forward from *cis*-Golgi to the *trans*-Golgi and eventually reach the TGN. In this context, the TGN holds a central role as this organelle is key in protein sorting and segregating proteins in specific sets of membrane-enclosed carriers which deliver the cargoes to their final destinations (Griffiths and Simons 1986; Bonifacino and Rojas 2006; Lodish 2008). Certain proteins, however, are retrieved from the *cis*-Golgi to the ER via a different set of transport vesicles in a vectorial transport called retrograde (backward-moving) transport route (Lodish 2008). The endolysosomal system on the other hand, includes various types of endosomes (e.g. early, late, recycling endosome), lysosomes and lysosome-related organelles (Bonifacino and Rojas 2006). This trafficking pathway is used to internalise substances such as membrane components, receptor-associated ligands and solute molecules into the cell, by a process usually referred to as endocytose. Inside the cell, endocytosed cargoes in the early endosomes are delivered to various intracellular destinations (Maxfield and McGraw 2004). The early endosome is a central hub in deciding whether some proteins are destined for either lysosomal degradation via maturation of early to late endosomes that eventually fuse with lysosomes or for recycling via recycling endosomes (Huotari and Helenius 2011; Lu and Hong 2014; Lodish 2008). Many receptor proteins that were endocytosed need to be recycled. Major recycling pathways are i) endosome-to-PM pathways including contribution of the recycling endosome and ii) endosome-to-TGN pathways including those from early, late and recycling endosomes (Lu and Hong 2014). The exit from endosomes is termed retrograde sorting or retrograde trafficking which acts on cargoes shuttling between endosomes and the GA or the PM (Johannes and Popoff 2008).

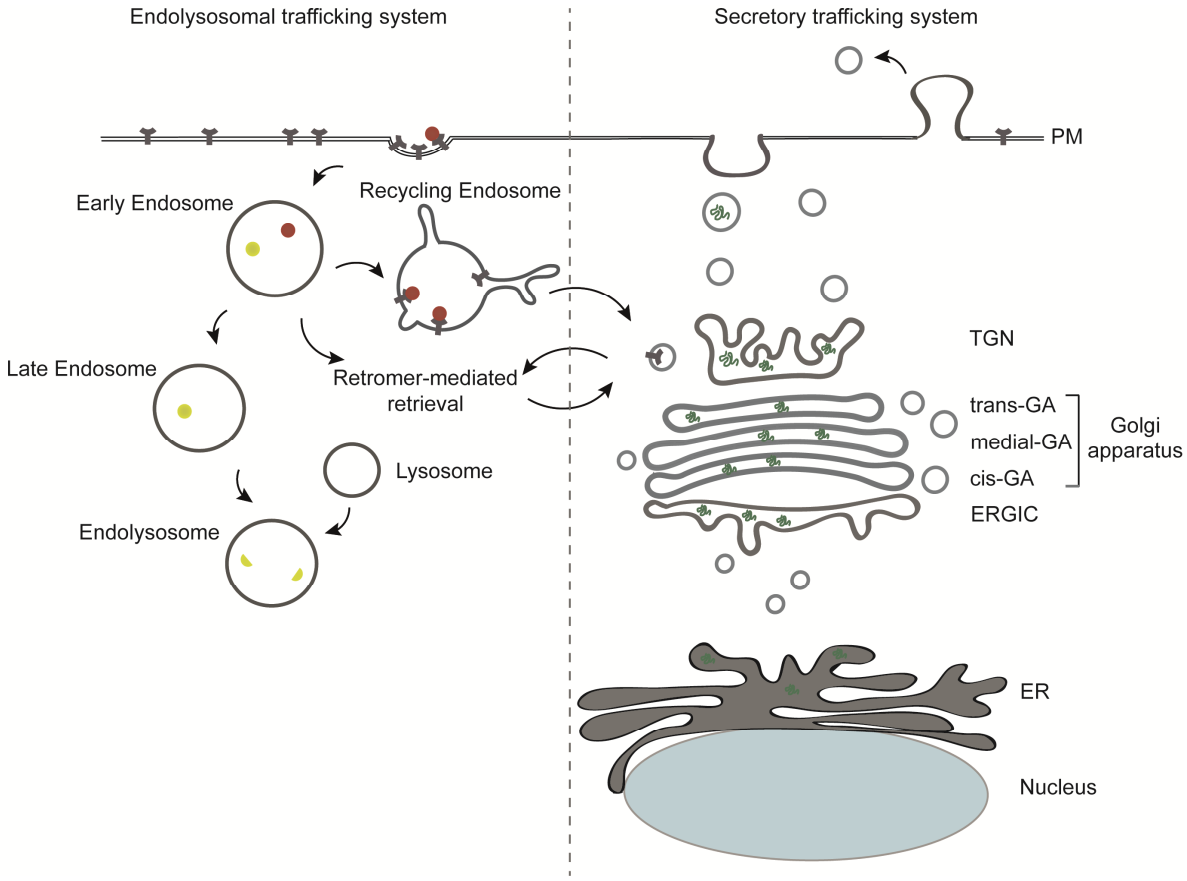

Figure 4. The eukaryotic endomembrane system.
Illustration of the main trafficking pathways within the eukaryotic endomembrane system. On the left-hand side, the endolysosomal trafficking system including various types of endosomes and lysosomes. On the right-hand side, the secretory trafficking system including ER, Golgi cisternae (*cis, media, trans*), TGN and the PM. Both systems involve transport vesicles that traffic cargoes from one compartment to another. See text for detailed explanation. ER: endoplasmic reticulum; ERGIC: ER-Golgi intermediate compartment; GA: Golgi apparatus; TGN: *trans*-Golgi network; PM: plasma membrane.

1.2.2 Retrograde trafficking

The TGN is a major traffic site and the main site of intersection between the secretory and the endolysosomal system as it receives not only secretory proteins by the anterograde transport route but also receives proteins from the retrograde transport route. In the latter case, proteins targeted from the GA or PM to endosomes (early, late, recycling) are transported back to the TGN, GA or the ER for re-use (Bonifacino and Rojas 2006; Johannes and Popoff 2008; Burd 2011). Cargoes can be categorised into four groups: i) cargo sorting receptors, ii) integral membrane proteases, iii) SNAREs and iv) nutrient transporters (Burd 2011). One of the best characterised retrograde cargoes are mammalian cation-dependent (CD-) and cation-independent (CI-) mannose phosphate receptors (MPRs) (Ghosh, Dahms, and Kornfeld 2003; Burd 2011). In the GA, mannose 6-phosphate (M6P) is incorporated into carbohydrate chains of soluble lysosomal acid hydrolase precursors functioning as lysosomal targeting signal (Burd 2011). In the TGN, M6P is then recognised by MPRs that serve to sort M6P-tagged proteins into vesicles which bud from the TGN and carry the hydrolases to endosomes. Endosomes

eventually maturate to lysosomes where hydrolase precursors become fully active (Munier-Lehmann, Mauxion, and Hoflack 1996). The receptors, however, return to the TGN to initiate new rounds of sorting (Seaman 2004; Arighi et al. 2004). Another well-characterised sorting receptor is sortilin (Nielsen et al. 2001; Lu and Hong 2014). An example of integral membrane proteins is the human furin, an enzyme harbouring a luminal protease and a cytoplasmic domain which contains both, anterograde and retrograde sorting signals (Burd 2011). Cycling between TGN and endosomes is thought to allow furin to function on numerous substrates (Bonifacino and Rojas 2006). SNAREs mediate vesicle fusion of endosome-derived transport carriers with the TGN as well as fusion of Golgi-derived vesicles with post-Golgi compartments. Hence, SNAREs need to be packaged with the retrograde cargo in the first case and need to be recycled to the TGN in the latter case (Burd 2011). Finally, nutrient transporters such as the insulin-responsive glucose transporter, GLUT4, cycle between the TGN and the PM (Shewan et al. 2003; Burd 2011).

Processes at the endosome-TGN interface include cargo selection, budding, translocation of transport intermediates, vesicle docking and fusion (Johannes and Popoff 2008). With regard to the molecular machinery of retrograde transport, studies have identified several elements that are involved (Johannes and Popoff 2008). Not all players involved in retrograde transport are going to be discussed here in detail. It will be rather focussed on a non-clathrin membrane coat: the retromer which is formed during one of the initial steps of retrograde trafficking. Retrograde trafficking plays important roles in endosomal sorting and cellular signalling, and disruption of the retromer is linked to neurodegenerative disorders such as Alzheimer's and Parkinson's disease (Lu and Hong 2014; Gallon and Cullen 2015).

The human retromer

Membrane coats are important key components for membrane deformation and cargo selection prior to retrograde trafficking. Clathrin membrane coats are essential for endosome-to-TGN trafficking (Lu and Hong 2014). Together with adaptor proteins, clathrin forms membrane coats that initiate membrane deformation required for emergence of transport carriers such as vesicles or tubules from endosomes. Transport carriers then tether and fuse at the TGN (Lu and Hong 2014).

Another way of endosomal sorting that involves the formation of transport carriers is mediated by a non-clathrin coat complex termed retromer (Johannes and Popoff 2008; McGough and Cullen 2011; Lu and Hong 2014). Its primary role is to select cargo proteins for endosome-to-TGN transport. Prominent retromer cargo proteins are CI-MPR, sortilin and Wnt transporter protein (Seaman 2012; Cullen and Korswagen 2012; Gallon and Cullen 2015).

The SNX-BAR retromer is a conserved, hetero-pentameric coat-like multi-protein complex consisting of a cargo-recognition subcomplex and a membrane-binding subcomplex (membrane-sensing subcomplex) (Figure 5). The cargo-recognition subcomplex comprises a stable VPS26-VPS29-VPS35 trimer while the membrane-binding subcomplex comprises a

sorting nexin (SNX) dimer (Bonifacino and Hurley 2008; Cullen and Korswagen 2012; Gallon and Cullen 2015). In mammalian cells, there are two yeast Vps26 orthologues, namely Vps26a and Vps26b and one yeast Vps29 and Vps35 orthologue each (Haft et al. 2000; Kerr et al. 2005). The VPS26-VPS29-VPS35 subcomplex participates in cargo selection as VPS35 directly binds to cytoplasmic domains of cargo proteins, though by low affinity and though no strong consensus motif has been described for most of the cargoes (Cullen and Korswagen 2012). VPS35 serves as a scaffold to which VPS26 and VPS29 bind independently in a 1:1:1 ratio (Hierro et al. 2007; Norwood et al. 2011; Gallon and Cullen 2015). VPS26 is incorporated into the retromer through interaction with the N-terminus of VPS35 (Shi et al. 2006; Collins et al. 2008). VPS29 associates with the C-terminus of VPS35 (Collins et al. 2005; Swarbrick et al. 2011). The trimer does not interact directly with membrane lipids but remains associated with endosomes due to interactions with the small GTPase Rab7 (Gallon and Cullen 2015; Klinger, Siupka, and Nielsen 2015). Recruitment of the retromer membrane-binding subcomplex to the endosomal membrane occurs concomitantly with the selection of cargo proteins (Seaman 2012). The membrane-interacting retromer subcomplex is formed by a dimer of various combinations of SNX proteins. The SNX dimer binds to phosphoinositides and mediates recruitment of the retromer to the endosome (Bonifacino and Hurley 2008; Gallon and Cullen 2015).

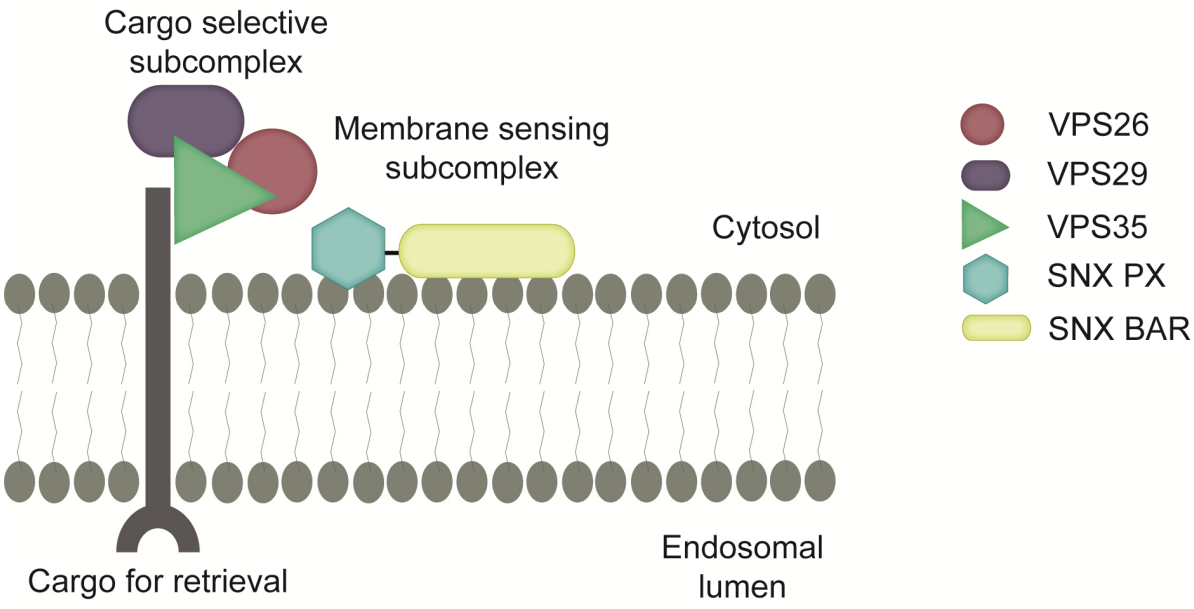

Figure 5. The structure of the human SNX-BAR retromer.
The retromer is a multi-protein complex consisting of two distinct subcomplexes: a cargo-selective and a membrane sensing subcomplex. The cargo recognition complex comprises a VPS26-VPS29-VPS35 trimer and the membrane-binding subcomplex comprises a SNX dimer. Retromer SNXs harbour two distinct domains: the PX and the BAR domain. VPS: vacuolar protein sorting protein; SNX: sorting nexin protein; PX: phox-homology; BAR: Bin/amphiphysin/Rvs. Adapted from Cullen and Korswagen 2012.

Sorting nexin proteins

SNX proteins (SNXs) constitute a family of proteins that are characterised by the presence of a phox-homology (PX) domain (Teasdale et al. 2001). At present, 33 mammalian sorting nexins have been identified (Cullen and Korswagen 2012). PX domains bind to phosphoinositides (phosphatidylinositol phosphates, PIPs) which are a group of phospholipids present in cell membranes and which function in numerous cellular processes including membrane trafficking, cytoskeleton and signal transduction (Di Paolo and De Camilli 2006; Mayinger 2012). The SNX family can be subdivided into five subfamilies based on their protein domain architecture: SNX-PX, SNX-BAR, SNX-FERM, SNX-PXA-RGS-PXC and SNX-MIT (Gallon and Cullen 2015). With regard to retromer function, SNX-BAR proteins (SNX-BARs), SNX3 and SNX27 are important players as these SNXs associate with the retromer. Classical retromer refers to SNX-BARs which were studied in this thesis. Apart from the PIP-binding PX domain, SNX-BARs bear a BAR (Bin/amphiphysin/Rvs) domain which is a dimerisation motif (Figure 6). In addition, the BAR domain senses membrane curvature and drives membrane remodelling towards membrane tubules due to its banana-shaped structure (Attar and Cullen 2010; van Weering, Verkade, and Cullen 2010; Frost et al. 2008). Combination of PX and BAR domain enables simultaneous detection of both, membrane composition by the PX domain and membrane curvature by the BAR domain. Coincidence detection and assembly are predicted to be required for protein recruitment and stabilisation of membrane curvature and induction of membrane tubulation (McMahon and Gallop 2005; Frost, Unger, and De Camilli 2009a).

SNX proteins were first discovered in budding yeats. Mammalian SNX1 and SNX2 are yeast VPS5 orthologues and mammalian SNX5 and SNX6 are yeast VPS17 orthologues (Seaman et al. 1997; Seaman, McCaffery, and Emr 1998; Wassmer et al. 2009). The membrane-interacting subcomplex is formed through a combination of SNX1 or SNX2 with either SNX5 or SNX6 (Carlton et al. 2004; Rojas et al. 2007; Wassmer et al. 2007), or with SNX32 (Gallon and Cullen 2015). Thus, the SNX-BAR dimer is a collaborative complex involving four proteins in recurring pairs: SNX1/5, SNX1/6, SNX2/5 and SNX2/6 (Trousdale and Kim 2015). While SNX1 and SNX2 are largely interchangeable, the same may be also true for SNX5 and SNX6 (Rojas et al. 2007; Wassmer et al. 2007; Wassmer et al. 2009). SNX PX domains bind to PIPs, most commonly to PI3P (Seet and Hong 2006; Teasdale and Collins 2012). Moreover, SNX proteins exhibit variations in the PIP-binding profile that may help to target the corresponding protein to distinct endosomal compartments and subdomains (Cullen 2008). For instance, binding of SNX1 and SNX2 to PI3P and PI3,5P_2 has been shown, whereas SNX5 and SNX6 have been shown to bind to PI4,5P_2 and PI4P, respectively (Cozier et al. 2002; Carlton et al. 2004; Carlton et al. 2005; Koharudin et al. 2009; Niu et al. 2013; Carlton and Cullen 2005). However, binding specificity of SNX PX domains other than to PI3P is still controversial (Teasdale and Collins 2012).

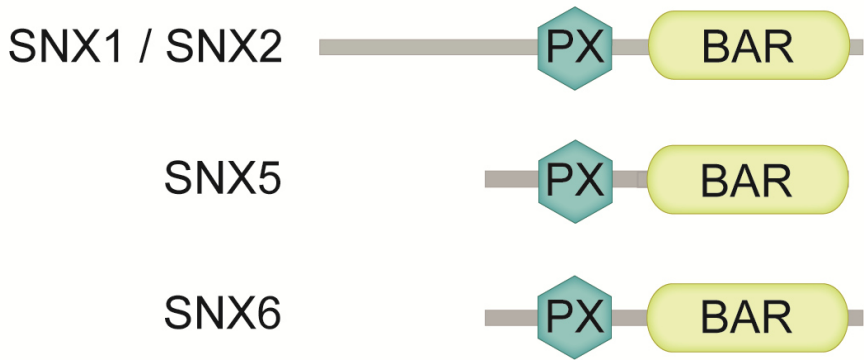

Figure 6. Retromer SNX-BAR domain architecture.
SNX-BARs harbour two distinct domains. The PX domain binds to membrane phosphoinositides, the BAR domain senses membrane curvature and drives membrane remodelling. SNX: sorting nexin protein; PX: phox-homology; BAR: Bin/amphiphysin/Rvs. Adapted from Teasdale and Collins 2012 and Gallon and Cullen 2015.

Tubular based endosomal sorting mediated by retromer

Recruitment of the retromer subcomplexes to the endosome membrane occurs concomitantly with cargo selection. In parallel, the SNX-BAR dimer assembles to promote formation of membrane tubules into which cargoes are sorted (Seaman 2012). There are two hypotheses of how the retromer is recruited to the endosomal membrane: One proposes association of the SNX dimer with endosome first to be required for recruitment of the VPS26-VPS29-VPS35 trimer to endosomes (Rojas et al. 2007; van Weering, Verkade, and Cullen 2012) while the other proposes recruitment of the cargo-recognition subcomplex before the membrane-sensing subcomplex (Harbour et al. 2010; Trousdale and Kim 2015). Either way, assembly of the retromer to the early-to-late endosome occurs as the cargo is captured prior to binding of cargo-specific adaptors resulting in formation of the nucleation complex. An effective concentration of retromer SNX-BARs results in curvature-inducing action to remodel endosomal membrane since BAR domains drive the formation of membrane tubules (van Weering, Verkade, and Cullen 2010). Through binding of accessory proteins, the membrane is further remodelled to mature tubules. In line with this, binding of SNX5 and SNX6 to the $p150^{glued}$ component of dynactin allows the retromer to be functionally linked to the microtubule system whose motors, in parallel, mediate minus-end directed endosomal sorting (Wassmer et al. 2009; Hong et al. 2009; Hunt et al. 2013). In addition, recruitment of Wiskott–Aldrich syndrome protein and SCAR homologue (WASH) complex connects actin polymerisation to the maturing tubules. Remodelling and scission is coordinated with actin assembly and microtubule cytoskeleton which both generate additional push and pull forces that eventually drive scission of tubules towards an uncoated vesicle (Cullen and Korswagen 2012) (**Fehler! Verweisquelle konnte nicht gefunden werden.**). These tubules form a tubular endosomal network which - as a key feature of the endosomal system - is a focal point of retrograde trafficking (Burd 2011).

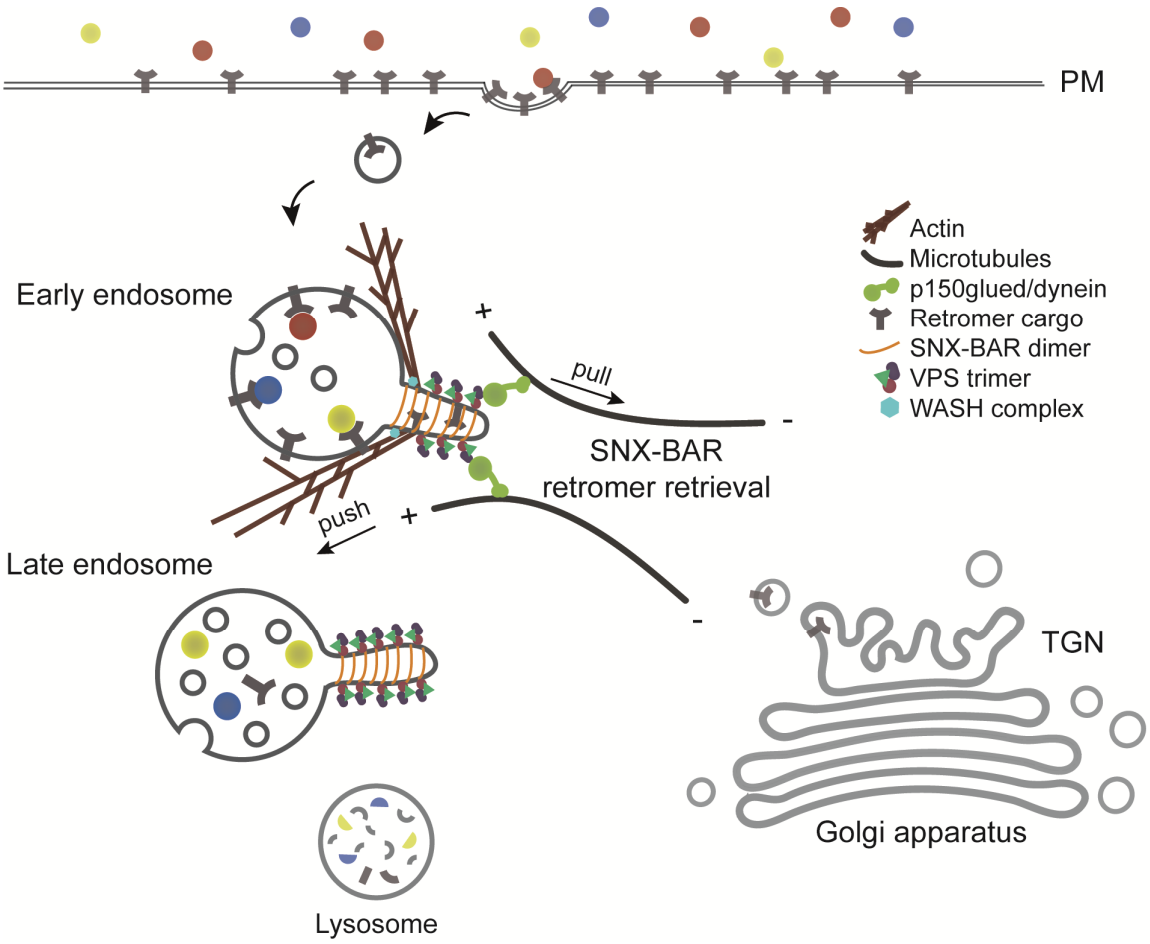

Figure 7. SNX-BAR retromer-mediated retrieval.
Illustration of retromer-mediated retrieval including SNX-BAR-mediated tubulation of the endosomal membrane. The retromer assembles to the endosomes concomitantly with cargo selection followed by binding of adaptor proteins. SNX-BARs drive membrane remodelling resulting in membrane tubules which are linked to the microtubule system. Recruitment of WASH complex connects actin to maturing tubules. Pull and push forces through microtubule and actin cytoskeleton, respectively, drive scission of tubules towards vesicles. Vesicles are transported towards the TGN. VPS: vacuolar protein sorting protein; SNX= sorting nexin; WASH: Wiskott–Aldrich syndrome protein and SCAR homologue; TGN: *trans*-Golgi network; GA: Golgi apparatus. Adapted from Maxfield and McGraw 2004, Carlton and Cullen 2005, Cullen and Korswagen 2012.

1.2.3 Subversion of the retrograde transport by intracellular pathogens

Endocytic pathways are opportune targets for viral and bacterial pathogens (Gallon and Cullen 2015; Personnic et al. 2016; Wang et al. 2018). After entry into the host cell, pathogens either escape from primary endosomal compartments into the cytosol or reside within a pathogen-containing vacuole (Goebel and Kuhn 2000). The intracellular bacterial pathogens *Chlamydia trachomatis, Legionella pneumophila* and *Salmonella enterica* serovar Typhimurium create replication-permissive compartments termed pathogen-containing vacuoles within the eukaryotic host cell by subverting the endocytic pathways (Hilbi and Haas 2012). This is achieved by hijacking the endolysosomal system whilst modifying the structure of the endosomal membrane early after entry. This enables the pathogens to evade endosome-to-lysosome maturation thus avoiding lysosomal degradation (Hilbi and Haas 2012). The

intracellular pathogen-containing vacuole allows replication and nutrient acquisition. Concurrently, it avoids host cell apoptosis and host immune recognition. Furthermore, *C. trachomatis, L. pneumophila* and *S.* Typhimurium interact with the retromer to decorate pathogen-containing vacuoles possibly to prevent recognition and to modulate bacterial replication. Effector proteins are not only utilised to create pathogen-containing vacuoles but also target host cellular trafficking and signalling pathways such as the retromer (Personnic et al. 2016). *Chlamydia* spp. likely secretes effector proteins into the host cellular cytosol or localises them into the inclusion membrane to manipulate host trafficking pathways (Moorhead et al. 2010). Chlamydial species insert inclusion membrane proteins (Incs) into the inclusion membrane that specifically interact with host cellular proteins. Recent studies demonstrated recruitment of retromer's SNX-BARs to the inclusion of *C. trachomatis* at mid-infection whereas retromer's VPS35 of the trimer localised adjacent to the inclusion (Aeberhard et al. 2015; Mirrashidi et al. 2015). In addition, SNX5 and SNX6 were shown to directly bind to chlamydial IncE (Mirrashidi et al. 2015; Paul et al. 2017; Elwell et al. 2017). During infection with *L. pneumophila*, the effector protein RidL targets the retromer through interaction with VPS29 (Finsel et al. 2013; Romano-Moreno et al. 2017; Bärlocher et al. 2017; Yao et al. 2018). Furthermore, at least SNX1 and SNX3 decorate the *S.* Typhimurium-containing vacuole (Bujny 2008, Braun 2010).

The host cellular endomembrane system with its retrograde and anterograde trafficking pathways constitute an extensive vesicular transport system. Intracellular pathogens reside within that system and several studies illuminate how intracellular pathogens hijack host cellular endolysosomal trafficking pathways in order to ensure intracellular survival.

1.3 Intracellular survival of *C. trachomatis*

1.3.1 The chlamydial inclusion: a spot from where to perturb the host cell

Chlamydia spp. are obligate intracellular bacteria that reside within a pathogen-containing vacuole, termed 'inclusion'. Inside the inclusion, *Chlamydia* spp. undergo their entire developmental cycle including replication and transition from one stage to the other. Through a specific interaction of an inclusion membrane protein with the microtubule system, *Chlamydia* spp. are trafficked towards a peri-Golgi region near the MTOC, where bacteria establish and maintain their niche throughout the developmental cycle (Grieshaber, Grieshaber, and Hackstadt 2003). Hence, the intracellular survival requires strategies to evade host immune recognition and degradation while host cellular nutrients need to be continuously acquired (Cocchiaro and Valdivia 2009; Bastidas et al. 2013; Elwell, Mirrashidi, and Engel 2016). This begs the question: How is the chlamydial inclusion preserved as a favourable intracellular niche?

Early modifications of the inclusion membrane

Soon after entry of *C. trachomatis* into the host cell, an inclusion is formed whose membrane initially resembles the host PM but is rapidly remodelled as bacterially-derived proteins are produced and inserted into the inclusion membrane to prevent the inclusion to maturate and fuse with lysosomes (Scidmore, Fischer, and Hackstadt 2003). Early understanding of the pathogen residing within the inclusion assumed that the inclusion is disengaged from classical vesicular trafficking pathways but later studies reassessed this model to a picture in which the inclusion co-opts host cell machinery to enable extensive interaction with the host cell (Cocchiaro and Valdivia 2009). Early in infection, the inclusion traffics along microtubules to a peri-Golgi region near the MTOC in a dynein-dependent but dynamitin-independent manner (Grieshaber, Grieshaber, and Hackstadt 2003). In parallel, the inclusion quickly dissociates from the endolysosomal pathway, thereby avoiding fusion with lysosomes but promoting fusion with sphingomyelin-containing exocytic vesicles (Hackstadt et al. 1996; Hackstadt 2000). The inclusion is a relatively neutral compartment with a pH at around 6. It lacks lysosomal markers such as lysosomal glycoproteins LAMP1, LAMP2 and the vacuolar H+-ATPase but recruits specific members of at least three families of fusion regulation namely Rab GTPases, phosphoinositide lipid kinases and SNARE proteins (SNAREs) (Heinzen et al. 1996; Schramm, Bagnell, and Wyrick 1996; Fields and Hackstadt 2002; Elwell, Mirrashidi, and Engel 2016). Rab GTPases are key regulators of vesicle fusion and some Rabs were among the first proteins identified to be selectively recruited to the inclusion in a species-specific manner (Rzomp et al. 2003; Damiani, Gambarte Tudela, and Capmany 2014). For *C. trachomatis* infection for instance, Rab1, Rab4, Rab6A, Rab11A, Rab14 and Rab39A are recruited to the inclusion. Rab4, Rab11 and Rab14 mediate recycling of endosomes while Rab1, Rab6 and Rab10 mediate ER-Golgi traffic (Rzomp et al. 2003; Rzomp, Moorhead, and Scidmore 2006; Brumell and Scidmore 2007; Capmany and Damiani 2010; Moorhead, Rzomp, and Scidmore 2007; Moorhead et al. 2010). Rab39A associates with late endosomes and lysosomes and regulates among others endocytosis (Seet and Hong 2006; Seto et al. 2013; Gambarte Tudela et al. 2015). In the context of *C. trachomatis* infections, Rab6A, Rab11A and Rab14 recruitment contributes to sphingomyelin acquisition whereas Rab4 and Rab11A recruitment facilitates iron acquisition (Rejman Lipinski et al. 2009; Rzomp et al. 2003; Rzomp, Moorhead, and Scidmore 2006; Capmany and Damiani 2010; Ouellette and Carabeo 2010). Rab39A is involved in delivery of multivesicular bodies and sphingolipid transport (Gambarte Tudela et al. 2015; Gambarte Tudela et al. 2019). Furthermore, proteins associated with phosphoinositol-4-phosphate (PI4P) metabolism such as phosphatidylinositol 4-kinase (PI4KIIα) and ADP-ribosylation factor 1 (ARF1) are recruited to the inclusion. The latter is a GTPase that regulates secretory membrane transport and modulates Golgi structure (D'Souza-Schorey and Chavrier 2006; Moorhead et al. 2010; Elwell et al. 2011). Interestingly, ARF1 was also shown to regulate actin cytoskeleton on the Golgi membrane (Godi et al. 1998; Fucini et al. 2000; Fucini et al. 2002). In addition, *Chlamydia* spp. interact with SNAREs such as syntaxin proteins STX6 and

STX10 and vesicle-associated membrane proteins VAMP3, VAMP7 and VAMP8 to control vesicle fusion (Bastidas et al. 2013; Elwell, Mirrashidi, and Engel 2016). SNAREs are key components during intracellular membrane fusion and responsible for all membrane fusion (Sudhof and Rothman 2009). Lastly, *C. trachomatis* recruits sorting nexin proteins (SNX) of the host cellular retromer which is a protein sorting machinery in trafficking from endosomes to the Golgi apparatus (see section 1.2.2).

Inclusion membrane proteins

While *Chlamydia* spp. acquire numerous nutrients from the host cell, the overall function of the host cell is not greatly disturbed (Moore and Ouellette 2014). In this context, the inclusion serves as a pathogen-specific compartment in order to interact with the host cell (Dehoux et al. 2011). The surface of the inclusion and the membrane itself are rapidly modified soon after entry into the host cell through the secretion of effector proteins and the insertion of inclusion membrane proteins into the inclusion membrane via the type III secretion system (T3SS) (Scidmore et al. 1996; Subtil, Parsot, and Dautry-Varsat 2001; Scidmore, Fischer, and Hackstadt 2003). Effector proteins are secreted at all infection stages (Rzomp et al. 2003; Mehlitz et al. 2010). Key proteins during intracellular survival are inclusion membrane proteins (Inc proteins, Incs) that are involved in inclusion membrane biogenesis (Scidmore-Carlson et al. 1999; Shaw et al. 2000; Mital et al. 2013). First discovered in *C. psittaci* infections and later on found in *C. trachomatis* infections, Incs share low primary sequence identity but display a common bi-lobed hydrophobic domain as secondary structure motif (Rockey and Rosquist 1994; Rockey, Heinzen, and Hackstadt 1995; Bannantine et al. 1998; Bannantine, Rockey, and Hackstadt 1998; Bannantine et al. 2000; Rockey et al. 2002; Scidmore-Carlson et al. 1999). The set of encoded Incs is species-specific. However, a core set of 23 Incs is shared by all species. The variance in expression of species-specific and core set Incs among chlamydial species might explain different host tropism and pathogenesis (Lutter, Martens, and Hackstadt 2012). As Incs are expressed at different time points during the developmental cycle, Incs are thought to carry out time-specific functions (Shaw et al. 2000; Belland et al. 2003). Furthermore, Incs are exposed at the cytosolic site of the inclusion membrane and are localised around the inclusion membrane in discrete microdomains and thus may facilitate interaction within host cells (Mital et al. 2013; Rockey et al. 1997; Hackstadt et al. 1999).

Functional analyses of at least a few Incs have driven understanding of cellular or Inc-Inc interactions (Figure 8). The best characterised Inc is IncA which mediates homotypic fusion of inclusions at mid-cycle of multiple infections (Hackstadt et al. 1999; Suchland et al. 2000). IncD interacts with the lipid transfer protein CERT and an ER-resident protein (Derre, Swiss, and Agaisse 2011; Agaisse and Derre 2014) and IncG interacts with the host cell protein 14-3-3ß (Scidmore and Hackstadt 2001). IncV interacts with an ER integral membrane protein, thus contributing to membrane contact sites (MCS) between ER and inclusion (Stanhope et al. 2017). Incs have also been shown to interact with host-cellular Rab proteins as CT229, for

instance, binds to Rab4 (Rzomp, Moorhead, and Scidmore 2006; Cortes et al. 2007). Through interaction with Rab GTPases, CT229 regulates multiple host vesicular trafficking pathways (Faris et al. 2019). Besides, CT228 recruits elements of the myosin phosphatase pathway (Lutter, Martens, and Hackstadt 2012). In addition, CT288 binds the human centrosomal protein CCDC146 whose interaction at the periphery of inclusion may modulate function of the host-cellular protein (Almeida et al. 2018). CT850 interacts with the dynein light chain DYNLT1 by which chlamydial inclusions are trafficked along microtubules (Mital et al. 2015). A study demonstrated recently that InaC regulates actin assembly and Golgi redistribution at the inclusion, presumably through ARF and/or 14-3-3s interactions (Kokes et al. 2015). SNX-BARs of the retromer complex were shown to be recruited to the inclusion (Aeberhard et al. 2015; Mirrashidi et al. 2015). In this context, it was demonstrated that IncE binds to SNX5 and SNX6 (Mirrashidi et al. 2015).

C. psittaci IncB interacts with the host protein Snapin which associates with SNAREs (Bocker et al. 2014a).

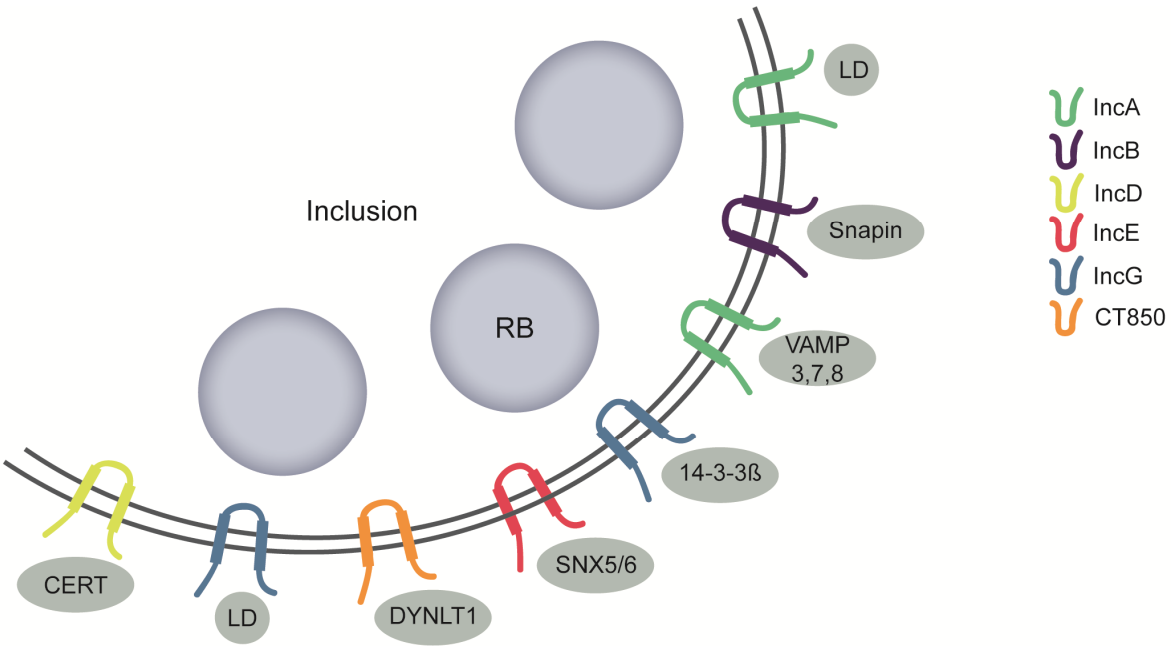

Figure 8. Interactions of Inc proteins with host cellular proteins.
For a few Incs, interacting host cellular proteins are identified, for other Incs cellular or Inc-Inc interaction have not been identified yet. See text for detailed explanation. Inc: inclusion membrane protein.

1.3.2 Reorganisation of the host-cellular cytoskeleton

Internalisation of *Chlamydia* spp. into the host cell is accompanied by GTPase-dependent reorganisation of the cytoskeleton throughout the developmental cycle, starting from entry of *C. trachomatis* via mid-infection to late infection (Cocchiaro and Valdivia 2009; Bastidas et al. 2013; Elwell, Mirrashidi, and Engel 2016). At the binding and entry sites, *C. trachomatis* induces actin remodelling and requires the GTPase Rac1 to enter the host cell (Carabeo et al. 2002;

Carabeo et al. 2004). Upon infection with *C. trachomatis*, Rac1 is activated resulting in recruitment of actin regulators to promote actin-related protein (Arp) 2/3-dependent actin recruitment (Carabeo et al. 2002; Carabeo et al. 2004). An early secreted chlamydial effector protein, the translocated actin-recruiting phosphoprotein (TARP) is able to nucleate actin polymerisation, thus facilitating internalisation (Jewett et al. 2006). Another effector protein, CT694 which is translocated into the host cell at attachment sites, interacts with the actin-binding protein AHNAK (Hower, Wolf, and Fields 2009). To maintain inclusion integrity and stability at mid-to-late stages, structural scaffolds of actin and intermediate filaments encase the inclusion (Kumar and Valdivia 2008a, 2008b). *Chlamydia* spp. co-opt the GTPase RhoA for assembly of actin filaments at the inclusion surface followed by recruitment of Intermediate filament proteins (Kumar and Valdivia 2008a). Moreover, it has been proposed that modulation of the host cytoskeleton by *Chlamydia* spp. may constitute a mechanism to evade immune response as destabilisation of the inclusion through actin disruption resulted in increased pro-inflammatory cytokine production (Kumar and Valdivia 2008a, 2008b). During the late infection stage, newly formed EBs are released by either cell lysis or extrusion. The latter requires actin polymerisation, myosin and GTPase RhoA (Hybiske and Stephens 2007). Taken together, *Chlamydia* spp. hijack host cellular cytoskeleton components in order to stabilise their niche (Kumar and Valdivia 2008b).

1.3.3 Host-pathogen interactions for nutrient acquisition

Chlamydia spp. rely on host-derived nutrients as species are capable of synthesising phosphatidylethanolamine, phosphatidylglycerol phosphatidylserine (Wylie, Hatch, and McClarty 1997; Hatch and McClarty 1998) but lack some lipid biosynthetic enzymes for replication, homotypic fusion, growth and stability of the inclusion membrane (Elwell and Engel 2012; Elwell, Mirrashidi, and Engel 2016). Once established their niche, *Chlamydia* spp. acquire sphingolipids, cholesterol and the glycerophospholipids phosphatidylcholine and phosphatidylinositol from the host cell (Hackstadt et al. 1996; Van Ooij et al. 2000; Carabeo, Mead, and Hackstadt 2003; Su et al. 2004; Moore et al. 2008). Strategies for lipid acquisition include subversion of the vesicular lipid transport from the GA and multivesicular bodies, hijacking of non-vesicular lipid transport, recruitment of lipid-modifying enzyme and lipid transporters as well as activation of signalling pathways. The GA acts as a central player in vesicular lipid transport of both, endocytic and exocytic pathways and between organelles (Elwell and Engel 2012). *Chlamydia* spp. intercept sphingomyelin- and cholesterol-containing exocytic vesicles from the GA (Bastidas et al. 2013). The GA is fragmented into discrete Golgi ministacks during mid-stages of *C. trachomatis* infection. These ministacks locate around the inclusion and are hypothesised to facilitate lipid delivery (Heuer et al. 2009). In this process, Rab GTPases Rab6A and Rab11A, ARF GTPase and dynamin are involved (Rejman Lipinski et al. 2009; Gurumurthy et al. 2014; Kokes et al. 2015). Interaction of inclusion membrane proteins with Rab proteins were shown to be implicated specifically in sphingomyelin acquisition

(Rejman Lipinski et al. 2009; Capmany and Damiani 2010). In addition, fragmentation requires remodelling of microtubules to recruit Golgi ministacks to the inclusion (Al-Zeer et al. 2014). However, since a recent study revealed that Golgi fragmentation was dispensable for dynamin-mediated lipid acquisition to *C. trachomatis*, the role of Golgi fragmentation for *C. trachomatis* growth and boost of lipid delivery is a subject of debate (Gurumurthy et al. 2014; Kokes et al. 2015). In addition to vesicular transport, non-vesicular lipid transport is involved in nutrient acquisition (Elwell and Engel 2012). The ER is an appealing target for *Chlamydia* spp. to be co-opted as the ER is key in folding protein molecules in sacs termed cisternae and in transport of synthesised proteins to the GA. ER tubules were shown to be in close proximity to *C. trachomatis* inclusions and studies characterised the connections between ER and the inclusions membrane and defined them as ER-inclusion MCSs (Giles and Wyrick 2008; Derre, Swiss, and Agaisse 2011; Dumoux et al. 2012; Derre 2017). These MCSs are thought to participate in a non-vesicular lipid transport from the ER to *C. trachomatis* inclusions (Derre, Swiss, and Agaisse 2011; Elwell et al. 2011; Derre 2015; Dumoux and Hayward 2016). ER-derived lipids serve as nutrients for bacterial replication and lipids are used to modify inclusion membrane composition and/or to subvert host immune response. The ceramide endoplasmic reticulum transport protein (CERT) is a non-vesicular lipid transporter which transports ceramide from the ER to the *trans*-Golgi where at least one of sphingomyelin synthase 1 or 2 (SMS1 or 2) uses CERT-transported ceramide to synthesise sphingomyelin (Hanada et al. 2003; Huitema et al. 2004). During infection with *Chlamydia* spp., CERT and SMS2 are recruited to the inclusion suggesting that CERT mediates ceramide transfer from the ER to the inclusion where SMS2 likely converts ceramide to sphingomyelin to promote the chlamydial infection (Koch-Edelmann et al. 2017). Other non-vesicularly transported lipids are host glycerophospholipids (Wylie, Hatch, and McClarty 1997; Hatch and McClarty 1998; Su et al. 2004). Furthermore, the inclusion interacts with multivesicular bodies which possibly act as post-Golgi trafficking intermediate to serve as sphingolipid and cholesterol source (Beatty 2006, 2008; Robertson et al. 2009; Gambarte Tudela et al. 2015). *Chlamydia* spp. also interact with i) lipid droplets serving as a source for neutral lipids such as long fatty acids (Kumar 2006, Cocchiaro 2008), ii) mitochondria possibly serving as a source for ATP (Matsumoto et al. 1991; Derre et al. 2007; Liang et al. 2018) and iii) lysosomes serving as a source for amino acids which are derived from host-protein degradation (Ouellette et al. 2011; Bastidas et al. 2013). However, interaction of the inclusion with lipid droplets is controversially debated as the host-cell derived proteome of isolated *C. trachomatis* inclusions did not identify lipid droplet marker (Aeberhard et al. 2015). In addition, *C. trachomatis* is able to scavenge fatty acids from the host cell by a lipid droplet-independent mechanism (Sharma et al. 2018). Recently, translocation of peroxisomes into the lumen of *C. trachomatis* inclusions was described. Peroxisomes may serve as a metabolic enzymes source (Boncompain et al. 2014). Altogether, *Chlamydia* spp. employ numerous strategies to acquire nutrients from the host cell which all ensure intracellular survival (Figure 9). Moreover, in the genome of *C. trachomatis*, ABC (ATP-binding cassette)

transporters were identified whose identification corresponds to the limited ability to synthesise amino acids (Stephens et al. 1998). ABC transporters constitute a family of membrane proteins and are associated with active amino acid and oligopeptide transport. Finally, *C. trachomatis* imports nucleotides from the host cell by a nucleotide transporter system that involves two nucleotide transporter proteins Npt1 and Npt2 expressed in *C. trachomatis* (Tjaden et al. 1999). Npt1 catalyses ATP and ADP transport in an exchange mode whereby *C. trachomatis* is provided with energy. Npt2 in contrast transports all four ribonucleoside triphosphates required for anabolic reactions (Tjaden et al. 1999).

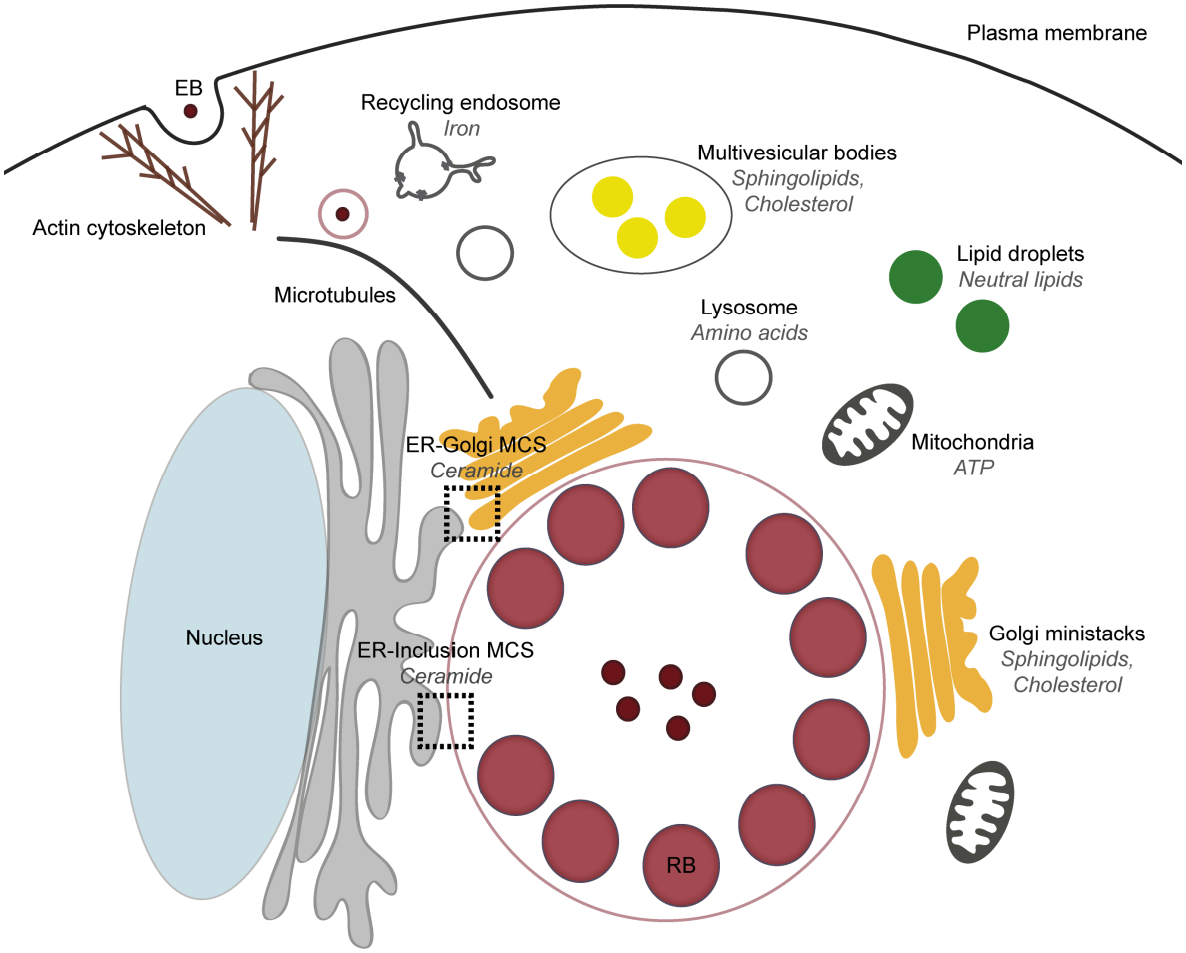

Figure 9. Host-pathogen interactions.
Chlamydia spp. reside in the inclusion from where *Chlamydia* spp. acquire nutrients from vesicular and non-vesicular transport pathways to ensure intracellular survival. The GA, multivesicular bodies and lipid droplets serve as lipid sources. MCSs between the ER and Golgi and between the ER and the inclusion participate further in lipid transport. Lysosomes serve as amino acids source and mitochondria possibly as ATP source. GA: Golgi apparatus; ER: endoplasmic reticulum; MCS: membrane contact sites. Adapted from Bastidas et al. 2013.

1.4 Ribosomes – the central hub for protein translation

1.4.1 Protein synthesis on ribosomes

The ribosome is a large ribonucleoprotein complex composed of two subunits (Figure 10 A). In eukaryotes, the ribosome consists of a small 40S subunit and a large 60S subunit; both are built from RNA and proteins and together they assemble to the 80S ribosome. Eukaryotic ribosomes contain 18S rRNA and 33 ribosomal proteins in the small subunit and 5S, 5.8S and 25S/28S rRNA and in most eukaryotic species 47 ribosomal proteins in the large subunit (Wilson and Doudna Cate 2012; Kressler, Hurt, and Bassler 2017).

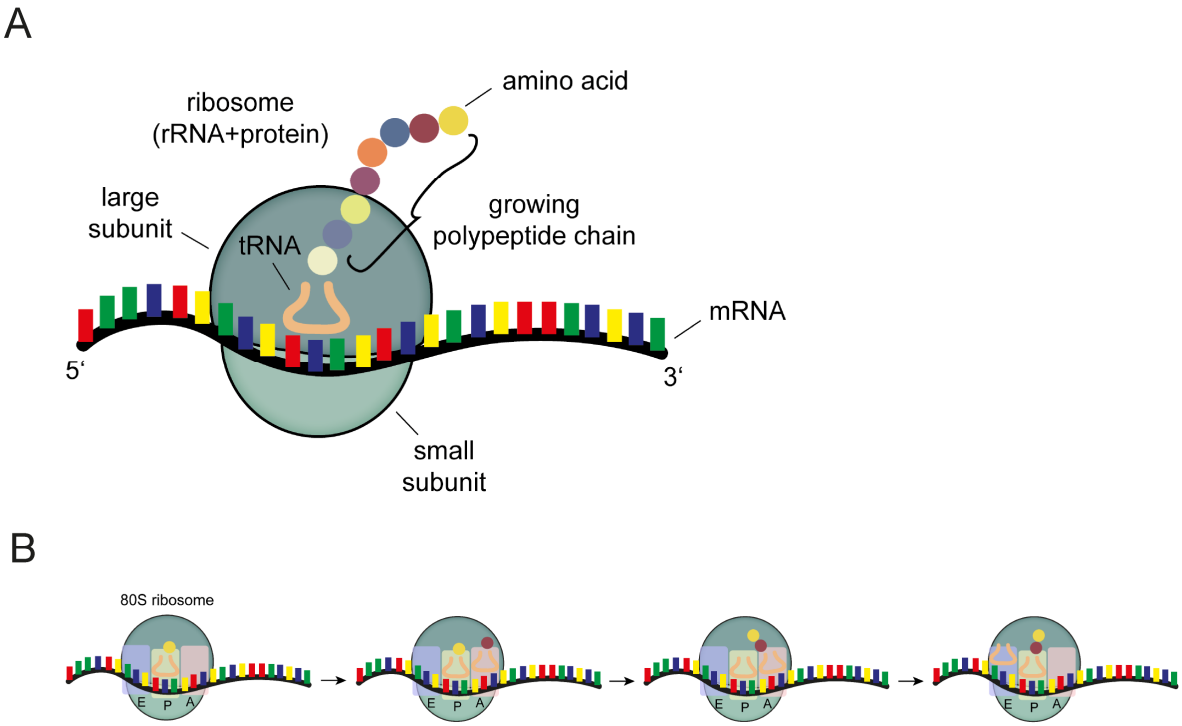

Figure 10. Protein synthesis on eukaryotic ribosomes.
(A) Eukaryotic ribosome structure. The eukaryotic ribosomes consist of two subunits: a large 60S subunit and a small 40S subunit. Both subunits are built from RNA and proteins and together form the 80S ribosome which translates mRNA templates into proteins. Adapted from Lodish 2008. (B) Elongation of polypeptidyl chain on the ribosome during translation. Once the 80S ribosome and the start codon are assembled in the P site, a second amino acid bound to tRNA binds to the A site followed by peptide bond formation through GTP hydrolysis. Another GTP hydrolysis results in translocation of one codon along the mRNA and the start codon-tRNA shifts to the E site while the second tRNA shifts to the P site. Adapted from Lodish 2008.

Central function of ribosomes is the stepwise protein synthesis - decoding mRNA templates into a polypeptide chain in three stages: initiation, elongation and termination/recycling. The ribosome is thus a translational machinery catalysing protein synthesis in all cells (Lodish 2008; Khatter et al. 2015). In parallel, ribosomes ensure protein quality control and coordination of polypeptide synthesis and proper folding (Pechmann, Willmund, and Frydman 2013). The mRNA binds to the small subunit where trinucleotide codons of mRNA interact with anticodons of tRNA. At the beginning of one translation round, the initiation complex, a multi-component

complex is formed. Recruitment of the large subunit forms the 80S ribosome ready to translate the mRNA at the initiation stage. Hereafter, the polypeptide chain is formed during the elongation stage (Figure 10 B) until the ribosome bearing a nascent protein chain reaches a stop codon site. Release factors enter the ribosomal complex, tRNAs and mRNA are released and the two ribosomal subunits disassemble (termination) (Ramakrishnan 2002; Schmeing and Ramakrishnan 2009).

1.4.2 Ribosome biogenesis

Eukaryotic ribosomes are pre-assembled in the nucleolus before export to the cytoplasm (Tschochner and Hurt 2003; Kressler, Hurt, and Bassler 2017) (Figure 11). In the nucleolus, ribosomal DNA is transcribed into a pre-rRNA (35S pre-rRNA) that is then modified (e.g. methylated or pseudouridinylated) by so-called small nucleolar ribonucleoproteins (snoRNPs) and snoRNAs. In the cytoplasm, ribosomal proteins and assembly factors (= biogenesis factors) are synthesised and subsequently transported into the nucleolus. There, pre-rRNAs and ribosomal proteins with assistance of assembly factors assemble and together form the 90S pre-ribosome (Kressler, Hurt, and Bassler 2017; Bassler and Hurt 2018). The 90S pre-ribosome is subsequently cleaved to yield 43S and 66S pre-ribosomal particles that are then exported from the nucleoplasm to the cytoplasm as mature 40S and 60S subunits, respectively. In the cytoplasm, ultimate maturation of both subunits into translation-competent subunits occurs, including incorporation of further ribosomal proteins and release plus recycling of assembly factors (Fatica and Tollervey 2002; Tschochner and Hurt 2003; Kressler, Hurt, and Bassler 2017; Bassler and Hurt 2018). Several quality checkpoints at both locations, the nucleus and the cytoplasm, ensure that only fully functional ribosomal subunits participate in translation (Kressler, Hurt, and Bassler 2017). As ribosome assembly requires extensive regulation and coordination with other cellular pathways, this is the most energy-consuming process in a growing cell (Bassler and Hurt 2018).

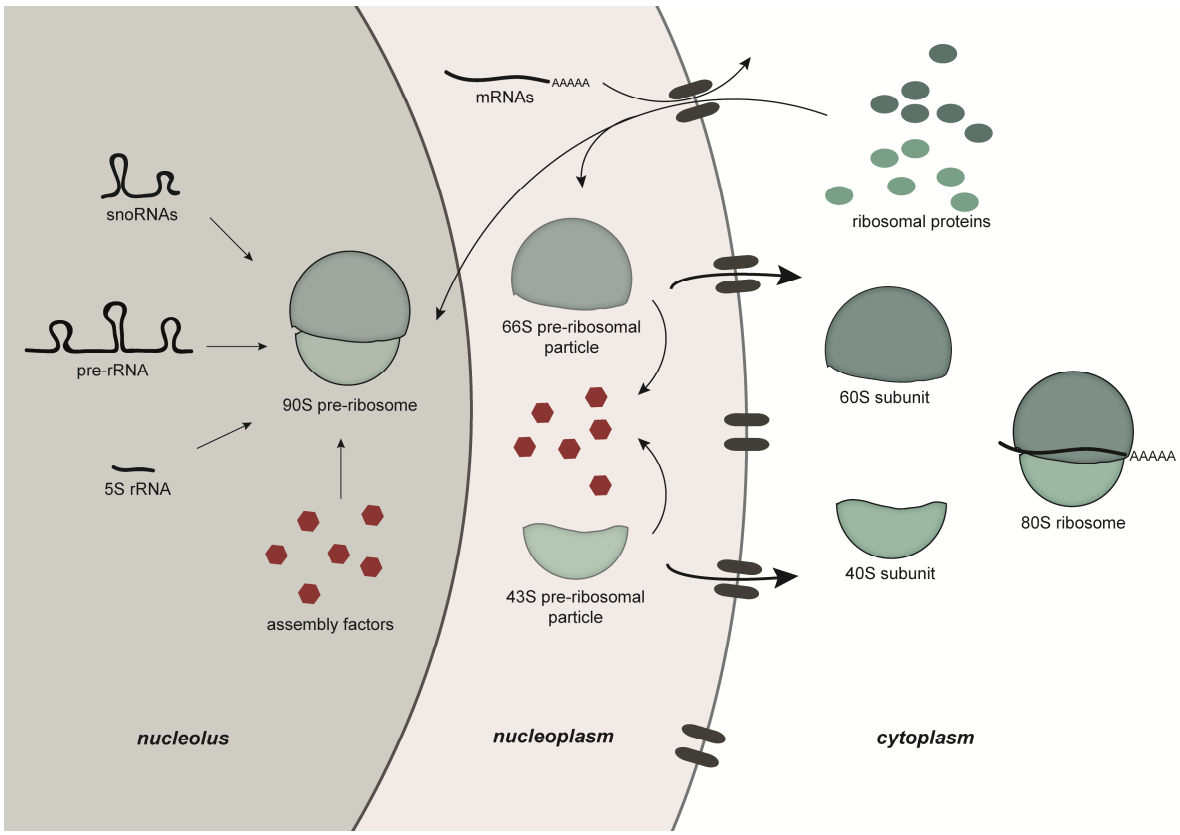

Figure 11. Ribosome biogenesis.
In the nucleolus, ribosomes are pre-assembled to the 90S pre-ribosome. The 90S pre-ribosome is cleaved in the nucleoplasm to yield 43S and 66S pre-ribosomal particles that are exported as mature 40S and 60S subunits. In the cytoplasm, ultimate maturation of both subunits occurs and 40S and 60S subunits join to the 80S ribosome ready for the translation process. snoRNA: small nucleolar RNA; pre-rRNA: pre-ribosomal RNA; rRNA: ribosomal RNA; mRNA: messenger RNA; r-protein: ribosomal proteins. Adapted from Bassler and Hurt 2018.

1.4.3 RPL13a: a ribosomal protein with an extra-ribosomal function

Ribosomal proteins are RNA-binding proteins present in every cell. Some ribosomal proteins have a clear and essential function in the assembly of ribosomal subunits but are dispensable for fully assembled ribosomal function. They remain in the mature ribosome and might improve their stability (Wilson and Nierhaus 2005). However, there is an increasing number of reports revealing that other ribosomal proteins carry out extra-ribosomal functions (= ribosome-independent functions) despite their housekeeping functions (Wilson and Nierhaus 2005). Hence, functional moonlighting of ribosomal proteins seems to be more widespread than previously thought (Wool 1996; Lindstrom 2009; Warner and McIntosh 2009; Zhou et al. 2015). One of the ribosomal proteins with an extra-ribosomal function is the ribosomal protein L13a (RPL13a). Mammalian RPL13a is a component of the 60S large subunit and present in the mature 80S ribosome but its function within the 80S ribosome is unknown (Das et al. 2013). In the 80S ribosome, RPL13a localises distal from the tRNA binding and exit site of the protein (Ben-Shem et al. 2011). It has no known function in the translation process as RNAi-mediated depletion of RPL13a did not affect total protein synthesis (Chaudhuri et al. 2007). Furthermore,

depletion of RPL13a did not cause defects in ribosome biogenesis and translational fidelity and was thus shown to be dispensable for general ribosome function. During processing of the 90S pre-ribosome, however, RPL13a is incorporated and is essential in rRNA methylation (Chaudhuri et al. 2007; Das et al. 2013). Apart from that, RPL13a functions extra-ribosomally in the GAIT complex (Mazumder et al. 2003; Vyas et al. 2009). The GAIT complex is a transcript-selective translational control system (Figure 12). Upon stimulation with IFNy, assembly of GAIT complex is induced which consists of 4 proteins: EPRS, NSAP1, RPL13a and GAPDH (Mukhopadhyay et al. 2009; Jia et al. 2012; Arif et al. 2018). Upon IFNy stimulation, EPRS is phosphorylated and released from the tRNA multisynthetase complex. EPRS and NSAP1 form a pre-GAIT complex. Later, RPL13a is phosphorylated and released from the 60S ribosomal subunit (Mazumder et al. 2003). Phosphorylated RPL13a associates with GAPDH and both proteins join the pre-GAIT complex thereby forming the functional GAIT complex (Mazumder et al. 2003). Complete GAIT complex is able to repress translation of GAIT element harbouring transcripts in the 3‘ untranslated region (UTR) such as 3‘ UTR of ceruloplasmin mRNA (Sampath et al. 2003; Mukhopadhyay et al. 2009; Jia et al. 2012; Arif et al. 2018).

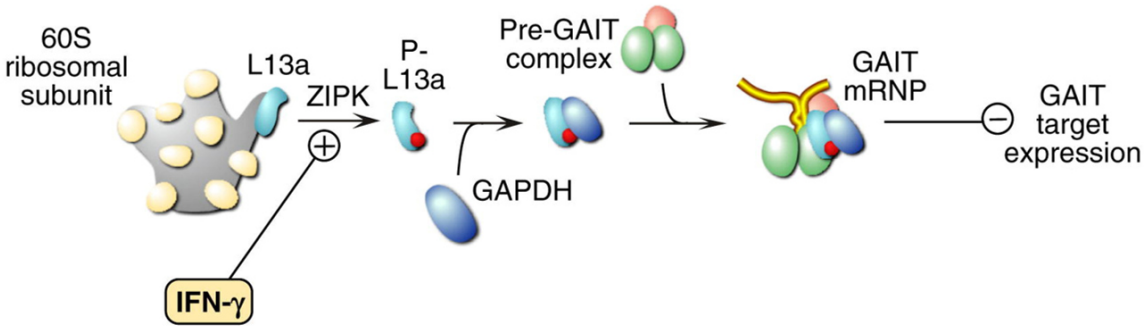

Figure 12. Formation of the GAIT complex.
Upon stimulation of with IFNγ, EPRS is phosphorylated and together with NSAP1 forms a pre-GAIT complex in a first step. In a second step, RPL13a is phosphorylated and together with GAPDH joins the pre-GAIT complex forming the functional GAIT complex. The GAIT complex represses translation of GAIT element harbouring transcripts. Modified from Jia et al. 2012.

1.5 Aim of this thesis

Chlamydia spp. reside within an inclusion and have evolved numerous sophisticated strategies that are highly adapted to the host in order to maintain intracellular survival. *C. trachomatis* is a major public health concern and one of the most prevalent sexually transmitted bacterial pathogens. Its inclusion is embedded in the host cellular endomembrane system from where *C. trachomatis* acquires several nutrients. They are required for the establishment and maintenance of the inclusion and inclusion integrity. Among recruited proteins are sorting nexins (SNX) of the human retromer which sorts proteins from endosomes to the *trans*-Golgi network. Moreover, tubular-like structures that seem to emanate from the inclusion and that are positive for SNX-BARs and Inc proteins have been observed. Function and the underlying mechanisms of the recruitment of SNXs and the tubular-like structures, however, are so far elusive. With this thesis, we aimed to decipher spatio-temporal dynamics of SNXs from early to mid-infection stages of *C. trachomatis* and we aimed to gain a greater understanding of the function of SNX recruitment and the tubular-like structures at both infection stages.

In the first part of this thesis, we examined the early infection stage and analysed the localisation of retromer components (SNX-BARs, VPS35) and one of its cargo CI-MPR in *C. trachomatis* infected cells in a time course. By use of generated SNX single and double knockout cell lines, we performed a functional analysis of early *C. trachomatis* trafficking.

In the second part, we examined the mid-infection stage. Here, we analysed the localisation of SNX-BARs, VPS35 and CI-MPR as wells as functional domains of SNX-BARs at mid-infection time point. In addition, we focussed on the co-localisation of SNX-BARs with the chlamydial inclusion membrane protein IncE. We went one step further and addressed the ultrastructure of tubular structures which likely emanate from the inclusion. By use of SNX KO cell lines, we analysed primary and secondary *C. trachomatis* infection.

In the third part, we applied a proximity-dependent biotinylation assay followed by nLC-MS/MS analysis to identify SNX1-proximal proteins. This approach allows us to draw conclusions from the mechanism and function of SNX-BAR recruitment and further involved proteins.

2 Materials and Methods

2.1 Materials

2.1.1 Organisms

Cell lines

Table 1. Cell lines

Cell line	Origin	Source
HeLa	isolated from human cervix carcinoma	ATCC: CCL-2
DF-1	chicken embryo fibroblast	ATCC: CRL-12203

For CRISPR/Cas9-mediated knockout cell lines, see section 2.2.7.

Bacteria

Table 2. *Chlamydia*

Species	Strain	Origin	Source
C. trachomatis	D	human cervix isolate UW-3/Cx	ATCC: VR-885
C. trachomatis	L2	lymphatic isolate 434 Bu	ATCC: VR-902B
C. psittaci	02DC15	bovine isolate	(Schofl et al. 2011)

Table 3. *Escherichia coli*

Strain	Purpose	Source
BIOBlue	Cloning	Bioline USA Inc.
BL21-CodonPlus-RIL	Expression	Agilent Technologies
DH5α	Retransformation	New England Biolabs
Rosetta	Expression	Novagen by Merck

2.1.2 Nucleic Acids

All Oligonucleotides were ordered from Eurofins MWG.

Primers for cloning

Table 4. Primers for cloning

Gene product	Domain	Back-bone	Source	Restriction site	Sequence	Direction
SNX1	Full	pEGFP-	this work	EcoRI	CAGAATTCGATG	for

	length	C1			GCGTCGGGTGGT	
				SalI	TAGTCGACGGAGATGGCCTTTGCCTCA	rev
SNX1	BAR domain (aa 302 – 522)	pEGFP-C1	this work	EcoRI	GGGAATTCGAATGAATCAGACATTTGGTTTGA	for
				SalI	GTCGACGGAGATGGCCTTTGCCTC	rev
SNX1	PX domain (aa 143 – 272)	pEGFP-C1	this work	EcoRI	GCGAATTCGTTTGATTTGACAGTCGGTATAA	for
				SalI	GTGTCGACACGTGGCAGCTCTTCTTTT	rev
SNX2	Full length	pEGFP-C1	this work	EcoRI	GAATGAATTCAATGGCGGCCGAGAGGGAAC	for
				SalI	GTTAGTCGACCTAGGCAATGGCTTTGGCTTC	rev
SNX2	BAR-domain (aa 283-514)	pEGFP-C1	this work	HindIII	GATAAAGCTTTAATGGTGAACAAGGCTGCCG	for
				EcoRI	GAATGAATTCTTCAGGTAGGAATGCTTCCCAG	rev
SNX2	PX-domain (aa 142-265)	pEGFP-C1	this work	HindIII	GATAAAGCTTTAGAAATTGGTGTATCAGATCCAG	for
				EcoRI	GAATGAATTCTGAACTTTCCAAGAACTGCCTT	rev
SNX5	Full length	pEGFP-C1	(Aeberhard et al. 2015)	EcoRI	CTTAGAATTCAATGGCCGCGGTTCCCGAG	for
				SalI	CAATGTCGACTCAGTTATTCTTGAA	rev

					CAAGTCAATACAGC	
SNX5	BAR-domain (aa 185-402)	pEGFP-C1	this work	HindIII	GATAAAGCTTTATTCTTCAAAAGTGTGGTGAAAAGTG	for
				BamHI	CTATGGATCCCTTGAACAAGTCAATACAGCTC	rev
SNX5	PX-domain (aa 29-169)	pEGFP-C1	this work	HindIII	GATAAAGCTTTATCGCTTCAGATTGACATACCTG	for
				BamHI	CTATGGATCCATCATATTCCAGGAAAACATGAAAG	rev
SNX6	Full length	pEGFP-C1	(Aeberhard et al. 2015)	HindIII	GATAAAGCTTTAATGACGAAGGAAGAATTCACAAAGATG	for
				BamHI	CTATGGATCCTTATGTGTCTCCATTTAACACTGCCAG	rev
SNX6	BAR domain (aa 203 – 406)	pEGFP-C1	this work	XhoI	GATACTCGAGGCGACTTCTTTAAAAACATG	for
				BamHI	TATGGATCCGTCTCCATTTAACACTGC	rev
SNX6	PX domain (aa 26-173)	pEGFP-C1	this work	XhoI	GACTCGAGGCCTTCAAAGTGATGCTGCTC	for
				BamHI	CTATGGATCCCAAATCTTGATTATATTCCAAGAAGACATG	rev
IncE	cytosolic domain (aa 88-132)	pGEX-3X	this work	EcoRI	GAAGAATTCGGCTTTGGATGTTCTAGAGGATCA	for
				BamHI	CCGAGGATCCTT	rev

SNX1	Full length	pcDNA3.1 mycBirA	this work	NotI EcoRI	GAGTTACTAAAA TCACTTTGTCTG AAGCGGCCGCAA ATGGCGTCG GTGAATTCGGAG ATGGCCTTTGCC TCAGG	for rev

SNX5 full length and SNX6 full length fusion proteins were used from Aeberhard et al. 2015.

Primers for quantitative real-time PCR (qPCR)

Table 5. Primers for qPCR

Target sequence	For Sequence (5' to 3')	Rev Sequence (5' to 3')	RefSeq ID (NCBI Reference Sequence Database) ID/ Reference
5‘ ETS	GCGCACGTCCCGT GCTC	GAGGGGGAAGCG GAGGAGG	(Chaudhuri et al. 2007)
18S	GCGCTGACCCCCT TCGC	CTCCCCGGGTCG GGAGTG	(Chaudhuri et al. 2007)
SNX1	GAGGGGGAGGACA TTTTCAC	ATCCCATTTTCTT TGGAGCC	NM_003099
SNX2	TTCACCAGCACTGT CTCCAC	GGCCATTGGAGT TTGCACTA	NM_003100
SNX5	AGCAGCAGGAGGA GGACC	GAGCGCATCAGG TATGTCAA	NM_152227
SNX6	CCCGGACTTCCTCT CAGAA	CATCAGAAATGTC CACCTGC	NM_152233
GAPDH	GCAAATTCCATGGC ACCGT	GCCCCACTTGATT TTGGAGG	NM_002046
ACTB	GTTGTCGACGACG AGCG	GCACAGAGCCTC GCCTT	http://primerdepot.nci.nih.gov/
c16S rDNA	CCGCCAACACTGG GACT	GGAGTTAGCCGG TGCTTCTTTAC	(Lienard et al. 2011)

Sequencing primers

Table 6. Sequencing primers

Name	Sequence (5' to 3')	Backbone	Direction
pEGFP C1	CATGGTCCTGCTGGAGTTCGTG	pEGFP	for
pEGFP C1	GAAATTTGTGATGCTATTGC	pEGFP	rev
CMV	CGCAAATGGGCGGTAGGCGTG	pcDNA3.1 mycBioID	for
BGH	TAGAAGGCACAGTCGAGG	pcDNA3.1 mycBioID	rev
mycBioID 1681	CGCTCTGGAGCTGTTCGA	pcDNA3.1 mycBioID	for
pGEX-3x	GGG CTG GCA AGC CAC GTT TGG TG	pGEX-3x	for
pGEX-3x	CCG GGA GCT GCA TGT GTC AGA GG	pGEX-3x	rev
pSpCas9	CGTAGAAAGTAATAATTTCTTGGGTAGTTTGCA	pSpCas9(BB)-2A-Puro (PX459) V2.0	for
pSpCas9	GAGCCATTTGTCTGCAGAATTGGCGCA	pSpCas9(BB)-2A-Puro (PX459) V2.0	rev

Expression plasmids

Table 7. Expression plasmids

Expressed insert	Plasmid name	Provider	Expressed insert
GST	pGEX-3X	GE Healthcare	GST
eGFP	peGFP-C1	Invitrogen	eGFP
Myc-BirA*	pcDNA3.1 mycBirA	www.addgene.org/35700/	Myc-BirA*
Cas9	pSpCas9(BB)-2A-Puro (PX459) V2.0	www.addgene.org/62988/	Cas9

Small Interfering RNAs

Table 8. Small interfering RNAs

Target	Target Sequence (5' to 3')	Manufacturer | Cat. No.	Target
AllStars	Not publicly available	Qiagen | SI03650318	AllStars
Luciferase	TCGAAGTACTCAGCGTAAGTT	Qiagen | 1027423	Luciferase
RPL13a	CTCCTGGTCTGAGCCCAATAA	Qiagen Hs_RPL13A_5 | SI04156845	RPL13a
RPL13a	ACAGCTCATGAGGCTACGGAA	Qiagen Hs_RPL13A_6 |	RPL13a

		SI04289607	
RPL13a	CCGCAAGCGGATGAACACCAA	Qiagen Hs_RPL13A_7 | SI04321779	RPL13a
RPL13a	CACAGGGTATTTCTAGAAGCA	Qiagen Hs_RPL13A_8 | SI04325902	RPL13a

2.1.3 Media and solutions

Cell culture media

Table 9. Cell culture media

Application	Composition	Manufacturer
Cell growth	RPMI 1640	Gibco
	10 % (v/v) FCS, heat-inactivated	Biochrom
	1 mM sodium pyruvate	Gibco
	5 mM L-glutamine	Gibco
Infection	DMEM high glucose (4.5 g/L)	Gibco
	1 mM sodium pyruvate	Gibco
	5 mM L-glutamine	Gibco
SILAC “light” cell growth	DMEM Media for SILAC	Thermo Fisher Scientific
	10% (v/v) dialysed FCS, heat-inactivated	Biochrom
	L- arginine (42 mg/mL)	SILANTES
	L- lysine (96 mg/L)	SILANTES
	1 mM sodium pyruvate	Gibco
SILAC “light” infection	DMEM Media for SILAC	Thermo Fisher Scientific
	5 % (v/v) FCS	Biochrom
	L- arginine (42 mg/mL)	SILANTES
	L- lysine (96 mg/L)	SILANTES
	1 mM sodium pyruvate	Gibco
SILAC “heavy” cell growth	DMEM Media for SILAC	Thermo Fisher Scientific
	5 % (v/v) dialysed FCS, heat-inactivated	Biochrom
	$^{13}C_6{}^{15}N_4$ L- arginine (42 mg/mL)	SILANTES
	$^{13}C_6{}^{15}N_2$ L-Lysine (96 mg/L)	SILANTES
	1 mM sodium pyruvate	Gibco
SILAC “heavy” infection	DMEM Media for SILAC	Thermo Fisher Scientific
	5 % (v/v) dialysed FCS, heat-inactivated	Biochrom

	$^{13}C_6{}^{15}N_4$ L- arginine (42 mg/mL)	SILANTES
	$^{13}C_6{}^{15}N_2$ L-Lysine (96 mg/L)	SILANTES
	1 mM sodium pyruvate	Gibco
Transfection	OptiMEM	Gibco
Passaging	Trypsin EDTA	Gibco
LB medium (liquid)	10 g/L trypton, 5 g/L yeast extract, 5 g/L NaCl	RKI
LB-agar plates	LB medium, 1.5 % (w/v) bacto agar supplemented with appropriate antibiotic	RKI

Buffers and Solutions

Table 10. Buffers and Solutions

Buffer	Composition
4% PFA	4% (v/v) PFA, 4% (w/v) sucrose in PBS
5x Separating gel SDS-PAGE buffer	1 M Tris/HCl, pH 9.0
5x Stacking gel SDS-PAGE buffer	1 M Tris/HCl, pH 6.8
6x SDS-PAGE loading buffer (Laemmli buffer)	375 mM Tris/HCl, pH 6.8, 48% (v/v) glycerol, 9% (v/v) β-mercaptoethanol, 6% (w/v) SDS, 0.03% (w/v) bromphenol blue
Coomassie staining solution	0.1% (w/v) Coomassie Blue R-250, 10% (v/v) acetic acid
Destaining solution	10 % (v/v) acetic acid, 40% (v/v) ethanol
Elution buffer I (Sample preparation for MS analysis)	2 M urea (prepare fresh the same day), 100 mM Tris/HCl, pH 8.5, 5 mM DTT, 6 ng/µL Trypsin
Elution buffer II Elution buffer I (Sample preparation for MS analysis)	2 M urea (prepare fresh the same day), 100 mM Tris/HCl, pH 8.5, 15 mM IAA, 6 ng/µL Trypsin
IF blocking buffer	0.2% (w/v) BSA in PBS
IF permeabilisation buffer	0.2% (w/v) BSA in PBS, 0.2% (v/v) Triton X-100
Mowiol mounting medium	2.4 g Mowiol 4-88, 6 g glycerol, 6 mL H_2O, 12 mL 0.2 M Tris pH 8.5
PBS	137 mM NaCl, 2.7 mM KCl, 10 mM Na_2HPO_4 + 2 H_2O, 1.76 mM KH_2PO_4, pH 7.4
Polyribosome buffer	20 mM Tris/HCL, 10 mM $MgCl_2$, 150 mM KCl, 0.5% (v/v) IGEPAL-CA630, pH 8.5
Pulldown Bead Wash buffer	40 mM Tris/HCl, 150 mM NaCl, pH 7.5
RIPA lysis buffer	40 mM Tris/HCl, 150 mM NaCl, 0.1% (v/v) NP40, 0.01% (v/v) Triton X-100, 0.1% (w/v) SDS pH 7.5
SDS-PAGE running buffer	25 mM Tris/HCl, 192 mM glycine, 0.1% (w/v) SDS

Separating gels, 10% (sufficient for 4 gels)	5 mL separating gel buffer, 6.6 mL 30% bisacrylamide, 200 µL 10% (w/v) APS, 20 µL TEMED, 8.2 mL ddH_2O
Separating gels, 12% (sufficient for 4 gels)	5 mL separating gel buffer, 7.9 mL 30% bisacrylamide, 200 µL 10% (w/v) APS, 20 µL TEMED, 6.9 mL ddH_2O
Stocking buffer	250 mM sucrose in PBS
Stripping buffer	200 mM Glycin, 1.5% (w/v) SDS, 1% (v/v) Tween 20
TBE	89 mM Tris/HCl, 89 mM borat, 2 mM EDTA, pH 8.0
TBS	137 mM NaCl, 10 mM Tris/HCl, pH 7.5
TBST	0.05% (v/v) Tween 20 in TBS
TBST-M (Western Blot blocking buffer)	3% (w/v) milk powder in TBS
Urea buffer	8 M urea, 2M Thiourea in 0.1 M Tris/HCl, pH 8.5
Western blot wet transfer buffer	25 mM Tris/HCl, 192 mM glycine, 0.1% (w/v) SDS, 20% (v/v) methanol
Stacking gels, 5% (sufficient for 4 gels)	2.5 mL stacking gel buffer, 1.6 mL 30% bisacrylamide, 100 µL 10% (w/v) APS, 10 µL TEMED, 5.8 mL ddH_2O
4xSP buffer	0.4 M sucrose, 16 mM Na_2HPO_4 pH 7.1

2.1.4 Antibodies

Primary antibodies

Table 11. Primary antibodies

Antigen	Species	Source	Catalog No.	Dilution WB	Dilution IF (/EM)
CI-M6PR	mouse	AbD seroTec	MCA2048	1:1000	1:100
c-myc (9E10)	mouse	Santa Cruz Biotechnology	sc-40	-	1:1000
EPRS	rabbit	Novus Biologicals	NBP1-84929	-	1:100
ERP57	rabbit	GeneTex	GTX113719	1:1000	1:500
GAPDH	mouse	Pierce	MA5-15738	1:2000	-
GFP	rabbit	Invitrogen	A6455	1:2000	-
GFP (for EM)	rabbit	Rockland	600-401-215	-	1:300 - 1:900
hnRNP Q (NSAP1)	mouse	Abcam	ab10687	-	1:100
Hsp60	mouse	Enzo Life Sciences	ALX-804-072	-	1:300
Hsp60	mouse	Enzo Life Sciences	ALX-804-071	1:5000	-
IncA (N80-	rabbit	self-made,	-	1:2000	1:500

S246) (*C. trachomatis*)		RKI, see (Aeberhard et al. 2015)			
IncB *(C. psittaci)*	rabbit	HKI, Jena, (Bocker et al. 2014b)			
LPS	rabbit	Milan	6	-	1:200
MOMP	mouse	(Gurumurthy et al. 2010)	-	-	1:500
Myc-Taq (71D10)	rabbit	Cell Signaling Technology	2278S	1:1000	-
p62	mouse	BD Biosciences	610497	1:1000	-
Pericentrin	rabbit	Abcam	ab4448	-	1:300
p-Ser (16B4)	mouse	Santa Cruz Biotechnology	sc-81514	1:500	-
RPL13a	rabbit	Novus Biologicals	NBP1-92345	1:1000	1:100
RPL13a (C-11)	mouse	Santa Cruz Biotechnology	sc-390131	1:1000	1:200
RPL19	rabbit	Abcam	ab224592	1:1000	1:75
RPL3	rabbit	Novus Biologicals	NBP1-81332	1:2000	-
RPL3	rabbit	Sigma Life Science	HPA003365	1:250	1:100
RPS26	rabbit	Sigma Life Science	HPA043961	1:500	1:50
RPS6	mouse	Santa Cruz Biotechnology	sc-74459	1:2000	1:200
RPS9	rabbit	Thermo Fisher Scientific	PA5-49950	1:1000	1:100
Sam68 (7-1)	mouse	Santa Cruz Biotechnology	sc-1238	1:1000	-
Sam68	mouse	Santa Cruz Biotechnology	sc-1238	-	1:500
SNX1	mouse	BD Transduction Lab.	611482	1:1000	1:100

SNX1	rabbit	Sigma Life Science	HPA047373	1:1000	1:100
SNX2	mouse	BD Transduction Lab.	611308	1:1000	1:100
SNX2	rabbit	Sigma Aldrich	HPA037400	1:1000	1:100
SNX5	rabbit	Abcam	ab180520	1:500	1:100
SNX6 (D5)	mouse	Santa Cruz Biotechnology	sc-365965	1:1000	1:100
VPS35	mouse	Abcam	ab57632	1:1000	1:300
β-Actin	mouse	Sigma Aldrich	A5441	1:4000	-

Table 12. Self-made primary antibodies

Antigen	Species	Source	Catalog No.	Dilution WB	Dilution IF
IncE (*C. trachomatis*)	mouse	BioGenes GmbH	Animal no: 14295	1:1000	1:100
IncE (*C. trachomatis*)	rabbit	BioGenes GmbH	Animal no: 25511	1:1000	1:50

Secondary antibodies

Table 13. Secondary antibodies

Name	Use	Source	Catalog No.	Dilution
Alexa Fluor 488: goat anti mouse IgG	IF	Dianova	115-545-003	1:100
Alexa Fluor 488: goat anti rabbit IgG	IF	Dianova	111-545-144	1:100
Alexa Fluor 647: goat anti mouse IgG	IF	Dianova	115-605-146	1:100
Alexa Fluor 647: goat anti rabbit IgG	IF	Dianova	111-605-144	1:100
Cy3: Goat anti-mouse IgG	IF	Dianova	115-165-146	1:200
Cy3: Goat anti-rabbit IgG	IF	Dianova	111-165-144	1:200
ECL™ anti-mouse IgG, HRP conjugated	WB	GE Healthcare, formerly Amersham Biosciences,	NA931	1:5000

ECL™ anti-rabbit IgG, HRP conjugated	WB	GE Healthcare, formerly Amersham Biosciences,	NA934	1:4000
anti-GFP 10 nm gold colloid for EM	EM	British Biocell	EM.GAR10	1:20

2.1.5 Chemicals

Table 14. Chemicals

Chemical	Manufacturer
3M Empore C18 Disk	3M
Acetic acid	Carl Roth
Acetone	Carl Roth
Acetonitrile	Sigma-Aldrich
Agarose	Carl Roth
Aktivkohle	Carl Roth
Ammonium bicarbonate	Sigma-Aldrich
Ammonium persulfate	Carl Roth
Ampicillin	Sigma-Aldrich
Benzonase Nuclease HC	Novagen
Boric acid	Carl Roth
Bovine Serum Albumin (BSA) Fraction V	Carl Roth
Bromophenol blue	Carl Roth
Calcium chloride	Carl Roth
Coomassie Brillant Blue R 250	Carl Roth
Cycloheximide	Carl Roth
DAPI	Sigma-Aldrich
Dextran, Alexa Fluor 647, 10,000 MW	Molecular Probes
Dipotassium phosphate	Carl Roth
DMSO	Carl Roth
Dnase and RNase-free Sucrose	Carl Roth
DTT	Carl Roth
ECL Reagent	Pierce
EDTA	Carl Roth
EGTA	Carl Roth
Ethanol	Carl Roth
Ethidium bromide	Carl Roth
Formaldehyde 37%	Carl Roth

Formic acid	Pierce
GelRed	VWR
Glutaraldehyde	TAAB Laboratory and Microscopy
Glycerol	Carl Roth
Glycin	Carl Roth
HCl	Carl Roth
HEPES	Sigma-Aldrich
IGEPAL-CA630	Sigma-Aldrich
Iodoacetamide	Sigma-Aldrich
IPTG	Carl Roth
Kanamycin sulfate	Sigma-Aldrich
KCl	Carl Roth
KOH	Carl Roth
Lowicryl HM20 resin	Polysciences
Magnesium chloride	Carl Roth
Methanol	Carl Roth
Milk powder	Carl Roth
Monopotassium phosphate	Carl Roth
Monosodium phosphate	Carl Roth
Mowiol 4-88	Carl Roth
NaCl	Carl Roth
NaOH	Carl Roth
Nuclease free water	Carl Roth
Paraformaldehyde	Carl Roth
Percoll	Sigma-Aldrich
Phosphoric acid	Carl Roth
Poly-D-Lysine	Sigma-Aldrich
Potassium chloride	Carl Roth
Puromycin	Carl Roth
SDS	Carl Roth
Sodium azide	Carl Roth
Sucrose	Carl Roth
TBE Buffer (10x)	Sigma-Aldrich
TEMED	Carl Roth
TFA	Sigma-Aldrich
Trichloracetic acid	Carl Roth
TRIS	Carl Roth
Triton X-100	Carl Roth
Tween® 20	Carl Roth

Uranyl acetate	Merck
Urea	Sigma-Aldrich
Water for LC/MS	Sigma-Aldrich
Xylene cyanol	Carl Roth
β- mercaptoethanol	Carl Roth

2.1.6 Kits and Consumables

Table 15. Kits and consumables

Name	Use	Manufacturer
µ-Dish 35 mm high	Live cell microscopy	ibidi
µ-Dish 35 mm high, Grid-50 Glass Bottom	Live cell microscopy	ibidi
$^{12}C_6{}^{14}N_2$ L-Lysine (=light, K0)	SILAC	SILANTES
$^{12}C_6{}^{14}N_4$L- arginine (= light, R0)	SILAC	SILANTES
$^{13}C_6{}^{15}N_2$ L-Lysine (=heavy, K8)	SILAC	SILANTES
$^{13}C_6{}^{15}N_4$ L- arginine (= heavy, R10)	SILAC	SILANTES
6x DNA Gel Loading Dye	PCR / Agarose gel	Thermo Fisher Scientific
Antarctic phosphatase	Molecular cloning	New England Biolabs
Benzonase	DNA digest	Merck Millipore
Biotin	Cell culture	Sigma-Aldrich
Cell culture flasks/dishes	Cell culture	TPP
Cell scraper	Cell culture	Biochrom
Centrifuge tubes (15 mL, 50 mL)	Cell culture / General use	TPP
cOmplete EDTA free	Protease inhibition	Roche
Dialysed FCS	SILAC	Biochrom
DNase I	DNA digest	New England Biolabs
DNeasy Blood &Tissue Kit	DNA purification	Qiagen
dNTPs	PCR	New England Biolabs
Electroporation cuvette BRIDGE 2 mm	Transformation	Carl Roth
FastDigest restriction enzymes	Molecular cloning	Thermo Fisher Scientific
FastDigest restriction enzymes	Molecular cloning	Thermo Fisher Scientific
GeneRuler 1 kb DNA ladder	PCR / Agarose gel electrophorese	Thermo Fisher Scientific
GeneRuler 100 bp Plus DNA ladder	PCR / Agarose gel electrophorese	Thermo Fisher Scientific
Glass beads 2.2 mm	Cell lysis	Roth

Glass coverslips	Immunofluorescence	Carl Roth
Glutathione	Protein purification	Carl Roth
Glutathione HiCap Matrix	Protein purification	Qiagen
HRP-conjugated streptavidin	Western Blot (1:30 000)	Jackson Laboratories
Immobilon-P PVDF membranes	Western Blot	Millipore
Injekt Solo 5 mL	Syringe	Braun
Interferon γ	Cell culture	Merck Millipore
Invisorb Spin Plasmid Mini Two	Plasmid isolation	STRATEC Molecular GmbH
IPTG	Antigen expression	Carl Roth
KOVA Glasstic Slides 10	Cell counting	Hycor
Lactacystin	Cell culture	Sigma-Aldrich
Lipofectamine2000	Transfection	Invitrogen
Live cell culture dishes	Cell culture and live cell microscopy	Ibidi
LoBind 1.5 and 2 mL tubes	Proteomics	Eppendorf
Lysozyme	Protein purification	Carl Roth
MB Taq DNA Polymerase	Mycoplasma detection	Biochrom
Midori Green	PCR / Agarose gel electrophorese	Biozym Scientific GmbH
Nocodazole	Cell culture	Sigma Life Science
OneStep RT-PCR	RT-PCR	Qiagen
PageRuler Plus Prestained	SDS-PAGE	Thermo Fisher Scientific
PageRuler Plus Prestained Protein Ladder	Western Blot	Thermo Fisher Scientific
PageRuler Unstained Protein Ladder	SDS-PAGE	Thermo Fisher Scientific
Parafilm	Immunofluorescence, general use	Pechiney Plastic Packaging
Pipette tips	General use	Sarstedt
Plasticware cell culture	Cell culture	TPP
Plastic ware other	General use	Sarstedt/ TPP/ BD
Polynucleotide kinase	CRISPR/Cas9-mediated knockout	New England Biolabs
Power SYBR Green RNA-to-Ct	qPCR	Applied Biosystems
Phusion High-Fidelity PCR Master Mix with HF Buffer	PCR	Thermo Fisher Scientific

Primers	PCR / RT-PCR / qPCR	Eurofin MWG
Qiagen Plasmid Midi Kit	Plasmid isolation	Qiagen
Qiagen Plasmid Mini Kit	Plasmid isolation	Qiagen
QuantiTect SYBR Green RT-PCR	qPCR	Qiagen
Reaction tubes (0.2 mL, 1.5 mL, 2.0 mL)	General use	Sarstedt
Restriction Enzymes	Molecular cloning	New England Biolabs
RNAeasy Kit	RNA extraction	Qiagen
RNAiFect	Transfection	Qiagen
Roti®-Quant Bradford Protein Assay	Protein quantification	Carl Roth
Rotiphorese® Gel 30 (37,5:1)	SDS-PAGE	Carl Roth
Sapphire disc	Electron microscopy	Engineering Office M. Wohlwend GmbH
Sequencing grade modified trypsin	Proteomics	Promega
Serological pipettes (2 mL, 5 mL, 10 mL, 20 mL)	Cell culture	neoLab
Standard Microscopy Slide	Microscopy	Carl Roth
Sterican 23G	Needle	Braun
Sterican 26G	Needle	Braun
Steritop-GP Filter Unit 250	Sterile filtration	Millipore
Streptavidin Agarose beads	Pulldown	PierceTM Thermo Fisher Scientific
Streptavidin-Alexa Fluor®488 Conjugate	Immunofluorescence (1:3000)	Thermo Fisher Scientific
T4 DNA ligase	Molecular cloning	New England Biolabs
Universal indicator paper	pH measurement	Carl Roth
VenorGeM	Mycoplasma detection	Biochrom
Wizard SV	Molecular cloning	Promega
X-ray film	Western Blot	Amersham

2.1.7 Equipment

Work was performed in standard modernly equipped laboratories.

Table 16. Equipment

Name	Type	Manufacturer
Acclaim™ PepMap™ column	LC column	Thermo Fisher Scientific
Agfa Citrix 60 developer	X-ray developer	Agfa
Allegra X-15 R	Benchtop centrifuge	Beckman Coulter
AxioCam HRc	Microscopy	ZEISS
Branson Sonifier 450	Sonicator	Branson
Butterfly heater	nano-LC systems heater	Phoenix S&T
CB 150	Incubator	Binder
Centrifuge 5417 R	Microfuge	Eppendorf
Digital Camera	Microscopy	Realtime Imaging
Dynamag-2	Magnetic particle concentrator	Invitrogen
EASY nLC II	nano HPLC	Proxeon
EASY-nanoLC 1200	nano-LC instrument	Thermo Fisher Scientific
Ecotron	Incubator	Infors HT
Electrospray with a stainless steel emitter	Electrospray emitter	Proxeon, Odense, Denmark
FlexCycler	PCR thermocycler	analytikjena
Gene Pulser Xcell™ Electroporation Systems	Electroporator	Bio-Rad
HL-2000 HybriLinker	Hybridisation oven	UVP Laboratory Products
HPF compact 01	High-pressure freezing machine for EM	Engineering Office M. Wohlwend
HS2020	Safety cabinet	Thermo Fisher Scientific
Infinite 200 Pro	Microplate reader	Tecan
LTQ Orbitrap Discovery	Mass spectrometer	Thermo Fisher Scientific
Mini-Protean Tetra	Electrophoresis cell	BioRad
Mr Frosty	Freezing container	Nalgene
NanoDrop ND-1000	Spectrophotometer	NanoDrop
Optima XPN-1000	Ultracentrifuge	Beckman Coulter
Orion 2 Star	pH meter	Thermo Fisher Scientific
PowerPac HC	Power Supply	BioRad
Q Exactive™ Plus	Mass spectrometer	Thermo Fisher Scientific
REAX	Overhead shaker	Heidolph
RM 50	Rotating mixer	Assistent

S-2002	Scale	Denver Instrument
Scanjet G4050	Flatbed scanner	Hewlett Packard
Severin 700 & Grill	Microwave oven	Severin
Sorvall® RC-6™ Plus	High speed centrifuge	Beckman Coulter
SpeedVac	Centrifugal evaporator	Eppendorf
Standard Power Pack P25	Power Supply	Biometra
Stratagene Mx3000P	qPCR thermocycler	Agilent Technologies
SW 40 Ti	Swinging-Bucket Rotor	Beckman Coulter
Thermomixer compact	Thermomixer	Eppendorf
Thermotron	Incubator	Infors HT
Trans-Blot SD	Semi-dry transfer cell	Biorad
Transmission electron microscope	electron microscope	Tecnai Spirit, ThermoFisher
Ultra-Clear Tube 344060	Ultracentrifuge tubes	Beckman Coulter
Vibramax 100	Shaker	Heidolph
Vibrofix VF1 Electronic	Vortex mixer	IKA
Vortex mixer SA8	Vortex mixer	Stuart
Water bath	Water bath (Cell culture / general use)	Gesellschaft für Labortechnik mbH / P-D Industriegesellschaft mbH Prüfgerätewerk Dresden

Microscopes

Table 17. Microscopes

Name	Configuration
ZEISS LSM780	Plan-Apochromat 100x/1.40 Oil Ph3 M27
	Plan-Apochromat 63x/1.40 Oil DIC M27
ZEISS Axio Observer Z1	LD Plan-Neofluar 40x/0.6 Corr Ph1 Ph2- M27
ZEISS Axiovert 40 CLF	LD Plan-Neofluar 40x/0.6 Corr Ph2 M27
ZEISS Axiovert 200	Plan-Neofluar 63x/1.25 oil Iris 0.7 1.25 ∞/0.17 DIC

2.1.8 Software

Table 18. Software

Name	Use	Company
AriaMx 1.5	qPCR	Agilent Technologies
EndNote X9.2	Literature management	Thomson Reuters
Excel 2016	Data processing	Microsoft
Geneious Version 7.1.4	Data processing	Biomatters
Graph Pad Prism 7.04 and 8.2	Data processing	Graph Pad Software
Illustrator CS6	Image processing	Adobe®
ImageJ Version 1.52a	Data processing	US National Institute of Health, Bethesda
MaxQuant Version 1.3.0.5	Mass spectrometry	ZBS6, RKI
Perseus Version 1.5.0.31	Bioinformatics	ZBS6, RKI
Photoshop CS6	Image processing	Adobe®
Realtime Capture	Microscopy	Realtime Imaging, Michael Schmauder
Skyline Version 4.0	PRM analysis	(Zauber, Kirchner, and Selbach 2018)
Word 2016	Word processing	Microsoft
XCalibur	Mass spectrometry	Thermo
ZEN 2012, black edition 64-bit, Version 8.0	Microscopy	ZEISS

2.2 Methods

2.2.1 Cell culture

HeLa cells were cultured in growth medium (RPMI) at 37°C in a humidified incubator with 5% CO_2 and regularly passaged for up to ten passages maximum. For passaging, growth medium was aspirated and cells were washed once with PBS. Addition of Trypsin-EDTA allowed cells to detach at 37°C for about 5 min. Addition of an appropriate volume of growth medium stopped detachment of cells which were then distributed to new flasks (usually 75 and 150 cm^2), plates (6-, 12-, 24- or 96-well plates) or live cell culture dishes to adhere. Cell culture was generally performed without antibiotics and contaminations of *Mycoplasma* were routinely excluded via PCR (see section 2.2.4).

DNA transfection of adherent cells

Prior to transfection of HeLa cells with plasmid DNA encoding genes of interest, cells were grown in wells of 6- or 12-well plates to a confluence of 70-80%. Two reaction mixes were prepared separately, one containing 0.5 to 1 µg of plasmid DNA in 50 or 100 µL OptiMEM depending on well size, one containing 1 or 2 µL of Lipofectamine2000 in 50 or 100 µL OptiMEM, respectively followed by separate incubation of 5 min at RT. Both reaction mixes were pooled, gently mixed by flipping the tube and transfection mix incubated for 20 min at RT to allow formation of liposomes. Meanwhile, cells were washed with PBS and incubated in 400 µL or 800 µL fresh media depending on well size. Cells were transfected with liposome complexes containing plasmid DNA by dropwise addition to cells. Cells incubated in transfection mix at least 6 h or overnight and were washed followed by culture of cells in standard growth volume in growth medium.

DNA transfection of cells in suspension

Cells were passaged one day before transfection and splitted appropriately to a confluence of 70%. Prior to transfection, cells were passaged as described in 2.2.1 and pelletised by centrifugation at 300 x *g* for 5 min. Cells were resuspended in appropriate volume of growth medium, mixed 1:1 with transfection mix (see *DNA transfection of adherent cells*) and filled up to half of standard volume. Cells adhered for at least 6 h or overnight. Cells were washed followed by culture of cells in standard growth volume in growth medium.

siRNA (small interfering RNA)-mediated knockdown

Specific knockdown (depletion) of target host cell proteins was mediated by target-specific small interfering RNAs. Cells were grown in 12 well plates to a confluence of 70% and transfected with 1 µg siRNA (equally to 80 pmol) per single knockdown and cells in a well of a

12-well plate. For preparation of the reaction mix, siRNA was added to 92 µL Qiagen RNAi transfection buffer, followed by addition of 6 µL RNAi Fect. Reaction mix incubated for 15 min at RT to allow formation of liposomes. Meanwhile, cells were washed with PBS and incubated in 600 µL fresh medium. Then, cells were transfected with siRNA by dropwise addition to cells followed by incubation of cells in transfection mix overnight. 24 h post transfection, cells were passaged and prepared for follow up assays. Efficient knockdown was assessed by Western Blot analysis (see section 2.2.5) and qPCR (see section 2.2.4).

2.2.2 Infection with *Chlamydia*

In this thesis, the human pathogen *C. trachomatis* was mainly employed as infection model unless indicated otherwise.

All infections were performed in DMEM at 35°C in a humidified incubator with 5% CO_2.Cells were grown to a confluence of 80% and washed once with infection medium. For inoculum preparation, bacterial stock suspension of EBs was diluted to desired multiplicity of infection (MOI) (determination of bacterial titer) in infection medium. For infections with *C. trachomatis* serovar D and *C. psittaci* isolate 02DC15, the inoculum (half of the standard culture volume) was adsorbed through pre-incubation at 35°C for 30 min followed by centrifugation at 600 x *g* for 30 min at RT and incubation of 1 h at 35°C and 5% CO_2. Centrifugation in culture flask was performed at 800 x *g* to increase infection rate. For infections with *C. trachomatis* L2, the inoculum (half of the standard culture volume) was adsorbed through incubation at 35°C for 2 h. After incubation for 2 h, cells were washed with DMEM and *Chlamydia* spp. were propagated in standard culture volume of DMEM at 35°C and in a humidified incubator 5% CO_2.

Preparation of Chlamydia spp. stock suspension

To prepare stock solutions of chlamydial species, cells were grown in 150 cm^2 culture flasks to a confluence of 70-80% and infected with an MOI 2 according to standard infection protocol (see above). At 48 h p.i. or 72 h p.i., depending on the chlamydial species and *C. trachomatis* serovar (one complete developmental cycle), cells were harvested with a cell scraper in a 50 mL centrifugation tube containing glass beads. Bacteria were mechanically released by vortexing for 3 min and infectious lysate was transferred to a new 50 mL centrifugation tube which was centrifuged at 600 x *g* for 5 min to remove cell debris. Cleared lysates were used as inoculum for a second round of infection of fresh naïve cells. At 48 h p.i. or 72 h p.i. cells were harvested as described before at 4°C. Cleared supernatant was transferred to sterile Sorvall® centrifuge tubes and EBs were enriched by centrifugation at 42858 x *g* for 1 h. Bacterial pellet was resuspended in 4xSP buffer at 4°C and suspension was transferred to a well of a 6-well plate in which the suspension was homogenised by passing through 23G and 26G syringes several times at 4°C. Aliquots of bacterial stock suspension were stored at -80°C.

Determination of bacterial titer

HeLa cells were grown to a confluence of 80-90% in wells of a 24-well plate containing glass coverslips. Cells were infected with serial dilutions of *Chlamydia* and fixed 24 h p.i. with 2% PFA for 30 min at RT. Subsequently, cells were immunostained for bacterial heat shock protein 60 (Hsp60) (see Immunofluorescence staining) and evolved inclusions were counted in at least ten fields of view per dilution using a ZEISS Axiovert 40 CFL microscope with 40x magnification. The following calculation was used to determine the number of inclusion forming units (IFU) per millilitre:

$$\text{IFU/mL} = \bar{x} \text{ inclusions per field of view} \times 454 \times \text{dilution factor} \times 4$$

$\bar{x}$ is the average of inclusions of 10 microscopic fields of view. The calculation includes the factor 454 to correct for the number of HeLa cells visible in a microscopic section at 40 x magnification. Factor 4 corrects for the infectious volume of 250 µL.As the unit IFU describes the absolute number of bacteria per millilitre, the unit MOI describes the ratio of bacteria per cell. Accordingly, an MOI of 2 corresponds to 2 IFUs per cell.

Infectious progeny formation assay

The infectious progeny formation assay (also known as reinfection assay) was used to assess alterations in infectious progeny formation under certain treatment conditions since chemical treatment, knockdown or knockout of host genes may affect infectious chlamydial progeny formation. Therefore, cells were infected with equal infectious doses of *C. trachomatis* D and L2 at an indicated MOI for 72 h p.i. and 48 h p.i., respectively (one complete developmental cycle). Cells were mechanically detached with a cell scraper and lysed by vortexing for 3 min with glass beads. Fresh naïve cells were infected with serial dilutions of previously infected cells and IFU was determined as described above (determination of bacterial titer).

2.2.3 Microscopy

Immunofluorescence staining

Cells were cultured in 12- or 24-well cell culture plates on glass coverslips. At indicated time points, cells were washed with PBS and fixed with 2% PFA for 30 min at RT or with ice-cold MeOH for 20 min at -20°C. Fixative agents were aspirated and cells were washed three times with PBS. Fixation with 2% PFA required blocking and permeabilisation of cells in IF permeabilisation buffer for 25 min at RT. Fixation with ice-cold MeOH required blocking of cells in IF blocking buffer for 25 min at RT. After blocking and permeabilisation, cells incubated with primary antibodies diluted in IF blocking buffer. Therefore, coverslips were placed face down on top followed by incubation in a wet chamber at for 1 h at RT. Cells were washed three times with PBS for 10 min each and incubated with fluorophore-coupled secondary antibodies and

DAPI both diluted in IF blocking buffer in the dark for 1 h at RT in a wet chamber. Coverslips were washed three times with PBS for 10 min each, finally dipped into ddH_2O to remove residual PBS and transferred onto glass slides prepared with Mowiol as mounting medium.

Phase contrast and epifluorescence microscopy

Standard phase-contrast microscopy for constant cell culture quality control was performed using a ZEISS Axiovert 40 CLF microscope equipped with Realtime Imaging software. A combination of phase contrast and epifluorescence microscopy was used to determine the number of infectious progeny (see section 2.2.2) or measurement of bacterial inclusion size.

Laser scanning confocal microscopy

Laser scanning confocal microscopy was applied on fixed and immunostained cell samples using a ZEISS LSM780 confocal laser scanning microscope (cLSM), Plan-Apochromat 100x/1.40 Oil Ph3 M27 and Plan-Apochromat 63x/1.40 Oil DIC M27 objectives equipped with ZEISS ZEN software and using optimised optical settings. Where necessary, images were processed and corrected (brightness/colour/colour intensity/contrast) with ZEN 2012 black edition software. Figures were assembled in Adobe® Illustrator CS6 and post-processed with Adobe® Photoshop CS6.

Correlative light and electron microscopy (cLEM)

For correlative light and electron microscopy, two approaches of fixation were applied.
For cLEM including chemical fixation, HeLa cells were cultured, infected with *C. trachomatis*, transiently transfected with fusion protein of interest in live cell culture dishes and microscoped with a ZEISS LSM780 LSCM in a pre-heated live-cell chamber (35-37°C, 5% CO_2) using optimised optical settings. For chemical fixation and EM analysis using a TEM, see Madela et al. 2014 (Madela et al. 2014).
For cLEM including high-pressure freezing (HPF, cryofixation), HeLa cells were cultured on sapphire discs (50 µm thick; 3 mm diameter) coated with a carbon pattern to localise cells of interest and with either ECM or collagen to improve cell adherence. After infection with *C. trachomatis*, cells were transiently transfected with fusion protein of interest. Cells were microscoped with a ZEISS LSM780 LSCM in a pre-heated live cell chamber (35 - 37°C, 5% CO_2) using optimised optical settings and cells of interest were localised. Subsequently, sapphire discs were high-pressure frozen with an HPF compact 01. Frozen samples were freeze-substituted in 0.1% glutaraldehyde, 0.05% uranyl acetate in acetone and embedded in Lowicryl HM20 resin at -35°C. Ultrathin sections (70-80 nm) were labelled with anti-GFP antibodies and a secondary antibody coupled to gold colloid (10 nm). Sections were stained with lead citrate and analysed with TEM.

2.2.4 Standard molecular-biological methods

Isolation of nucleic acids

DNA was cleaned up or gel-purified using the Wizard SV Kit according to manufacturer's instructions. Isolation of DNA from cells was performed by using DNeasy Blood &Tissue Kit according to manufacturer's instructions.
RNA was isolated using RNAeasy Kit according to manufacturer's instructions under RNase free conditions.

Amplification Polymerase Chain reaction

DNA fragments were amplified by polymerase chain reaction (PCR). For all DNA applications dedicated to cloning, polymerase PCR Master Mix, specific primers and template DNA were used in one reaction (Table 19).

Table 19. Standard reaction mixture for PCR

Reagent	50 µL reaction	Final concentration
2x Phusion Master Mix	25 µL	1x
10 µM Forward Primer	2,5 µL	0,5 µM
10 µM Reverse Primer	2,5 µL	0,5 µM
Template DNA	vol. depending on template concentration	< 250 ng
Nuclease-free water	ad 50 µL	-

Polymerase chain reactions were performed with a standard cycling protocol (Table 20) in a thermocycler, taking melt temperature of the primer and product length into account:

Table 20. Standard cycling protocol for PCR

Reaction step	Time	Temperature	Cycle
Initial denaturation	5 min	95°C	1x
Denaturation	10 s	95°C	35x
Annealing	30 s	60-65°C	
Elongation	30 s/kb	72°C	
Final elongation	10 min	72°C	1x

If needed, PCR conditions were optimised by changing annealing temperature, number of cycles and elongation times.
PCR products were separated by agarose gel electrophoresis to verify amplicon quality and obtained products. Therefore, PCR products mixed with loading dye were loaded onto agarose

gel supplemented with Midori Green and gel was run at 100 V for about 1.5 h and visualised under UV light.

Cloning by restriction enzyme digest

Sequences for cloning were retrieved from UniProt (https://www.uniprot.org), RNA was extracted from HeLa cells and transcribed to cDNA followed by cloning into backbone vector.
Cloning was performed by restriction digest and ligation. Relevant PCR amplicons were purified directly from solution or gel-purified using the Wizard SV Gel and PCR Clean-Up System according to manufacturer's instructions. DNA was eluted in 20 µL nuclease-free ddH_2O.
Standard cloning workflow included restriction enzyme-mediated digest of PCR product and backbone plasmid, ligation of insert and vector and transformation of ligation product. In detail, 200 ng of purified PCR product and 1 µg of pure destination vector plasmid with appropriate restriction enzymes and buffers were incubated at 37°C for 1 h or for 15 min in case of FastDigest restriction enzymes. After heat-inactivation of restriction enzymes, the digested backbone vector was dephosphorylated by Antarctic phosphatase at 37°C for 1 h followed by heat-inactivation at 65°C for 5 min. Digested DNA was purified and the ligation reaction was prepared (Table 21). For this, the amount of insert to be used was calculated using the following formula whereby 'factor' stands for an excess factor of insert (usually within three- to fivefold):

$$\text{amount of insert [ng]} = \frac{\text{size of insert [bp]} \times \text{factor} \times \text{amount of vector [ng]}}{\text{size of vector [bp]}}$$

Table 21. Ligation reaction

Reagent	Ligation	Blank
10x T4 Ligase buffer	2 µL	2 µL
Vector	75 ng	75 ng
Insert	calculated	-
ddH_2O	ad 20 µL	ad 20 µL
T4 Ligase	1 µL	1 µL

Ligation reaction incubated at 37°C for 3 h or at 16°C overnight. Then, the enzyme was heat-inactivated at 70°C for 5 min.

Colony PCR and control digest

Colony PCR was performed with the same programme used for amplification as stated above. Instead of DNA, a colony of transformed bacteria was used as template by dipping a pipette tip into the colony followed by dipping the same tip into the PCR reaction, onto a fresh antibiotic-containing LB agar plate as backup plate and finally ejecting the tip into liquid LB-medium supplemented with appropriate antibiotic (for plasmid preparation and control digest). *E. coli* strains were grown overnight for plasmid DNA preparation.

Transformation of constructs into competent bacteria

Purified ligation product was transformed into BioBlue chemically competent *E. coli* with 2-5 µL of the reaction mixture according to manufacturer's protocol.
Clones were selected on LB agar plates supplemented with appropriate antibiotics depending on the resistance gene in backbone vector. The insertion of DNA was verified by control restriction digest and colony PCR. DNA sequences of positively tested clones were verified by Sanger sequencing.

Plasmid DNA preparation

DNA extraction of plasmid-DNA from 5 mL or 50 mL liquid LB cultures was performed with Invisorb Spin Plasmid Mini Two (Miniprep) or Plasmid Midi Kit (Midiprep), respectively according to the manufacturer protocols. DNA was eluted in 50 µL ddH_2O. DNA quality and concentration were verified by UV spectrophotometry using a NanoDrop-1000 taking the absorption of DNA at 260 nm (1 $A_{260\ nm}$ = 50 µg/mL) and the absorption of tryptophan and tyrosine at 280 nm into account. A ratio of $A_{260\ nm}/A_{280\ nm}$ above 1.8 was considered to be sufficiently pure DNA.
0.5 µg DNA was digested according to the protocol described above and analysed on an agarose gel to visualise correct digest of ligation product. A clone's DNA determined as positive was sent for sequencing (Sanger sequencing).

Quick-change mutagenesis

The quick-change mutagenesis method introduces DNA modifications by specific oligonucleotides harbouring desired mutations (Zheng, Baumann, and Reymond 2004). Primer pairs containing mutations were designed with the tool PrimerX (http://www.bioinformatics.org/primerx/index.htm) unless stated otherwise and are shown in Table 22. The reaction mixture was prepared as described previously (Table 19) using 50 ng of template DNA to be mutated. PCR cycling parameters for mutagenesis are shown in Table 23.

Table 22. Primers for quick-change mutagenesis

Mutation	Sequence	Direction	Source
Y132D	CAAGAACTGGAAGCTGAGGATCTCGC TGTCTTTAAGA	for	(Elwell et al. 2017)
	TCTTAAAGACAGCGAGATCCTCAGCTT CCAGTTCTTG	rev	(Elwell et al. 2017)
Y132D	CAAGAACTGGAAGCTGAGGATCTCGC TGTCGATAAGA	for	
	TCTTATCGACAGCGAGATCCTCAGCTTC AGTTCTTG	rev	
F136D	CTGAGTATCTCGCTGTGGATAAGAAG ACTGTGTCC	for	
	GGACACAGTCTTCTTATCCACAGCGA GATACTCAG	rev	
F136D	CTGAGTATCTCGCTGTGGATAAGAAG ACTGTGTCCTC	for	
	GAGGACACAGTCTTCTTATCCACAGC GAGATACTCAG	rev	

Primers for the generation of the mutation Y132D in eGFP-SNX5 PX domain were retrieved from (Elwell et al. 2017).

Table 23. Cycling protocol for mutagenesis PCR

Reaction step	Time	Temperature	Cycle
Initial denaturation	5 min	95°C	1x
Denaturation	30 s	95°C	16x
Annealing	30 s	55°C	
Elongation	1 min/kb + 1min	68°C	
Final elongation	10 min	68°C	1x

After visualisation of correct PCR amplicon and purification of the PCR product, the methylation-sensitive restriction enzyme DpnI enzyme was added according to the reaction mixture (Table 24) to digest parental DNA at 37°C for 1 h.

Table 24. DpnI digest reaction for parental DNA digest

Reagent	Volume
10x Tango buffer	1 µL
DNA	500 ng
DpnI	1 µL
dd H_2O	ad 10 µL

The enzyme DpnI was heat-inactivated for 20 min at 80°C followed by purification of mutated DNA and transformation into chemically competent *E. coli* with 2-5 µL of the reaction mixture according to manufacturer's protocol (see *Transformation of constructs into competent bacteria*). Resulting mutants were verified by Sanger sequencing and cultured for plasmid DNA preparation.

Sanger sequencing

All final constructs were verified by Sanger sequencing using Big Dye according to manufacturer's instructions at the in-house sequencing facility at Robert Koch Institute, Berlin.

Reverse-transcriptase-PCR (RT-PCR)

Isolated DNA from HeLa cells was reversely transcribed and amplified with specific primers using the OneStep RT-PCR Kit according to manufacturer's instructions. See the following PCR programme:

Table 25. Reverse-transcriptase-PCR cycling protocol

Step	Time	Temperature	Cycle
Reverse transcription	30 min	50°C	1x
Initial PCR activation step	15 min	95°C	1x
Denaturation	45 s	94°C	33x
Annealing	45 s	60°C	33x
Extension	2 min	72°C	33x
Final extension	10 min	72°C	1x

For verification, PCR products were mixed with loading dye and loaded onto an agarose gel supplemented with Midori Green. Gel run at 100 V for about 1.5 h and was visualised under UV light.If multiple bands appeared, the band at correct size was cut out (on a UV table) and purified using Wizard®SV Gel and PCR Clean-Up System. In case of one band at the correct size, the PCR product was directly cleaned-up using Wizard®SV Gel and PCR Clean-Up System. DNA concentration was monitored using a NanoDrop-1000.

Quantitative real-time PCR (qPCR)

Relative amounts of chlamydial DNA were analysed by quantitative real-time PCR using target-specific primers. Reactions were prepared using the QuantiTect SYBR Green RT-PCR kit according to manufacturer's instructions. Dilutions of heat-inactivated cell culture samples served as template DNA. All reactions were run on a Stratagene Mx3000P thermocycler.

2.2.5 Standard protein methods

Prior to cell lysis, cells were washed with PBS. Cells were then lysed in various lysis buffers depending on the assay.For SDS-PAGE, cells were grown in cell culture dishes and washed with PBS. For whole-cell extracts, 2x Laemmli buffer pre-heated to 95°C was directly added to cells. Lysate was collected by scraping with a kinked pipette tip and then transferred to tubes. Samples were boiled at 95°C for 10 min to denaturate proteins followed by pelletising insoluble material by centrifugation at 20 000 x *g* for 5 min. Samples were stored at -20°C until further analysis.

SDS-PAGE and immunoblot analysis (Western blot)

One sample per lane was loaded onto 10% to 15% denaturing separating gels depending on the molecular weight of proteins to be analysed. Protein separation by electrophoresis was performed according to standard procedures (http://www.molecularcloning.com/index.php) and Laemmli et al. 1970 (Laemmli 1970). For Western Blot (WB), proteins separated by SDS-PAGE were transferred to an activated PVDF-membrane by standard wet blot procedure (200 mA for 2 h). Membranes were blocked at RT in TBST-M for at least 1 h. Membranes incubated with primary antibody diluted in TBST-M under continuous agitation at 4°C overnight unless stated otherwise. Membranes were washed three times with TBS-T for 10 min each followed by incubation with HRP-coupled secondary antibody diluted in TBST-M at RT for 1 h. After washing three times with TBS-T for 10 min each, ECL solution using the ECL Plus kit was added and the resulting chemiluminescent signal was detected by exposure to X-ray films. Films were developed in an Agfa Citrix 60 developer and scanned for digitalisation.

Protein quantification by Bradford Assay

Protein concentrations of cell lysates were determined colourimetrically by Bradford assay according to manufacturer's protocol. Absorption was measured at 595 nm using a Tecan Infinite 200 device. Protein concentrations were calculated using a standard curve with diluted albumin.

TCA precipitation

TCA was added to the protein solution to a final concentration of 10% TCA. Precipitation was performed by tumbling end-over-end for 1.5 h at 4°C. Proteins were pelletised by centrifugation at 20 000 x *g* for 45 min at 4°C. Pellet was washed with ice-cold acetone, thoroughly vortexed and centrifuged again at 20 000 x *g* for 45 min at 4°C. Washing was repeated two times. Pellet was dried for 30 min at RT.
For WB analysis, protein pellet was resuspended in 1x Laemmli buffer. In case of residual acid, protein solution was buffered with 1/10 vol 1 M Tris/HCl pH 8.5 to fully resuspend proteins. For MS analysis, protein pellet was resuspended in 8 M urea buffer.

Protein expression and purification of chlamydial protein IncE

Proteins expressing glutathione S-transferase (GST) tagged fusion proteins were purified by affinity purification. For overexpression of the fusion protein GST-IncE, *E. coli* RIL strain was transformed with pGEX3x-IncE. For cloning see 2.2.4.
After an overnight culture on LB agar plates supplemented with the appropriate antibiotic, a 1 L culture of *E. coli* was grown overnight to get a high yield of expressed protein. At an OD_{600nm} = 0.4, a cold shock was performed for 2 min at 15°C in a water bath to allow a proportion of protein to be soluble. Protein expression was induced by addition of 1 mM IPTG to bacterial culture which grew at 26°C overnight while shaking in an orbital shaker at 200 rpm. Protein expression was verified by SDS-PAGE and staining of gel with Coomassie solution.
Bacterial cells after overnight growth were pelletised by centrifugation at 4000 x *g* for 10 min at 4°C and stored at -20°C for at least 20 min. Bacterial cells were lysed in in PBS supplemented with cOmplete EDTA free protease inhibitor cocktail, 1 mM EDTA, 0.1% Triton X-100 and 1 mg/mL lysozyme for 45 min at 4°C while gently mixing every 15 min. During lysis, 500 U of Benzonase and $MgCl_2$ to a final concentration of 2 mM were added to the suspension. Three freeze-thaw cycles were performed using a 37°C water bath and N_2 (liquid) to enhance lysis efficiency. Then, lysate was cleared by centrifugation at 15 000 x *g* for 15 min at 4°C to pelletise cellular debris. Soluble GST tagged protein was purified using Glutathione HiCap Matrix according to manufacturer's instructions. Protein was eluted with PBS supplemented with 1 mM EDTA (PBS-EW) and 10 mM Glutathione, pH 8-9. Protein yield was quantified by Bradford assay. The final eluate was used as antigen for immunisation.

Antibody production and Affinity purification

Production of polyclonal mouse and rabbit anti-IncE antibodies was carried out by immunisation of mice and rabbits with the C-terminal cytoplasmic fragment of *C. trachomatis* D IncE (aa 88-132) fused to GST (GST-IncE). Immunisation of animals and animal keeping were handled by BioGenes GmbH, Berlin, Germany, order number 43640. The antigen (GST-IncE) was

expressed in *E. coli* strain RIL using pGEX 3x N-terminal GST expression vector as described above.

GST-IncE and GST-only (purified from empty pGEX-3X vector) were overexpressed and purified as described above. Qiagen Glutathione HiCap Matrix beads were equilibrated in PBS-EW. Both separately, GST-IncE and GST-only were coupled to Qiagen Glutathione HiCap Matrix beads by incubation at 4°C overnight and crosslinked using BS3 (Suberic acid-bis-(3-sulfo-N-hydroxysuccinimide ester)) at a molar protein to crosslinker ratio of 1:45 by incubation at 4°C overnight after bead washing. Crosslinking reaction was saturated with TBS and non-covalently-bound proteins were removed by washing with 0.2 M glycine pH 2.0. Coupled beads were washed two times with TBS for 10 min each in an end-to-end shaker.

For affinity purification of antibodies from antiserum, serum was first heat-inactivated at 56°C for 30 min and then incubated with beads coupled to GST-only to deplete anti-GST antibodies for 8 h at 4°C in an end-to-end shaker. Depleted anti-GST serum incubated with antigen-coupled beads at 4°C overnight. Beads were washed with TBS before and after washing with 0.1 M borate, 0.5 M NaCl, pH 8.0 and finally eluted with 0.2 M glycine pH 2.0 into 2 M Tris to neutralise the pH. Protein yield was quantified using a NanoDrop-1000. Affinity-purified antibodies dialysed against PBS using a QuixSep Micro Dialyzer were diluted 1:1 in glycerol, 0.06% sodium azide for storage at -20°C.

2.2.6 Mass spectrometry (MS) and related methods

Labelling of cells by Stable isotope labelling by amino acids in cell culture

Stable isotope labelling by amino acids in cell culture (SILAC) is a method used for relative quantification of proteins by mass spectrometry via labelled isotopes (Ong et al., 2002). A mass spectrometer recognises mass differences between heavy-labelled and light-labelled (unlabelled) peptides which allows for relative quantification by comparing their respective signal intensities. Consequently, different physiological states in a biological system can be quantified.

HeLa cells were labelled by culturing for 5 passages in high glucose DMEM containing either isotope heavy-labelled ($^{13}C_6{}^{15}N_4$ L-arginine, $^{13}C_6{}^{15}N_2$ L-lysine) or light-labelled ($^{12}C_6{}^{14}N_4$ L-arginine, $^{12}C_6{}^{14}N_2$ L-lysine) L-lysine and L-arginine supplemented with 1 mM sodium pyruvate and 10% dialysed FCS (dFCS). All SILAC media was sterile filtered before use. To minimise metabolic proline to arginine conversion due to an oversupply of arginine in the growth medium (Blagoev and Mann 2006), the concentration of L-arginine and L-lysine has been titrated (Aeberhard et al. 2015).

Cells were expanded for stock preparation and stocked in dFCS supplemented with 10% DMSO using Mr Frosty freezing containers according to manufacturer's instructions. Samples of these cells were taken, tryptic peptides prepared by in-solution digestion (see below) and

desalted by STAGE (stop and go extraction) Tips before analysis with nLC-MS/MS to control for complete incorporation of isotope labelled amino acids (Rappsilber, Mann, and Ishihama 2007). SILAC incorporation rate was assessed by nLC-MS/MS after tryptic digest of SILAC cells, peptide purification (desalinisation) using StageTips. Tryptic peptides were analysed by nLC-MS/MS at the Proteomics and Spectroscopy facility at Robert Koch Institute, Berlin (Aeberhard et al. 2015).

BioID assay

BioID proximity-dependent biotinylation assay (in short BioID assay) was performed in SILAC cells where HeLa WT cells were heavy-labelled and SNX5 KO cells were light-labelled. Both, WT and SNX5 KO labelled cells were transfected in suspension with either myc-BirA*-SNX1 vector or myc-BirA* vector (control vector) and infected with *C. trachomatis* serovar D with an MOI 2. At 9 h p.i., biotinylation as a crucial step of BioID assay was induced by addition of 50 µM biotin. At 30 h p.i. cells were washed with PBS and lysed in RIPA lysis buffer for 30 min on ice while vortexing every 10 min. Cellular debris was pelletised at 20 000 x *g* for 15 min at 4°C. Protein amount was quantified by Bradford assay and cleared lysates of heavy-labelled cells and light-labelled cells, for myc-BirA*-SNX1 expressing cells or myc-BirA* control expressing cells in parallel, were pooled 1:1. Biotinylated proteins were purified by streptavidin pulldown.

Streptavidin pulldown

Binding of biotin to streptavidin is a strong non-covalent interaction. Therefore, it is used to purify biotinylated molecules such as proteins by their binding to streptavidin which has been covalently coupled to agarose beads.

Prior to streptavidin pulldown, cells were lysed in the appropriate lysis buffer whereof 10% were kept as whole cell lysate for subsequent WB analysis. Equilibrated streptavidin-agarose beads in lysis buffer that was used in the respective assay were loaded with remaining lysate considering binding capacity of streptavidin-agarose beads. Pulldown was performed by tumbling end-over-end for 2 h at 4°C. Beads were washed five times in wash buffer by centrifugation at 2000 x *g* for 2 min whereby the last two washing steps were performed with detergent-free wash buffer.

For WB analysis, bound proteins were eluted with 2x Laemmli buffer in a 1:1 ratio for 10 min at 95°C with gentle shaking. Beads were pelletised by centrifugation at 2000 x *g* for 2 min. Elution was repeated and supernatants pooled. Prior to nLC-MS/MS analysis, proteins were digested on-bead after washing of bound proteins to streptavidin-agarose beads.

On-bead tryptic digest

Following pulldown of biotinylated proteins by binding to streptavidin-agarose beads, affinity-purified proteins were digested on-bead with trypsin. Briefly, beads were washed stringently with detergent-free buffer (bead-wash buffer) as SDS containing RIPA buffer inhibits tryptic activity. Bound proteins were first digested in elution buffer I for 1.5 h at 37°C during gentle shaking, followed by a second digestion step in elution buffer II (equal volume as elution buffer I) overnight at 37°C during gentle shaking. Afterwards, beads were pelletised by centrifugation at 2000 x *g* for 2 min. Supernatant containing digested peptides were stored at -20°C until nLC-MS/MS analysis of peptides using intensity based absolute quantification (iBAQ). iBAQ is a label-free quantification method based on peak intensity assuming that most of the proteins contributing to the total protein pool are identified and quantified (Arike et al. 2012; Cox et al. 2014).

Sample preparation for nLC-MS/MS (cell lysates, TCA pellets)

Cell lysates

Prior to cell lysis, cells were washed with PBS, then mechanically detached with cell scrapers and centrifuged at 300 x *g* for 5 min at 4°C. Cells were lysed in urea buffer followed by five freeze-thaw cycles in liquid N_2 (freeze in liquid N_2, thaw at 37°C in a water bath, each cycle for 3 min) and disruption of cells with sonicator (3x 1 min, 50% cycles, 50-60% power).

TCA pellets

Precipitated proteins by TCA were resuspended in 8 M urea buffer for 30 min at 37°C.

In-solution digestion

Protein amount was quantified by Bradford assay. For in-solution digestion, DTT was added to 50 µg of lysed cells to a final concentration of 3 mM and incubated for 45 min at 37°C to reduce disulfide bonds. Free thiol groups on cysteines were alkylated by addition of IAA at a final concentration of 6 mM and incubated for 20 min at 37°C in the dark. Unreacted IAA was quenched by DTT at a final concentration of 3 mM for 15 min at RT. Proteins were digested by trypsin (trypsin to protein ratio of 1:20 - 1:50) in urea buffer at a final concentration of 1M urea at 37°C overnight, while gently shaking in a thermomixer. Trypsin was inactivated by TFA at a final concentration of 0.1% TFA, pH 2. Samples were centrifuged at 13 000 x *g* for 1 h at RT.

Peptide purification with C18 StageTips

Desalting of tryptic peptides and purification of peptides is based on reversed-phase extraction and was performed according to StageTip method as described (Rappsilber, Ishihama, and

Mann 2003; Rappsilber, Mann, and Ishihama 2007). StageTips are composed of small disks of C_{18}- linked silica beads embedded in a Teflon mesh material (C18 Empore Disk, 3M) inserted into a standard plastic pipette tip. Peptide purification includes equilibration of mesh material, loading and elution of peptides. Equilibration comprises activation with 100 µL MeOH, acidification with 100 µL 80% (v/v) ACN in 0.5% (v/v) FA and 100 µL 0.2% TFA. Then, peptides were loaded in steps of 50-100 µL onto StageTips. After washing twice with 100 µL 0.2% (v/v) TFA, peptides were eluted by addition of 20 µL 80% (v/v) ACN in 0.1 % (v/v) FA. Following this, peptides were concentrated in a SpeedVac and resuspended in 15 µL 0.1% (v/v) FA for quantification of peptide yield using a NanoDrop-1000 UV spectrophotometer at A_{280nm}. Peptides were again concentrated in a SpeedVac and stored at -20°C until nLC-MS/MS analysis.

nLC-MS/MS Analysis

Peptides were analysed on an EASY-nanoLC 1200 coupled online to a Q Exactive™ Plus mass spectrometer. 1 µg peptides were separated on a 50 cm Acclaim™ PepMap™ column (75 µm i.d., 100 Å C18, 2 µm) using a linear 120 min gradient of 3 to 28% acetonitrile in 0.1% FA at 200 nL/min flow rate. Column temperature was kept at 50°C using a butterfly heater. The Q Exactive™ Plus was operated in a data-dependent manner in the m/z range of 300 – 1650. Full scan spectra were recorded with a resolution of 70 000 using an automatic gain control (AGC) target value of 3×10^6 with a maximum injection time of 20 ms. Up to the 10 most intense 2+ - 6+ charged ions were selected for higher-energy c-trap dissociation (HCD) with normalised collision energy (NCE) of 25%. Fragment spectra were recorded at an isolation width of 2 Th and a resolution of 17,500@200m/z using an AGC target value of 1×10^5 with a maximum injection time of 50 ms. The minimum MS^2 target value was set to 1×10^4. Once fragmented, peaks were dynamically excluded from precursor selection for 30 s within a 10 ppm window. Peptides were ionised using electrospray with a stainless steel emitter, I.D. 30 µm at a spray voltage of 2.2 kV and a heated capillary temperature of 275°C. Mass spectra were analysed using MaxQuant (Version 1.5.1.2). At first, parent ion masses were recalibrated using the 'software lock mass' option before the MS^2 spectra were searched using the Andromeda algorithm against sequences from the UniProt knowledgebase. Spectra were searched with a tolerance of 4.5 ppm in MS^1 and 20 ppm in HCD MS^2 mode, strict trypsin specificity (KR not P) and allowing up to two missed cleavage sites. Cysteine carbamidomethylation was set as a fixed modification and methionine oxidation as well as N-terminal acetylation of proteins as variable modifications. The false discovery rate was set to 1 % for peptide and protein identifications. Identifications were transferred between samples using the 'match between run' option within a match window of 0.7 min and an alignment window of 20 min. Statistical analysis of MaxQuant results was done in Perseus (Version 1.5.0.31). At first, reverse protein hits, contaminants and proteins only identified by site were removed. Relative protein quantification was done based on log(2)-transformed LFQ intensities using a minimum ratio count of 2.

Proteins which were not quantified in at least 2/3rd of all preparations were removed and remaining missing values were replaced after normalisation to median intensity for each protein from a normal distribution (width 0.3, downshift 1.8). Significant protein expression differences between samples were identified using FDR-adjusted p-values from an ANOVA test with a permutation-based FDR of 0.01 and 250 randomisations. Tandem mass spectrometry (MS/MS) spectra were matched to peptide sequences in a specific sequence database using Andromeda which is a search engine based on scoring of peptide-spectrum matches. Andromeda is fully integrated into the MaxQuant quantitative proteomics software package designed for the analysis of large-scale mass spectrometric data sets (Cox and Mann 2008; Cox et al. 2009; Cox and Mann 2009; Cox et al. 2011). In case of MS/MS spectra, peptide and fragment masses are searched in an organism-specific sequence database prior to scoring them by a probability-based approach (peptide score). Peptide sequence hits were assembled into protein hits in order to identify candidate proteins (Cox and Mann 2008; Cox et al. 2009; Cox and Mann 2009; Cox et al. 2011).

Parallel reaction monitoring (PRM)

PRM assay was designed according to Zauber et al. and analysed with Skyline (Zauber, Kirchner, and Selbach 2018). Peptide detection criteria were dotp>0.9, min. 2 peptides with 5 transitions. PRM parameters are listed in Table 26.

Table 26. PRM Parameters

Parameter	PRM
nLC	
Peptide Amount	1 µg
Column	50 cm, 1.9 µm
Loading Solvent	0.1% FA, 2% ACN
Column Temperature	40°C
Flow Rate	250 nL/min
Gradient % B	10 to 33
Gradient Length	1 h
Q Exactive™ Plus	
Spray Voltage	2,2
S-lens RF Level	50
Heated Capillary	275°C
Scan Resolution	70000@200m/z
MS² Resolution	35000@200m/z
Full Scan Target	3x10^6, 20 ms max
Mass Range	300-1650

MS² Target	1x10^5, 50 ms max
Loop Count	12
Isolation Width	1.4 Th
Fixed First Mass	no
NCE	25

2.2.7 Generation of CRISPR/Cas9-mediated stable knockout cell lines

The CRISPR/Cas system originates from prokaryotes that have succeeded in numerous 'innate' defence strategies against mobile genetic elements from prokaryotic viruses (Al-Attar et al. 2011). Hence, the CRISPR/Cas system is a defence mechanism that comprises a unique type of repetitive DNA stretches, termed Clustered Regularly Interspaced Short Palindromic Repeats (CRISPRs), CRISPR-associated (Cas) genes and noncoding RNAs (Jansen et al. 2002; Ran et al. 2013). Together, they constitute the CRISPR RNA array. The repeated sequences are interspaced by short variable sequences referred to as protospacers which originate from phages or plasmids constituting the immunological memory of prokaryotes (Horvath and Barrangou 2010; Al-Attar et al. 2011; Ran et al. 2013).

In this work, we used Type II CRISPR system derived from *Streptococcus pyogenes* which consists of Cas9, the CRISPR RNA array encoding guide RNAs and a trans-activating CRISPR RNA array in order to facilitate processing of the CRISPR RNA array. Within the target DNA, the protospacer must be associated with a protospacer adjacent motif (PAM) for correct targeting of sgRNA (Ran et al. 2013). The PAM sequence is located downstream of the genomic DNA target. Cas9 nuclease from *S. pyogenes* is targeted to genomic DNA by a single guide RNA (sgRNA) consisting of a 20-nucleotide guide sequence, illustrated in Figure 13. The sgRNA binds to the DNA target by Watson-Crick base pairing, followed by a DNA double-strand break mediated by Cas9 3 bp upstream of PAM (Ran et al. 2013).

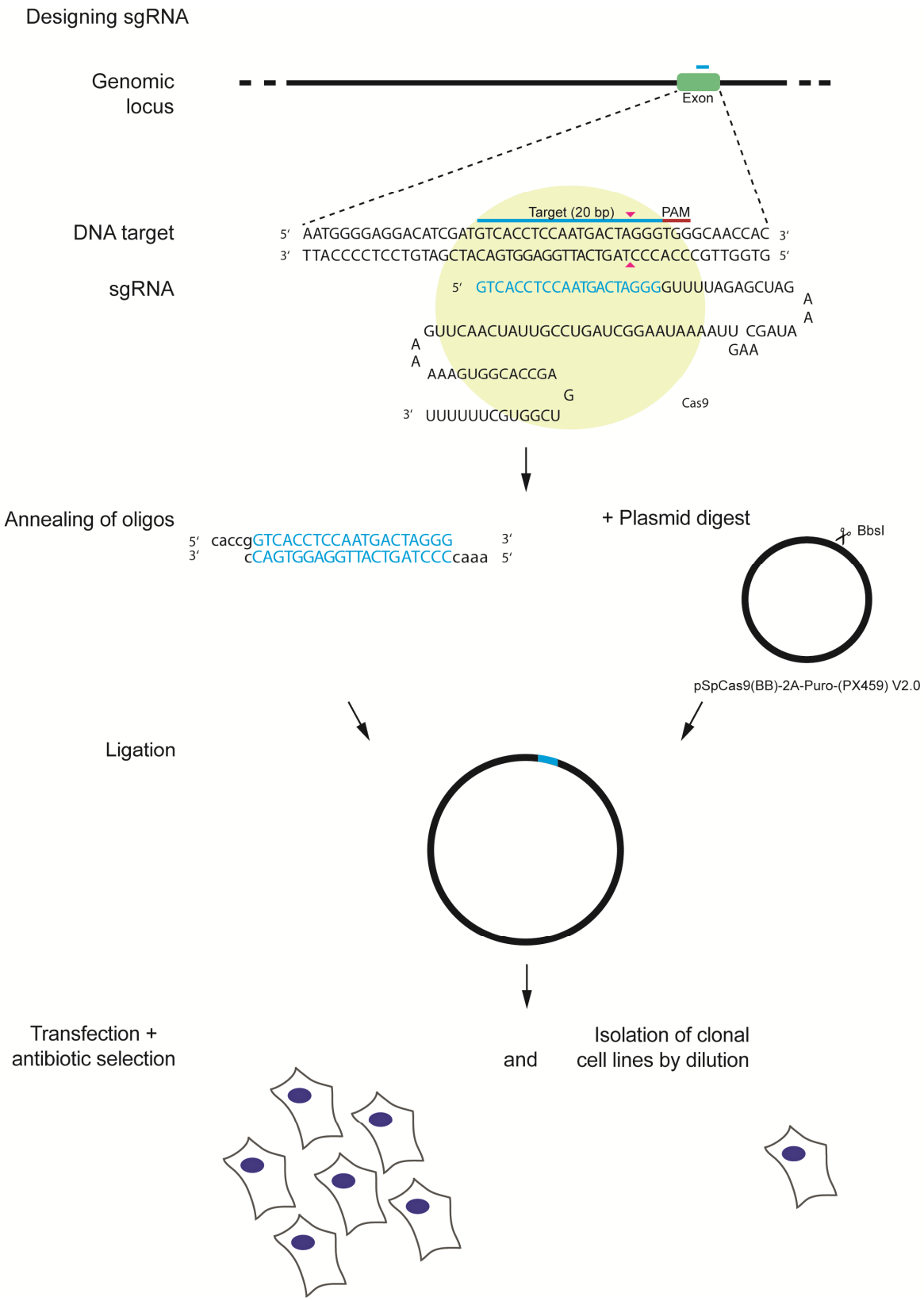

Figure 13. Schematic workflow of the generation of stable knockout cell lines using the CRISPR/Cas9 system.
The 20 bp genomic DNA sequence objected/destined/designated for gene editing is selected and sgRNA sequences that target Cas9 to the specific locus are designed *in silico* using a CRISPR design tool (Ran et al. 2013). sgRNA sequences are cloned into an expression vector using restriction enzyme BbsI. Ligated and sequence-verified plasmid bearing both, Cas9 and sgRNA scaffold backbone is transfected into HeLa cells. After antibiotic selection, cells are first isolated and afterwards clonally expanded to derive isogenic cell lines. Adapted from Ran et al. 2013.

Target selection for sgRNA design

For selection of sgRNA sequences, exons ideally being part of all transcript variants of the gene to be edited were retrieved using Ensembl Genome Browser (http://www.ensembl.org/index.html). Optimally, exons near the 5` end of transcripts were selected and coding sequences were submitted to CRISPR design tool provided by the Zhang Lab (Ran et al. 2013). sgRNAs were ranked by an off-target and quality score and those with best scores were selected. Each of selected guide sequences was cloned into pSpCas9n(BB)-2A-Puro (PX462) (Addgene #48141) via BbsI restriction enzyme digest (Ran et al. 2013).

CRISPR/Cas9 vector generation

sgRNA harbouring Cas9-plasmids were synthesised via plasmid digest, oligonucleotide annealing and ligation. For plasmid digest, the reaction mixture is shown in Table 27.

Table 27. Cas9-plasmid digest reaction

Reagent	Volume
10x FastDigest Buffer	2 µL
Plasmid	1 µg
FastAP	1 µL
FastDigest BbsI	1 µL
ddH2O	ad 20 µL

Plasmid was digested at 37°C for 30 min and gel purified. Following this, oligonucleotides were phosphorylated and annealed according to Table 28.

Table 28. Oligonucleotide annealing reaction for CRISPR/Cas9 vector generation

Reagent	Volume
10x T4 Ligation Buffer	1 µL
Oligo for (final concentration of 100 µM)	1 µL
Oligo rev (final concentration of 100 µM)	1 µL
T4 PNK	0.5 µL
ddH_2O	ad 10 µL

Oligonucleotides were annealed at 37°C for 30 min followed by incubation at 95°C for 5 min. Then, the temperature ramped down to 25°C at 0.1°C/s. Annealed oligonucleotides were ligated into digested vector as follows and ligation was performed at RT for 2 h or at 4°C overnight.

Table 29. Ligation reaction for CRISPR/Cas9 vector generation

Reagent	Volume
10x Ligation buffer	1 µL
digested plasmid	1 µL
Oligo duplex (1:200 dilution)	1 µL
T4 ligase	1 µL
ddH_2O	ad 10 µL

Sequenced plasmids were transformed into competent cells using the appropriate selection marker (see 2.2.4).

Transfection and Expansion of cell lines

(Clonal isolation by dilution for single-clone screen)

HeLa cells were grown in cell culture dishes and transfected with 1 µg total plasmid DNA and 2 µL Lipofectamine2000 in 50 µL OptiMEM each according to standard transfection protocol. After incubation overnight, cells incubated under antibiotic pressure of 1.5 µg/mL puromycin for 72 h by replacing medium each day. For single-clone screen, cells were passaged according to standard cell culture. Cells were serially diluted to a final concentration of 0.14 cells per 100 µL/well followed by an expansion period in order to generate a clonal cell line. Positive cell lines were validated by IF, WB, qPCR and MS analysis (parallel reaction monitoring) as well as genomic sequencing of target region. The following CRISPR KO cell lines were generated:

Table 30. CRISPR/Cas9 knockout cell lines

Name	Gene to be edited	Mode
CRISPR Ctrl - clone 087_1 5D	--	single- clone screen
HeLa-SNX1-KO - clone 16_1 2D	SNX1	single- clone screen
HeLa-SNX5-KO - clone 17_1 7D	SNX5	single-clone screen
HeLa-SNX5/SNX6 double KO - clone #2 8C	SNX5, SNX6	single-clone screen

2.2.8 Isolation of ribosome

Cells were seeded in cell culture flasks in standard growth medium and infected with *C. trachomatis* D or left uninfected. At 48 h p.i., cells were washed three times with cold PBS supplemented with 10 µg/mL CHX (DPBS) to inhibit eukaryotic translation. During the ribosome isolation procedure, all work was performed on ice or at 4°C. Cells were mechanically detached with a cell scraper in DPBS and pelletised by centrifugation at 500 x *g* for 5 min. Cells were lysed in polyribosome buffer supplemented with cOmplete EDTA-free protease inhibitor, 2 mM DTT and 10 µg/mL CHX and 100 µM lactacystin which inhibits the proteolytic activity of the

chlamydial protease- or proteasome-like activity factor (Zhong et al. 2001). Cell lysis was performed for 15 min while homogenising the suspension by gentle pipetting at the beginning of incubation and 5 min following incubation. Subsequently, lysate was centrifuged at 1000 x *g* for 10 min to pelletise nuclei. Supernatant was cleared of cell debris and mitochondria by centrifugation at 20 000 x *g* for 10 min. In case of extant DNA, cleared lysate was homogenised by 23G and 26G syringes and centrifuged again at 20 000 x *g* for 10 min. Then, cleared lysate was gently layered over a sucrose density gradient (60%-15%) in polyribosome buffer. Centrifuge tube was filled up with polyribosome buffer supplemented with 2 mM DTT and 10 µg/mL CHX. Ultracentrifugation was performed at 82 000 x *g* for 21 h at 4°C. Fractionation was performed by piercing the bottom of tube and collecting fractions of 1 or 300 µL each depending on subsequent analysis. 1 mL fractions were taken for WB analysis while 300 µL fractions were taken for MS analysis. Aliquots were saved for subsequent SDS-PAGE analysis during the entire process. For Western Blot analysis, proteins of half volume of fractions were precipitated by TCA precipitation (2.2.5) and subsequently analysed via SDS-PAGE and WB. For MS analysis, SILAC labelled cells were cultured in appropriate SILAC medium and passaged to a maximum passage of 5. Cells were infected with *C. trachomatis* D (light labelled, K0R0) or mock-infected (heavy labelled, K8R10) and incubated in appropriate SILAC infection medium. Mock-infected and infected cells were pooled 1:1 after protein quantification and 200 µg of total protein amount were layered over a sucrose gradient. After ultracentrifugation, proteins of fractions were precipitated by TCA precipitation.

2.2.9 Computational methods

In silico cloning, sequence alignment

Geneious was used for *in silico* cloning. DNA sequences were imported from NCBI databases and oligo design, alignments and cloning steps were performed using Geneious built-in algorithms. Sequence alignments were performed with the Geneious alignment option using the type of global alignment with free end gaps. For comparative sequence analysis, the basic logarithmic alignment search tool (BLAST) by NCBI was used. Protein alignments were performed with the built-in Geneious alignment using blosum62 cost matrix.

2.2.10 Statistical analysis

Data from at least two biologically independent experiments were used for data analysis and technical replicates were included to correct for internal variations. Measure of central tendency and standard deviation were plotted (median; mean ± SD) using GraphPad Prism 7 and 8. Statistical significance was determined by indicated statistical test (*: p-value< 0.05; **: p-value< 0.005).

3 Results

Quantitative proteomic studies by Aeberhard et al. revealed host cell-derived proteins, especially proteins of the human retromer complex to be enriched on the inclusion of *Chlamydia trachomatis* (Aeberhard et al. 2015). Of the retromer, proteins of the sorting nexin (SNX) family were highly concentrated in the inclusion fraction. The retromer is a protein sorting complex involved in retrograde trafficking (Gallon and Cullen 2015). It comprises two subcomplexes: the membrane-sensing subcomplex composed of a SNX-BAR dimer and the cargo-recognition complex composed of a VPS trimer (Rojas et al. 2008). In the study by Aeberhard et al., immunofluorescence analyses confirmed localisation of retromer SNX-BARs on the inclusion and showed partial co-localisation with the bacterial inclusion marker IncA during mid-infection (24 h p.i.) whereas VPS35 and CI-M6PR, the latter being one of retromer's cargo, were depicted as punctuated structures adjacent to the inclusion of *C. trachomatis* (Aeberhard et al. 2015). In contrast to SNX-BARs, SNX3 and SNX12 did not localise on the inclusion membrane suggesting specific recruitment of SNX-BARs (Aeberhard et al. 2015). Based on these findings, we hypothesised SNX-BAR recruitment during early stages of *C. trachomatis* infections (0 – 8 h p.i.). First, we characterised SNX recruitment during early chlamydial infection. Second, we analysed SNX recruitment during mid-infection as we aimed to examine the function of SNX recruitment and the mechanisms behind. Third, we assessed SNX1-associated proteins by proximity-dependent biotinylation in order to identify candidate proteins that may play a role in SNX recruitment and tubule formation.

3.1 SNX recruitment during early infection

In the study by Aeberhard et al., inclusions of *C. trachomatis* L2 infected cells were analysed by a proteomic approach (Aeberhard et al. 2015). Hence, we assessed spatiotemporal dynamics of SNX-BAR recruitment during early *C. trachomatis* infection by analysing localisation of bacteria, retromer components and CI-MPR with indicated antibodies at indicated time points.

3.1.1 SNX-BARs of the retromer complex are recruited to *C. trachomatis* early in infection

Localisation of SNX1

Chlamydia spp. enter the cell by endocytosis and establish their niche at the MTOC in a peri-Golgi region (Grieshaber 2003). We investigated the localisation of SNX1 protein and *C. trachomatis* L2 in HeLa cells in a time course during early infection by immunofluorescence (IF) and Immunoblot (Western Blot, WB) (Figure 14). HeLa cells were infected with *C. trachomatis* L2 or left uninfected and co-stained for host cellular protein SNX1 and bacterial protein LPS at indicated time points (Figure 14 A). In uninfected cells, SNX1 localised in a disperse punctuate pattern in the cytosol. At 2 h p.i., *C. trachomatis*, indicated by staining of

LPS, and host cellular SNX1 localised in a punctate pattern in the cytosol. At 4 h p.i., LPS localised in spatial proximity of the nucleus while SNX1 localised adjacent to bacteria and started to accumulate. In addition, we observed SNX1-positive tubular structures at 4 h p.i.. At 8 h p.i., LPS accumulated in a perinuclear region supposed to be the MTOC (see Figure 16). In parallel, SNX1 accumulated in a perinuclear region, in close proximity to *C. trachomatis*.

Analogous to SNX1 localisation in *C. trachomatis* L2 infected HeLa cells, cells were infected with *C. trachomatis* D or left uninfected (Figure 14 B). In uninfected cells, we confirmed the localisation of SNX1 in a disperse punctuate pattern. In infected cells, in contrast, LPS localised in spatial proximity of the nucleus while SNX1 accumulated close to LPS signal at 8 h p.i. In addition, SNX1-positive tubules were visible as observed for *C. trachomatis* L2 presuming SNX1 recruitment at early infection time point for *C. trachomatis* serovars. Accumulation of SNX1 protein suggested regulation of protein expression levels during early infection. Thus, HeLa cells were infected with *C. trachomatis* or left uninfected and harvested at indicated time points for WB analysis (Figure 14 C). WB analysis revealed no change in protein expression levels.

In sum, infection with *C. trachomatis* resulted in a rearrangement of SNX1 proteins that accumulated close to bacteria at 8 h p.i. in a perinuclear region. In addition, we observed early SNX1-positive tubular structures in *C. trachomatis* infected cells at 8 h p.i.. In parallel, protein levels remained unaffected by infection with *C. trachomatis*.

A

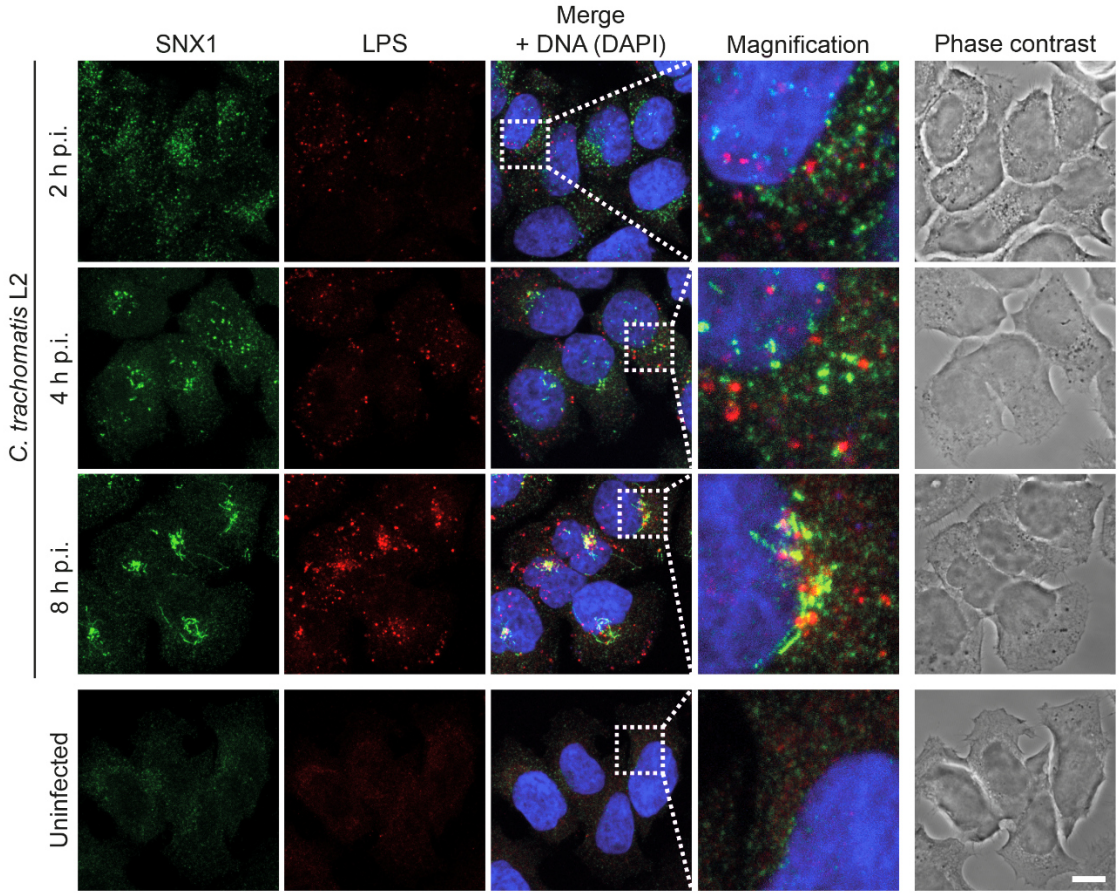
SNX1
LPS
Merge
+ DNA (DAPI)
Magnification
Phase contrast
C. trachomatis L2
2 h p.i.
4 h p.i.
8 h p.i.
Uninfected

B

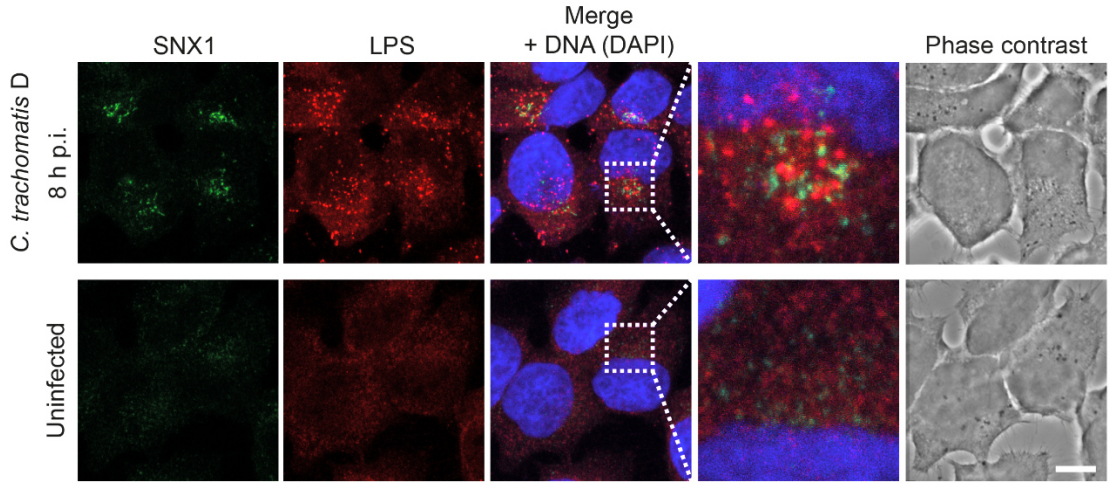
SNX1
LPS
Merge
+ DNA (DAPI)
Phase contrast
C. trachomatis D
8 h p.i.
Uninfected

C

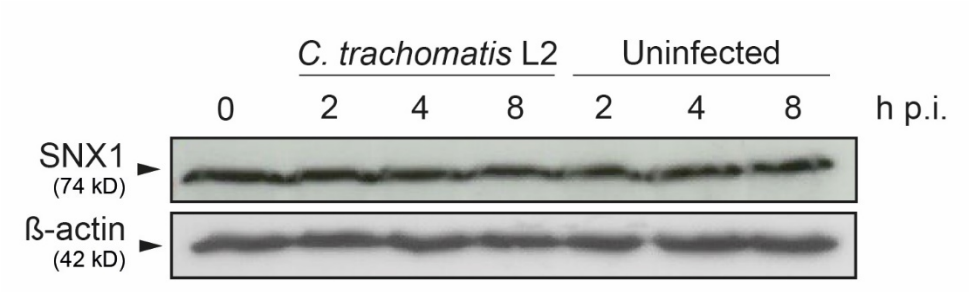

Figure 14. SNX1 is recruited to *C. trachomatis* early in infection.
Confocal IF images showing localisation of SNX1 in (A) *C. trachomatis* L2 and (B) *C. trachomatis* D infected (MOI 10) HeLa cells visualised at indicated time points. Cells were fixed at indicated time points and stained with indicated antibodies and DAPI. SNX1 (green) was immunostained to visualise localisation of host-cellular retromer SNX dimer component. LPS (red) was immunostained to visualise localisation of bacteria. Merge depicts SNX1, *C. trachomatis* (LPS) and DNA (DAPI). Localisation analysis using cLSM; MIP; Scale bar, 10 µm; Representative images shown for n=3. (C) Immunoblot of SNX1 protein levels during *C. trachomatis* L2 infection (MOI 10) in HeLa cells at indicated time points. ß-actin as loading control, Representative immunoblot shown for n=3.

Next, we examined whether SNX1 phenotype during *C. trachomatis* infection is limited to human pathogenic species or whether SNX1 is also recruited in zoonotic species. HeLa cells were infected with the avian pathogen *C. psittaci* or left uninfected for 8 h and cells were co-stained for SNX1 and LPS (Figure 15 A). As a result, in infected cells, SNX1 localised in a disperse punctuate pattern in the cytosol and did not accumulate in close proximity to *C. psittaci* at a perinuclear region as observed for *C. trachomatis*. Taken together, we observed accumulation of SNX1 in HeLa cells infected with the human pathogenic species *C. trachomatis* but not in zoonotic species while all examined chlamydial species localised in a perinuclear region at 8 h p.i. This suggests that recruitment of SNX1 in HeLa cells is specific for *C. trachomatis*.

Each chlamydial species has its predominant host (Andersen and Vanrompay 2000). Since HeLa cells are not the natural host, we performed *C. psittaci* infection in DF-1 cells. DF-1 cells are chicken fibroblast cells and as *C. psittaci* is an avian pathogen, DF-1 cells are reasonable host cells. In DF-1 cells, we observed SNX1 accumulation in a perinuclear region and in spatial proximity of *C. psittaci* in DF-1 cells in contrast to the observation in HeLa cells (Figure 15 B). This suggests that SNX1 recruitment is a natural host-specific phenotype.

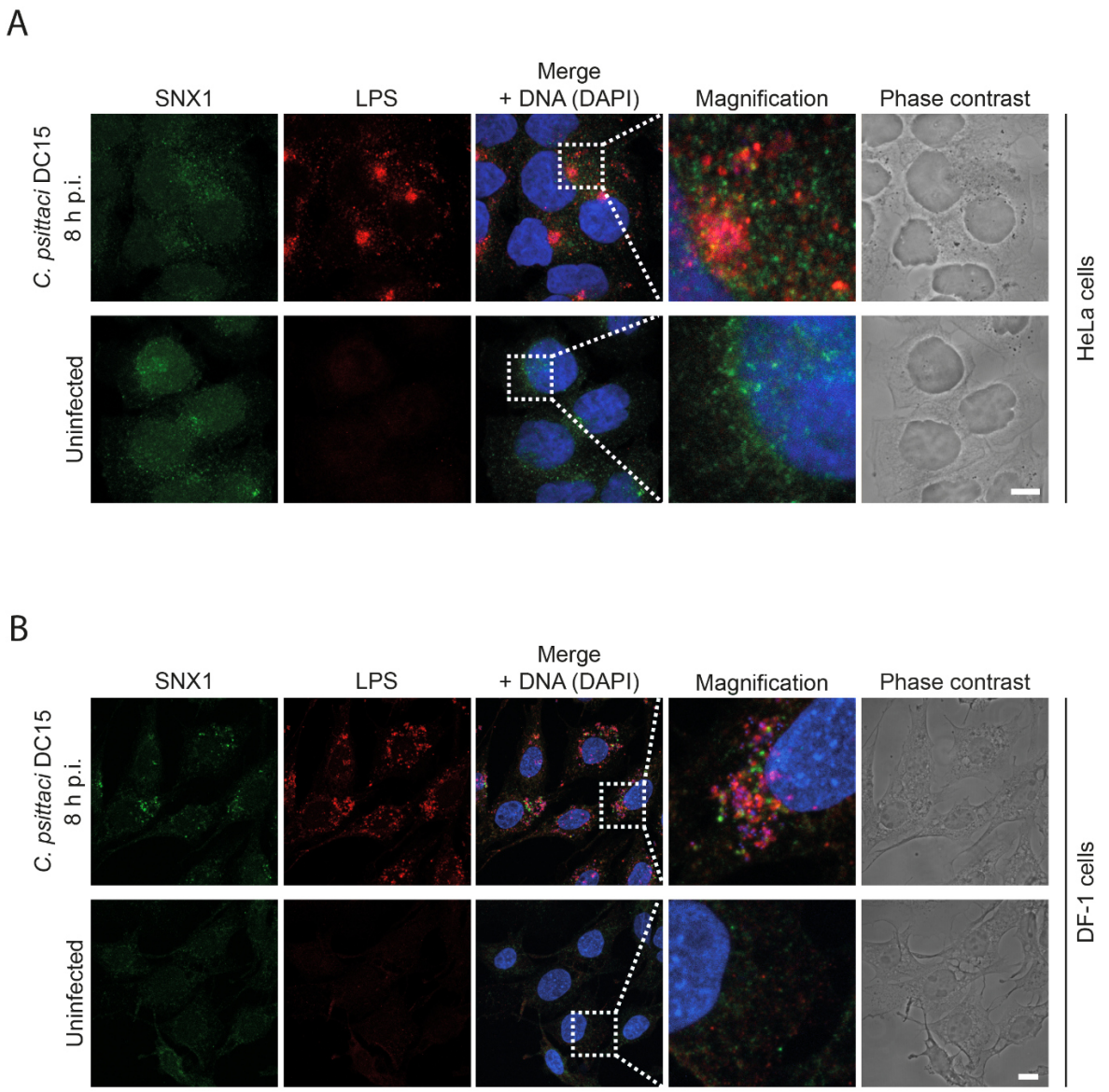

Figure 15. SNX1 localisation in *C. psittaci* infected cells.
Confocal IF images showing localisation of SNX1 in *C. psittaci* DC015 infected (MOI 10) and uninfected (A) HeLa cells and (B) DF-1 cells visualised at indicated time points. Cells were fixed 8 h p.i. and stained with indicated antibodies and DAPI. SNX1 (green) was immunostained to visualise localisation of host-cellular retromer SNX dimer component. LPS (red) was immunostained to visualise localisation of bacteria. Merge depicts SNX1, *C. trachomatis* (LPS) and DNA (DAPI). Localisation analysis using cLSM; MIP; Scale bar, 10 µm; Representative images shown for n=3.

To verify whether the perinuclear region is the MTOC, HeLa cells were infected with *C. trachomatis* and co-stained for pericentrin, a marker for the MTOC and MOMP, one of the predominant surface protein of EBs and RBs at early infection (Caldwell and Judd 1982; Caldwell and Schachter 1982). We observed that *C. trachomatis* is trafficked towards the MTOC during early infection as it accumulated at the MTOC at 8 h p.i. (Figure 16). Trafficking and recruitment of SNX1 was conserved between *C. trachomatis* serovars. Thus, we focussed on analysing *C. trachomatis* L2 during early infection in further experiments.

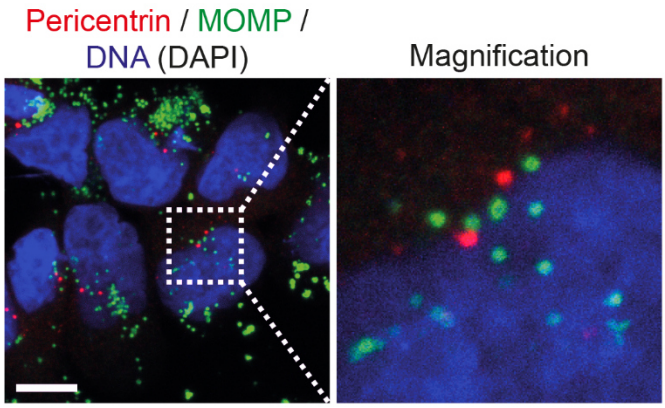

Figure 16. *Chlamydia* spp. are trafficked towards the MTOC.
Confocal IF images showing *C. trachomatis* D infected HeLa cells (MOI 10) visualised at 8 h p.i.. Cells were fixed 8 h p.i. and stained with indicated antibodies and DAPI (DNA). MOMP (green) was immunostained to localise bacteria. Pericentrin (red) was immunostained to localise the MTOC. Localisation analysis using cLSM; MIP; Scale bar 10 µm; Representative images shown for n≥3.

Localisation of SNX-BARs SNX2, SNX5 and SNX6

We assessed whether SNX-BARs of the human retromer differ in the localisation pattern during early *C. trachomatis* infection as observed for SNX1. Hence, we analysed localisation of SNX2, SNX5 and SNX6 at early *C. trachomatis* infection (Figure 17). HeLa cells were infected with *C. trachomatis* or left uninfected for 8 h and cells were stained for either SNX2, SNX5 or SNX6, each co-stained with LPS or MOMP. In uninfected cells, SNX-BARs localised in disperse punctuate pattern in the cytosol. In infected cells, in contrast, SNX2, SNX5 and SNX6 accumulated at the MTOC in close proximity to *C. trachomatis* L2 at 8 h p.i. (Figure 17). We observed co-localisation of SNX and LPS signals indicating proximity of these signals in time and place and possible interaction.

Taken together, all SNX-BARs of the membrane-sensing subcomplex of the human retromer were recruited to *C. trachomatis* early in infection.

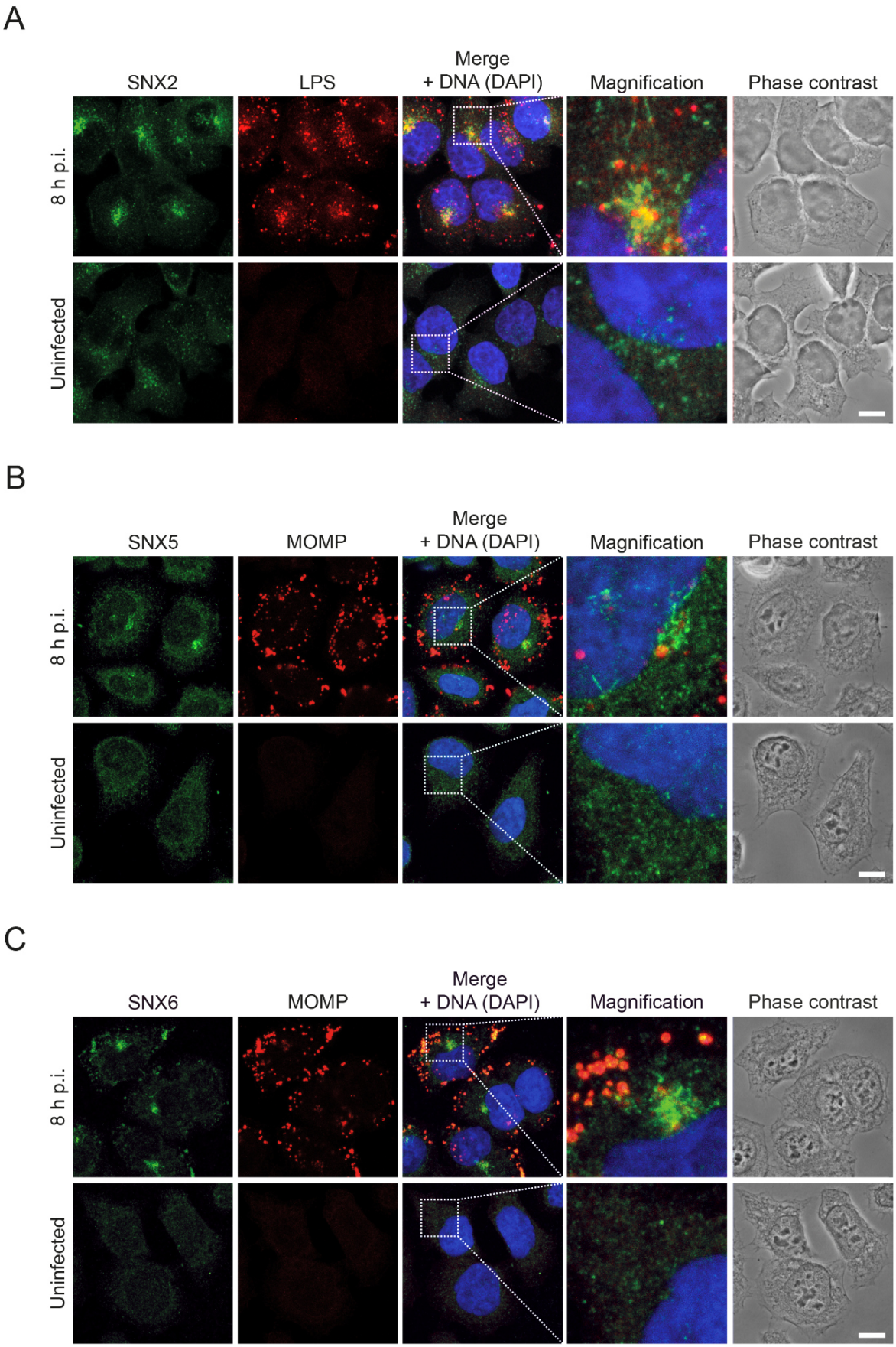

Figure 17. SNX-BARs are recruited to *C. trachomatis* early in infection.
Confocal IF images showing localisation of (A) SNX2, (B) SNX5 and (C) SNX6 in *C. trachomatis* L2 infected HeLa cells (MOI 10) visualised at 8 h p.i.. Cells were fixed 8 h p.i. and stained with indicated antibodies and DAPI. SNX (green) was immunostained to analyse localisation of host-cellular

retromer component in *C. trachomatis* infected cells. LPS and MOMP (red) were immunostained to visualise localisation of bacteria. Merge depicts SNX proteins, *C. trachomatis* (LPS, MOMP) and DNA (DAPI). Localisation analysis using cLSM; MIP; Scale bar, 10 µm; Representative images shown for n=3.

SNX-BARs localised in close proximity to inclusion membrane protein IncE

Mirrashidi et al and Paul et al. reported direct binding of host cellular protein SNX5 to IncE (Mirrashidi et al. 2015; Paul et al. 2017). IncE is an inclusion membrane protein which is expressed at 2 h p.i. (Stephens et al. 1998). To examine the localisation of IncE at 8 h p.i., HeLa cells were infected with *C. trachomatis* and co-stained for SNX-BARs and IncE (Figure 18). At early infection time point, *C. trachomatis* indicated by IncE staining is proximally localised to SNX-BARs. Furthermore, we observed co-localisation of SNX-BARs and IncE at early infection.

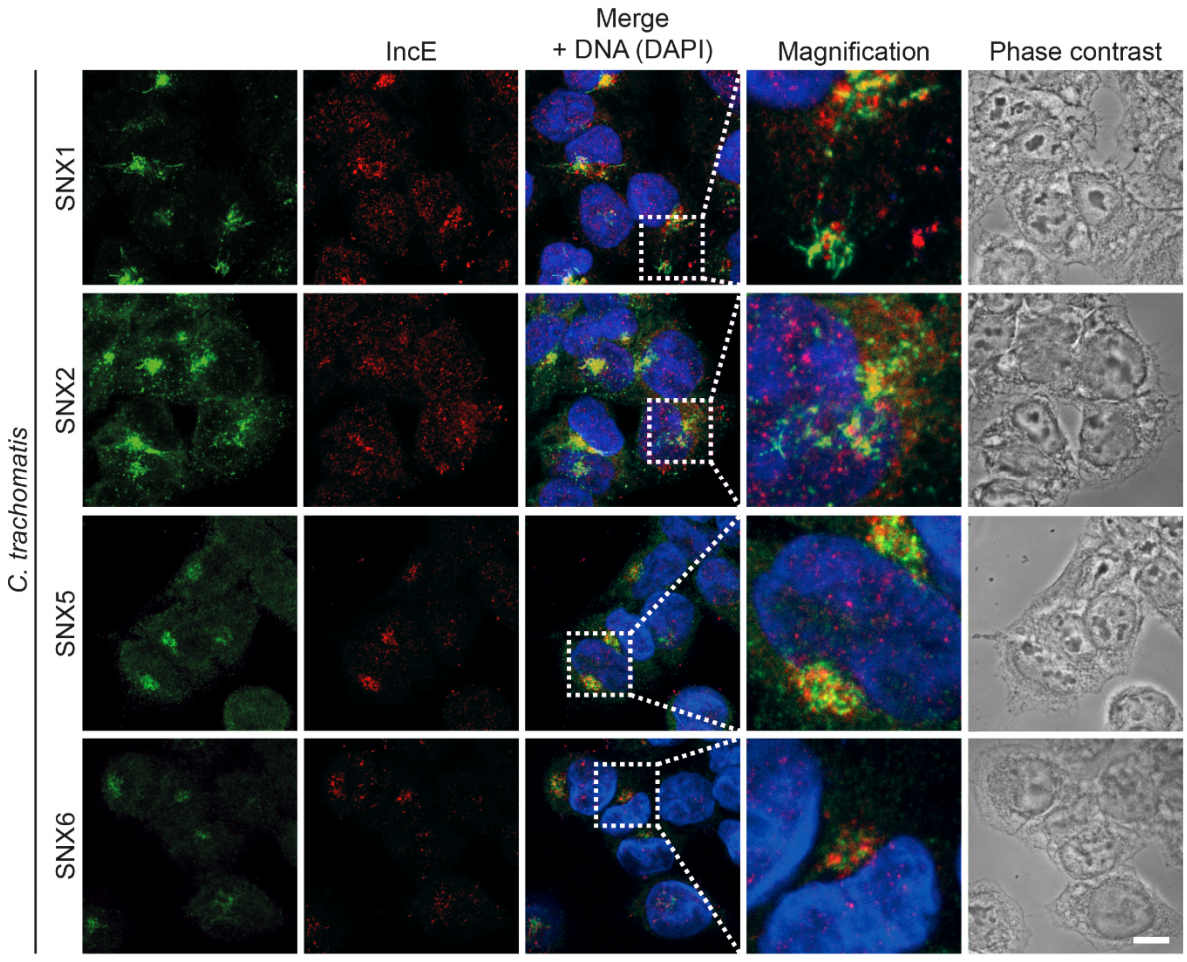

Figure 18. Localisation of SNX-BARs and inclusion membrane protein IncE.
Confocal IF images showing localisation of SNX-BARs and IncE in *C. trachomatis* L2 infected HeLa cells (MOI 10) visualised at 8 h p.i.. Cells were fixed 8 h p.i. and stained with indicated antibodies and DAPI. SNX-BARs (green) were immunostained to visualise localisation of retromer's membrane-sensing subcomplex. IncE (red) was immunostained to visualise localisation of *C. trachomatis* L2 inclusion membrane protein. Merge depicts SNX-BARs, IncE and DNA (DAPI). Localisation analysis using cLSM, MIP; Scale bar, 10 µm; Representative images shown for n=2.

Localisation of VPS35 and CI-MPR

The cargo-recognition subcomplex consists of three VPS proteins namely VPS26, VPS29 and VPS35. The VPS trimer binds to the cargo which is aimed for recycling (Cullen and Korswagen 2012).

We next addressed whether VPS35, exemplarily for retromer components of the cargo-recognition complex, is recruited to the inclusion as it was observed for SNX-BARs. By studying the localisation of VPS35, we examined whether retromer complex separates into the two subcomplexes during early infection. HeLa cells were infected with *C. trachomatis* or left uninfected and co-stained for VPS35 and SNX-BARs at indicated time points (Figure 19). In uninfected cells, SNX1 and VPS35 in part co-localised in punctate structures in the cytosol. In infected cells, SNX1 and VPS35 remained in part co-localised at all indicated time points (Figure 19 A). In addition, at 8 h p.i. both, SNX1 and VPS35 in part co-localised in a perinuclear region at the MTOC and VPS35 accumulated at the MTOC as it was observed for SNX-BARs (Figure 19 A). Furthermore, localisation of the other SNX-BARs of the retromer namely SNX2, SNX5 and SNX6 was examined in *C. trachomatis* infected and uninfected HeLa cells at 8 h p.i. (Figure 19 B-D). In uninfected cells, SNX-BARs and VPS35 in part co-localised in punctate structures in the cytosol. In infected cells at 8 h p.i., VPS35 and SNX-BARs accumulated at the MTOC and in part co-localised assuming on the one hand that both, the cargo-recognition complex and the membrane-sensing are recruited to the early inclusion and on the other hand that the retromer is maintained as a complex at early infection stage.

A

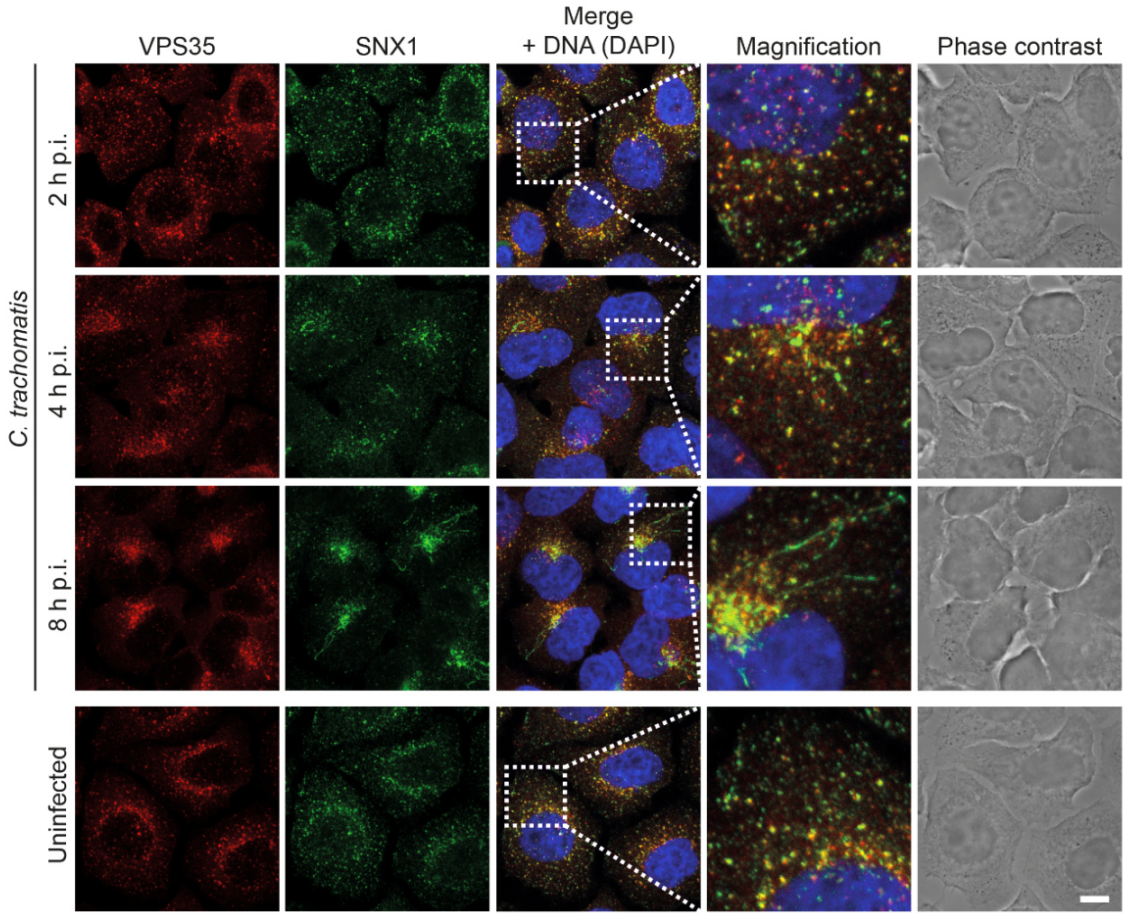
VPS35
SNX1
Merge
+ DNA (DAPI)
Magnification
Phase contrast
C. trachomatis
2 h p.i.
4 h p.i.
8 h p.i.
Uninfected

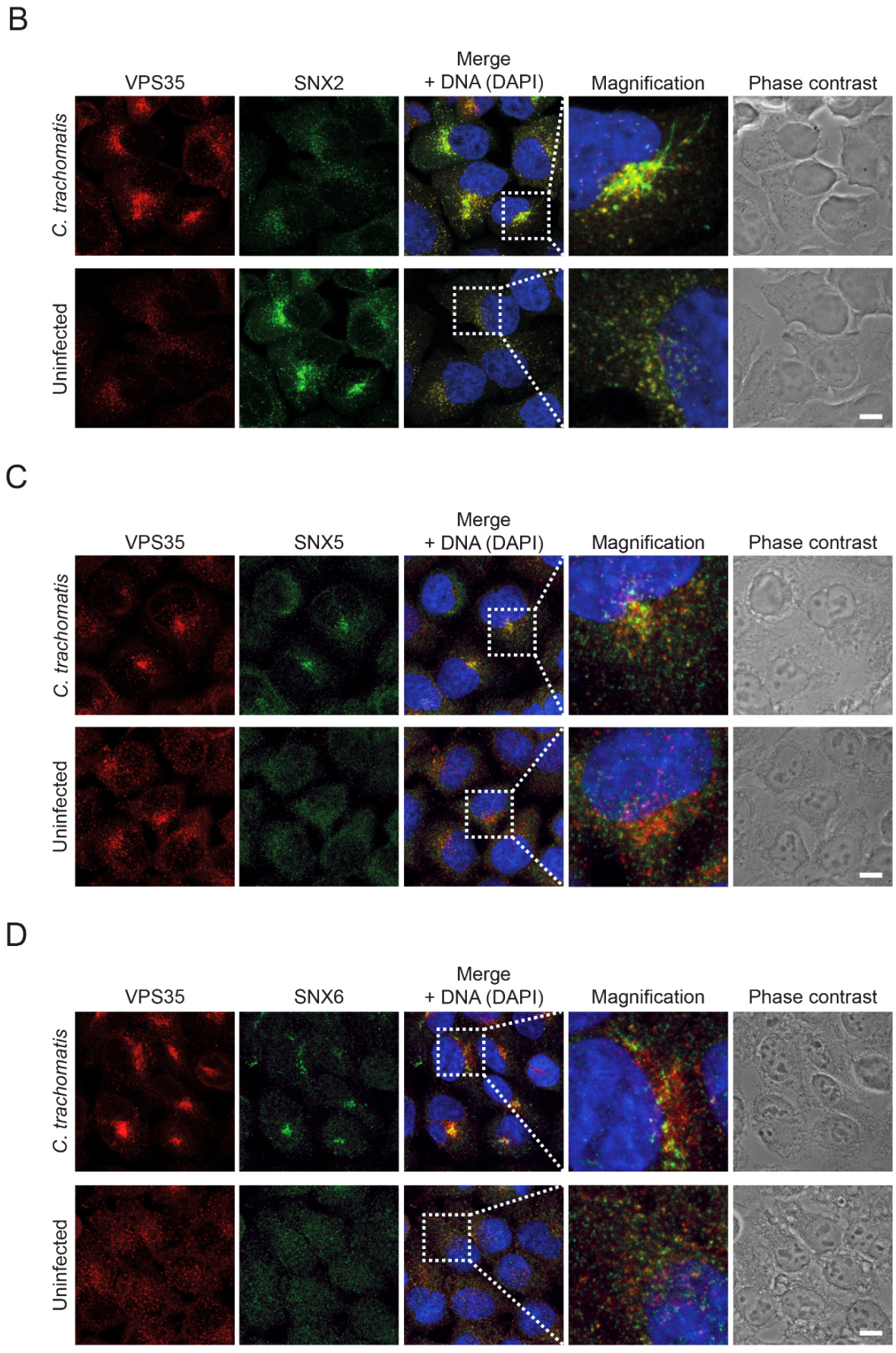

Figure 19. Localisation of VPS35 in *C. trachomatis* infected cells.
Confocal IF images showing localisation of VPS35 in *C. trachomatis* L2 infected HeLa cells (MOI 10) visualised at 8 h p.i.. Cells were fixed 8 h p.i. and stained with indicated antibodies and DAPI.

VPS35 (red) was immunostained to visualise localisation of cargo-selective subcomplex. (A) SNX1, (B) SNX2, (C) SNX5 and (D) SNX6 (green) were immunostained to analyse localisation of membrane-sensing subcomplex. Merge depicts VPS35, SNX-BARs and DNA (DAPI). During early infection, VPS35 protein accumulated in close proximity of SNX-BARs at the MTOC. Localisation analysis using cLSM, MIP; Scale bar, 10 µm; Representative images shown for n=3.

We next examined the localisation of one of retromer's cargo, CI-MPR since Figure 6 suggests a connection of the two subcomplexes of the retromer forming an intact retromer during early infection. HeLa cells were infected with *C. trachomatis* or left uninfected and cells were co-stained for CI-MPR and SNX-BARs at indicated time points (Figure 20). In uninfected cells, CI-MPR localised in close proximity of the nucleus while SNX1 localised in punctuate structures in the cytosol (Figure 20 A). In infected cells, in contrast, both, CI-MPR and SNX1 localised in close proximity at indicated time points (Figure 20 A). At 8 h p.i., CI-MPR and SNX1 accumulated at the MTOC. Analogous to localisation analysis of SNX1, HeLa cells were infected with *C. trachomatis* or left uninfected for 8 h. Cells were stained for CI-MPR and co-stained with SNX2, SNX5 and SNX6 to investigate spatial localisation of CI-MPR to the other SNX-BARs at 8 h p.i. (Figure 20 B-D). In uninfected cells, CI-MPR localised in close proximity of the nucleus and SNX-BARs localised in punctuate structures in the cytosol. In infected cells at 8 h p.i., CI-MPR and SNX-BARs revealed localisation of both in close proximity at the MTOC at 8 h p.i.

In sum, CI-MPR and SNX-BARs accumulated at the MTOC and in part co-localised at early infection time points.

A

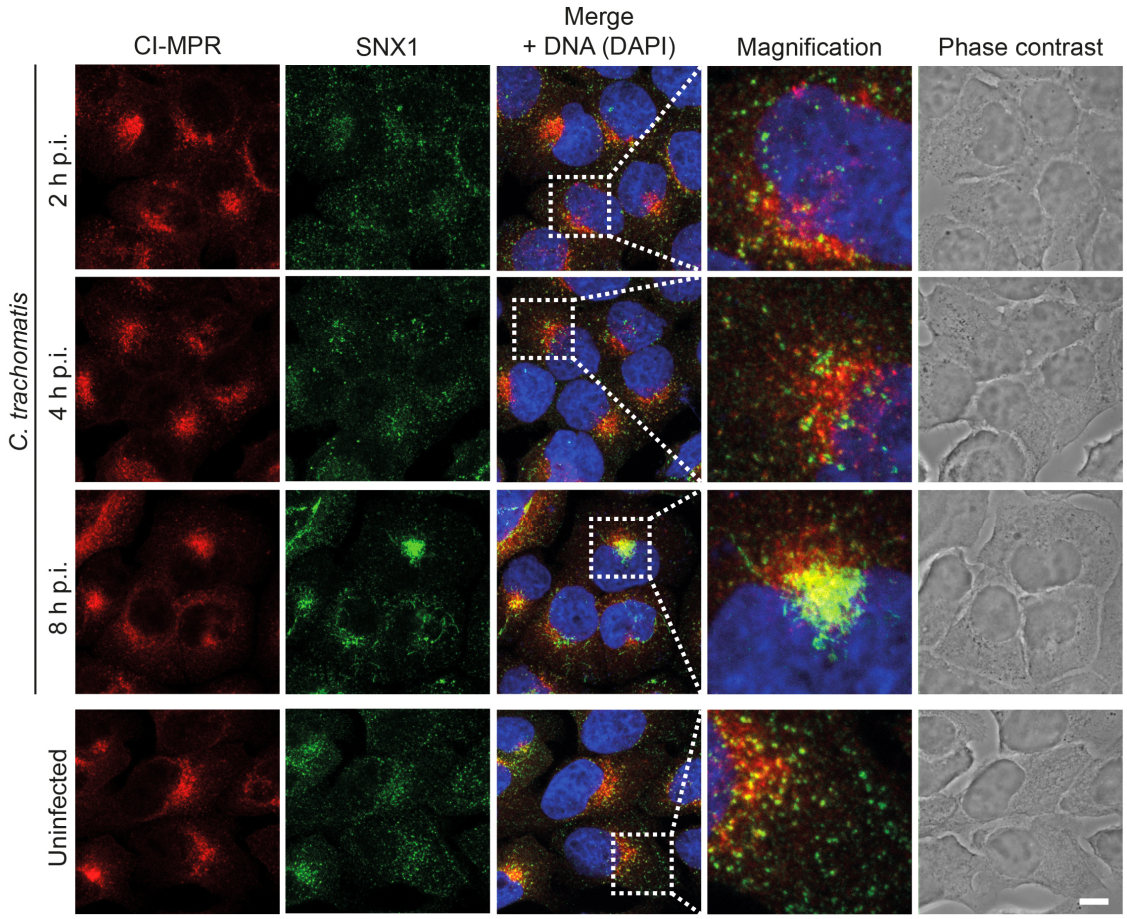
CI-MPR
SNX1
Merge
+ DNA (DAPI)
Magnification
Phase contrast
C. trachomatis
2 h p.i.
4 h p.i.
8 h p.i.
Uninfected

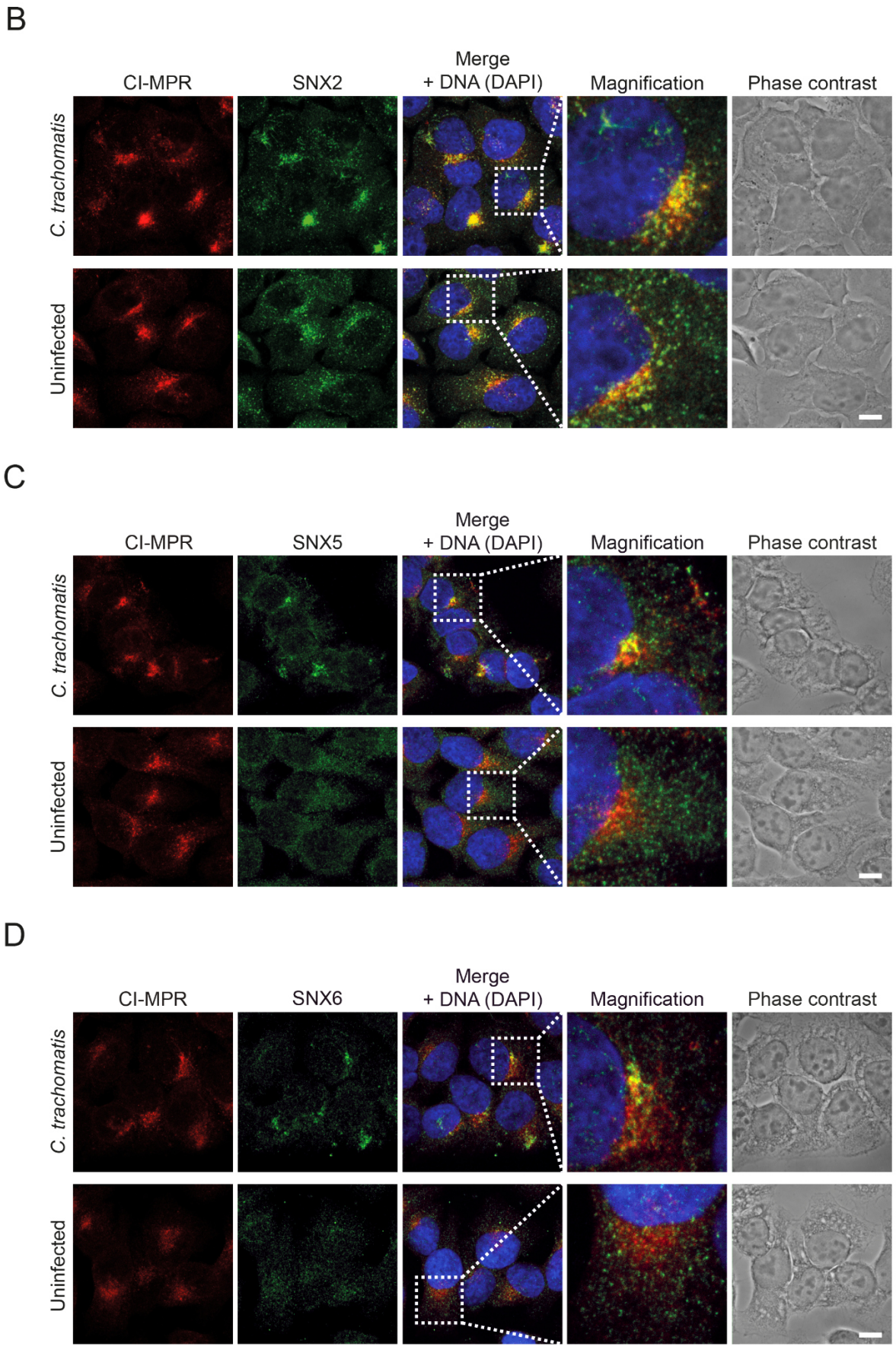

Figure 20. Localisation of CI-MPR in *C. trachomatis* infected cells.
Confocal IF images showing localisation of CI-MPR in *C. trachomatis* L2 infected HeLa cells (MOI 10) visualised at 8 h p.i.. Cells were fixed 8 h p.i. and stained with indicated antibodies and DAPI. CI-

MPR (red) was immunostained to visualise localisation of one of retromer's cargo. (A) SNX1, (B) SNX2, (C) SNX5 and (D) SNX6 (green) were immunostained to analyse localisation of membrane-sensing subcomplex. Merge depicts CI-MPR, SNX-BARs and DNA (DAPI). During early infection, VPS35 protein accumulated in close proximity of SNX-BARs at the MTOC. Localisation analysis using cLSM, MIP; Scale bar, 10 µm; Representative images shown for n=2.

Taken together, we examined localisation of retromer components and localisation of one of retromer's cargo (CI-MPR) during early *C. trachomatis* infection. At 8 h p.i., both, the membrane-sensing subcomplex and VPS35 of the cargo-recognition complex localised in close proximity to *C. trachomatis* and accumulated at the MTOC where *C. trachomatis* establishes its niche. Besides, the cargo CI-MPR accumulated at the MTOC regardless of whether the cells were infected or uninfected.

3.1.2 Early SNX1 tubular structures

Phenotyping of early SNX1 tubular structures

By studying the early infection with *C. trachomatis* in HeLa cells at an early infection time point (8 h p.i.), we observed peripheral and perinuclear SNX cluster phenotypes that are exemplarily illustrated for SNX1 based on cellular location in Figure 21 A, 1. Furthermore, we categorised early SNX-positive tubules according to the formed tubular structure phenotype, again SNX1 being representative for SNX-BARs (Figure 21 A, 2). Using the IF images of early SNX1 tubular structures (Figure 21 B), we quantified the proportion of tubular structure phenotypes per cell (Figure 21 C) and the length of tubular structures per cell (Figure 21 D). In more than 95% of cells, we detected SNX1 clustered structures (99% of cells). In 54% of cells, we observed singular SNX1 structures while aligned SNX1 structures were visible in 18% of cells (Figure 21 C). Moreover, we quantified the length of tubular structures per cell (Figure 21 D). Tubules of SNX1 clustered structure and singular SNX1 structures were mainly 0.5 to 1 µm in length while aligned SNX1 tubules were 5 to 6 µm in length in 95% of cases (95% CI of mean) but also had the widest range of 11.20 µm (minimum 0.3 µm, maximum 11.50 µm).

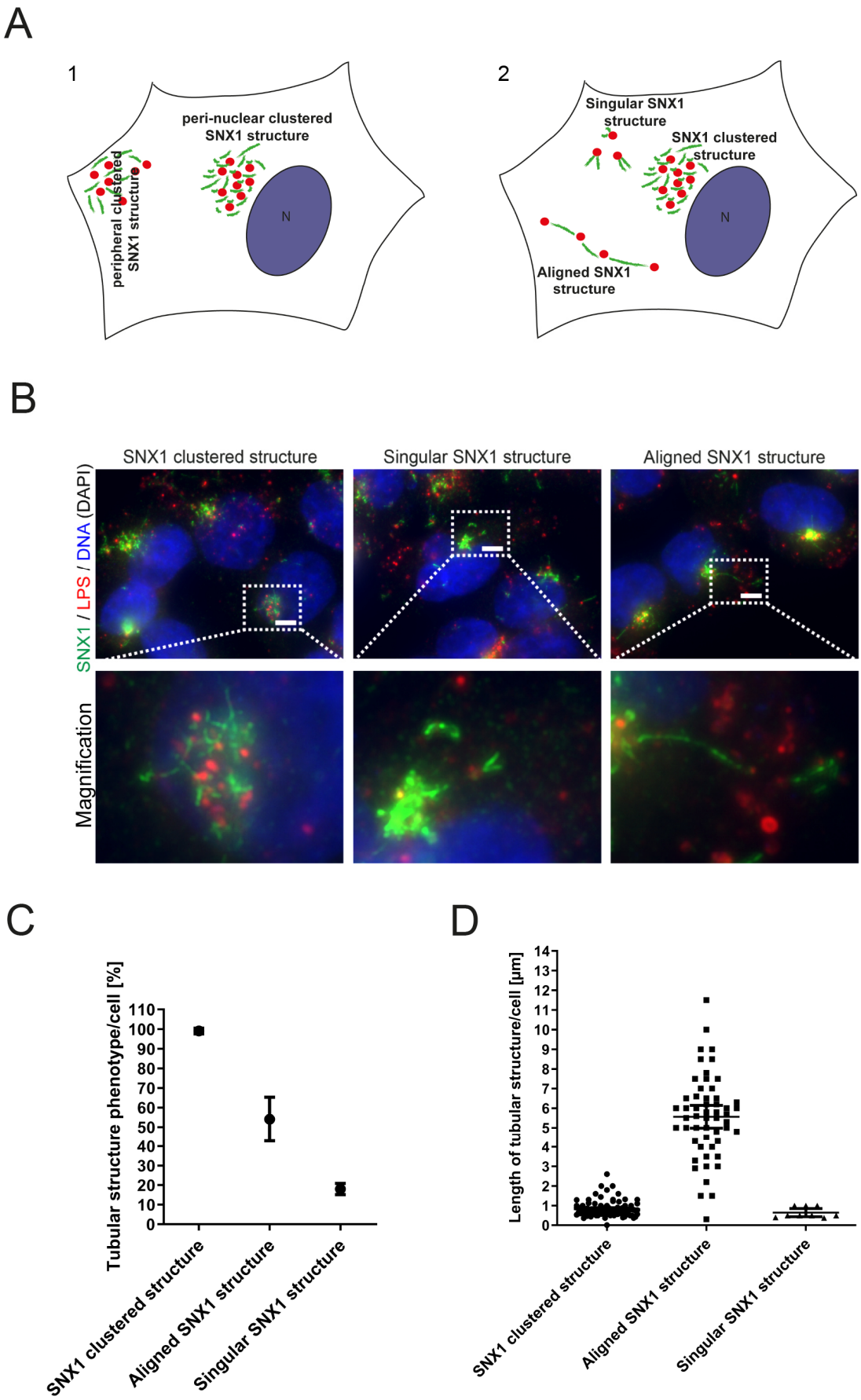

Figure 21. SNX1 tubular structures exhibit different phenotypes.
(A) Graphical model of phenotypes of SNX1 tubular structures based on 1) cellular location and 2) formation of tubular structures. (B) IF images showing phenotypes of SNX1 tubular structures.

Localisation analysis using Axio Observer Z1, MIP; Scale bar, 5 µm; Representative images shown for n=2 (C) Proportion of tubular structure phenotypes per cell [%] quantified in at least 10 fields of view. HeLa cells infected with *C. trachomatis* L2 were fixed at 8 h p.i. and immunostained with SNX1 and LPS (mean ± SD, n=2). (D). Length of tubular structures per cell [µm]. HeLa cells infected with *C. trachomatis* L2 were fixed at 8 h p.i. and immunostained with SNX1 and LPS (mean, upper and lower 95% CI of mean, N=50, n=2).

Nocodazole affects early C. trachomatis trafficking and disrupts early tubules

Microtubules are essential for trafficking of endolysosomal vesicles and trafficking of *Chlamydia* spp. inside the host cell along microtubules (Clausen et al. 1997; Grieshaber, Grieshaber, and Hackstadt 2003; Grieshaber et al. 2006). Thus, we examined the role of cytoskeleton in SNX recruitment at early and mid-infection with *C. trachomatis* by treating infected cells with the microtubule-disrupting agent nocodazole (Figure 22). In addition, we tested whether treatment with nocodazole disrupts SNX1 tubular structures at early and mid- infection time points (Figure 22 A). Nocodazole is a synthetic agent that causes microtubule depolymerisation by binding to free tubulin dimers thereby preventing tubulin from incorporation into microtubules (Hoebeke, Van Nijen, and De Brabander 1976). HeLa cells were infected with *C. trachomatis* or left uninfected for 8 h and 24 h and either treated with nocodazole or control-treated with DMSO for 4 h (Figure 22 A). Cells were co-stained for SNX1 and LPS. In uninfected, DMSO-treated HeLa cells, SNX1 remained localised in a disperse punctate pattern as visualised before (see Figure 14). In DMSO-treated HeLa cells infected with *C. trachomatis*, SNX1 accumulated in close proximity to bacteria, visualised by LPS, at the MTOC at early infection (8 h p.i.). At mid-infection (24 h p.i.), SNX1 was recruited to the chlamydial inclusion. In addition, tubular structures at early and mid- infection time point were intact. Treatment with nocodazole for 4 hours, however, resulted in a strong reduction of SNX1 accumulation at 8 h p.i. but did not inhibit SNX1 recruitment at 24 h p.i.. Moreover, tubular structures positive for SNX1 were disrupted by treatment with nocodazole at both, early and mid-infection. In sum, upon nocodazole treatment, SNX1 recruitment to the inclusion was reduced at early infection but was not inhibited at mid-infection. Treatment with nocodazole disrupted tubular structures suggesting that formation of tubules is dependent on microtubules.

We next quantified the ratio of *C. trachomatis* at the MTOC to *C. trachomatis* in cells, treated with either DMSO as control or with nocodazole (Figure 22 B). We used pericentrin and MOMP as markers for the MTOC and for *C. trachomatis*, respectively. By use of ImageJ, we set a region of interest (ROI) around the cell and placed an ROI of a diameter of 3.5 µm around the pericentrin signal followed by measurement of MOMP signal within the cell and around the MTOC. This measurement was applied to examine *C. trachomatis* trafficking towards the MTOC upon treatment with nocodazole. Treatment with nocodazole resulted in strong reduction of *C. trachomatis* at the MTOC by nearly 50% confirming dependence of *C. trachomatis* on microtubules during trafficking of *Chlamydia* spp. towards the MTOC.

A

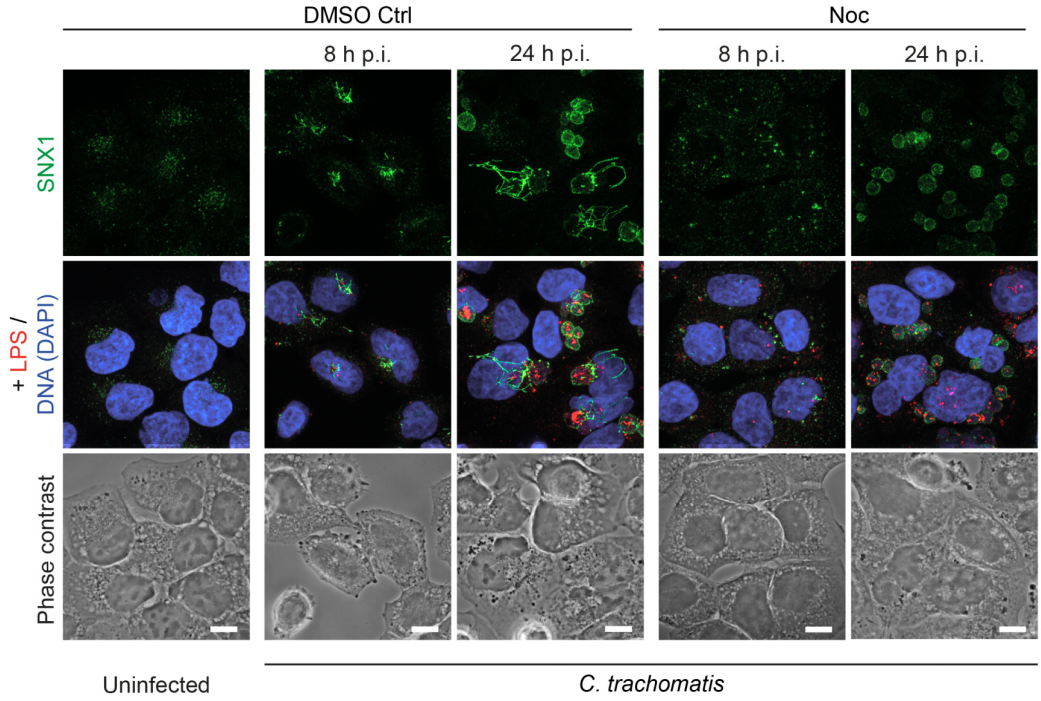

B

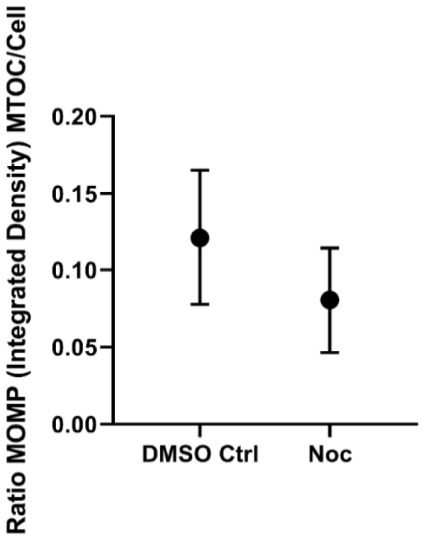

Figure 22. SNX1-positive tubular structures are dependent on microtubules.
(A) Confocal IF images of *C. trachomatis* infected nocodazole- and DMSO-treated HeLa cells. HeLa cells were infected with *C. trachomatis* L2 (MOI 10 or MOI 2) fixed at indicated time points and immunostained with indicated antibodies and DAPI (DNA). SNX1 (green) was immunostained to analyse localisation of host-cellular retromer component in *C. trachomatis* L2 infected cells. LPS (red) was immunostained to visualise localisation of bacteria. Treatment with 1 µg/mL nocodazole (Noc) at 4 h p.i. resulted in a strong reduction of SNX1 recruitment at 8 h p.i. (MOI 10) but did not inhibit SNX1 recruitment to the chlamydial inclusion at 24 h p.i. (MOI 2). Localisation analysis using cLSM, Scale bar, 10 µm, Representative images shown for n=2. (B) Analysis of *C. trachomatis* trafficked towards the MTOC in HeLa cells. HeLa cells were infected with *C. trachomatis* D (MOI 10), fixed at 8 h p.i. and immunostained with MOMP and pericentrin. MOMP was immunostained to localise *C. trachomatis* and pericentrin was immunostained to localise the MTOC. Signal intensities per cell were quantified in at least 30 cells per treatment condition using ImageJ after MIP of confocal IF images. Only cells with visible pericentrin signals were analysed (mean ± SD, n=2).

We applied this quantification also to study the effect of SNX knockout on the trafficking of *C. trachomatis* towards the MTOC (see section 3.1.3).

3.1.3 Functional analysis of early SNX recruitment by CRISPR/Cas9-mediated knockout

We hypothesised that *C. trachomatis* uses host's cellular retromer-mediated retrograde trafficking in order to establish its niche at the MTOC by avoiding fusion of endosomes with lysosomes thereby escaping the degradative trafficking pathway. Therefore, we generated stable SNX1, SNX5 single knockout and SNX5/SNX6 double knockout cell lines to examine the function of SNX-BARs during early chlamydial infection.

Generation of stable knockout cell lines

We used the CRISPR/Cas9 system as a genome editing tool for the generation of knockout (KO) cell lines by using HeLa cells as a human model cell line. Briefly, sgRNAs were cloned into a backbone vector and HeLa cells were transfected with CRISPR/Cas9 plasmid for co-expression of Cas9 and sgRNA sequences. Following antibiotic selection, clonal cell lines were isolated by dilution and eventually expanded. Single KO cell lines of SNX1, SNX5 and double KO cell lines of SNX5/SNX6 were validated by Western Blot (Figure 23 A and B), targeted protein analysis (PRM, see section 2.2.6) (Figure 23 C), qPCR (data not shown) and immunofluorescence (data not shown). SNX1 KO clones 16_1 2D and 16_1 6E as well as SNX5 KO clone 17_1 7D were among others positively validated by WB analysis (Figure 23 A) and did not exhibit SNX1 and SNX5 protein expression, respectively (Figure 23 C). SNX6 KO was generated in SNX5 KO cell line for SNX5/SNX6 KO cell line generation. SNX5/SNX6 KO clone #2 8C was also positively validated by WB analysis (Figure 23 B) and did not exhibit either SNX5 or SNX6 protein expression (Figure 23 C). Each KO cell line revealed reduced protein expression levels of the other SNX-BARs suggesting a mutual dependence of protein expression of SNX-BARs. Identified positive KO cell lines were used for further studies.

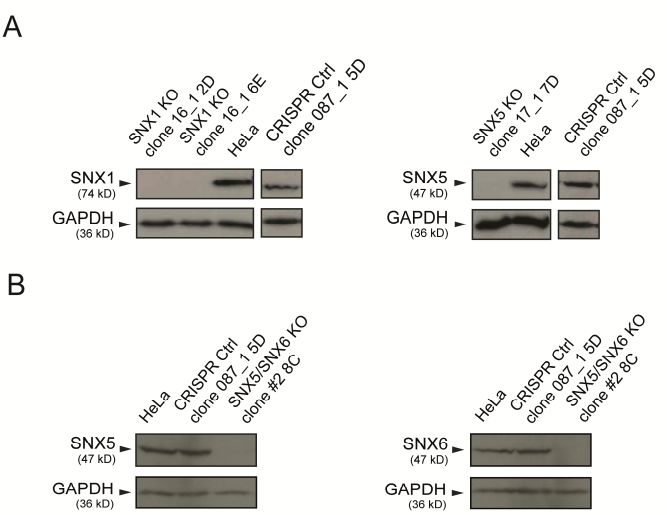

C

Cell line	Protein expression [in %] SNX1	SNX5	SNX6
SNX1 KO (clone 16_1 2D)	n.d.	21.5	57.0
SNX5 KO (clone 17_1 7D)	69.3	n.d.	89.6
SNX5/6 KO (clone #2 8C)	54.6	n.d.	n.d.
CRISPR Ctrl (clone 087_1 5D)	100.0	100.0	100.0

Figure 23. Validation of stable SNX knockout cell lines.
(A) Immunoblot of SNX1 (16_1 2D, 16_1 6E) and SNX5 (17_1 7D) knockout clones infected with *C. trachomatis* L2 (MOI 2) at 24 h p.i. using indicated antibodies. GAPDH as loading control. (B) Immunoblot of SNX5/SNX6 double knockout clone (#2 8C) using indicated antibodies, GAPDH as loading control. SNX6 was knocked out in the previously generated SNX5 knockout cell line. (C) SNX knockout cell lines were validated using parallel reaction monitoring as described in Koch-Edelmann et al. 2017 following in-solution digest and peptide purification using StageTips (see section 2.2.6). Table shows protein expression of indicated proteins relative to CRISPR Ctrl cell line, n.d.:not detected.

Early C. trachomatis infection in SNX knockout cell lines

To study the effect of SNX KO on uptake of *C. trachomatis* and early trafficking of *C. trachomatis* towards the MTOC, HeLa, CRISPR Ctrl and SNX1 and SNX5 KO cell lines were infected with *C. trachomatis* or left uninfected for 8 h and co-stained for indicated proteins (Figure 24). Analogous to studying the role of cytoskeleton during infection with *C. trachomatis* after treatment with nocodazole, pericentrin and MOMP were used as markers for MTOC and for *C. trachomatis*, respectively (Figure 24 A). We examined the *C. trachomatis* infection rate per cell at 8 h p.i. (total MOMP signal within cell) in SNX1 and SNX5 single KO cell lines from Figure 24 A (Figure 24 B). Infection of SNX1 and SNX5 KO cell lines with *C. trachomatis* resulted in a similar infection rate to HeLa and CRISPR Ctrl cell lines. We detected a slight decrease in total MOMP signal in CRISPR Ctrl cell line of about 25% compared to HeLa cells. In SNX1 and SNX5 KO cell lines, total MOMP signal was slightly decreased compared to HeLa cells and slightly increased compared to CRISPR Ctrl cell lines. As a result, single KO of neither SNX1 nor SNX5 affected uptake of *C. trachomatis* into the cell. In addition, we examined trafficking of *C. trachomatis* in SNX1 and SNX5 single KO cell lines by quantifying the ratio of *C. trachomatis* at the MTOC to *C. trachomatis* within the cell at 8 h p.i. as used to quantify *C. trachomatis* at the MTOC upon treatment with nocodazole (Figure 24 C). The ratio of MOMP at the MTOC to MOMP within the cell was similar to HeLa and CRISPR Ctrl cell lines. MOMP signal ratio was slightly increased in CRISPR Ctrl cell line. In SNX1 and SNX5 KO cell line, ratio of MOMP at the MTOC to MOMP within cell was similar to HeLa and CRISPR Ctrl cell lines

indicating that SNX1 and SNX5 single KO did not affect early trafficking of *C. trachomatis* towards the MTOC.

Taken together, SNX1 and SNX5 single KO did not affect uptake into the cell and early trafficking of *C. trachomatis*.

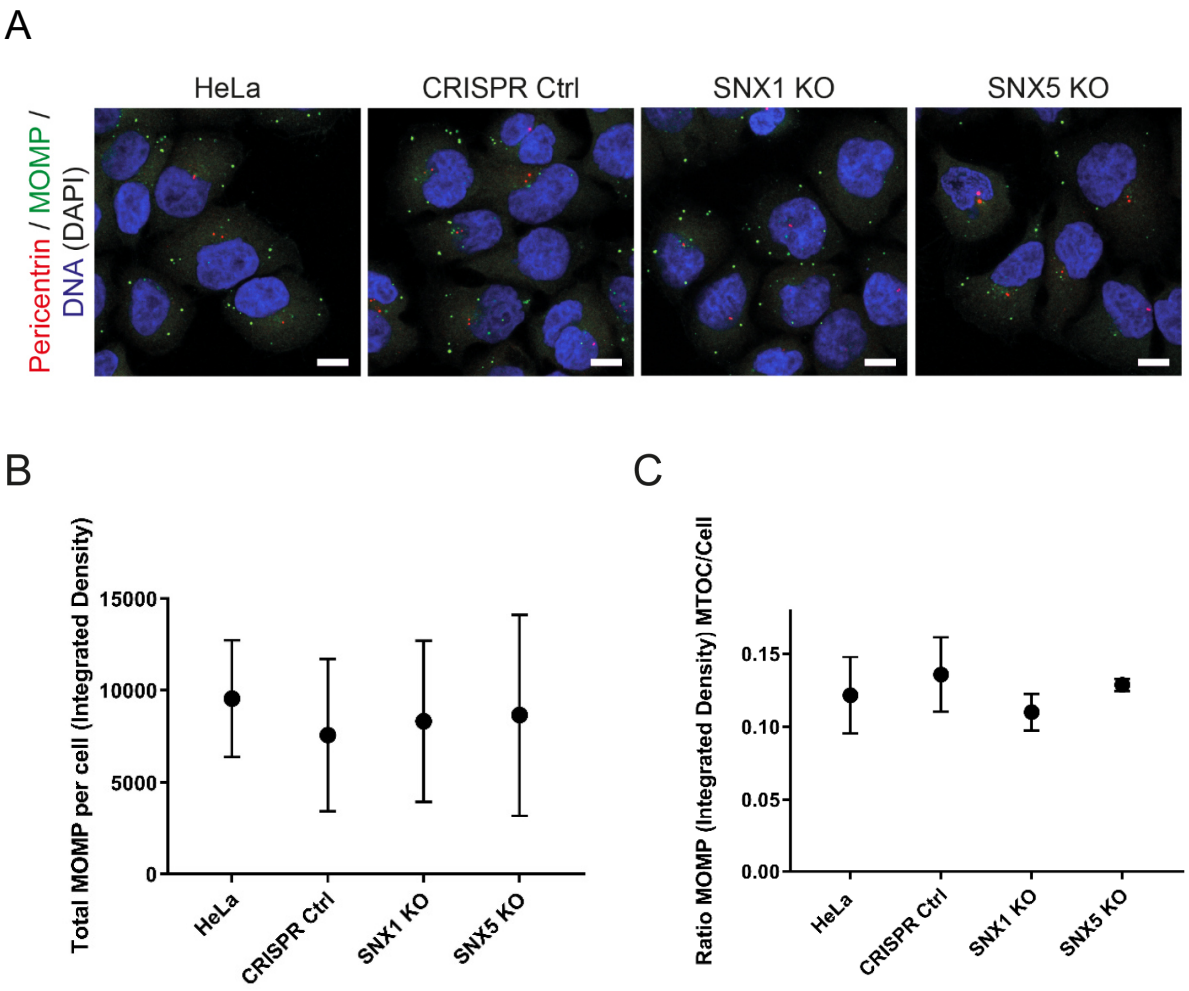

Figure 24. Early trafficking of *C. trachomatis* towards the MTOC is not altered in SNX single knockout cell lines.
HeLa, CRISPR Ctrl, SNX1 and SNX5 single knockout cell lines were infected with *C. trachomatis* L2 (MOI 10) and visualised 8 h p.i.. Cells were fixed 8 h p.i. and stained with indicated antibodies and DAPI (DNA). MOMP (green) was immunostained to localise *C. trachomatis*. Pericentrin (red) was immunostained to localise the MTOC. (A) Confocal IF images showing *C. trachomatis* infected HeLa, CRISPR Ctrl, SNX1 and SNX5 single knockout cell lines. Localisation analysis using cLSM, MIP, Scale bar, 10 µm, n=3. (B) Analysis of uptake of *C. trachomatis* into HeLa, CRISPR Ctrl, SNX1 and SNX5 single knockout cell lines from panel A. Signal intensities per cell in at least 8 fields of view per cell line were quantified using ImageJ after MIP of confocal IF images (mean ±SD, n=3; Ordinary one-way ANOVA, Tukey's multiple comparison test). (C) Analysis of *C. trachomatis* trafficked towards the MTOC in HeLa, CRISPR Ctrl, SNX1 and SNX5 single knockout cell lines from panel A. Signal intensities per cell in at least 8 fields of view per cell line were quantified using ImageJ after MIP of confocal IF images. Only cells with visible pericentrin signal were analysed (mean ±SD, n=3; Ordinary one-way ANOVA, Tukey's multiple comparison test).

During the analysis of early *C. trachomatis* infection, infected SNX KO cell lines, HeLa, CRISPR Ctrl and SNX single and KO cell lines, were in parallel co-stained for SNX1 and LPS to assess

whether SNX1 trafficking and *C. trachomatis* trafficking is disrupted in SNX5/SNX6 KO cell lines. We observed disruption of SNX1 accumulation at MTOC and loss of SNX1 tubular structures in SNX5/SNX6 KO cell line suggesting that early retrograde trafficking of *C. trachomatis* is in addition to SNX1 accumulation affected in SNX5/SNX6 KO (Figure 25).

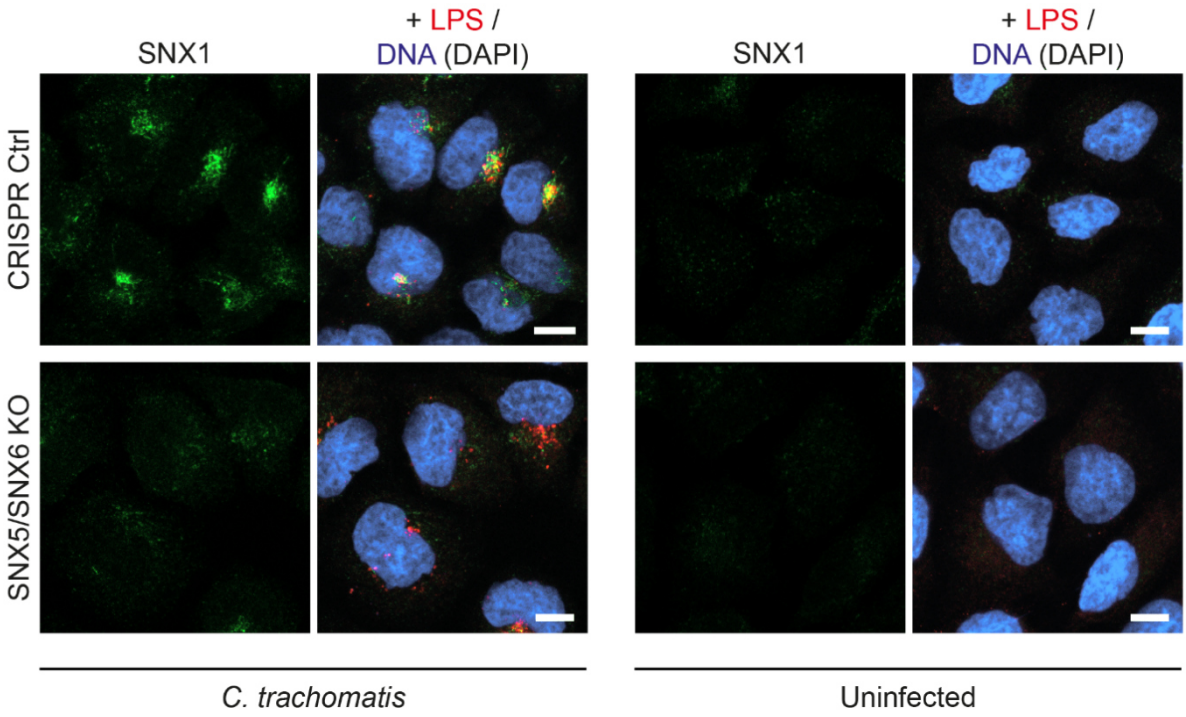

Figure 25. SNX1 accumulation at the MTOC and early tubular structures are disrupted in *C. trachomatis* infected SNX5/SNX6 double knockout cell line.
Confocal IF images showing *C. trachomatis* L2 infected CRISPR Ctrl and SNX5/SNX6 double knockout cell lines (MOI 10) visualised at 8 h p.i.. Cells were fixed at 8 h p.i. and immunostained with indicated antibodies. SNX1 (green) was immunostained to visualise retromer component and LPS (red) was immunostained to localise *C. trachomatis*. Localisation analysis using cLSM, MIP, Scale bar, 10 µm, Representative images shown for n=3.

Hence, we tested whether uptake of *C. trachomatis* and early *C. trachomatis* trafficking towards the MTOC is affected in SNX5/SNX6 KO cell line (Figure 26). Since HeLa cells and CRISPR cell line were only slightly different in the previous analysis, we decided to perform the following analysis in CRISPR cell line as sole control. SNX5/SNX6 KO cells were infected with *C. trachomatis* or left uninfected for 8 h and co-stained for indicated proteins (Figure 26 A). Again, pericentrin and MOMP were used as markers for MTOC and for *C. trachomatis*, respectively and early *C. trachomatis* infection was analysed in cell lines from Figure 26 A. Analysis was performed analogously to the analysis in SNX1 and SNX5 single KO (see Figure 24). Double KO of SNX5/SNX6 did not affect total MOMP signals within SNX5/SNX6 KO cells as MOMP signal in SNX5/SNX6 KO was only slightly increased compared to CRISPR Ctrl cell line (Figure 26 B). However, double KO of SNX5/SNX6 resulted in a significant decrease of MOMP signal at MTOC of 43% (Figure 26 C). Taken together, loss of SNX5 and SNX6 did not

affect *C. trachomatis* uptake into cells but resulted in a strong decrease of *C. trachomatis* at the peri-Golgi region/MTOC at early infection time point.

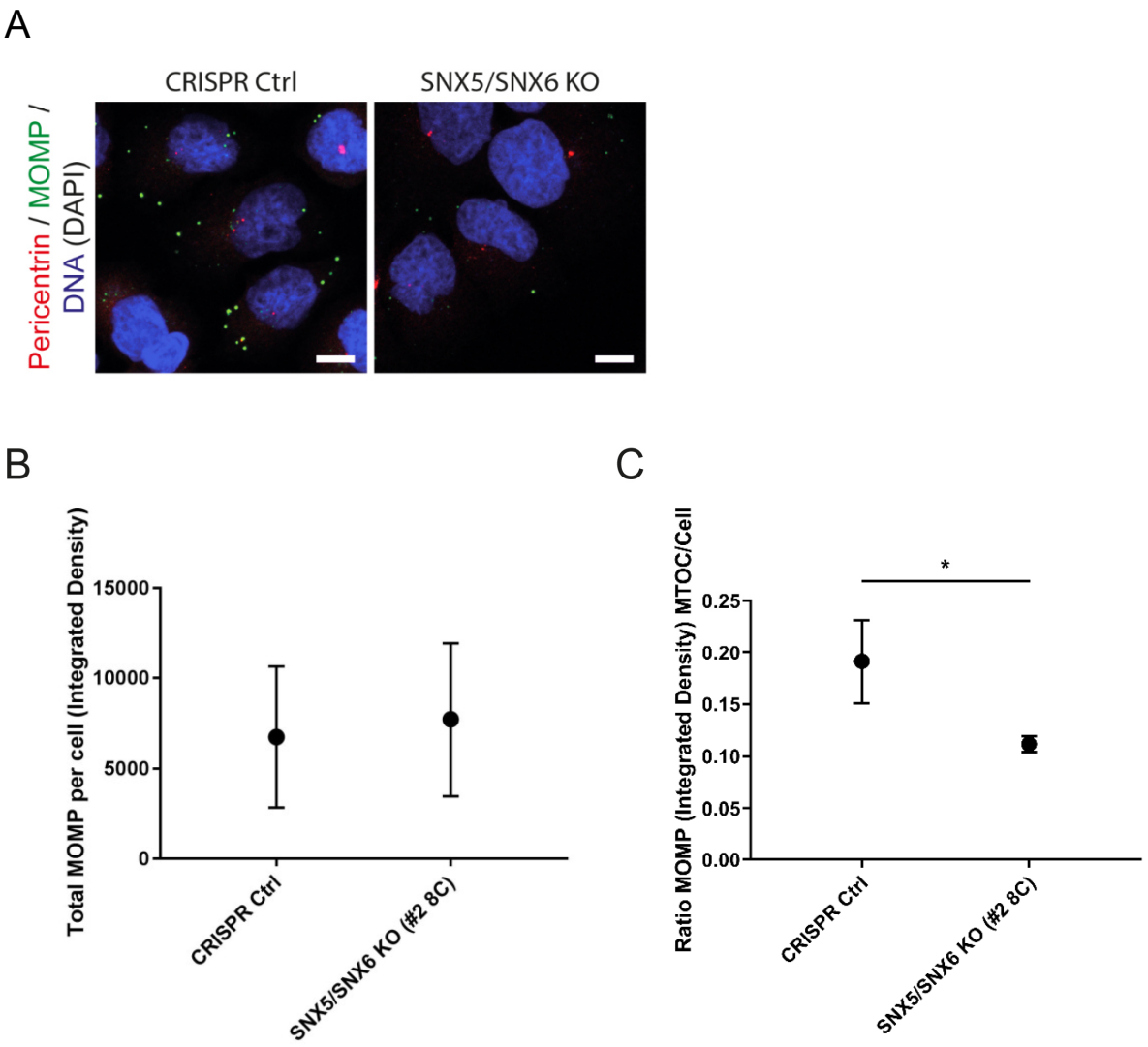

Figure 26. Early trafficking of *C. trachomatis* towards the MTOC is reduced in SNX5/SNX6 double knockout cell line.
(A) CRISPR Ctrl and SNX5/SNX6 double knockout cell lines were infected with *C. trachomatis* L2 (MOI 10) and visualised 8 h p.i.. Cells were fixed 8 h p.i. and stained with indicated antibodies and DAPI (DNA). MOMP (green) was immunostained to localise *C. trachomatis*. Pericentrin (red) was immunostained to localise the MTOC. (A) Confocal IF images showing *C. trachomatis* infected CRISPR Ctrl and SNX5/SNX6 double knockout cell lines. Localisation analysis using cLSM, MIP, Scale bar, 10 µm, Representative images shown for n=3. (B) Analysis of uptake of *C. trachomatis* into CRISPR Ctrl and SNX5/SNX6 double knockout cell lines from panel A. Signal intensities per cell in at least 8 fields of view per cell line were quantified using ImageJ after MIP of confocal IF images (mean ±SD, n=3; two-tailed Mann-Whitney test). (C) Analysis of *C. trachomatis* trafficked towards the MTOC in CRISPR Ctrl and SNX5/SNX6 double knockout cell lines from panel A. Signal intensities per cell in at least 8 fields of view per cell line were quantified using ImageJ after MIP of confocal IF images. Only cells with visible pericentrin signal were analysed (mean ±SD, n=3; two-tailed unpaired t test, * indicates p-value < 0.05).

Localisation of VPS35 in SNX5/SNX6 KO

Since loss of SNX5 and SNX6 resulted in a decrease of *C. trachomatis* at the MTOC, we assessed whether loss of these SNXs affects association of retromer cargo-recognition complex to membrane-binding subcomplex. CRISPR Ctrl, SNX1 single and SNX5/SNX6 KO cells were infected with *C. trachomatis* or left uninfected for 8 h and co-stained for VPS35 and LPS (Figure 27). In *C. trachomatis* infected CRISPR Ctrl and SNX1 single KO cell lines, VPS35 accumulated at the MTOC at 8h p.i.. In *C. trachomatis* infected SNX5/SNX6 KO cell lines, clustering of VPS35 at the MTOC decreased in approximately two-third of cells suggesting that loss of SNX5/SNX6 affects trafficking of cargo-recognition complex.

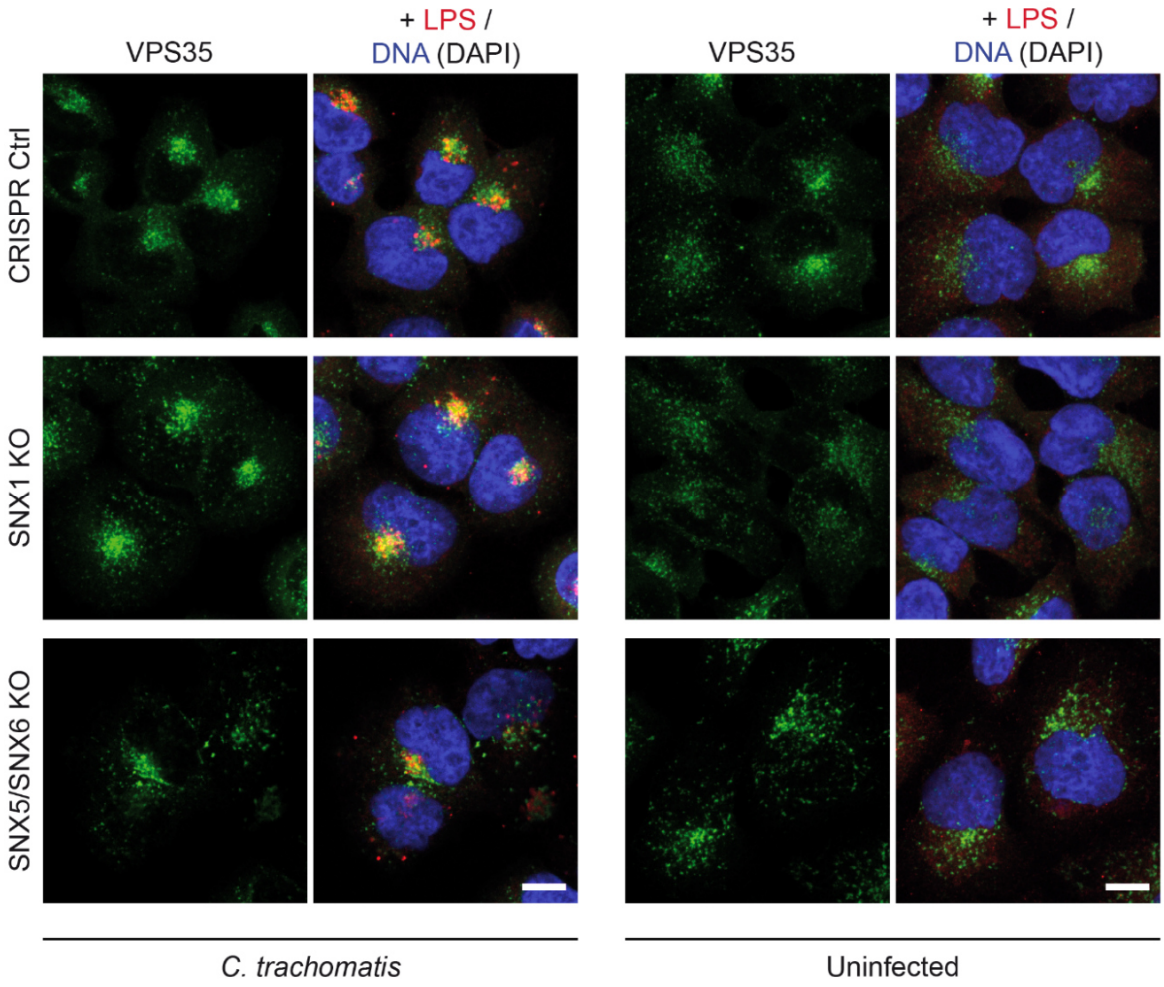

Figure 27. Clustering of VPS35 at the MTOC at 8 h p.i. is affected in *C. trachomatis* infected SNX5/SNX6 double knockout cell line.
Confocal IF images showing *C. trachomatis* L2 infected CRISPR Ctrl, SNX1 single and SNX5/SNX6 double knockout cell lines (MOI 10) visualised at 8 h p.i.. Cells were fixed at 8 h p.i. and immunostained with indicated antibodies and DAPI (DNA). VPS35 (green) was immunostained to visualise retromer component and LPS (red) was immunostained to localise *C. trachomatis*. Localisation analysis using cLSM, MIP, Scale bar, 10 µm, Representative images shown for n=2.

3.1.4 Summary of early *C. trachomatis* infection

At the early infection stage, *C. trachomatis* is trafficked towards the MTOC. In parallel, both, SNX-BARs of the membrane-sensing and VPS35 of the cargo-recognition complex of the host-cellular retromer accumulated at the MTOC adjacent to *C. trachomatis*. Moreover, we observed early SNX tubular structures. Early trafficking and the formation of tubular structures were dependent on microtubules. By use of CRISPR/Cas9-mediated KO of SNX-BARs, we analysed the function of SNX-BARs during early *C. trachomatis* infection. Uptake of *C. trachomatis* into the cell and early *C. trachomatis* trafficking were not affected in SNX1 and SNX5 KO but were affected in SNX5/SNX6 KO suggesting dependence of early *C. trachomatis* trafficking on SNX5/SNX6.

3.2 SNX recruitment during mid-infection

The membrane-binding subcomplex comprises a dimer of SNX-BARs which mediates recruitment of the retromer to endosomes (Bonifacino and Hurley 2008). SNX-BARs are composed of two domains with distinct functions. The N-terminal PX domain most commonly binds to PI3P-rich endosomal membranes though PIP-binding profile of SNX PX domains are discussed to vary (Teasdale and Collins 2012). The C-terminal BAR domain is a dimerisation motif. In addition, this domain senses membrane curvature and drives membrane tubulation.
Aeberhard et al. showed that in *C. trachomatis* L2 infected cells at mid-infection, endogenous SNX1 and SNX2 as well as transiently expressed eGFP-SNX5 and eGFP-SNX6 localised on the inclusion and in part co-localised with the inclusion membrane protein IncA (Aeberhard et al. 2015). Aeberhard et al. postulated at least a partial separation of the retromer complex at mid-infection time point since VPS35 and the retromer's cargo CI-MPR did not show a rim-like inclusion-staining pattern. VPS35 and CI-MPR localised in small punctuate pattern adjacent to the inclusion. Moreover, Aeberhard et al. observed tubular structures emanating from the inclusion. These structures were positive for SNX-BARs and IncA. Recruitment of SNX-BARs was examined in parallel by Mirrashidi et al. (Mirrashidi et al. 2015). Therein, endogenous SNX1, SNX2, SNX6 and transiently expressed FLAG-SNX5 co-localised with the inclusion membrane protein IncE.
C. trachomatis serovar D differs to serovar L2 in that way as it forms substantial more tubular structures which are in addition considerably longer (data not quantified). Because of that, we used *C. trachomatis* D, unless stated otherwise, to study mid-infection time points. Furthermore, we addressed which functional SNX-BAR protein domain mediates recruitment to the inclusion. By using our generated KO cell lines, we aimed to gain a deeper understanding of the function of SNX recruitment. Finally, we focussed on SNX1-interacting proteins in order to deduce a role for SNX recruitment.

3.2.1 Localisation of SNX-BARs of the retromer

Analogously to data from Aeberhard et al. we analysed the localisation of endogenous SNX-BARs at mid-infection of *C. trachomatis* D. HeLa cells were infected with *C. trachomatis* or left uninfected for 36 h and cells were stained for one of each SNX-BARs and the inclusion membrane protein IncE (Figure 28). In uninfected cells, endogenous SNX-BARs localised in disperse punctuate pattern in the cytosol consistent with reported endosomal localisation of SNX proteins (Aeberhard et al. 2015). In cells infected with *C. trachomatis* in contrast, SNX-BARs clearly localised around the chlamydial inclusion in a rim-like pattern and at least in part co-localised with the inclusion membrane protein IncE suggesting specific recruitment of SNX-BARs. Recruitment of SNX-BARs did not differ between *C. trachomatis* serovars L2 and D (data not shown) suggesting no species-specific but host-specific recruitment. In addition, tubular structures emanating from the inclusion were positive for both, SNX-BARs and the inclusion membrane protein IncE.

In sum, SNX-BARs were recruited to the inclusion of *C. trachomatis* and host-cellular SNX-BARs and chlamydial IncE localised along tubular structures.

A

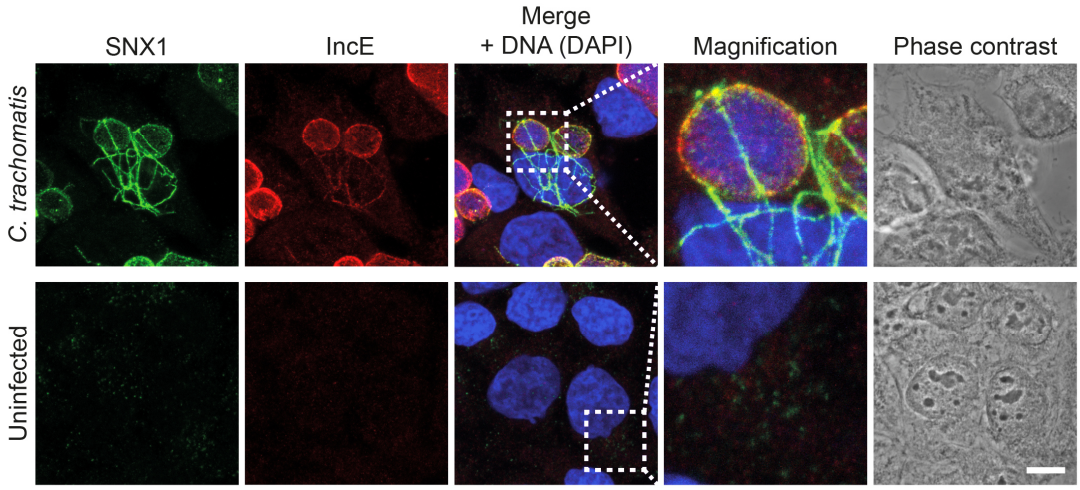
SNX1
IncE
Merge
+ DNA (DAPI)
Magnification
Phase contrast
C. trachomatis
Uninfected

B

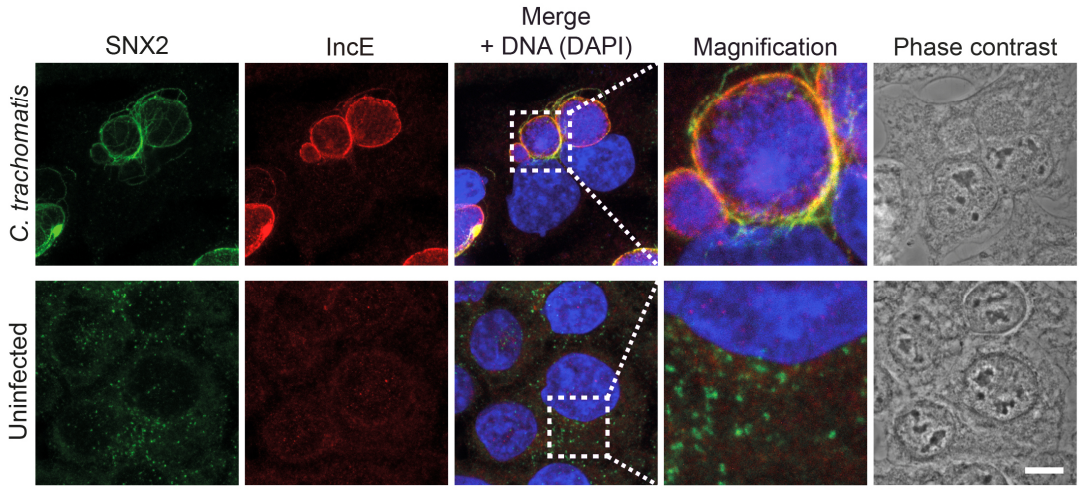
SNX2
IncE
Merge
+ DNA (DAPI)
Magnification
Phase contrast
C. trachomatis
Uninfected

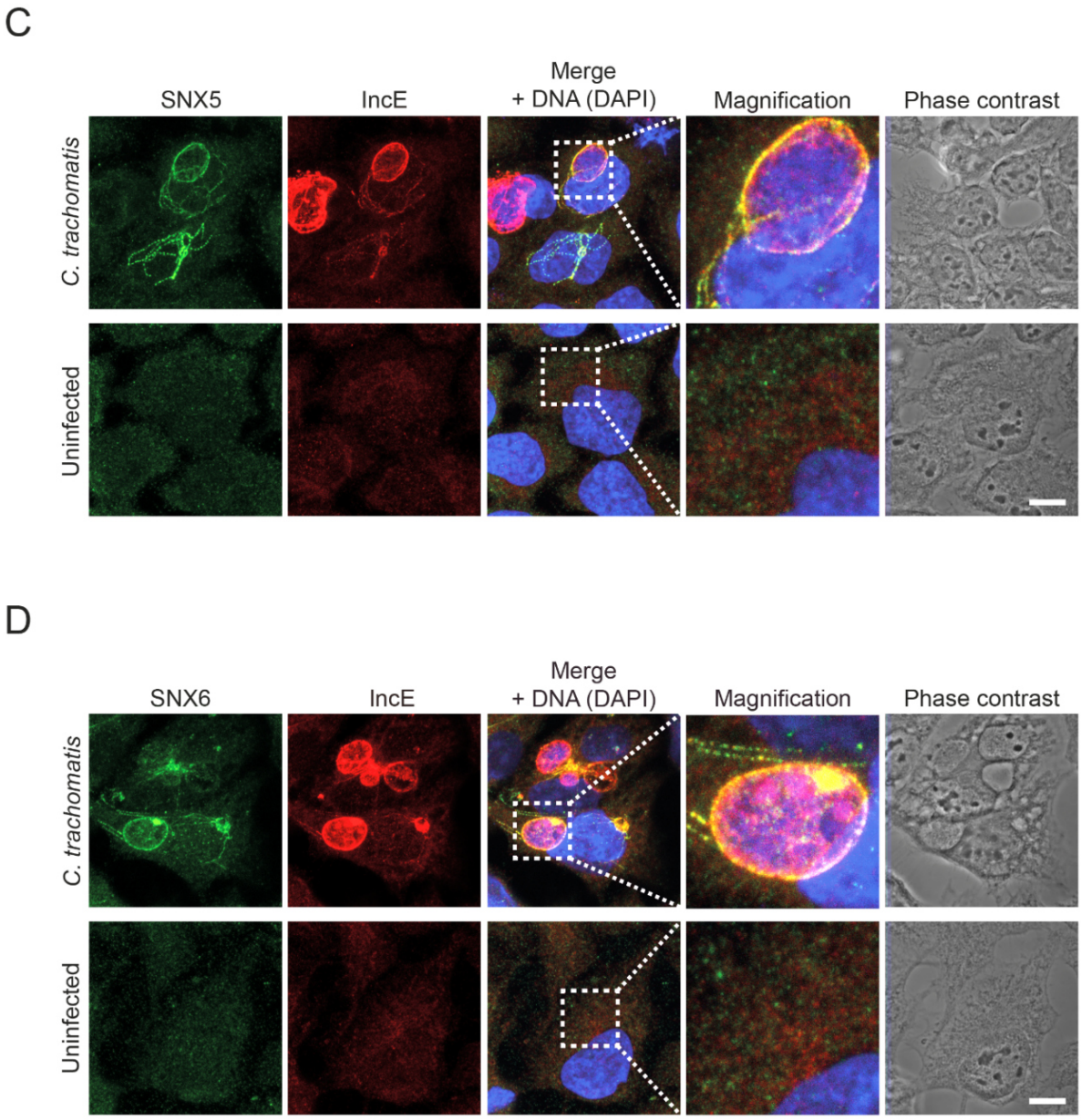

Figure 28. SNX-BARs are recruited to *C. trachomatis* inclusions at mid-infection.
Confocal IF images showing localisation of SNX-BARs in *C. trachomatis* D infected HeLa cells (MOI 2) visualised at 36 h p.i.. Cells were fixed 36 h p.i. and stained with indicated antibodies and DAPI. (A) SNX1, (B) SNX2, (C) SNX5 and (D) SNX6 (green) were immunostained to analyse localisation of membrane-sensing subcomplex. IncE (red) was immunostained to visualise localisation of chlamydial inclusion. Merge depicts SNX-BARs, IncE and DNA (DAPI). At mid-infection time point, SNX-BARs localised on the inclusion. Localisation analysis using cLSM, MIP; Scale bar, 10 µm; Representative images shown for n=2.

3.2.2 Localisation of the cargo-recognition complex protein VPS35

Next, we assessed whether the two subcomplexes of the retromer are separated at mid-infection with *C. trachomatis* D as postulated for *C. trachomatis* L2 by Aeberhard et al. (Aeberhard et al. 2015).

HeLa cells were infected with *C. trachomatis* D or left uninfected for 24 h and co-stained for VPS35 and SNX-BARs (Figure 29). In uninfected cells, VPS35 is localised in a punctuate

pattern as observed for SNX-BARs (SNX1, SNX2, SNX5 and SNX6) (Figure 29 A-D). VPS35 and SNX-BARs localised in close proximity. In infected cells, in contrast, we observed a separation of the signals from VPS35 and SNX-BARs. VPS35 localised in a punctuate pattern adjacent to the inclusion while SNX-BARs localised on the inclusion (Figure 29 A-D). Moreover, tubular-structures emanating from the inclusion were positive for SNX-BARs but not for VPS35 suggesting specific recruitment of SNX-BARs or of the membrane-binding subcomplex.

In sum, SNX-BARs of the membrane-binding subcomplex localised on the chlamydial inclusion while VPS35 being a component of the cargo-recognition subcomplex localised in a punctuate pattern adjacent to the inclusion. This suggests a separation of the two subcomplexes at mid-infection.

A

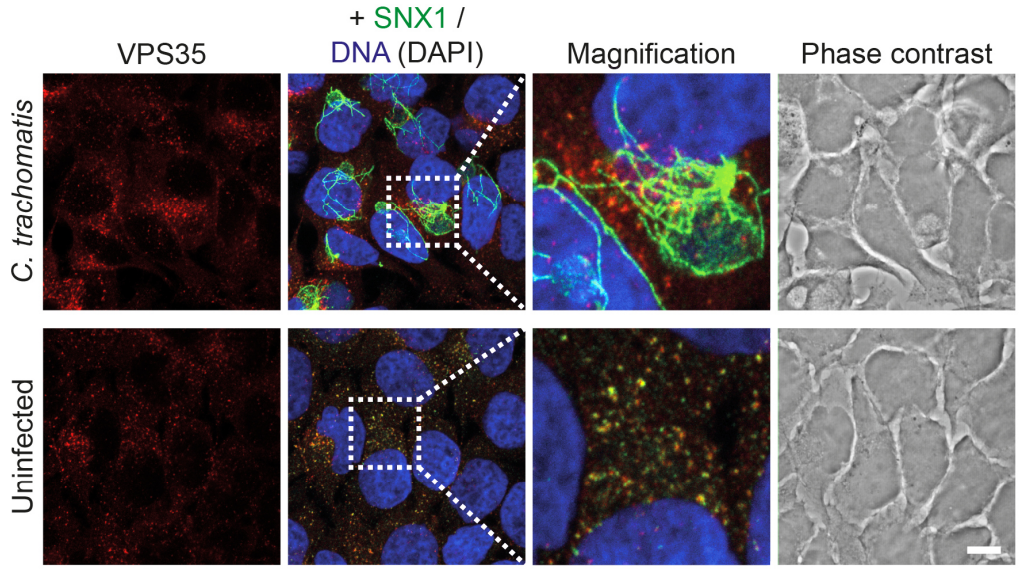
VPS35
+ SNX1 /
DNA (DAPI)
Magnification
Phase contrast
C. trachomatis
Uninfected

B

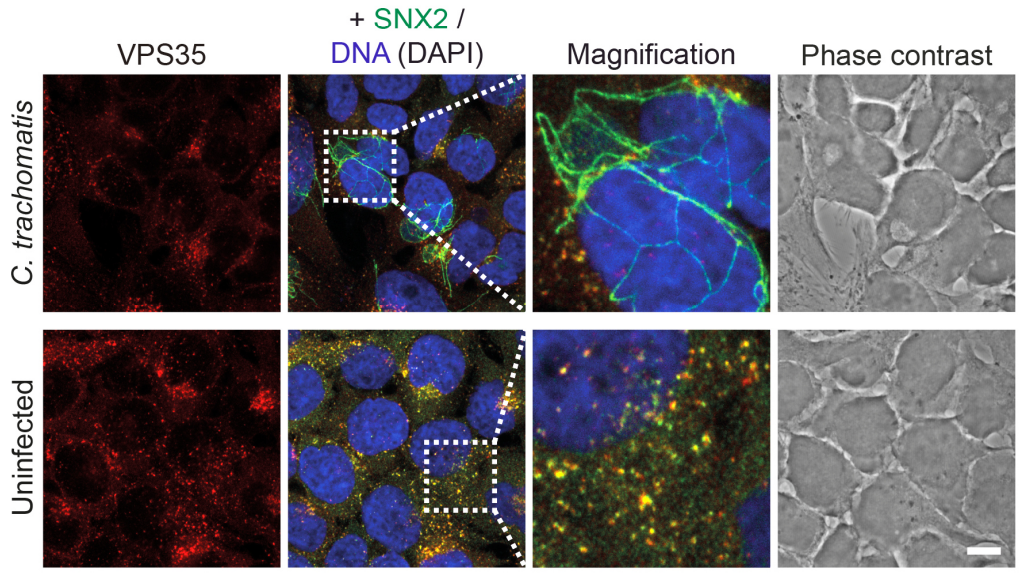
VPS35
+ SNX2 /
DNA (DAPI)
Magnification
Phase contrast
C. trachomatis
Uninfected

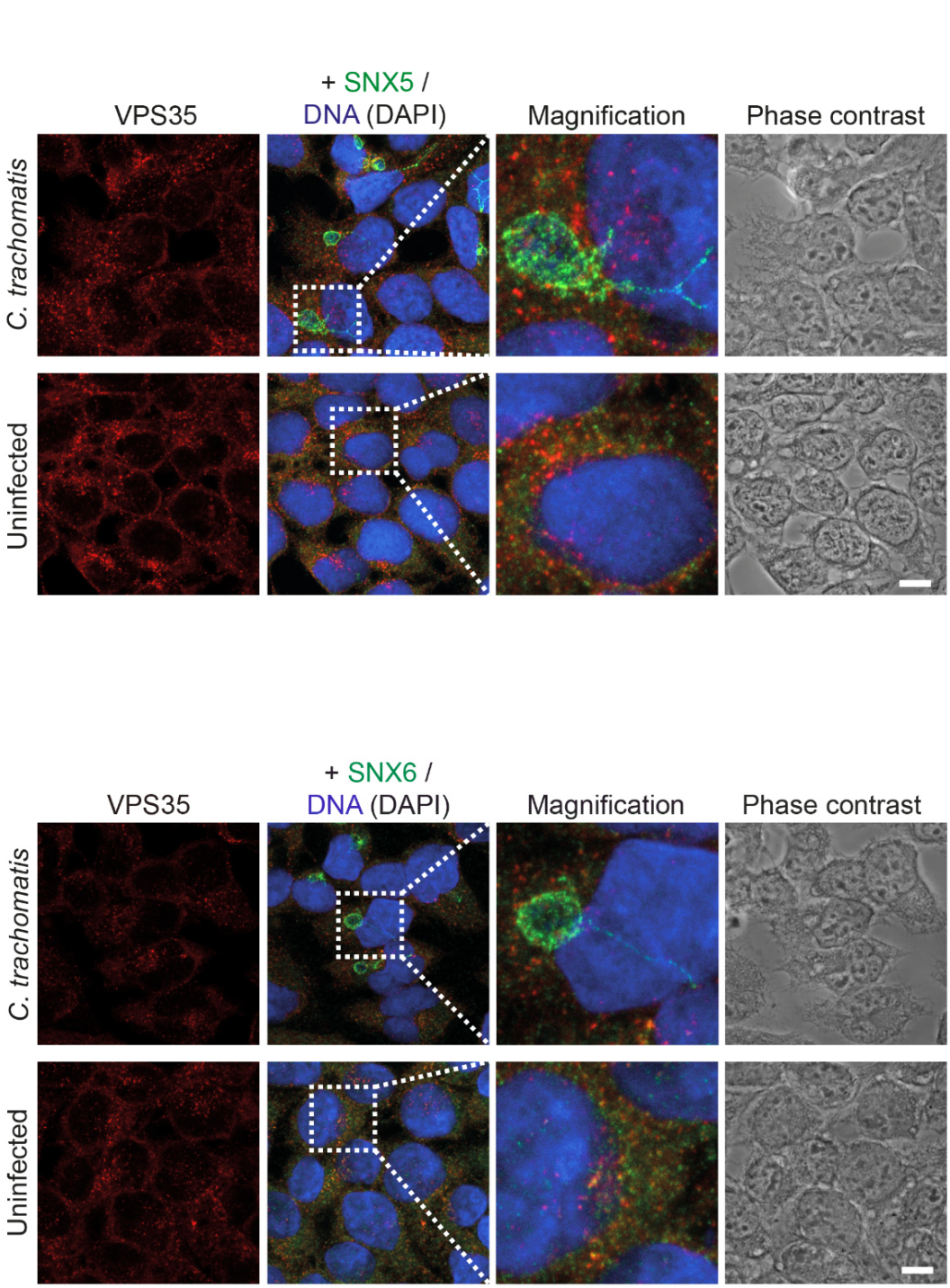

Figure 29. VPS35 localises in a punctuate pattern adjacent to the chlamydial inclusion. Confocal IF images showing localisation of VPS35 in *C. trachomatis* D infected HeLa cells (MOI 2) visualised at 24 h p.i.. Cells were fixed 24 h p.i. and stained with indicated antibodies and DAPI. (A) SNX1, (B) SNX2, (C) SNX5 and (D) SNX6 (green) were immunostained to analyse localisation of membrane-sensing subcomplex. VPS35 (red) was immunostained to visualise localisation of cargo-selective subcomplex component. Merge depicts SNX-BARs, VPS35 and DNA (DAPI). At mid-infection time point, membrane-sensing and cargo-selective subcomplex of the retromer are separated. Localisation analysis using cLSM, MIP; Scale bar, 10 µm; Representative images shown for n=2.

3.2.3 Localisation of SNX functional domains

To assess whether functional domains are solely sufficient to localise properly on the inclusion membrane, we examined the localisation of full length SNX-BARs and their domains during *C. trachomatis* infection. We generated a set of SNX fusion proteins that considered functional features (Figure 30 A). To study subcellular protein localisation of fluorescent eGFP fused to either full length SNXs or SNX protein domains, HeLa cells were infected with *C. trachomatis* or left uninfected for 24 h and transiently expressed eGFP-SNX fusion proteins. Cells were stained for the inclusion membrane protein IncA (Figure 30 B).

In uninfected cells, signals for full length SNXs localised in punctuate structures in the cytosol consistent with the reported endosomal localisation of endogenous SNX proteins by Aeberhard et al. and Mirrashidi et al. (data not shown). In *C. trachomatis* infected cells, expression of eGFP control exhibited disperse localisation in the cytosol omitting the area of inclusion (Figure 30 B). In infected cells transiently expressing full length eGFP-SNX1, eGFP-SNX2, eGFP-SNX5 and eGFP-SNX6 fusion proteins, SNXs localised on the inclusion confirming recruitment of endogenous SNXs at mid-infection (see 3.2.1). Interestingly, SNX1 and SNX2 BAR domains localised on the inclusion while SNX1 and SNX2 PX domains did not. As opposite to SNX1 and SNX2, SNX5 and SNX6 PX domains localised on the inclusion while SNX5 and SNX6 BAR domains did not. In addition, full length eGFP-SNX fusion proteins as well as domains that were specifically recruited to the inclusion at least in parts co-localised with the inclusion membrane protein IncA.

In sum, BAR domains but not PX domains of SNX1 and SNX2 were recruited to the inclusion whereas PX domains but not BAR domains of SNX5 and SNX6 localised on the inclusion.

A

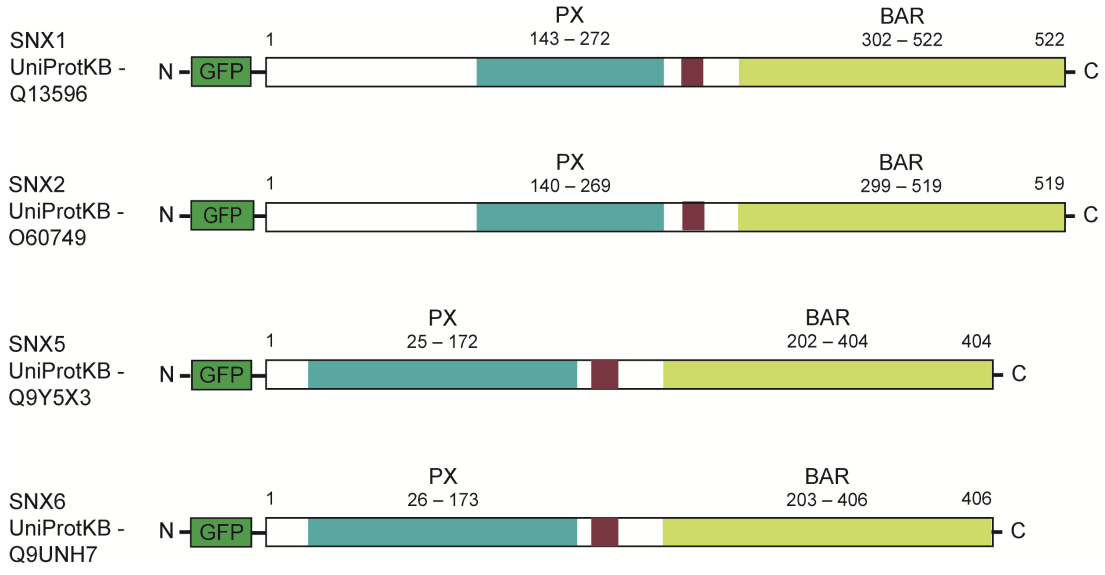

B

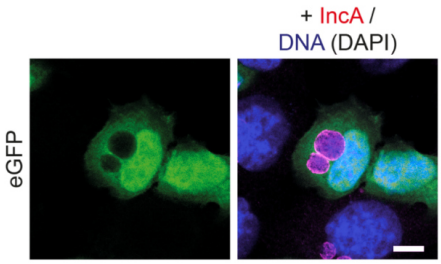
+ IncA /
DNA (DAPI)
eGFP

C

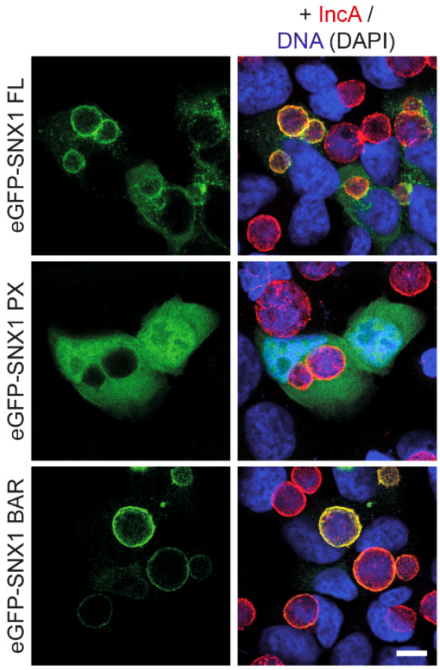
+ IncA /
DNA (DAPI)
eGFP-SNX1 FL
eGFP-SNX1 PX
eGFP-SNX1 BAR

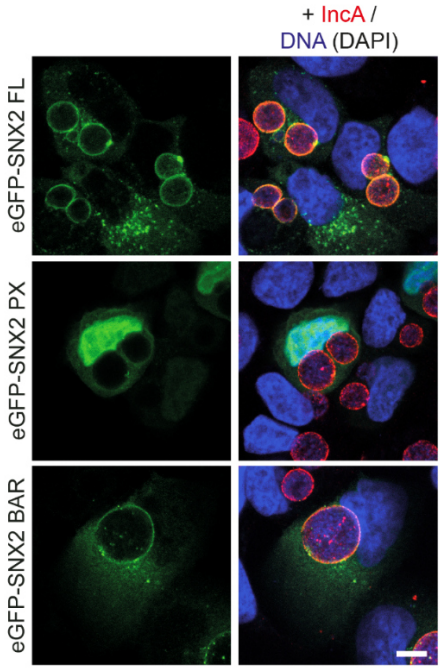
+ IncA /
DNA (DAPI)
eGFP-SNX2 FL
eGFP-SNX2 PX
eGFP-SNX2 BAR

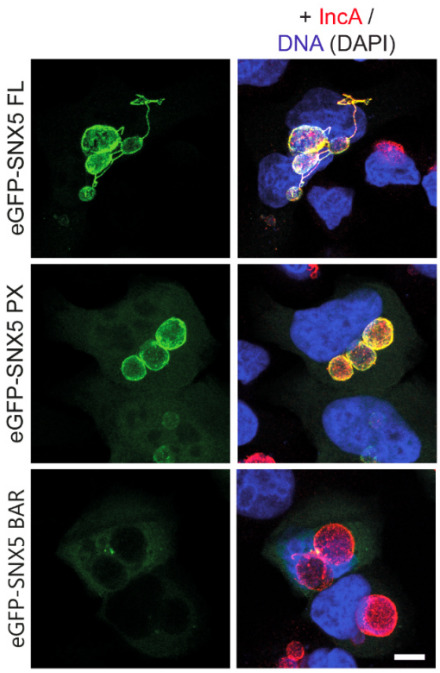
+ IncA /
DNA (DAPI)
eGFP-SNX5 FL
eGFP-SNX5 PX
eGFP-SNX5 BAR

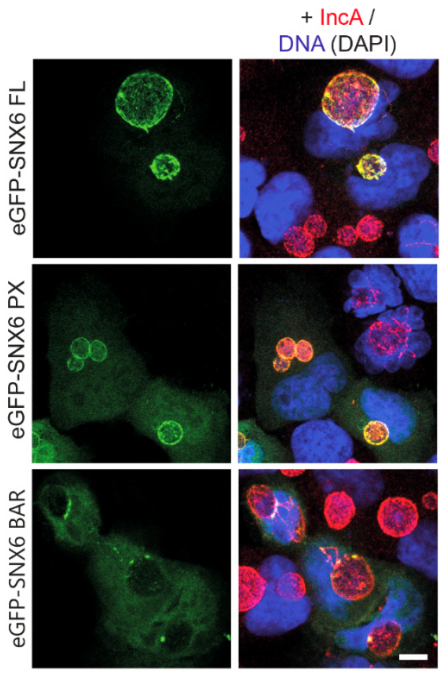
+ IncA /
DNA (DAPI)
eGFP-SNX6 FL
eGFP-SNX6 PX
eGFP-SNX6 BAR

Figure 30. Domain-specific localisation of SNX-BARs on the chlamydial inclusion.
(A) Schematic illustration of SNX-BAR fusion proteins cloned into pEGFP-C1 backbone vector enabling expression of N-terminally eGFP-tagged fusion proteins. Full length or functional domains of SNX-BARs of the human retromer were cloned by sticky end cloning. Numbers indicate the number of amino acids. (B) Confocal IF images showing HeLa cells transiently expressing eGFP control infected with *C. trachomatis* L2 (MOI 2). Cells were fixed 24 h p.i. and immunostained with IncA and DAPI. IncA (red) was immunostained to visualise *C. trachomatis* inclusions. Merge depicts eGFP, IncA and DNA (DAPI). Localisation analysis using cLSM, Scale bar, 10 µm; Representative images shown for n=3. *Localisation analysis of eGFP performed by Stefanie Lüth, RKI Berlin*. (C) Confocal IF images showing HeLa cells transiently expressing SNX-BAR full length or functional domain fusion proteins infected with *C. trachomatis* L2 (MOI 2). Cells were fixed 24 h p.i. and immunostained with IncA and DAPI. IncA (red) was immunostained to visualise *C. trachomatis* inclusions. Merge depicts SNX-BARs, IncA and DNA (DAPI). *Localisation analysis of eGFP-SNX1 FL, PX, BAR and eGFP-SNX6 FL, PX, BAR fusion proteins performed by Stefanie Lüth, RKI, Berlin.* FL: full length, Localisation analysis using cLSM; Scale bar, 10 µm; Representative images shown for n=3.

In conclusion, we observed domain-specific recruitment of SNX-BARs as PX domain of SNX5 and SNX6 and BAR domain of SNX1 and SNX2 localised on the inclusion (Table 31). Hence, we hypothesised that SNX5 and SNX6 bind to an inclusion membrane protein via their PX domain and that SNX1 and SNX2 dimerise with the BAR domains of SNX5 and SNX6.

Table 31. Overview of the domain-specific localisation of SNX-BARs at the chlamydial inclusion. SNX1 and SNX2 BAR domain localised on the chlamydial inclusion. SNX5 and SNX6 PX domain localised on the inclusion.

SNX protein	PX domain	BAR domain
SNX1	-	+
SNX2	-	+
SNX5	+	-
SNX6	+	-

Next, we focussed on the co-localisation of IncE with eGFP-SNX5 and eGFP-SNX1 in more detail, as eGFP-SNX6 and eGFP-SNX2 revealed a similar phenotype as eGFP-SNX5 and eGFP-SNX1, respectively (Figure 31). HeLa cells were infected with *C. trachomatis* or left uninfected for 36 h and transiently expressed either eGFP-SNX5 or eGFP-SNX1 fusion proteins. Cells were stained for inclusion membrane protein IncE (Figure 31). Both, eGFP-SNX5 and eGFP-SNX1 were recruited to the inclusion and in part co-localised with IncE at mid-infection (Figure 31 A) confirming previous findings of endogenous SNX5 and SNX1 being recruited to the chlamydial inclusion. In addition, we observed co-localisation of IncE and eGFP-SNX fusion proteins at tubular structures emanating from the inclusion (Figure 31 B). Besides partial co-localisation at tubular structures, we observed an alternating localisation pattern of IncE and eGFP-SNX proteins which was more distinct when magnifying the image section.

In sum, eGFP-SNX1 and eGFP-SNX5 were recruited to the chlamydial inclusion and at least in part co-localised with postulated interaction partner IncE consistent with the findings by Mirrashidi et al. (Mirrashidi et al. 2015).

A

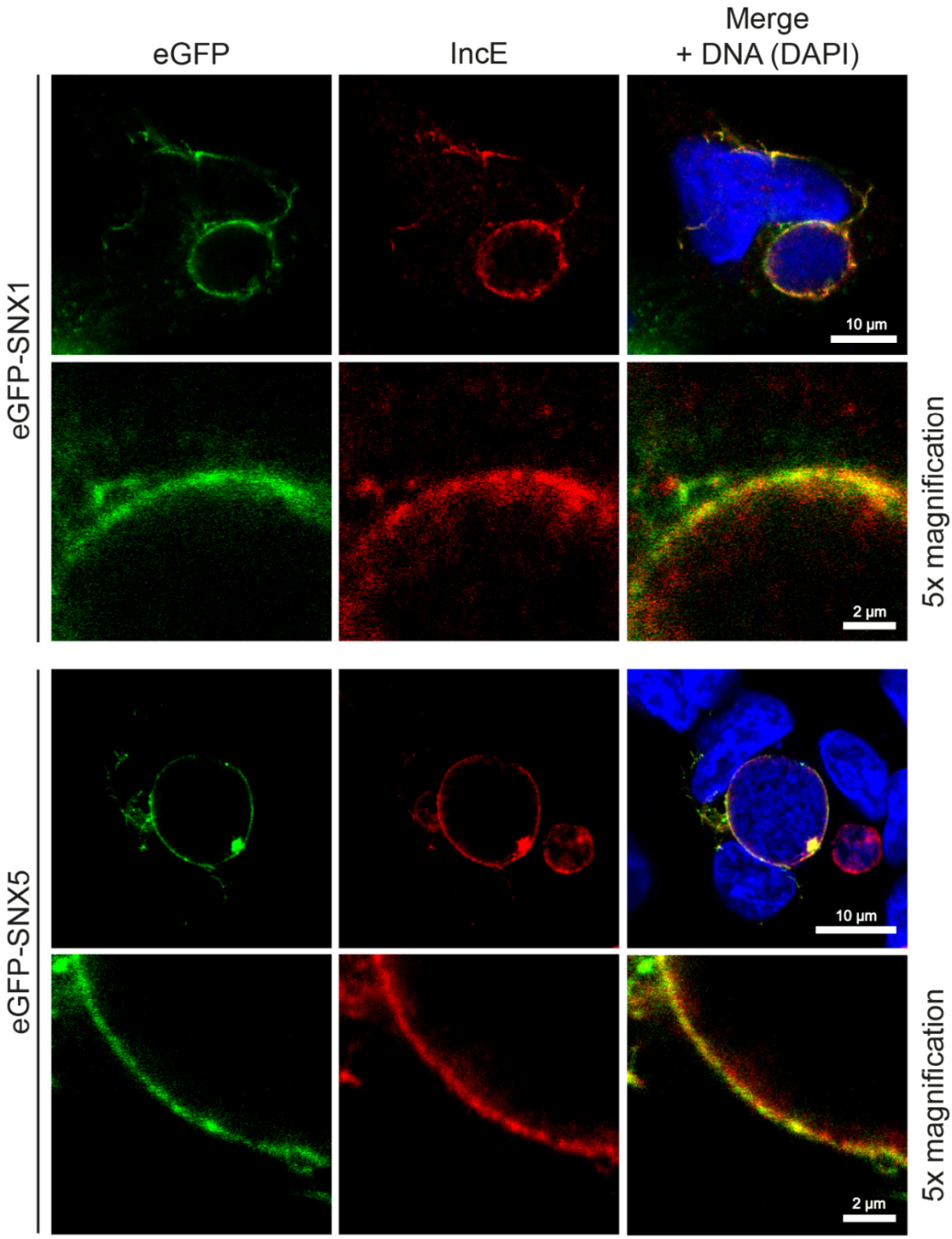

B

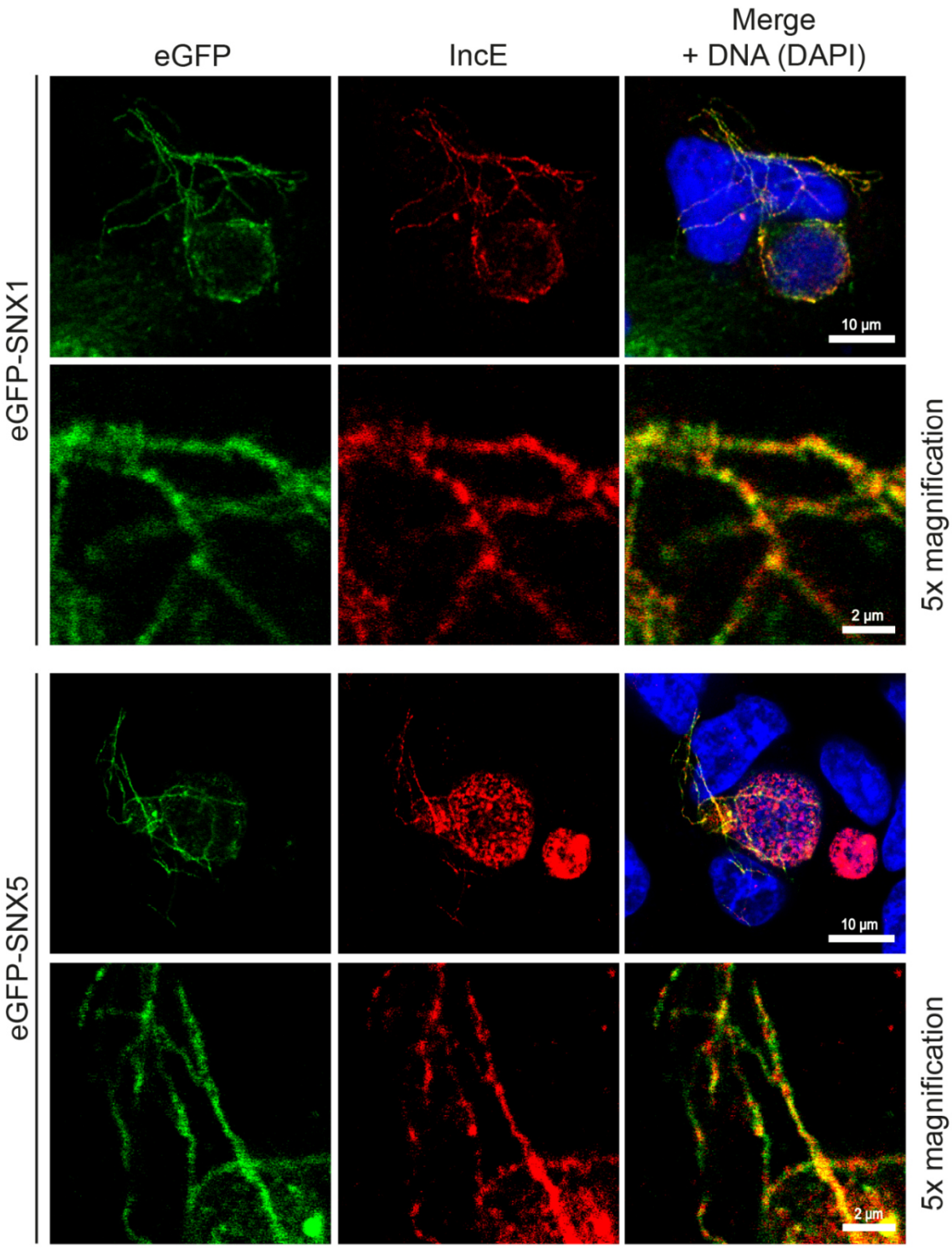

Figure 31. SNX1 and SNX5 fusion proteins in part co-localise with IncE.
(A) Confocal IF images showing localisation of HeLa cells transiently expressing eGFP-SNX1 and eGFP-SNX5 infected with *C. trachomatis* D (MOI 2) visualised at 36 h p.i.. Cells were fixed 36 h p.i. and immunostained with IncE and DAPI. IncE (red) was immunostained to visualise *C. trachomatis* inclusions and tubular structures. Merge depicts eGFP-SNX1 or eGFP-SNX5, IncA and DNA (DAPI). Images focus on inclusion membrane visualising co-localisation of SNX1 and SNX5 fusion proteins with IncE. Localisation analysis using cLSM, MIP; Representative images shown for n=2. *Experiment performed by Stefanie Lüth, RKI Berlin*. (B) Confocal IF images showing localisation of HeLa cells transiently expressing eGFP-SNX1 and eGFP-SNX5 infected with C. trachomatis D (MOI 2) visualised at 36 h p.i.. Cells were fixed 36 h p.i. and immunostained with IncE and DAPI. IncE (red) was immunostained to visualise *C. trachomatis* inclusions and tubular structures. Merge

depicts eGFP-SNX1 or eGFP-SNX5, IncA and DNA (DAPI). Images focus on tubular structures visualising alternating protein pattern of SNX1 or SNX5 and IncE. Localisation analysis using cLSM, MIP; Representative images shown for n=2. *Experiment performed by Stefanie Lüth, RKI Berlin*.

Recruitment of SNX1 and SNX2 to the inclusion is absent in SNX5/SNX6 knockout cell lines

Having shown distinct recruitment of host cellular SNX-BARs to the chlamydial inclusion, we aimed to elucidate a mutual effect of either SNX single or double KO on the SNX-BAR localisation. For this purpose, cells were infected with *C. trachomatis* for 36 h and stained for IncE and SNX-BARs. In infected cells, all SNX-BARs were recruited to the chlamydial inclusion (data not shown). In SNX1 and SNX5 single KO cell lines, SNX-BARs were recruited to the inclusion and SNX-BARs at least in part co-localised with IncE (Figure 32). In addition, tubular structures positive for inclusion membrane protein IncE and SNX-BARs were visible. In SNX5/SNX6 KO cell line, localisation of SNX1 and SNX2 on the inclusion was absent (Figure 33). However, tubular structures positive for IncE were yet evident (Figure 33).

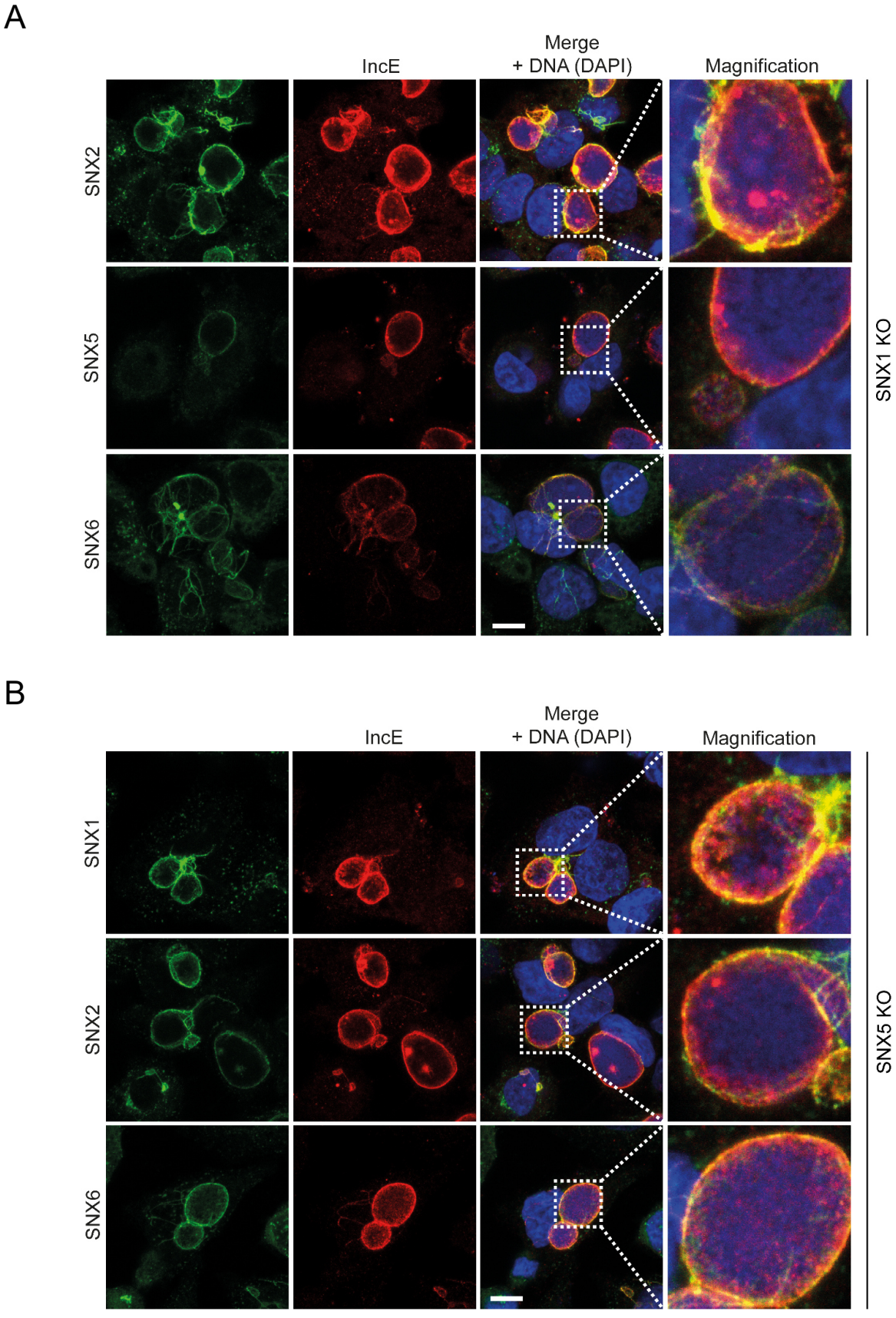

Figure 32. Recruitment of SNX-BARs is not affected in SNX1 and SNX5 single knockout cell lines.

(A) Confocal IF images showing localisation of SNX-BARs in HeLa cells infected with *C. trachomatis* D (MOI 2) visualised at 36 h p.i.. Cells were fixed 36 h p.i. and immunostained with SNX1, SNX2, SNX5 or SNX6 (green), IncE (red) and DAPI (DNA). SNX proteins were immunostained to visualise

retromer components. IncE (red) was immunostained to visualise *C. trachomatis* inclusions. Merge depicts SNX, IncE and DNA (DAPI). Localisation analysis using cLSM, MIP; Scale bar, 10 µm; Representative images shown for n=3.

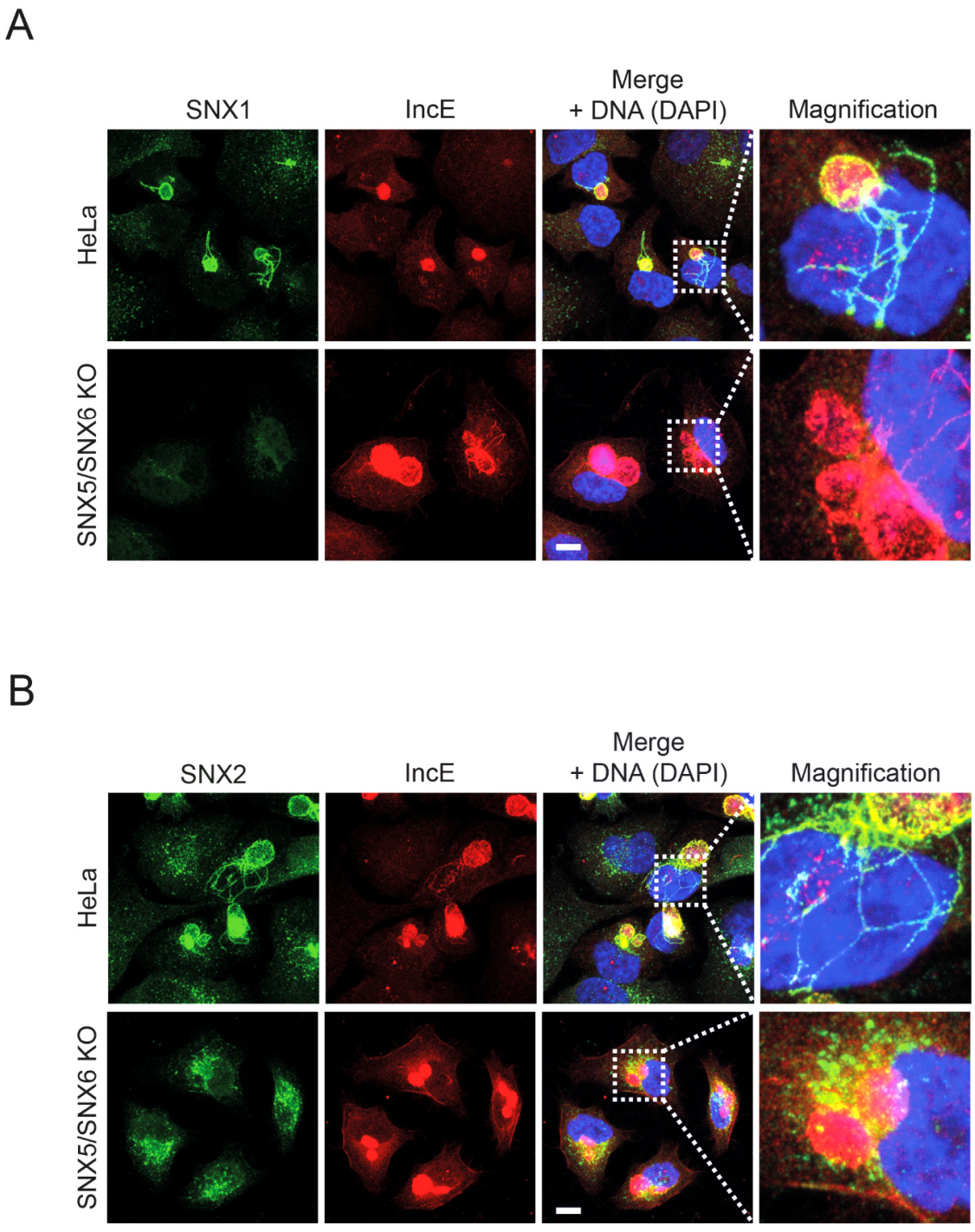

Figure 33. Recruitment of SNX1 and SNX2 is lost in SNX5/SNX6 knockout cell line.
Confocal IF images showing localisation of SNX1 and SNX2 in HeLa and SNX5/SNX6 double knockout cell line infected with *C. trachomatis* D (MOI 2) visualised at 24 h p.i.. Cells were fixed 24 h p.i. and immunostained with (A) SNX1 or (B) SNX2 (green), IncE (red) and DAPI (DNA). SNXs were immunostained to visualise retromer components. IncE (red) was immunostained to visualise *C. trachomatis* inclusions. Merge depicts SNX, IncE and DNA (DAPI). Localisation analysis using cLSM, MIP; Scale bar, 10 µm; Representative images shown for n=2.

3.2.4 *C. trachomatis* primary infection and infectious progeny formation in SNX KO cell lines

Depletion of SNX-BARs in the studies by Aeberhard et al. and Mirrashidi et al. suggested that SNX-BARs may function distinctly and that SNX5 and SNX5/SNX6, in particular, restrict *C. trachomatis* infection during mid-infection. Based on these findings, we examined *C. trachomatis* primary infection and infectious progeny formation in a more robust system in SNX-BAR KO cells than in SNX-BAR depleted cells.

C. trachomatis primary infection

To assess *C. trachomatis* primary infection in HeLa, CRISPR Ctrl and SNX KO cell line, cells were infected with *C. trachomatis* for 36 h and stained for chlamydial Hsp60 which belongs to a class of ubiquitous and evolutionary conserved chaperonins (Cappello et al. 2009). Primary infection as analysed by inclusion formation (ratio inclusions per nucleus; for ImageJ script see appendix) in HeLa, CRISPR Ctrl and SNX single KO cell lines resulted in inclusions per nucleus between 0.1 and 0.2 at an MOI 0.1 and inclusions per nucleus between 0.5 and 0.8 at an MOI 1, exhibiting no distinct differences (Figure 34 A). In SNX5/SNX6 KO cell line, primary infection increased by a factor of 3 at MOI 0.1. At an MOI 1, in SNX5/SNX6 KO cell line, primary infection increased by a factor of 1.4 (Figure 34 B).
In sum, loss of SNX1 or SNX5 did not affect primary infection regardless of the MOI. In contrast, loss of SNX5/SNX6 resulted in an increase in primary infection at an MOI 0.1 and 1.

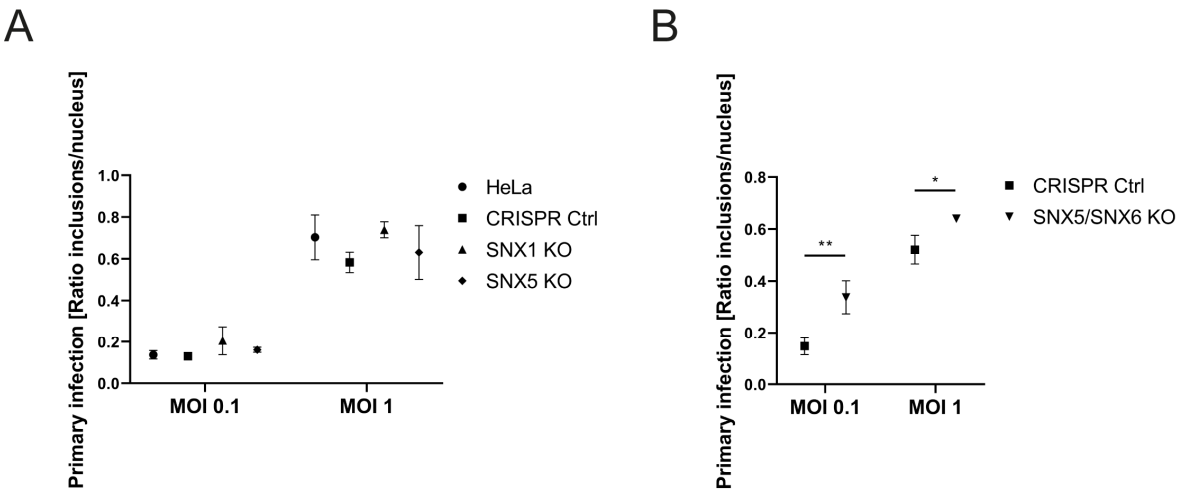

Figure 34. *C. trachomatis* primary infection in SNX single and double KO cell lines.
(A) Analysis of *C. trachomatis* D primary infection (inclusions per nucleus) (MOI 0.1 and MOI 1) in HeLa, CRISPR Ctrl, SNX1 and SNX5 single knockout cell lines at 36 h p.i.. Epifluorescence images of inclusions per cell in at least 8 fields of view per cell line were quantified using ImageJ (mean ±SD, n=3; 2way ANOVA, Sidak's multiple comparisons test). (B) Analysis of *C. trachomatis* D primary infection (inclusions per nucleus) (MOI 0.1 and MOI 1) in CRISPR Ctrl, SNX5/SNX6 double knockout cell lines. Epifluorescence images of Inclusions per cell in at least 8 fields of view per cell line were quantified using ImageJ (mean ±SD, n=3; 2way ANOVA, Sidak's multiple comparisons test, * indicates p-value < 0.05, ** indicates p-value < 0.005).

To examine *C. trachomatis* replication in SNX KO, we determined the genome copy number (chlamydial DNA) by quantitative real-time PCR with obtained lysates of infected HeLa, CRISPR Ctrl and SNX KO cell line at 72 h p.i. after completion of one round of a developmental cycle of *C. trachomatis* serovar D (Figure 35). Genome copy number increased in SNX1 (twofold increase) but not in SNX5 KO cell line (Figure 35 A). Moreover, we observed a more profound increase of genome copy number in SNX5/SNX6 KO cell line by a factor of 4.3 and 3 compared to HeLa and CRISPR Ctrl cells, respectively.

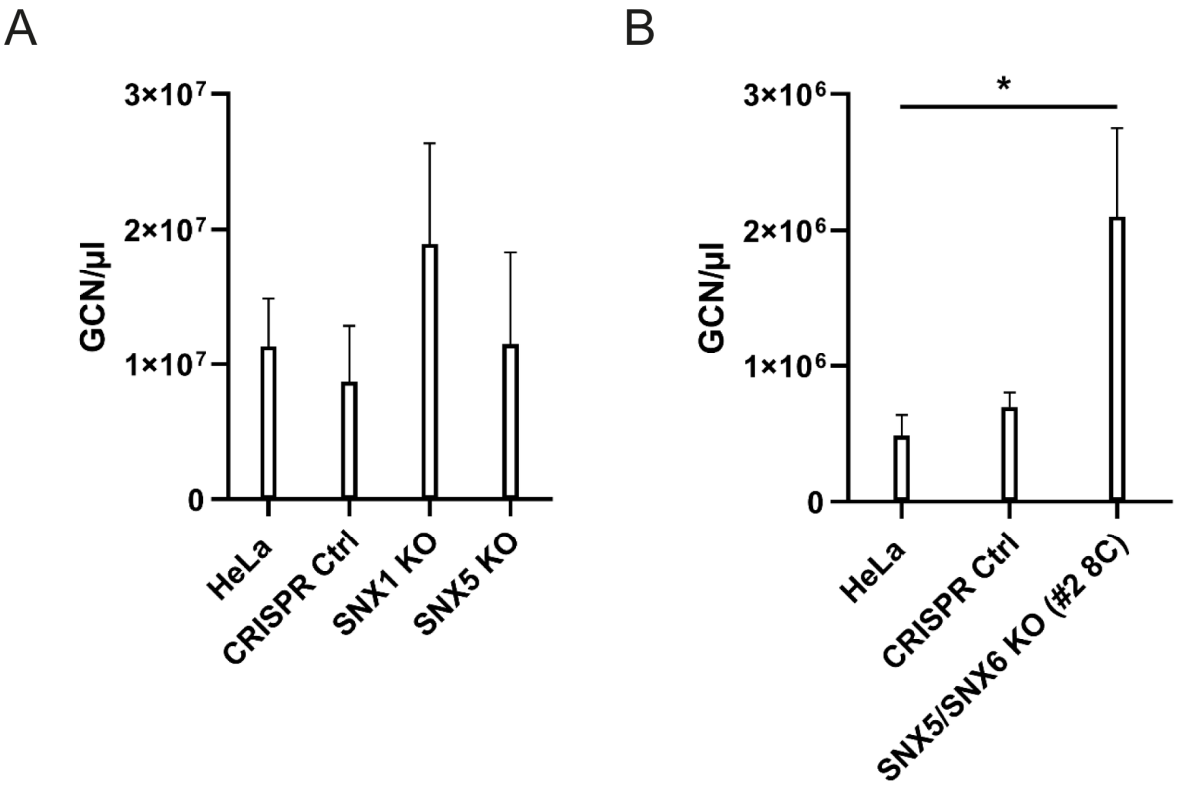

Figure 35. Loss of SNX5 and SNX6 promotes chlamydial replication.
(A) Analysis of bacterial genome copy numbers (GCN) in *C. trachomatis* D infected HeLa, CRISPR Ctrl, SNX1 and SNX5 single knockout cell lines (MOI 2) at 72 h p.i.. GCN was determined by qPCR (mean ±SD; n=3; Ordinary one-way ANOVA, Tukey's multiple comparison test). (B) Analysis of bacterial genome copy numbers (GCN) in *C. trachomatis* D infected CRISPR Ctrl and SNX5/SNX6 double knockout cell lines (MOI 2) at 72 h p.i.. GCN was determined by qPCR (mean ±SD, n=3, Kruskal-Wallis test, Dunn's multiple comparison test, * indicates p-value < 0.05).

C. trachomatis infectious progeny formation

To determine *C. trachomatis* infectious progeny formation in SNX KO cell lines, we performed a progeny formation assay (Figure 36). In brief, control (HeLa and CRISPR Ctrl) and SNX KO (SNX1, SNX5 and SNX5/SNX6 KO) cell lines were infected with *C. trachomatis* and lysed at 72 h p.i.. Fresh naïve HeLa cells were infected with serial dilutions of obtained lysates and subsequently, the infectious progeny was determined.

We determined progeny formation in single KO cell lines and observed a slight increase of infectious progeny in SNX1 KO cell line whereas SNX5 KO cell line revealed a slight decrease (Figure 36 A). In SNX5/SNX6 KO cell line, infectious progeny formation of *C. trachomatis* increased by a factor of 1.8 and 2.6 compared to Hela and CRISPR Ctrl cells, respectively.

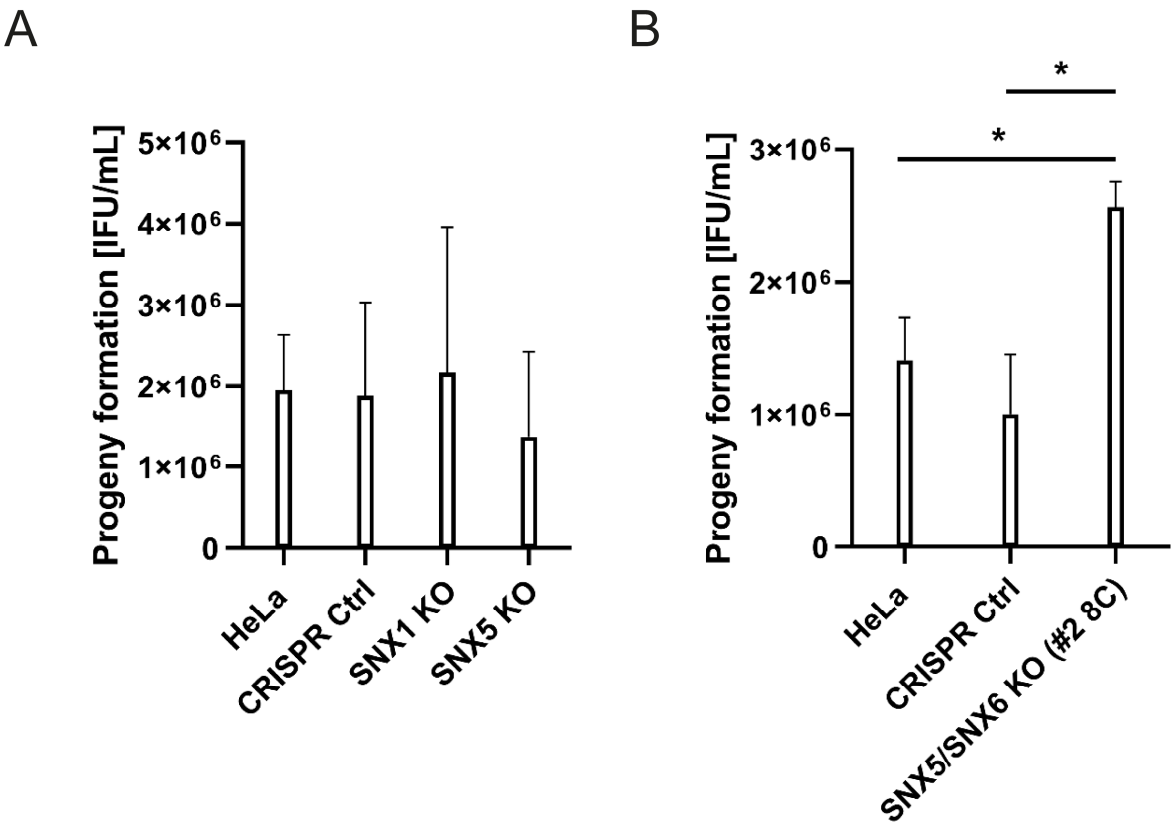

Figure 36. Loss of SNX5 and SNX6 promotes infectious progeny formation.
(A) Analysis of infectious progeny formation in *C. trachomatis* D infected HeLa, CRISPR Ctrl, SNX1 and SNX5 single knockout cell lines (MOI 2) at 72 h p.i.. Infectious progeny formation was determined by progeny formation assay (mean ±SD; n=3; Ordinary one-way ANOVA, Tukey's multiple comparison test). IFU: inclusion forming units. (B) Analysis of infectious progeny formation in *C. trachomatis* D infected CRISPR Ctrl and SNX5/SNX6 double knockout cell lines (MOI 2) at 72 h p.i.. Infectious progeny formation was determined by progeny formation assay (mean ±SD; n=3; Ordinary one-way ANOVA, Tukey's multiple comparison test, * indicates p-value < 0.05). IFU: inclusion forming units.

Taken together, KO of SNX5/SNX6 resulted in an increase of both, replication and infectious progeny formation while single KO of SNX5 had no effect on chlamydial replication but resulted in a slight decrease of progeny formation.

3.2.5 SNX tubules indicate ER structures

Ultrastructure of SNX tubular structures

Having observed prominent tubular structures by fluorescence microscopy which emanate from inclusions and which are positive for host cellular SNX-BARs and inclusion membrane proteins IncA/IncE, we addressed the ultrastructure by correlative light and electron microscopy (cLEM)

according to Madela et al. (Madela et al. 2014). In brief, HeLa cells seeded in live cell culture dishes were infected with *C. trachomatis* and transiently expressed eGFP-SNX5 fusion protein. First, positions of interest exhibiting eGFP-expressing infected cells were localised and documented by a confocal laser scanning microscope. Second, samples were chemically fixed, dehydrated and embedded, positions of interest were re-localised and trimmed for serial thin sectioning. Third, cells of interest were identified in sections at the transmission electron microscope (TEM) using the overview images documented before by confocal microscopy as described. Finally, confocal and TEM images taken from the serial sections were loaded in the TrakEM module of ImageJ and cross-faded to find matching correlation between fluorescence and ultrastructure pattern. The cLEM analysis revealed elongated tubular membranous structures as best match for the SNX-positive tubular fluorescence signal (Figure 37 A). Tubules were thin (30 - 100 nm in diameter) and seemed to be connected with each other when followed in successive sections. However, the technique of serial sectioning is limited in z-resolution and quality (e.g. section loss and deformation) which did not allow a reconstruction of the tubular network at sufficient quality. We never observed a connection between the lumen of the tubular membrane structures and the lumen of the inclusion.

To examine whether tubular membrane compartments are indeed positive for SNX-immunolabelling, we performed cLEM with high-pressure freezing (HPF) approach instead of chemical fixation (Figure 37 B). Here, HeLa cells seeded on sapphire discs were infected with *C. trachomatis* and transiently expressed eGFP-SNX5 fusion protein. Positions of interest were localised and documented by a cLSM followed by HPF. After freeze-substitution and pre-embedding, ultrathin sections of 60 - 70 nm were labelled with immunogold directed against GFP and sections were analysed with a TEM. As a result, data revealed tubular membranous structures by labelling of GFP with immunogold thereby confirming findings identified by cLEM using chemical fixation. Furthermore, these tubular structures had again a diameter of 30 to 100 nm and some of the tubular structures carried ribosomes.

In sum, elongated tubular SNX structures that emanate from the inclusion and that are positive at the ultrastructural level corresponded to membrane-bound tubules which are likely connected if not continuous.

A

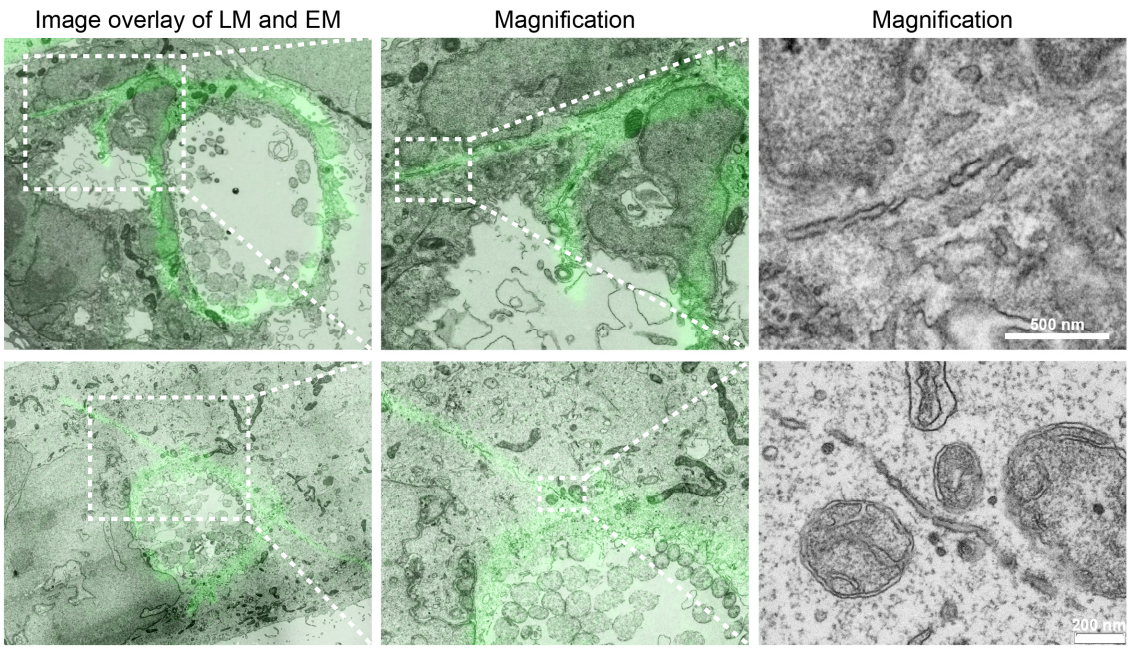
Image overlay of LM and EM
Magnification
Magnification
500 nm
200 nm

B

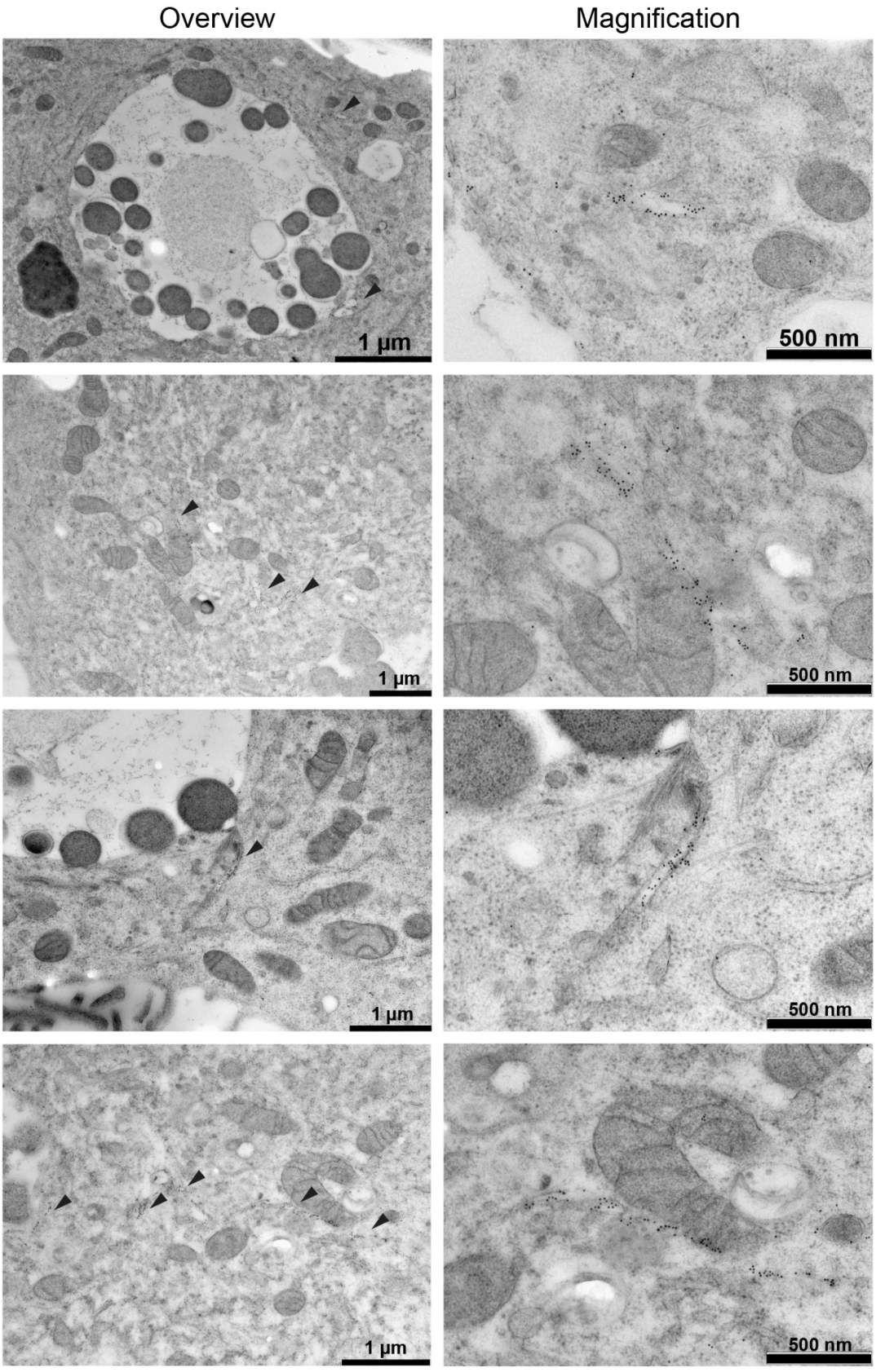

Figure 37. cLEM analysis of SNX tubular structures reveal thin membrane-bound tubules.
(A) TEM images of sections through HeLa cells infected with *C. trachomatis* L2 (MOI 0.5) and transiently expressing eGFP-SNX5 fusion protein. Cells were visualised at 32 h p.i. using a cLSM and chemically fixed prior to TEM. Two examples from different cells (upper and lower row), each

showing on section level from a section series through a target cell. LM: light microscopy; EM: electron microscopy; Representative images shown for n=2. *EM was performed by the Advanced light and electron microscopy facility of Michael Laue, RKI, Berlin*. (B) TEM images of anti-GFP immunogold labelled sections through HeLa cells infected with *C. trachomatis* D (MOI 1) and transiently expressing eGFP-SNX5 fusion protein. Cells were visualised at 24 h p.i. using a cLSM and high-pressure freezing prior to TEM; arrows in overview images point to immunogold labelled tubules; round black spots in magnification images = immunogold labelled GFP; n=1. *EM was performed by the Advanced Light and Electron Microscopy facility of Dr. Michael Laue, RKI, Berlin*.

Tubular structures are positive for ER marker RTN4

To verify whether tubular structures emanating from the inclusion are in part ER-related, we performed IF staining of Reticulon-4 (RTN4) in SNX5/SNX6 KO cell line as tubules positive for SNX1 and SNX2 were absent in this cell line (Figure 38). RTN4 belongs to the group of reticulon proteins that are morphogenic, ER membrane-shaping proteins and that induce formation and stabilisation of ER tubules (Diaz and Ahlquist 2012; Voeltz et al. 2006). RTN4 is thus a reasonable marker for the ER. For that purpose, HeLa and SNX5/SNX6 KO cells were infected with *C. trachomatis* for 29 h and stained for inclusion membrane protein IncA and ER membrane-shaping protein RTN4. In infected HeLa cells, RTN4 clearly localised along tubular structures but weakly localised on the inclusion. In infected SNX5/SNX6 KO cell line, in contrast, RTN4 was absent on tubular structures. However, tubular structures were yet evident indicated by staining of IncA suggesting that tubular structures are in part but not solely ER-related structures.

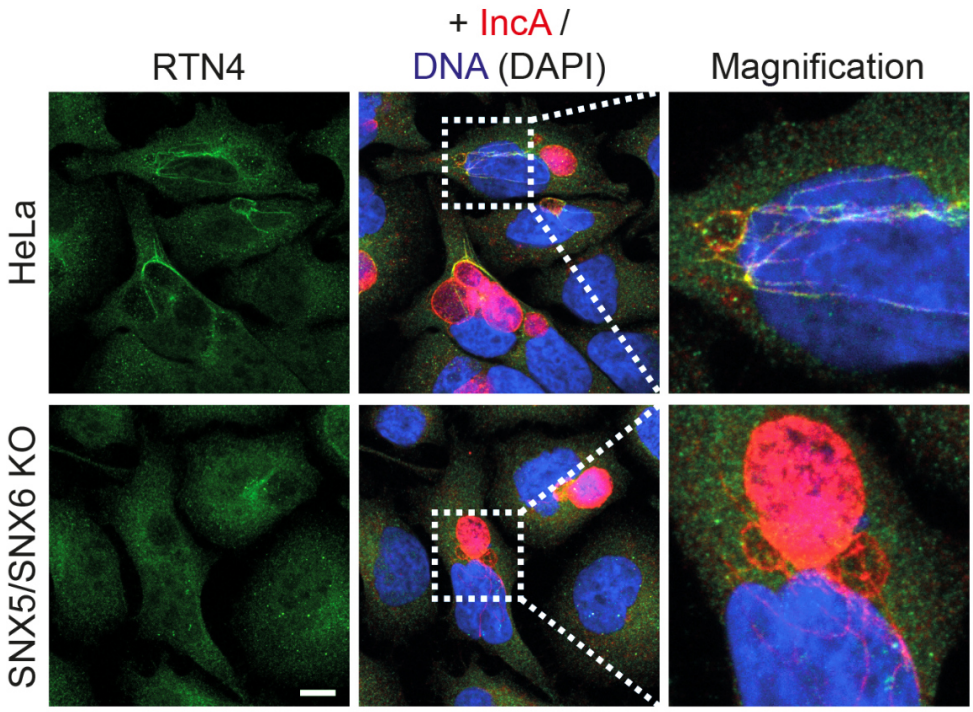

Figure 38. RTN4 localises along tubular structures that emanate from the inclusion.
Confocal IF images showing localisation of RTN4 in HeLa and SNX5/SNX6 double knockout cell line infected with *C. trachomatis* D (MOI 2) visualised at 29 h p.i.. Cells were fixed 29 h p.i. and immunostained with RTN4 (green), IncA (red) and DAPI (DNA). RTN4 was immunostained to

visualise ER-membrane shaping protein. IncA (red) was immunostained to visualise *C. trachomatis* inclusions. Merge depicts RTN4, IncA and DNA (DAPI). Localisation analysis using cLSM, MIP; Scale bar, 10 µm; Representative images shown for n=2.

3.2.6 Summary of mid-*C. trachomatis* infection

At mid-infection stage, the inclusion is decorated with SNX-BARs of retromer's membrane-sensing subcomplex while VPS35, a component of the cargo-recognition complex, localised adjacent to the inclusion. SNX-BARs comprise two functionally distinct domains. The PX domain binds to PIPs and the BAR domain senses membrane curvature and drives membrane tubulation. Studying the localisation of these functional domains in *C. trachomatis* infected cells, we observed domain-specific localisation of SNX-BARs as PX domains of SNX5 and SNX6 and BAR domains of SNX1 and SNX2 were recruited to the inclusion. All full-length SNX-BARs at least in part co-localised with the inclusion membrane protein IncE. Loss of SNX5/SNX6 resulted in disruption of SNX1 and SNX2 rim-like localisation pattern on the inclusion.
Loss of SNX1 or SNX5 did not affect primary infection. In contrast, loss of SNX5/SNX6 resulted in an increase in primary infection. Chlamydial replication increased in SNX5 and even more profound increased in SNX5/SNX6 KO cell line. Furthermore, infectious progeny formation increased in SNX5/SNX6 KO cell line. Lastly, the ultrastructure of elongated tubular SNX structures corresponded to membrane-bound tubules.

3.3 BioID – Recruitment of RPL13a to the chlamydial inclusion

Having shown recruitment of SNX-BARs to the chlamydial inclusion and suggesting that SNX5 and SNX6 PX domains bind to an inclusion membrane protein while SNX1 and SNX2 are assumed to bind to either SNX5 or SNX6 via their BAR domain, interacting proteins of SNX-BARs on the inclusion and the mechanism of recruitment remained still unidentified. Hence, we established a proximity-dependent biotinylation assay (BioID assay) in our system to identify putative SNX1-interacting proteins that would allow us to deduce a potential role for SNX-BAR recruitment.
BioID is based on a promiscuous biotin ligase fused to a protein of interest and is aimed to identify proximal and interacting proteins in cells (Roux et al. 2012; Roux, Kim, and Burke 2013), see Figure 39. The promiscuous biotin ligase is capable to biotinylate all proteins in a radius of 10 - 20 nm around the protein of interest upon addition of exogenous biotin (Firat-Karalar and Stearns 2015). Addition of biotin results in production of highly reactive and short-lived biotinyl-AMP which tags proximal proteins. Since SNX1 is targeted to the chlamydial inclusion, the promiscuous biotin ligase BirA* is targeted to a subcellular location by fusion to SNX1. Biotinylated proteins proximal to SNX1 can be affinity captured and subsequently analysed by nLC-MS/MS and immunoblot.

3.3.1 Identification of proximal and interacting proteins of SNX1

Proximity-dependent biotinylation (BioID) as a tool to identify SNX1-associated proteins

In order to identify SNX1-interacting proteins at the cytosolic site of chlamydial inclusions, myc-BirA* was N-terminally fused to SNX1 (Figure 39).

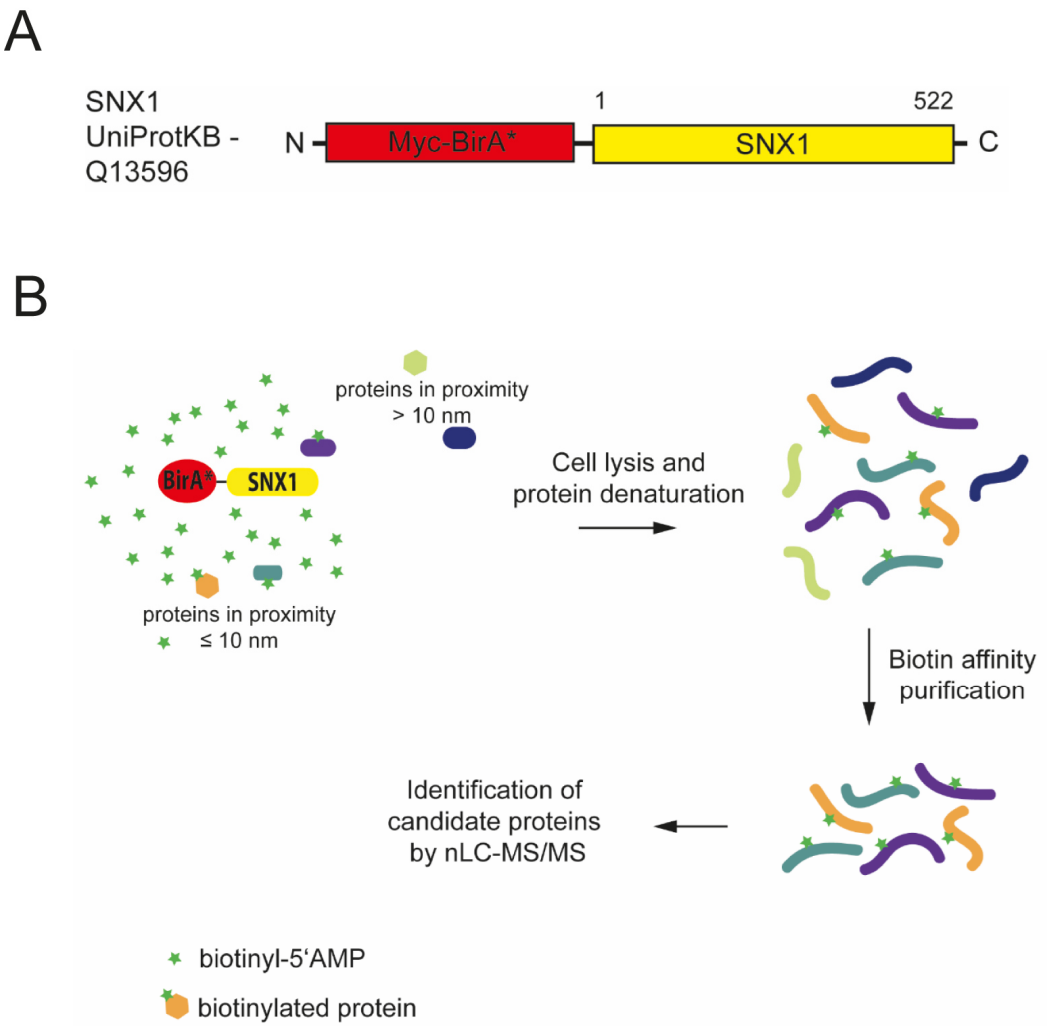

Figure 39. Schematic workflow of proximity-dependent biotinylation assay.
(A) Schematic illustration of myc-BirA*-SNX1 fusion proteins cloned into pcDNA3.1 mycBioID backbone vector enabling expression of N-terminally myc-tagged fusion protein bearing promiscuous biotin ligase BirA*. Full length SNX1 protein of the human retromer was cloned by sticky end cloning. Numbers indicate the number of amino acids. *Cloning performed by Stefanie Lüth, RKI, Berlin.* (B) Schematic illustration of the workflow of proximity-dependent biotinylation assay (BioID). Assay involves expression of fusion protein and addition of exogenous biotin resulting in biotinylation of proximal proteins. Biotinylated proteins are affinity-purified followed by nLC-MS/MS analysis.

Validation of fusion protein expression and correct localisation

Myc-BirA* tag of fusion protein enables detection of sufficient fusion protein expression and correct localisation. Myc protein tag is approximately 1 kD and BirA* is an approximately 33.5 kD protein. Myc-BirA* tag was not suggested to impact either localisation, stability or function of the protein of interest or BirA* activity. To test this, HeLa cells transiently expressing Myc-BirA*-SNX1 and Myc-BirA* only (negative control) and mock-transfected HeLa cells were infected with *C. trachomatis*. At 9 h p.i., exogenous biotin or DMSO as control was added to infected cells followed by WB and IF analysis.

We first tested protein expression and sufficient BirA* biotinylation activity by WB analysis (Figure 40 A). Immunoblot analysis revealed expression of myc-BirA*-SNX1 fusion protein at a correct molecular weight of expected 110 kD. In addition, expression of myc-BirA* only revealed a band at an expected size of about 35 kD. Treatment of cells with biotin resulted in a pronounced smear of the biotin signal compared to DMSO control indicating biotinylation of a variety of proteins of different sizes (Figure 40 A). The thicker band at the biotin blot showing cells that transiently expressed myc-BirA*-SNX1 indicated self-biotinylation of the fusion protein. In mock-transfected cells, addition of biotin did not alter the band pattern compared to DMSO control. Second, we assessed correct localisation of myc-BirA*-SNX1 fusion protein compared to myc-BirA* control by IF (Figure 40 B). In addition, we tested targeted biotinylation activity at subcellular location of fusion protein. Infected HeLa cells transiently expressing myc-BirA*-SNX1 fusion protein or myc-BirA* control were treated with biotin or DMSO and stained for biotin using fluorophore-coupled streptavidin, for myc and IncA. IF analysis by myc and IncA staining exhibited localisation of myc-BirA*-SNX1 fusion protein at the chlamydial inclusion regardless of whether cells were treated with biotin or DMSO indicating correct localisation and function of the fusion protein since SNX1 has shown to be recruited to the inclusion during infection with *C. trachomatis*. Treatment with biotin resulted in targeted biotinylation activity at subcellular location of myc-BirA*-SNX1 fusion protein while treatment with DMSO resulted in a disperse biotin staining pattern detected by fluorophore-coupled streptavidin. In comparison, analysis of myc-BirA* transfection control by myc staining revealed a disperse localisation in the cytosol regardless of whether cells were treated with biotin or DMSO.

Taken together, both, WB and IF analysis, revealed that myc-BirA*-SNX1 fusion protein was expressed at a correct molecular weight and localised at a correct subcellular location during infection with *C. trachomatis*. In addition, treatment with biotin resulted in targeted biotinylation activity at subcellular location of myc-BirA*-SNX1 fusion protein. Thus, using the BioID tool with myc-BirA*-SNX1 fusion protein was considered a reasonable approach to study interactions of SNX1 and proximal proteins during infection with *C. trachomatis* at mid-infection time point.

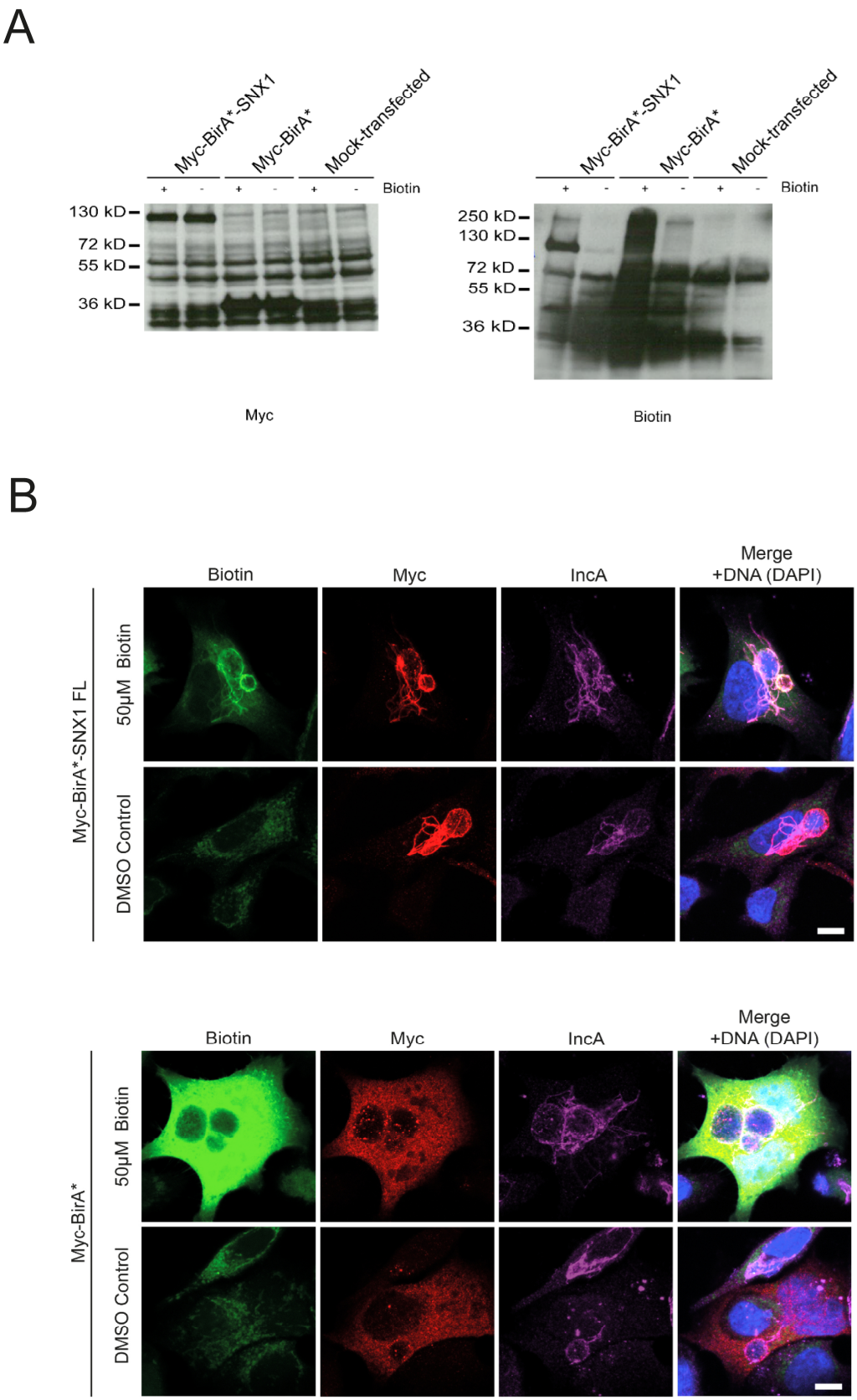

Figure 40. Myc-BirA*-SNX1 fusion protein is expressed at a correct molecular weight and localises on the chlamydial inclusion.
(A) Immunoblots of *C. trachomatis* D (MOI 2) infected HeLa cells transiently expressing fusion proteins or left mock-transfected at 30 h p.i. using indicated antibody or HRP-coupled streptavidin. Cells were treated with 50 µM biotin + or DMSO (-) at 9 h p.i.. Representative immunoblot shown for n=3. (B) Confocal IF images showing HeLa cells transiently expressing myc-BirA*-SNX1 fusion

protein or myc-BirA* transfection control infected with *C. trachomatis* L2 (MOI 2) visualised at 30 h p.i.. Cells were treated with 50 µM biotin or DMSO, fixed 30 h p.i. and immunostained with myc, IncA and DAPI. Biotin was detected by fluorophore-coupled streptavidin. Myc (red) was immunostained to visualise fusion protein expression. IncA (magenta) was immunostained to visualise *C. trachomatis* inclusions. Merge depicts biotin, myc, IncA and DNA (DAPI). Localisation analysis using cLSM, MIP; Scale bar, 10 µm; Representative images shown for n=3.

We used the BioID assay to identify protein candidates that presumably interact with SNX1 (Figure 41). This assay involved transfection of myc-BirA*-SNX1 fusion protein or myc-BirA* (control) and infection with *C. trachomatis*. Once the fusion protein is expressed, addition of exogenous biotin results in biotinylation of proximal proteins followed by protein denaturation, affinity capture of biotinylated proteins and subsequent nLC-MS/MS analysis of candidate proteins (Figure 41 A). In detail, HeLa cells transiently expressing myc-BirA*-SNX1 or myc-BirA* (control cells) were infected with *C. trachomatis* D. We used *C. trachomatis* D since this human pathogen exhibits more pronounced tubular structures than *C. trachomatis* L2. At 9 h p.i., exogenous biotin was added. At 30 h p.i., infected cells were harvested, proteins denatured during cell lysis and biotinylated proteins affinity purified prior to nLC-MS/MS analysis of peptides using label-free intensity based absolute quantification (iBAQ). In total, we identified 2194 protein hits (see appendix, Table 32) of which 40 proteins were identified as enriched proteins (see appendix, Table 33). Proteins were plotted in a volcano plot (Figure 41 B). Among enriched protein candidate hits were the SNX-BARs SNX1, SNX5 and SNX6 supporting our hypothesis of SNX-BARs interacting on the inclusion. In addition, we identified the chlamydial inclusion membrane protein IncE, again supporting our hypothesis of SNX-BARs interacting with IncE. Interestingly, we identified RPL13a among 10 enriched ribosomal proteins: RPL13a, RPL15, RPL18, RPL19, RPL27a, RPL28, RPL29, RPL34 and RPL36 of the large ribosomal subunit and RPS26 of the small ribosomal subunit.
In sum, we identified 40 enriched proteins out of 2194 in total identified proteins. These proteins were assumed to be biotinylated as these were affinity purified by streptavidin.

A

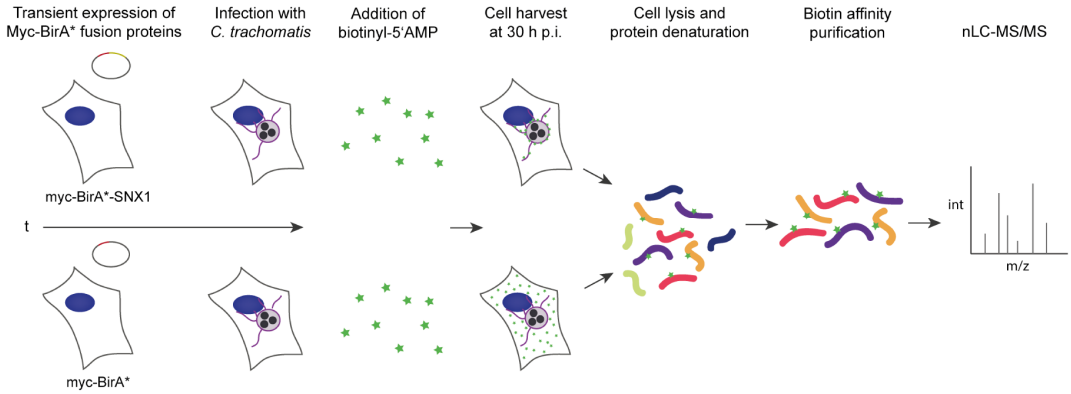

B

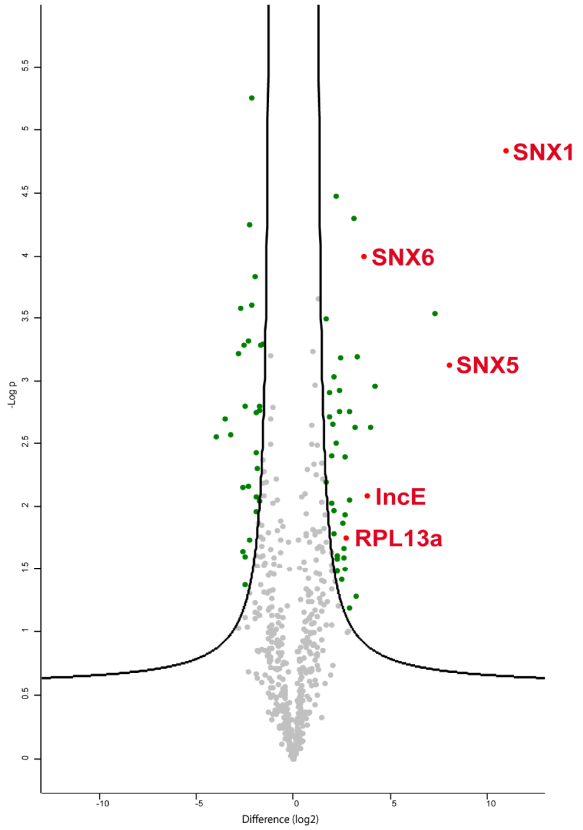

Figure 41. Identification of SNX1-associated proteins by proximity-dependent biotinylation assay.
(A) Schematic illustration of BioID assay workflow for identification of SNX1 interacting proteins. Assay involves transient expression of a fusion protein, infection with *C. trachomatis* D (MOI 2) and addition of biotinyl-5'-AMP. Biotin ligase BirA* biotinylates proteins in proximity of SNX1 in a 10 nm radius. Biotinylated proteins were affinity purified and analysed by nLC-MS/MS. (B) Candidate protein hits identified in BioID assay by nLC-MS/MS. Enrichment of proteins was calculated based on intensity based absolute quantification (iBAQ), minimum ratio count of 2, -log(p-value) >1, difference (log2) > 1.8, FDR 1%, no missing values; n=3. *MS analysis was performed by Dr. Jörg Döllinger, Proteomics and Spectroscopy facility, RKI, Berlin.*

3.3.2 RPL13a is recruited to the inclusion of *C. trachomatis*

Some ribosomal proteins exhibit extra-ribosomal functions or are related to ribosome heterogeneity (Xue and Barna 2012a). Due to the identification of ribosomal proteins in the BioID assay, we examined the hypothesis that *C. trachomatis* may interfere in the host cellular translation process. Hence, we validated certain ribosomal protein candidate hits from BioID assay during *C. trachomatis* D infection by immunofluorescence and immunoblot analysis after streptavidin pulldown (Figure 42). For IF analysis, HeLa cells were infected with *C. trachomatis* or left uninfected for 30 h and stained for ribosomal proteins of the large subunit RPL3 (not enriched protein candidate hit), RPL13a and RPL29 (enriched protein candidate hits) and of the small subunit RPS6, RPS9 (not enriched protein candidate hits) and RPS26 (enriched protein candidate hit), each protein co-stained with the inclusion membrane protein IncE (Figure 42 A). In uninfected cells, ribosomal proteins localised in a disperse punctuate pattern in the cytosol (data not shown). In infected cells, RPL13 and RPS9 localised on the inclusion presuming specific recruitment. In contrast, RPL3 and RPL29-directed antibodies stained bacteria indicating cross reaction of the antibody in IF studies. RPS6 and RPS26 localised in a disperse punctuate pattern in the cytosol during infection. Next, we validated these candidate hits via streptavidin pulldown followed by WB analysis. HeLa cells transiently expressing either myc-BirA*-SNX1 fusion protein or myc-BirA* transfection control were infected with *C. trachomatis* for 30 h followed by cell lysis and streptavidin pulldown of biotinylated proteins (Figure 42 B). Biotin blot confirmed biotinylation efficiency as biotinylated proteins were present after pulldown and bands were more distinct compared to whole-cell lysate. Then, we validated enriched protein candidate hits by detection of SNX-BARs SNX1, SNX5 and inclusion membrane protein IncE as positive controls and ribosomal protein RPL3, RPL13a and RPS9. ß-actin was detected as loading control. As expected, myc-BirA*-SNX1 fusion protein exhibited a distinct band in pulldown lanes as self-biotinylation takes place. In addition, we detected endogenous SNX1 suggesting that SNX1 proteins form homodimers. However, candidate hits with a high enrichment score such as SNX5 and IncE were only detected in whole-cell lysate. In addition, ribosomal proteins were detected in whole-cell lysate but not in pulldown.

In sum, validation of enriched proteins by IF resulted in localisation of RPL13a and RPS9 on the inclusion suggesting specific recruitment. However, validation of candidate protein hits by pulldown did not reveal the detection of at least enriched candidate proteins.

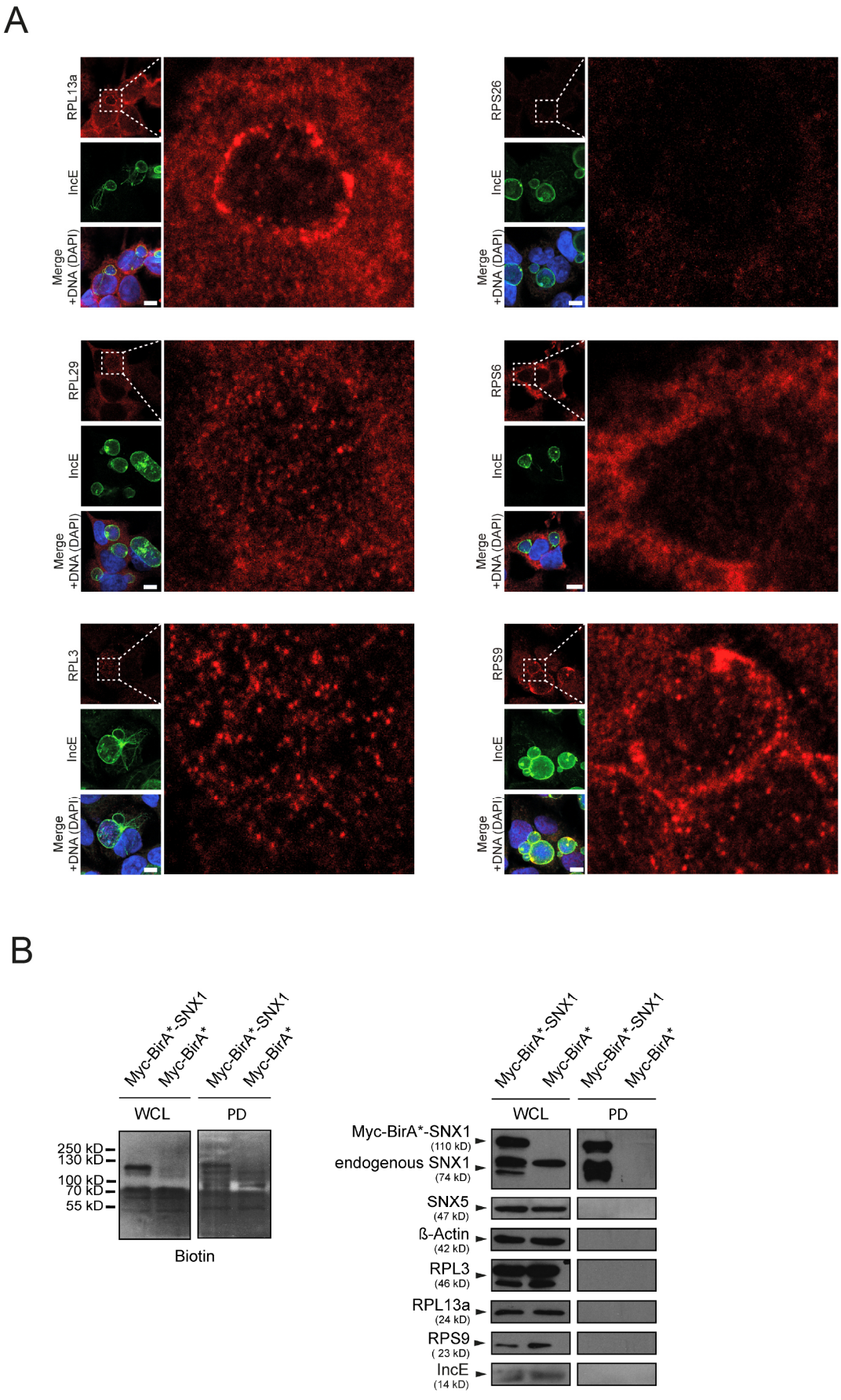

Figure 42. Validation of ribosomal proteins identified in BioID assay.
(A) Confocal IF images showing localisation of ribosomal proteins in *C. trachomatis* D infected HeLa cells (MOI 2) visualised at 48 h p.i.. Cells were fixed 48 h p.i. and immunostained with indicated

antibodies and DAPI (DNA). Ribosomal proteins (red) were immunostained to localise ribosomal proteins identified in BioID assay. IncE (green) was immunostained to visualise localisation of *C. trachomatis* inclusion. Merge depicts ribosomal proteins, IncE and DNA (DAPI). Localisation analysis using cLSM; Scale bar, 10 µm; Representative images shown for n=2. (B) Immunoblots after streptavidin pulldown of *C. trachomatis* D infected HeLa cells (MOI 2) transiently expressing fusion proteins or transfection control at 30 h p.i. using HRP-coupled streptavidin and indicated antibodies. Cells were treated with 50 µM biotin at 9 h p.i.. Representative immunoblot shown for n=2; WCL: whole-cell lysate, PD: pulldown, 20x.

RPL13a localisation in C. trachomatis D infected cells

To analyse the spatio-temporal localisation of RPL13a, we performed a time course during infection with *C. trachomatis* D (Figure 43). HeLa cells were infected or left uninfected and stained for RPL13a and IncE at indicated time points. In uninfected cells and at 16 h p.i., RPL13a localised in a disperse punctuate pattern in the cytosol. At 36 and 48 h p.i. in contrast, RPL13a localised on the inclusion which was yet more distinct at 48 h p.i. suggesting specific recruitment of ribosomal protein L13a to the inclusion.

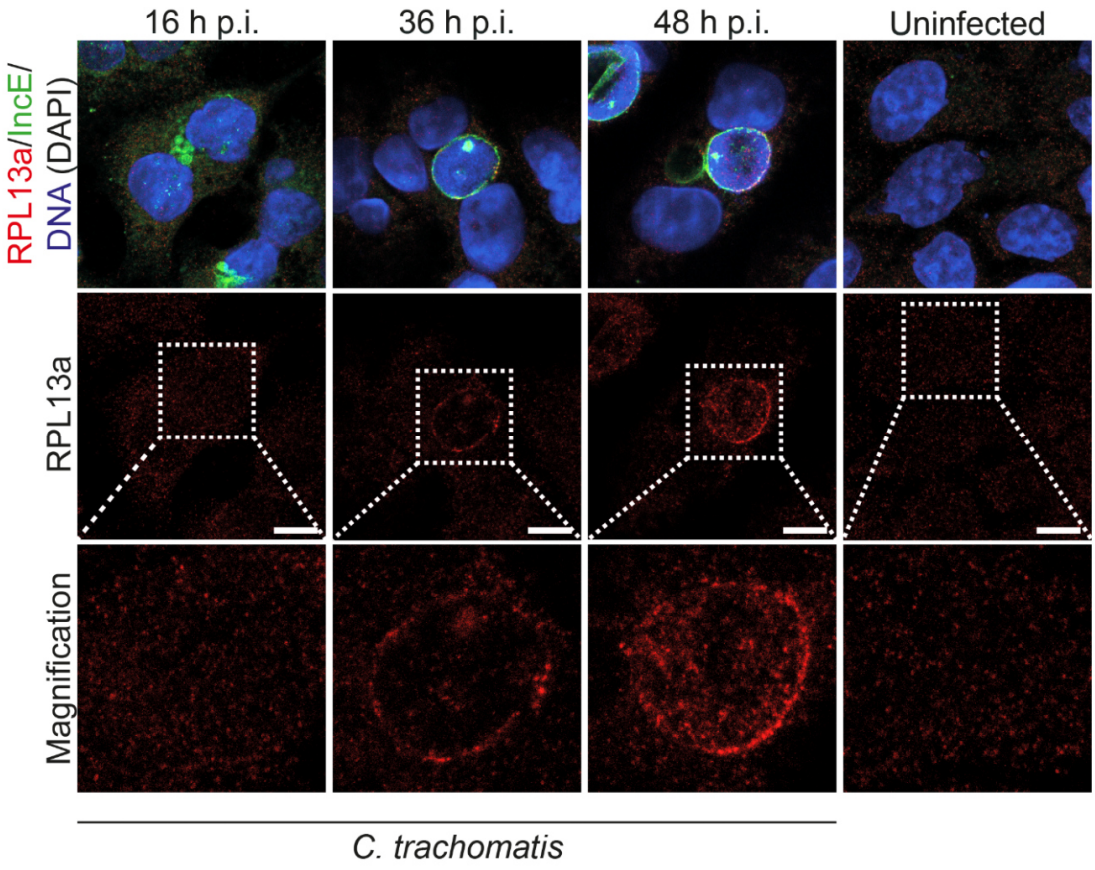

Figure 43. RPL13a is recruited to the inclusion of *C. trachomatis* at mid-infection time points. Confocal IF images showing localisation of RPL13a in *C. trachomatis* D infected HeLa cells (MOI 2) at indicated time points. Cells were fixed at indicated time points and immunostained with indicated antibodies and DAPI (DNA). RPL13a (red) was immunostained to localise host cellular ribosomal protein of large subunit. IncE (green) was immunostained to visualise *C. trachomatis* inclusion. Merge depicts RPL13a, IncE and DNA (DAPI). Localisation analysis using cLSM; Scale bar, 10 µm; Representative images shown for n=3. *Experiment performed by Sandra Oehlmann, RKI, Berlin.*

Recruitment of RPL13a to the inclusion is reduced in C. trachomatis L2 and C. psittaci DC15

Next, we compared the localisation of RPL13a to the human pathogen *C. trachomatis* L2 and zoonotic pathogen *C. psittaci* DC15 to assess whether RPL13a recruitment is species-specific (Figure 44). HeLa cells were infected with *C. trachomatis* L2 and *C. psittaci* DC15 or left uninfected for 40 h and co-stained for RPL13a and either IncA (*C. trachomatis* L2) or IncB (*C. psittaci* DC15) (Figure 44 A). In uninfected cells, RPL13a localised in a disperse punctuate pattern in the cytosol. In infected cells, either with *C. trachomatis* L2 or with *C. psittaci* DC15, RPL13a mainly localised in a disperse punctuate pattern in the cytosol. Quantification of RPL13a signal on the inclusion revealed that RPL13a localised on the inclusion in 5% of cells infected with *C. trachomatis* L2 and *C. psittaci* DC15 (Figure 44 B). In *C. trachomatis* D infected cells, in contrast, RPL13a localised on the inclusion in 60% of infected cells (Figure 44 B).
In sum, in *C. trachomatis* D infected cells, RPL13a localised on the inclusion in 60% of cells whereas, in *C. trachomatis* L2 and *C. psittaci* DC15 infected cells, RPL13a is rarely localised on the inclusion suggesting species-specific differences in the recruitment of large subunit's ribosomal protein L13a.

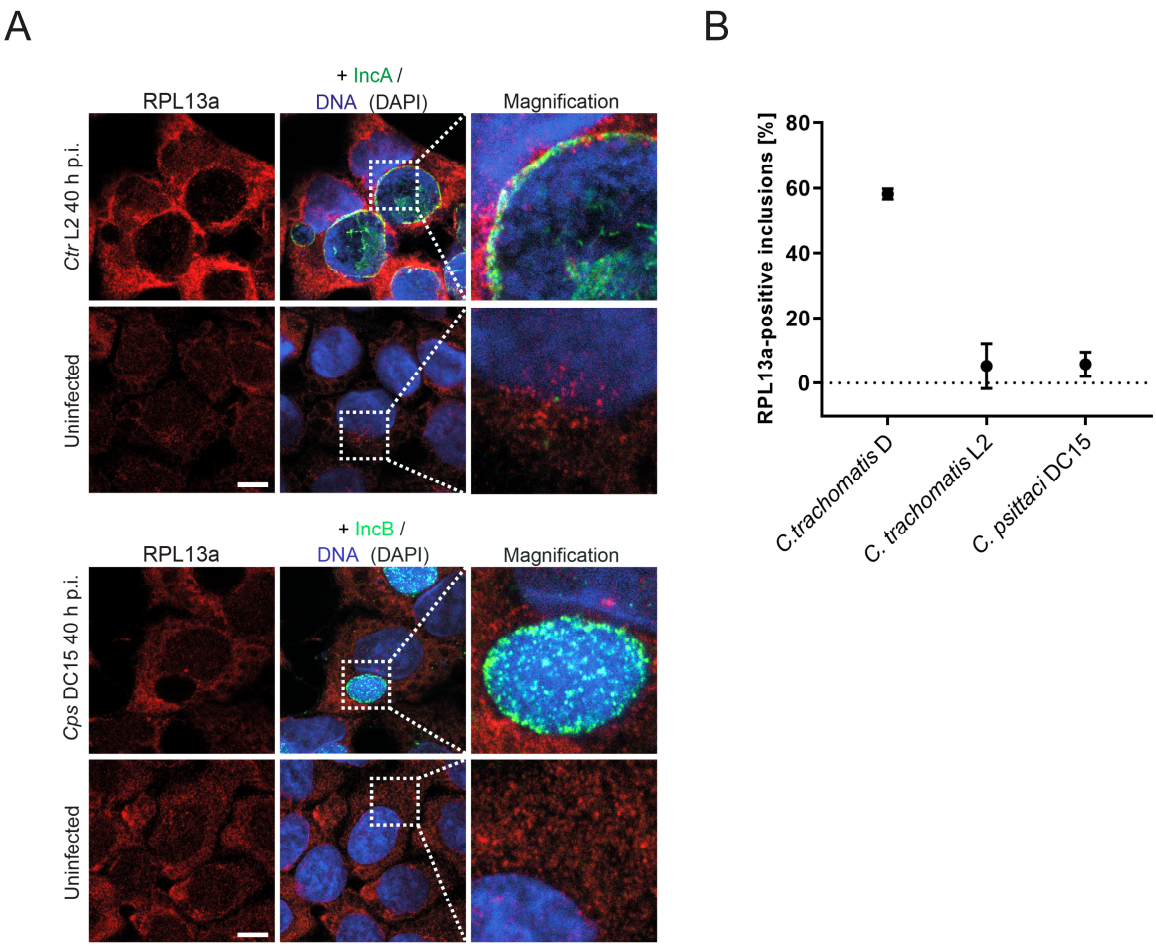

Figure 44. RPL13a is species-specifically recruited.
(A) Confocal IF images showing localisation of RL13a in *C. trachomatis* L2 (*Ctr* L2) and *C. psittaci* DC15 (*Cps* DC15) infected HeLa cells (MOI 2) visualised at 40 h p.i.. Cells were fixed 40 h p.i. and immunostained with indicated antibodies and DAPI (DNA). RPL13a (red) was immunostained to localise host cellular ribosomal protein of large subunit. IncA or IncB (green), depending on the

pathogen, were visualised to localise chlamydial inclusions. Merge depicts RPL13a, IncA/B and DNA (DAPI). Localisation analysis using cLSM; Scale bar, 10 µm; Representative images shown for n=3. *Experiment performed by Sandra Oehlmann, RKI, Berlin.* (B) Analysis of inclusions revealing recruitment of RPL13a in HeLa cells infected with *C. trachomatis* D, *C. trachomatis* L2 and *C. psittaci* DC15 (MOI 2) at 48 and 40 h p.i. depending on the pathogen. Cells were fixed 40 h p.i. (*C. trachomatis* L2, *C. psittaci* DC15) and 48 h p.i. (*C. trachomatis* D) and immunostained with indicated antibodies and DAPI (DNA). RPL13a was immunostained to localise host cellular ribosomal protein of large subunit. Inc protein was immunostained to localise chlamydial inclusions. RPL13a-positive chlamydial inclusions were counted using cLSM; n=3.

Recruitment of RPL13a is reduced in SNX1 KO cell line

As RPL13a was identified as enriched candidate protein hit in myc-BirA*-SNX1 transiently expressing HeLa cells, we assumed a link between SNX1 and RPL13a. Thus, we assessed whether RPL13a localisation is affected in SNX1 KO cell line. HeLa cells, CRISPR Ctrl cells and SNX1 KO cells were infected with *C. trachomatis* D for 48 h and co-stained for RPL13a and IncE. We used time point 48 h p.i. as this time point exhibited a pronounced localisation of RPL13a on the inclusion compared to 36 h p.i. time point. We observed an overall increasing trend of RPL13a signal intensity in the cytosol from HeLa over CRISPR Ctrl to SNX1 KO cell line. In addition, SNX1 KO cell line exhibited an increased RPL13a signal intensity in the cytosol compared to control cell lines suggesting that RPL13a recruitment to the inclusion is affected in SNX1 KO cell line.

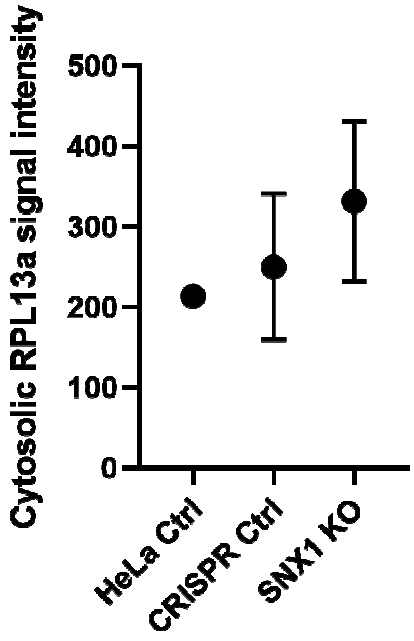

Figure 45. RPL13a recruitment to the inclusion is reduced in SNX1 knockout cell line.
Analysis of RPL13a signal intensity in *C. trachomatis* D infected HeLa, CRISPR Ctrl and SNX1 knockout cell lines (MOI 2) at 48 h p.i.. Cells were fixed at 48 h p.i. and immunostained for RPL13a, IncE and DAPI (DNA). Signal intensities of cytosolic RPL13a (without RPL13a signal around inclusions) in at least 30 cells per cell line of confocal IF images were quantified using ImageJ (mean ±SD, n=2).

GAIT complex components EPRS and NSAP1 are not localised on the inclusion

RPL13a exhibits an extra-ribosomal function being a component of the gamma interferon inhibitor of translation (GAIT) complex that is formed upon stimulation by IFNγ. The assembled functional GAIT complex is known to repress translation of specific transcripts that harbour GAIT elements. Thus, we analysed a possible formation of the GAIT complex during infections with *C. trachomatis*. To stimulate GAIT complex formation, HeLa cells were infected with *C. trachomatis* for 48 h and additionally treated with IFNγ at 24 h p.i. for 24 h or left untreated (UT). Cells were co-stained with GAIT complex components and IncE. We examined the localisation of RPL13a, EPRS and NSAP1 (Figure 46). In untreated and IFNγ treated infected cells, RPL13a localised on the inclusion. In contrast, in untreated and IFNγ treated infected cells, EPRS and NSAP1 did not localise around the inclusion suggesting no formation of GAIT complex on the inclusion.

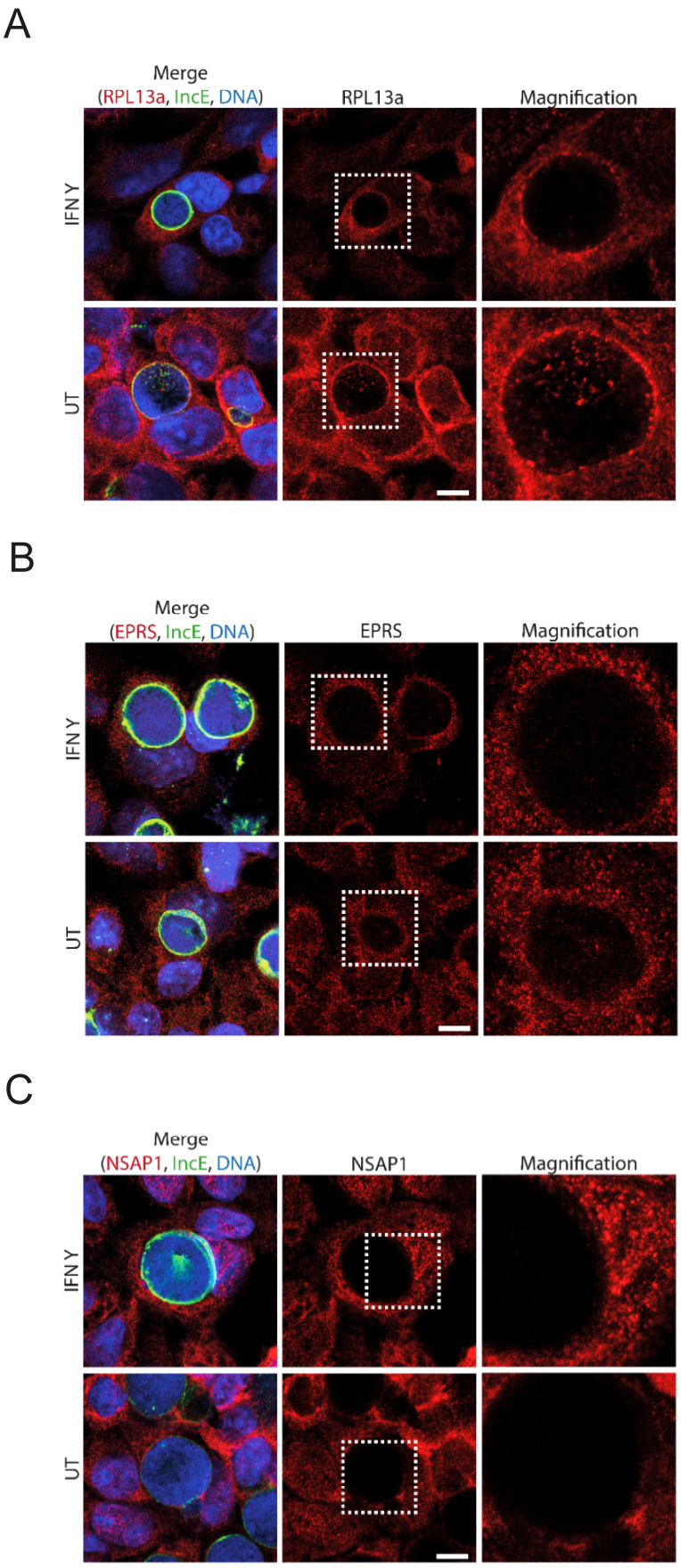

Figure 46. Localisation of GAIT complex components in *C. trachomatis* infected cells.
Confocal IF images showing localisation of GAIT complex components in *C. trachomatis* D infected HeLa cells (MOI 2) visualised at 48 h p.i.. Cells were fixed 48 h p.i. and immunostained with indicated antibodies and DAPI (DNA). RPL13a, EPRS and NSAP1 (red) were immunostained to

localise GAIT complex components. IncE (green) was visualised to localise chlamydial inclusions. Merge depicts GAIT complex component, IncE and DNA (DAPI). Localisation analysis using cLSM; Scale bar, 10 µm; Representative images shown for n=2; IFNγ: interferon γ; UT: Untreated.

3.3.3 Functional analysis of RPL13a by RNAi

We used RNAi to study function of RPL13a in infected cells by examination of replication, progeny formation, protein expression and inclusion size upon depletion of RPL13a (Figure 47). Therefore, HeLa cells were transfected with RPL13a siRNA pools 6+8, 7+8, control transfected with AllStars or mock-transfected prior to infection with *C. trachomatis* for 48 h or 72 h depending on the assay. Depletion of RPL13a resulted in a threefold increase of genome copy number indicating increased replication compared to control transfected cells (Figure 47 A). In addition, we observed a fourfold increase of infectious progeny formation upon depletion of RPL13a compared to control transfected cells (Figure 47 B). Both, increased genome copy number and increased infectious progeny formation was consistent to elevated expression of bacterial proteins IncA, IncE and Hsp60 at a fold change of three to four upon depletion of RPL13a detected by immunoblot analysis (Figure 47 C). Finally, we determined the inclusion size (Figure 47 D). Upon depletion of RPL13a, inclusions of infected cells were considerably enlarged compared to control transfected cells. Average inclusion size reached an area of 180 µm^2 whereas average inclusion size upon RPL13a depletion reached an area of 310 µm^2 stating a 1.7-fold enlargement.

In sum, replication, infectious progeny formation, bacterial protein expression and inclusion size increased upon depletion of RPL13a suggesting that RPL13a restricts *C. trachomatis* infection.

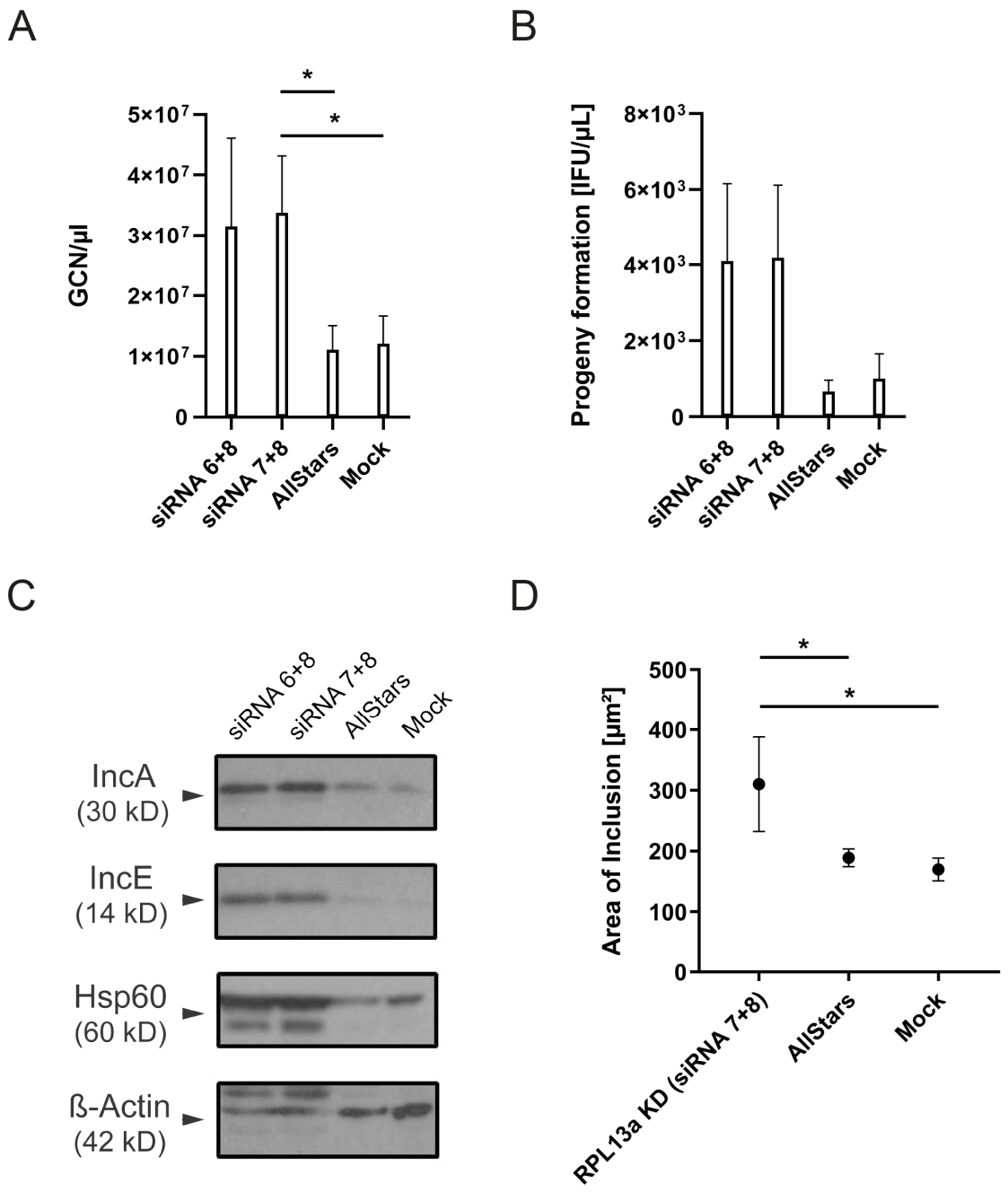

Figure 47. Functional analysis of RPL13a during *C. trachomatis* infection.
(A) Analysis of bacterial genome copy numbers (GCN) in *C. trachomatis* D infected HeLa cells (MOI 2) at 72 h p.i. upon depletion of RPL13a. Cells were transfected with indicated siRNA pools, control siRNA (AllStars) or left mock-transfected. GCN was determined by qPCR (mean ±SD, n=4; RM one-way ANOVA, Tukey's multiple comparison test). (B) Analysis of infectious progeny formation in *C. trachomatis* D infected HeLa cells at 72 h p.i. upon depletion of RPL13a. Cells were transfected with indicated siRNA pools, control siRNA (AllStars) or left mock-transfected. Infectious progeny formation was determined by progeny formation assay. (mean ±SD; n=4; RM one-way ANOVA, Tukey's multiple comparison test, * indicates p-value <0.05). (C) Immunoblot showing bacterial protein expression in *C. trachomatis* D infected HeLa cells (MOI 2) at 48 h p.i. upon depletion of RPL13a using indicated antibodies. ß-actin as loading control. Cells were transfected with indicated siRNA pools, control siRNA (AllStars) or left mock-transfected. Representative immunoblot shown for n=4. (D) Analysis of inclusion area in *C. trachomatis* D infected HeLa cells (MOI 2) at 48 h p.i. upon depletion of RPL13a. Cells were transfected with indicated siRNA pool, control siRNA (AllStars) or left mock-transfected and immunostained with RPL13a, IncA and DAPI (DNA). Areas of inclusions per cell of at least 15 fields of view per condition and replicate of confocal IF images were determined using ImageJ (mean ± SD, n=4; Ordinary one-way ANOVA, Tukey's multiple comparisons test, * indicates p-value <0.05). KD: knockdown.

3.3.4 Altered total ribosomal profile in *C. trachomatis* infected cells

RPL13a localised on the inclusion during infection with *C. trachomatis*. In addition, *C. trachomatis* infection was affected in RPL13a depleted cells. Thus, we examined whether the composition of ribosomal large and small subunits is altered during infection with *C. trachomatis*. Therefore, I implemented a workflow in order to isolate ribosomes to our infection system. This workflow involves lysis of cells, removal of nuclei and mitochondria by centrifugation followed by fractionation of polysomes, ribosomes and ribosomal subunits 60S and 40S using a sucrose density gradient (Figure 48 A). First, absorption of polysomes, ribosomes, ribosomal subunits and proteins after density centrifugation were monitored. Therefore, HeLa cells were infected with *C. trachomatis* or left uninfected for 48 h before ribosomes of the two conditions were isolated separately. Ribosomes and ribosomal subunits were fractionated by collecting fractions of 1 mL and absorption was monitored at absorption maxima of nucleic acids and proteins, 254 and 280 nm, respectively. As a result, we were able to fractionate ribosomes, large and small subunits indicated by three peaks in both, infected and uninfected cells (Figure 48 B). The first peak (fractions 1 and 2) indicates 80S ribosomes, the second peak (fractions 4 and 5) indicates the large ribosomal subunit and the third peak (fraction 7) indicates the small ribosomal subunit which was confirmed by immunoblot analysis (see appendix, Figure 55 and sheets ‘PCP ribosome’ per replicate in Table 34). The peak at fraction 10 indicates DNA as the sucrose density gradient had a volume of 10 mL before cleared lysates were layered over the gradient. We detected an altered ribosomal profile of *C. trachomatis* infected cells compared to uninfected cells expressed by lower absorption of ribosomes and ribosomal subunits. Furthermore, the large ribosomal subunit fractions of infected cells displayed a stretched peak. Monitoring absorption of proteins, we confirmed fractionation of ribosomes and ribosomal subunits as shown by three small-sized peaks (Figure 48 C). In contrast to an altered ribosome profile, we detected similar total protein profiles of fractions of infected and uninfected cells.

In sum, infection with *C. trachomatis* resulted in an altered ribosome profile whereas the total protein profile was unaffected compared to uninfected cells.

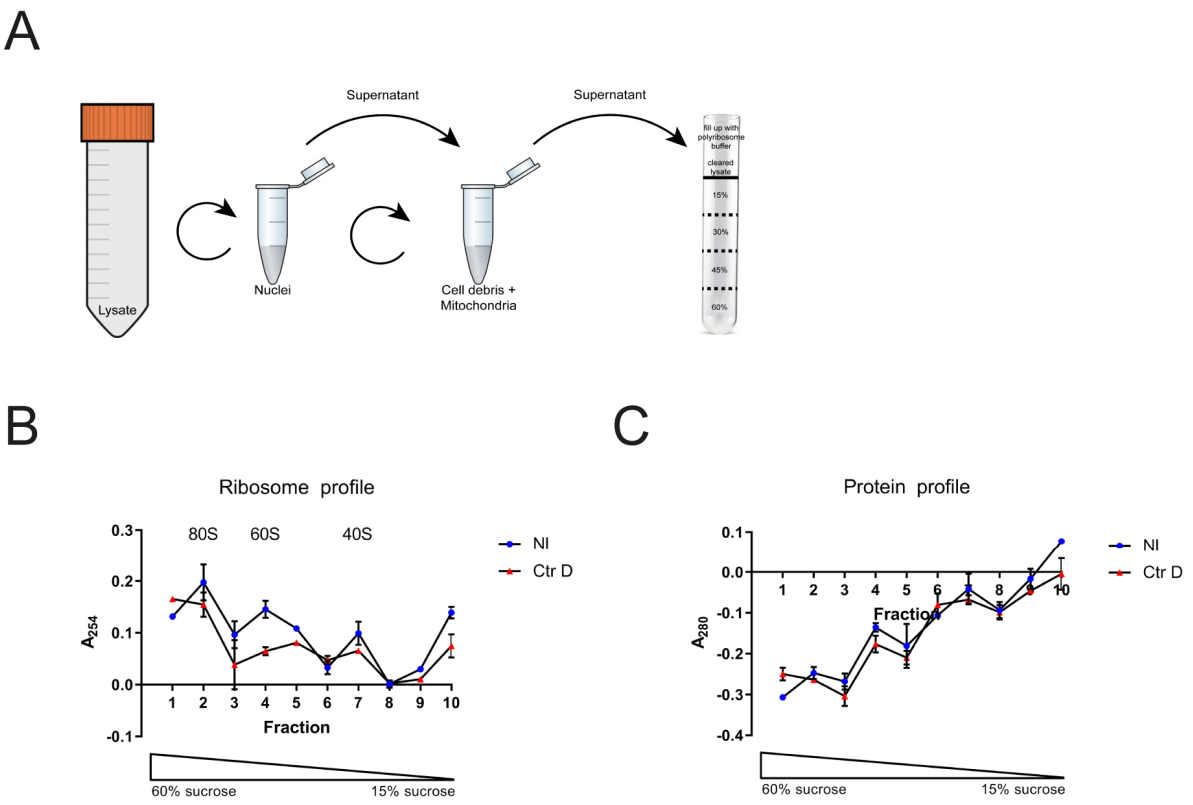

Figure 48. Total ribosome profile is altered in *C. trachomatis* infected cells.
(A) Schematic illustration of ribosome isolation workflow. Workflow involves cell lysis and subsequent removal of nuclei and mitochondria. Cleared lysate is layered over a 15%-60% sucrose gradient and ribosomes and ribosomal subunits fractionated by density gradient centrifugation. (B) Total ribosome profile of *C. trachomatis* D infected (MOI 5) and uninfected HeLa cells at 48 h p.i.. Ribosomes were isolated at 48 h p.i. followed by fractionation of ribosomes and ribosomal subunits by density gradient centrifugation. Fractions of 1 mL were collected and absorption recorded at a wavelength of 254 nm. Ribosomes and ribosomal subunits were detected indicated by peaks (mean ±SD; n=2); NI: uninfected; Ctr D: *C. trachomatis* D. (C) Total protein profile of *C. trachomatis* D infected (MOI 5) and uninfected HeLa cells at 48 h p.i.. Ribosomes were isolated at 48 h p.i. followed by fractionation of ribosomes and ribosomal subunits by density gradient centrifugation. Fractions of 1 mL were collected and absorption recorded at a wavelength of 280 nm. Proteins of ribosomes and ribosomal subunits were detected indicated by peaks (mean ±SD; n=2); NI: uninfected; Ctr D: *C. trachomatis* D.

3.3.5 Analysis of ribosomal protein profiles of C. trachomatis infected cells

Given that ribosome fractionation revealed an altered ribosome profile of infected versus uninfected cells, we assumed a heterogeneous ribosome composition during infection with *C. trachomatis*. Ribosomal heterogeneity includes diversity in composition, function, activity, post-translational modifications of subsets of ribosomal proteins and variations in ribosomal RNA sequences. All of these factors may contribute to the occurrence of heterogeneous ribosomes (Xue and Barna 2012b). Thus, we analysed individual ribosomal protein expression of isolated ribosomes of infected and uninfected cells by a proteomic approach using SILAC. Heavy (H, K8R10) and light (L, K0R0) labelled HeLa cells were prepared by SILAC method as described in Aeberhard et al. (Aeberhard et al. 2015). SILAC allows for relative quantification of

proteins of different conditions in cell culture by using differently labelled isotopes of amino acids which are incorporated in cell culture (Ong et al. 2002; Ong and Mann 2007). MS analysis recognises mass differences of peptide hits which are further assembled to protein hits thereby providing quantification of proteins between two physiological states within biological systems (Cox et al. 2009; Cox and Mann 2009; Cox et al. 2011). In this thesis, HeLa cells were infected with *C. trachomatis* (light label) or left uninfected (heavy label) for 48 h prior to isolation of ribosomes (Figure 48). After isolation of ribosomes and ribosomal subunits by density gradient centrifugation, fractions were collected and proteins precipitated using TCA followed by in-solution trypsin-mediated digest. Peptides were purified with StageTips prior to nLC-MS/MS analysis (Figure 49 A; see appendix for results matrix, Table 34). Summed ribosomal and ribosomal subunit protein ratios were plotted per fraction across the sucrose gradient and per replicate (ribosome fractionation data, Figure 49 B). An increasing fraction number corresponds to a decreasing sucrose concentration (fraction 1: 60% sucrose – fraction >25: 15% sucrose). In general, 80S and ribosomal subunit proteins exhibited summed protein ratios Heavy/Light (H/L) per fraction varying around zero indicating little changes of ribosomal protein expression in *C. trachomatis* infected cells. Proteins of the 60S subunit (green plots) clustered mainly around zero except between fractions 1 and 10 where proteins exhibited ratios around 0.5. Proteins of the 40S subunit (green plots) clustered mainly around zero except between fractions 14 and 25 where proteins exhibited ratios around 0.5. Next, we analysed BioID significantly enriched ribosomal proteins in relation to individual ribosomal proteins of 60S subunit obtained from ribosome fractionation data in more detail (Figure 49 C; ribosomal proteins of 60S subunit from replicate 2 of Figure 49 D). We observed that BioID significantly enriched ribosomal proteins (red plots) cluster similar to ribosomal proteins of the 60S subunit (grey plots). Moreover, BioID significantly enriched proteins (grey plots) were plotted in addition to individual protein profiles of 60S (blue plots) and 40S (green plots) subunit proteins from ribosome fractionation data (protein ratios per replicate). Analysis of protein plots revealed that BioID significantly enriched proteins cluster in particular in front and back fractions and exhibit protein profiles similar to 60S and 40S ribosomal protein profiles (ribosome fractionation data, Figure 49 D). The protein exhibiting a considerable negative ratio H/L in all replicates was identified as actin.

In sum, protein expression of individual ribosomal proteins was not altered in *C. trachomatis* infected cells.

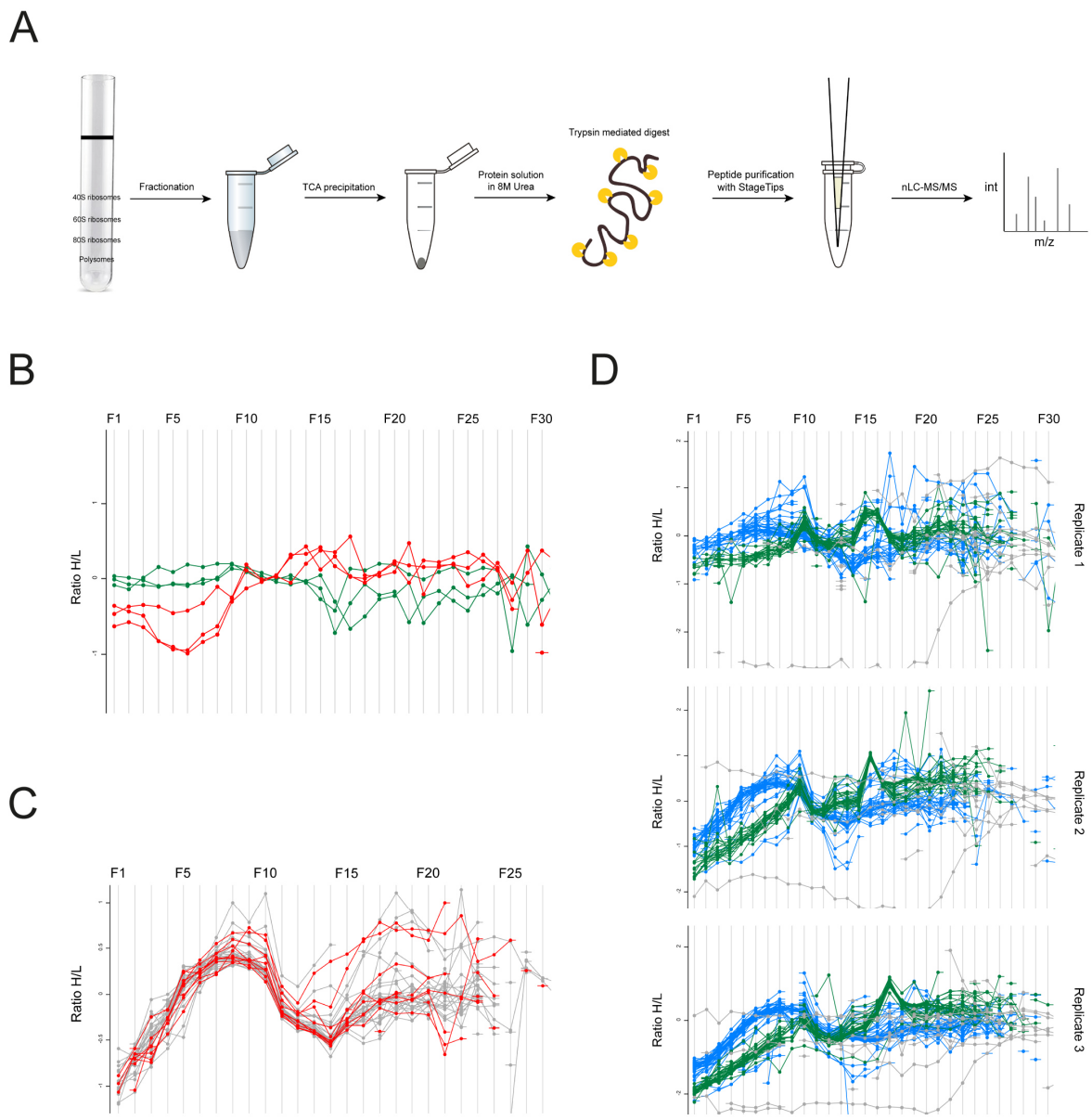

Figure 49. Ribosomal protein profiles of *C. trachomatis* infected cells.
(A) Schematic illustration of sample preparation of fractionated ribosomes and ribosomal subunits workflow. Workflow involves fractionation of ribosomes and ribosomal subunits followed by protein precipitation using TCA. Proteins are digested in-solution in 8 M urea buffer by trypsin. Peptides are purified with StageTips prior to nLC-MS/MS analysis. (B) Profile plots of summed ribosomal and ribosomal subunit protein ratios per fraction and replicate of *C. trachomatis* D (MOI 5) and uninfected SILAC-labelled HeLa cells per fraction (ribosome fractionation data). Ribosomes of infected (L, light labelled) and uninfected (H, heavy labelled) cells were isolated at 48 h p.i. followed by fractionation of ribosomes and ribosomal subunits by density gradient centrifugation. Fractions of 300 µL were collected and samples prepared according to workflow illustrated in (A). n=3; 60S subunit proteins: green; 40S subunit proteins: red; F: fraction. (C) Profile plots of BioID significantly enriched ribosomal proteins and 60S subunit protein ratios (replicate 2) from ribosome fractionation data. BioID significantly enriched ribosomal proteins: red, 60S subunit proteins: grey; F: fraction, replicate exemplarily shown for other replicates. (D) Profile plots of BioID significantly enriched proteins and 60S and 40S subunit protein ratios from ribosome fractionation data. n=3; 60S subunit proteins: blue, 40S subunit proteins: green, BioID significantly enriched proteins: grey; F: fraction. *MS analysis was performed by Dr. Jörg Döllinger, Proteomics and Spectroscopy facility, RKI, Berlin.*

4 Discussion

Intracellular pathogens depend on host cells for their survival. *L. pneumophila*, *S. enterica serovar* Typhimurium and *C. trachomatis*, for instance, subvert the host endomembrane system and establish a pathogen-containing vacuole. Once established, it allows intracellular pathogens to extensively interact with the host cell as they acquire nutrients from the host cell. Simultaneously, these pathogens avoid host cell apoptosis and host immune recognition (Hilbi and Haas 2012). *L. pneumophila*, *S.* Typhimurium and *C. trachomatis* have also been shown to interact with the host cellular retromer. Hence, the pathogen-containing vacuole is a favourable niche.

The human retromer is a multi-protein complex that associates with endosomes and recognises cargoes prior to retromer-mediated cargo retrieval from endosomes to the TGN. Retrieval processes were observed 30 years ago. Since then, retrograde trafficking machinery including tubular based endosomal sorting within the endomembrane system entered the limelight (Cullen and Steinberg 2018; Simonetti and Cullen 2018). Seaman originally identified the retromer by a genetic screen in yeast (Seaman et al. 1997). Its human orthologues were identified in the year 2000 (Haft et al. 2000). Furthermore, retromer's two subcomplexes and their components have been determined: Classical concept of the retromer comprises a cargo-recognition (VPS trimer) and a membrane-binding (SNX-BAR dimer) subcomplex. Retromer knowledge extended in a way that SNX-BAR architecture, retromer coat structure and function of retromer has been unveiled though future research will certainly uncover even more. SNX-BARs are composed of two domains. The N-terminal PX domain of SNX-BARs binds to PIP-rich endosomal membranes while the C-terminal BAR domain senses membrane curvature and is capable to drive membrane tubulation (Cullen and Korswagen 2012; Seaman 2012). Moreover, retromer-mediated retrieval and tubular-based endosomal sorting has been modelled. This model involves binding of SNX-BARs which results in curvature-inducing action to remodel endosomal membrane (van Weering, Verkade, and Cullen 2010). These findings opened the way for retromer to come into focus of cellular biology and later in the context of infection biology as, interestingly, intracellular pathogens have been demonstrated to hijack the retromer by recruiting components of it (Personnic et al. 2016). Altogether, importance of the retromer to general endosomal biology in mammalian cells has been markedly accredited and will increase further (Gallon and Cullen 2015).

C. trachomatis is a public health burden as it is the most prevalent sexually transmitted bacterial pathogen causing severe infections of the urogenital tract in both, women and men (WHO 2012). Quantitative proteomic analysis of isolated chlamydial inclusions revealed a host-derived proteome composition (Aeberhard et al. 2015). Aeberhard et al. identified 1400 host cellular proteins in the inclusion fraction. Plotting of proteins in the inclusion fraction with a SILAC ratio above 1.5 revealed proteins from cytoplasmic vesicles, ER-Golgi intermediate compartment (ERGIC), GA, lysosomes and the ER in the inclusion fraction. Statistical analysis identified 351

host cellular proteins to be enriched in the inclusion fraction. Interestingly, by assessing the enrichment of inclusion-associated proteins, components of the human retromer including proteins of the SNX family were identified to be highly enriched in the inclusion fraction. IF analyses in *C. trachomatis* infected human host cells exhibited presence of SNX-BARs of the human retromer at the inclusions but absence of SNX3 and SNX12 (Aeberhard et al. 2015). In addition, Mirrashidi et al. identified an Inc-human interactome that unveiled interaction of SNX1, SNX2, SNX5, SNX6 and SNX32 with the inclusion membrane protein IncE (Mirrashidi et al. 2015). Moreover, Mirrashidi demonstrated binding of SNX5 and SNX6 to IncE. Furthermore, SNX-BARs of the retromer localised on the inclusion consistent with the findings by Aeberhard et al (Aeberhard et al. 2015). While Aeberhard et al. analysed the host-derived inclusion proteome after purification of inclusions, Mirrashidi et al. performed affinity purification-mass spectrometry of host cellular proteins bound to Inc fusion proteins. Hence, two different approaches were applied to identify a *C. trachomatis*-host interactome on a global scale. Comparing them, 58 inclusion associated proteins were detected by both approaches where 7 out of these 58 proteins were published before (Banhart et al. 2017). Aeberhard et al. detected 40% of previously published protein-protein interactions whereas Mirrashidi et al. identified 20% of these interactions (Banhart et al. 2017). This difference clearly lies in the different methodologies which were discussed in more detail by Banhart et al. (Banhart et al. 2017). In sum, the studies by Aeberhard et al. and Mirrashidi et al. identified and characterised a global picture of the interactions between inclusions and host cellular proteins and both studies showed that *C. trachomatis* interacts with distinct cellular compartments and pathways (Aeberhard et al. 2015; Mirrashidi et al. 2015).

The recruitment of SNX-BARs (SNX1, SNX2, SNX5 and SNX6) to the chlamydial inclusion at mid-infection stages based on the study by Aeberhard et al. pointed to an association of SNX-BARs with *C. trachomatis* already at early infection stages. Hence, we characterised the localisation of SNX-BARs during early infection of *C. trachomatis*. Next, we aimed to study the mechanisms and the function of SNX-BAR recruitment to the chlamydial inclusion at mid-infection time points in SNX KO cell lines. In addition, we took a closer look at tubular structures emanating from the inclusions. Finally, we hypothesised that identifying SNX1-associated proteins will unveil greater understanding of functions of SNX-BAR recruitment in the host cell and infection context. Thus, we identified proteins associated with SNX1 which localised on inclusions and along inclusion tubules during mid-infection stage.

4.1 SNX recruitment to *C. trachomatis*

4.1.1 SNX recruitment during the early infection stage

Host cellular retromer is recruited to C. trachomatis early in infection

To our knowledge, this is a first study in which the localisation of SNX-BARs and VPS35 of the retromer was addressed at early infection time points in *Chlamydia*-infected cells. Early accumulation of SNX-BARs and VPS35 proximal to *C. trachomatis* started at 4 h p.i. (Figure Figure 14, Figure 17 and Figure 18). As from 8 h p.i., SNX-BARs and VPS35 accumulated in a perinuclear region in close proximity to *C. trachomatis*, while protein expression levels of SNX1 was not altered during early infection indicating that *Chlamydia* spp. rearrange localisation of the retromer but do not regulate its protein expression levels (Figure 14 - Figure 18). Since SNX5 was demonstrated to bind to IncE, we next assessed the localisation of SNX-BARs and IncE in *C. trachomatis* infected cells. IncE is an inclusion membrane protein encoded by an early operon. This operon encodes the four Inc proteins IncD, IncE, IncF and IncG but not IncA. Early Incs are expressed within the first 2 h, while IncA is expressed at 16 h p.i. (Scidmore-Carlson et al. 1999; Shaw et al. 2000). In this thesis, SNX-BARs and IncE localised in close proximity during early infection which corresponds to the localisation pattern of LPS and MOMP (Figure 18). Binding of SNX5 or SNX6 to IncE may apply at early infection time points. In uninfected HeLa cells, SNX-BARs and VPS35 localised in a disperse punctuate pattern. This is consistent with localisation studies of SNX1 and SNX2 in uninfected cells (Carlton et al. 2004; Carlton and Cullen 2005; Carlton et al. 2005; Kvainickas et al. 2017; Simonetti et al. 2017). These studies showed that SNX-BARs and VPS35 are endosomally localised and co-localised to each other (Gullapalli et al. 2004; Seaman 2004; Carlton et al. 2004; Carlton and Cullen 2005; Carlton et al. 2005; Kvainickas et al. 2017; Simonetti et al. 2017). With regard to the localisation of the VPS trimer, Seaman studied localisation of VPS26 whereas Kvainickas et al. and Simonetti et al. showed localisation of VPS35 (Seaman 2004; Kvainickas et al. 2017; Simonetti et al. 2017). Since VPS35 directly binds to the cargo, we considered VPS35 as a prototype marker to assess localisation of the cargo-selective subcomplex.

Chlamydia spp. are known to be trafficked along microtubules to the MTOC in a dynein-dependent but dynamitin-independent process (Grieshaber, Grieshaber, and Hackstadt 2003). Microdomains on the inclusion membrane of *C. trachomatis* are enriched in cholesterol, active Src-family kinases and at least four Incs (IncB, CT101, CT122 and CT850) (Mital et al. 2010). The inclusion microdomains tightly associate with microtubules. CT850 harbours a binding domain for a dynein light chain isoform, DYNLT1, thereby enabling association of CT850 with dynein (Mital et al. 2015). Hence, after being trafficked along microtubules, *Chlamydia* spp. accumulate at the MTOC in a peri-Golgi region where *Chlamydia* spp. establish their niche. All examined retromer components, SNX-BARs and VPS35, accumulated at the MTOC in a perinuclear region where *C. trachomatis* localised (Figure 19). Based on that, we conclude that *C. trachomatis* uses the retromer to traffic along microtubules to the MTOC or at least uses a

similar retrograde trafficking route as the retromer. Regardless of whether HeLa cells were uninfected or infected with *C. trachomatis*, VPS35 and SNX-BAR proteins co-localised suggesting connection of the two subcomplexes. Hence, we propose that the retromer is not disconnected during early infection stage assuming that retromer function remains intact. Throughout the early infection, we observed co-localisation of SNX-BARs, either with LPS or MOMP or with IncE as we observed co-localisation signals at early infection time points and at mid-infection time points of *C. trachomatis* L2. This suggests an association between *C. trachomatis* and retromer, though we did not analyse co-localisation in-depth. The developmental cycle of *C. trachomatis* D takes longer compared to *C. trachomatis* L2 resulting in decelerated trafficking at early infection time points, visibly by *C. trachomatis* D localising proximally to SNX1 at 8 h p.i. but not revealing co-localisation signals to a similar extent as observed in *C. trachomatis* L2. Due to the presence of distinct co-localisation in *C. trachomatis* L2 and likely at later infection time points in *C. trachomatis* D infected cells, we assume that *C. trachomatis* acts as a retromer cargo that is then sorted towards the TGN and finally localises at a perinuclear region. Final localisation of *C. trachomatis* was observed at 8 h p.i. (Figure 14 - Figure 17).

Taken together, we propose that after internalisation of *Chlamydia* spp. into the host cell, *Chlamydia* spp. reside in the endosomal-like compartment. Soon after entry, *C. trachomatis* rapidly remodels the membrane towards an inclusion membrane which still resembles the endosomal compartment (Scidmore, Fischer, and Hackstadt 2003). Furthermore, we assume that *C. trachomatis* either uses a similar trafficking route as the retromer or co-opts retromer-mediated retrieval to evade fusion with the lysosomes and to be trafficked to the MTOC during the early infection (Figure 50). Thereby, SNX5 and SNX6 bind to the $p150^{glued}$ component of dynactin in order to link the retromer to the microtubule system that together with the actin cytoskeleton generate push and pull forces to pinch off retromer coated transport vesicles (Wassmer et al. 2009; Hong et al. 2009; Cullen and Korswagen 2012). Synergy of both, binding of CT850 to dynein and binding of SNX-BARs to dynactin may ensure trafficking of the early inclusion to the MTOC. In parallel, IncE is able to bind the PX domains of SNX5 and SNX6 but fails to bind to SNX1 and SNX2 PX domains (Mirrashidi et al. 2015; Paul et al. 2017; Elwell et al. 2017). This binding may ensure trafficking of *C. trachomatis* along microtubules towards the MTOC while possible binding of VPS trimer to CI-MPR may not be affected as CI-MPR did not localise separately from the retromer (Figure 20). Altogether, we postulate a model in which *C. trachomatis* co-opts the retromer rather than it uses a similar retromer trafficking route.

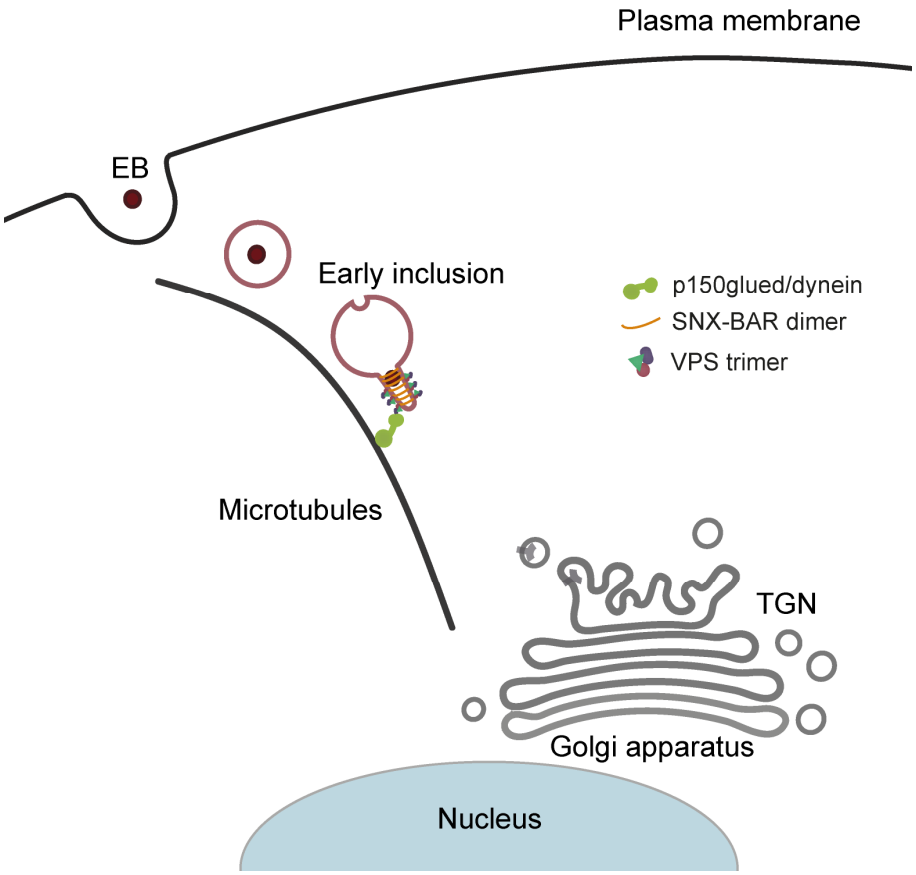

Figure 50. Model of early trafficking of *C. trachomatis*.
After entry of *Chlamydia* spp. into the host cell, the endosomal compartment is rapidly remodelled towards the inclusion. Synergy of both, binding of CT850 to dynein and binding of SNX-BARs to dynactin ensures trafficking of the early inclusion towards the MTOC which is proximally located to the TGN and GA. SNX-BAR: Sorting nexin-BAR proteins of the retromer; VPS: vacuolar protein sorting proteins; TGN: *trans*-Golgi network; GA Golgi apparatus.

Beyond SNX-BAR retromer-mediated cargo retrieval

Our results indicate a model in which trafficking of *Chlamydia* is mediated by an SNX-BAR retromer retrieval as SNX-BARs localised proximally to the bacteria at the early infection stage (Figure 14 - Figure 17). In addition, we showed that SNX-BARs co-localised with VPS35 at early infection time points. Apart from localisation studies of the retromer, CI-MPR co-localised with SNX-BARs in *C. trachomatis* infected cells at 8 h p.i. (Figure 20). Moreover, CI-MPR localised proximally to *C. trachomatis* visualised by LPS signal (n=2, data not shown) supporting our hypothesis that *C. trachomatis* uses the retromer to separate from the endolysosomal pathway for retromer-mediated cargo retrieval. In conclusion, cargo retrieval does not seem to separate from the retromer in *C. trachomatis* infected cells during early infection. VPS35 may bind to the cargo CI-MPR whose binding may not be affected during early infection as the cargo is thought to interact with the retromer through VPS35 (Arighi et al. 2004; Rojas et al. 2007). In parallel, SNX5 binds IncE. Hence, we assume that retromer-mediated CI-MPR trafficking is not affected during infection. In contrast, affinity-purification mass spectrometry of SNX5-transiently expressing cells identified CI-MPR to interact with SNX5

(Elwell et al. 2017). As Mirrashidi et al. showed that ectopic expression of IncE was sufficient to disrupt CI-MPR trafficking, Elwell et al. focussed on the interaction between SNX5 and CI-MPR and revealed that WT IncE interfered with CI-MPR binding to SNX5 while mutant IncE failed. This suggested that IncE is capable to disrupt SNX5:CI-MPR interaction through its conserved binding groove thereby displacing CI-MPR (Elwell et al. 2017). Altogether, binding of SNX5 to CI-MPR may add an additional cargo retrieval mechanism besides the interaction between VPS35 and CI-MPR that we propose based on our localisation data. Interestingly, retromer retrieval was further challenged recently (Chamberland and Ritter 2017). Two studies questioned the current retromer model of CI-MPR retrieval involving the two retromer subcomplexes as they demonstrated that SNX-BARs mediate a VPS trimer-independent transport of CI-MPR in a non-infection context (Kvainickas et al. 2017; Simonetti et al. 2017). So far, it is commonly accepted that cooperation of the VPS trimer and the SNX-BAR dimer is required for tubular endosomal sorting based on membrane deformation and membrane tubulation induced by association of retromer complex to endosomes. However, despite loss of VPS expression, SNX-BAR dimer recruitment was not affected indicating a much more variable mechanism of retromer retrieval (Gallon and Cullen 2015). In this regard, Kvainickas et al. and Simonetti et al. identified the SNX-BAR dimer as the cargo-selective element of CI-MPR retrograde transport in mammalian cells independently of the VPS trimer as KO of SNX-BARs but not KO of VPS35 caused a loss of retrograde sorting of CI-MPR (Kvainickas et al. 2017; Simonetti et al. 2017). Whether CI-MPR is retrieved by SNX-BAR/VPS retromer or by a VPS-independent retrieval in *C. trachomatis* infected cells, remains to be determined. Earlier RNAi-mediated loss-of-function screen to define the role of mammalian SNXs in retromer-mediated retrograde transport yet established that suppression of SNX1, SNX5 and/or SNX6 reduced the efficiency of endosome-to-TGN transport of CI-MPR (Wassmer et al. 2007). These data suggested that SNXs are either directly or indirectly associated with endosome-to-TGN retromer-mediated transport of for instance CI-MPR (Wassmer et al. 2007). Besides SNX-BAR retromer retrieval, other assembled retromer complexes have been described and are thus reasonably conceivable. Classical retromer consists of a VPS trimer and an SNX-BAR dimer. Beyond that, identification of SNX3 retromer and SNX27 retromer, each comprising the core VPS trimer, extended the retromer model to a concept of multiple different retromer complexes (Harterink et al. 2011; Lauffer et al. 2010; Temkin et al. 2011). These different retromer complexes associated with specific SNX proteins may enable trafficking pathways of different proteins, thereby emphasising the retromer as a master regulator of endosomal sorting (Gallon and Cullen 2015). Nonetheless, in the host-cell derived inclusion proteome by Aeberhard et al., SNX3 was identified but did not localise on the inclusion whereas SNX27 was not identified (Aeberhard et al. 2015). Thus, we focussed on SNX-BAR retromer as our localisation studies supported an SNX-BAR-mediated retrieval of *C. trachomatis*.

Recent studies revealed cargo retrieval mediated by retromer-independent mechanisms thus highlighting the variety of retrieval mechanisms (McNally et al. 2017; McNally and Cullen 2018)

(**Fehler! Verweisquelle konnte nicht gefunden werden.**). One of them is termed retriever-mediated retrieval which is, similarly to the retromer, a multi-protein complex but displays assembly of different proteins. It is a hetero-trimer consisting of DCSR3, chromosome 16 open reading frame 62 (C16orf62) and the retromer subunit VPS29 (McNally et al. 2017; McNally and Cullen 2018). Retriever and retromer share structural similarities as the most obvious one is that VPS29 is present in both. Furthermore, retriever and retromer undertake distinct cargo retrieval pathways but are localised to the same endosomal retrieval subdomain (McNally and Cullen 2018). WASH and CCC complexes are additional multi-protein complexes involved in retriever-mediated retrieval (Gershlick and Lucas 2017, McNally and Cullen 2018). The CCC complex is a heterodimer and the complex itself does not associate with endosomes but interacts with a subunit of the WASH complex which is present at the endosomal surface (Gershlick and Lucas 2017), McNally and Cullen 2018).

Altogether, recent findings started to shed light on the complexity of retrograde trafficking. In the context of chlamydial infections, several mechanisms of *C. trachomatis* retrieval from endosomes are conceivable. Although we think that *C. trachomatis* uses the retromer to be trafficked from endosomes to the MTOC, we are conscious that our hypothesis needs to be proven further and that future research on whether other retrieval mechanisms are involved in early *C. trachomatis* trafficking remains to be determined.

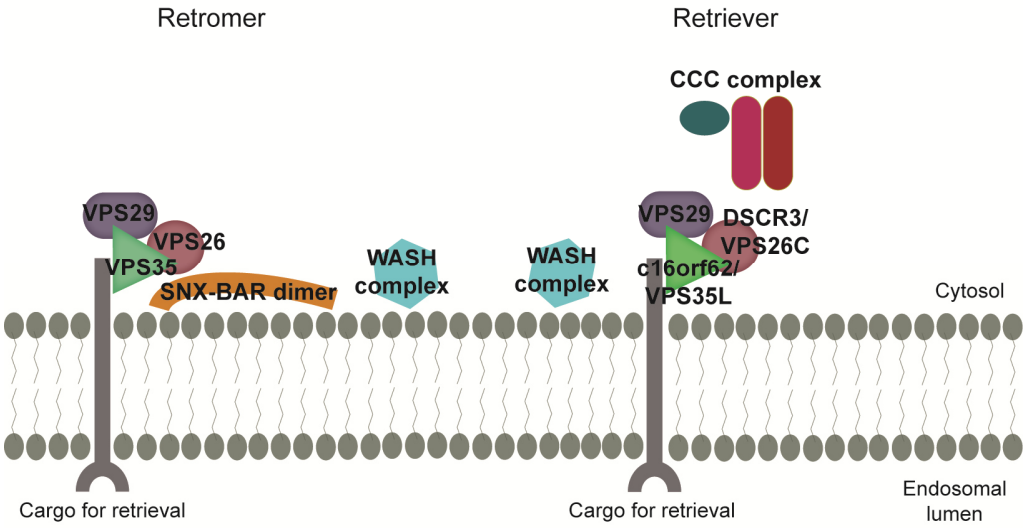

Figure 51. Retromer and retriever are two multi-protein complexes in retrograde trafficking. The retromer comprises a VPS trimer (VPS26-VPS29-VPS35) and an SNX-BAR dimer. The retriever is a hetero-trimer consisting of DCSR3, chromosome 16 open reading frame 62 (C16orf62) and VPS29. Both retrieval mechanisms require the WASH complex. Retriever-mediated retrieval also involves the CCC complex consisting of coiled-coil domain-containing protein 22 (CCDC22), coiled-coil domain-containing protein 93 (CCDC93) and the association of copper metabolism MURR1 domain-containing (COMMD) proteins. VPS: Vacuolar protein sorting protein, WASH: Wiskott–Aldrich syndrome protein and SCAR homologue. Adapted from McNally 2017, McNally and Cullen 2018.

4.1.2 SNX recruitment during mid-infection stages

Localisation of retromer components

At mid-infection, retromer SNX-BARs were recruited to the chlamydial inclusion while VPS35 localised in punctuate structures adjacent to the inclusion consistent with studies by Aeberhard et al. and Mirrashidi et al. (Figure 28 and Figure 29) (Aeberhard et al. 2015; Mirrashidi et al. 2015). In addition, tubular structures emanating from the inclusion were positive for retromer SNX-BARs but not for VPS35 indicating specific recruitment of the membrane-sensing subcomplex. This suggests further that the two subcomplexes of the retromer are at least in part disconnected on the inclusion membrane. In yeast cells, the retromer is a stable hetero-pentameric protein complex. In mammalian cells, in contrast, the interaction between SNX-BARs and the VPS trimer exhibits low affinity (Swarbrick et al. 2011). This may contribute to the capability of the retromer to separate during mid-infection time points. Moreover, the observed separation of the two subcomplexes at mid-infection time point supports the model that the two subcomplexes operate independently in cargo trafficking (Nisar et al. 2010; Prosser et al. 2010; Chua et al. 2012). In contrast to retromer SNX-BARs, SNX3, SNX12 and SNX27 were not recruited to the inclusion, indicating that *C. trachomatis* inclusions and tubules specifically associate with retromer SNX-BARs (Aeberhard et al. 2015; Mirrashidi et al. 2015).

SNXs bind to PIP-enriched membranes and in addition, seem to display a variable PIP-binding profile (Cullen 2008). SNX1 and SNX2 bind to PI3P and $PI3,5P_2$, SNX5 and SNX6 bind to $PI4,5P_2$ and PI4P (Cozier et al. 2002; Carlton et al. 2004; Carlton et al. 2005; Koharudin et al. 2009; Niu et al. 2013). PI4P has been detected in the inclusion membrane whose presence may facilitate recruitment of SNX-BARs (Moorhead et al. 2010). Association of the retromer with endosomes occurs through the interaction of VPS35 with Rab7 which is coordinated with the Rab switch from Rab5 to Rab7 (Rojas et al. 2007; Seaman et al. 2009). The retromer is associated throughout the maturation of endosomes for coordinated trafficking (Gallon and Cullen 2015), Rab7, however, was absent on the inclusion, again assuming possibly independent function of the two retromer subcomplexes (doctoral thesis from Sophia Edelmann 2016 (Edelmann 2016)).

Domain-specific recruitment of SNX-BARs to the inclusion

In this study, we examined the localisation of SNXs functional domains by generating GFP-tagged fusion proteins of full length SNX-BARs, PX or BAR domain. All full length fusion proteins localised on the inclusion consistent with the endogenous localisation of SNX-BARs and studies by Aeberhard et al and Mirrashidi et al. Interestingly, while SNX1 and SNX2 BAR domains were recruited to the inclusion, it was the opposite for SNX5 and SNX6, both exhibiting recruitment of PX domains to the inclusion (Figure 30). This indicates a domain-specific recruitment. SNX5 and SNX6 PX domains were sufficient to mediate recruitment which was the case for SNX1 and SNX2 BAR domains. SNX-BARs are composed of a PX and a BAR domain,

each domain exhibiting distinct functions. Membrane targeting specificity requires the N-terminal PX domain which binds to PIPs within membranes (Zhong et al. 2005). In this context, holo SNX1 localised precisely at endosomes while sole SNX1 PX domains were insufficient to localise properly to PI3P-enriched endosomal membrane. In this thesis, sole SNX1 and SNX2 PX domains were insufficient to bind to the inclusion membrane consistent with the study by Zhong et al. (Zhong et al. 2005). This indicates other structural features of SNX1 to be essential to enhance binding affinity (Seet and Hong 2006). Adjacent to the PX domain is the BAR domain. BAR domains are a curved dimerisation motif and function in membrane shaping as they sense and induce membrane curvature (Frost, Unger, and De Camilli 2009b). The C-terminal BAR domain lacks targeting specificity but drives dimerisation required to enhance binding affinity (Koharudin et al. 2009; Zhong et al. 2005). Other proteins may also stabilise SNX1 and SNX2 dimers (Zhong et al. 2005). Interestingly, SNX5 and SNX6 share a unique hydrophobic groove composed of a helix-turn-helix structural insertion that is absent in other SNX family members such as SNX1, except for SNX32 (Koharudin et al. 2009). This unique hydrophobic groove is likely to enable distinct binding specificity to PIPs in comparison to other SNXs. SNX5 and SNX6 are able to bind to $PI4,5P_2$ and PI4P, respectively (Koharudin et al. 2009). With regard to the chlamydial inclusion, different PIPs were found to be present in the inclusion membrane, among which PI4P has been detected (Moorhead et al. 2010). In conclusion, SNX5 and SNX6 may facilitate binding to PIPs other than PI3P in the inclusion membrane. SNX5 and SNX6 BAR domains seem to lack both, lipid- or protein binding properties. Given that PX domains are the membrane-binding domain and based on our data, we hypothesise an SNX-BAR interaction model in which SNX5 and SNX6 bind to the inclusion via their PX domain and SNX1 and SNX2, in turn, dimerise with either SNX5 or SNX6 via their BAR domain (**Fehler! Verweisquelle konnte nicht gefunden werden.**).

Loss of SNX5/SNX6 prevents SNX1/SNX2 recruitment

Recruitment of SNX1 and SNX2 to the chlamydial inclusion was absent in SNX5/SNX6 double KO cell line at mid-infection time point suggesting that SNX1 and SNX2 recruitment is dependent on SNX5 and/or SNX6 (Figure 33). This supports our hypothesis that SNX1 or SNX2 are associated with either SNX5 or SNX6. Furthermore, we observed tubular structures which are positive for SNX-BARs and IncE and which emanated from the mid-infection inclusion. Interestingly, in SNX5/SNX6 double KO cell line, tubular structures positive for IncE were yet evident, suggesting that SNX-BARs decorate tubular structure but formation of tubular structures is at least in part independent from SNX-BARs (Figure 33).

Interaction of SNX5 and SNX6 with IncE

At the time of characterising SNX recruitment at mid infection stages, IncE was shown to recruit and specifically bind to SNX5 and SNX6 (Mirrashidi et al. 2015; Paul et al. 2017; Elwell et al. 2017). The structure data, in particular, were published during our work on SNX-BAR and IncE localisation. Using GFP-tagged SNX1 and SNX5 fusion proteins in this thesis, we observed co-localisation of SNXs with IncE consistent with Mirrashidi et al. (Figure 31). In follow-up biochemical studies after SNX5 PX:IncE binding has been published, structures of direct binding of SNX5 and SNX6 PX domains to predicted IncE C-terminal ß-hairpin independently of phosphoinositides were shown by crystallography (Paul et al. 2017; Elwell et al. 2017; Sun et al. 2017). Accordingly, the unique hydrophobic groove of SNX5 and SNX6 enables binding to IncE (Paul et al. 2017). Paul et al. fused human SNX5 PX domain to the C-terminal part of IncE from *C. trachomatis* LGV L3, Elwell et al. determined the interaction structurally by using murine SNX5 and synthesised IncE $_{108-132}$ from *C. trachomatis* D. Sun et al. co-crystallised murine SNX5 with IncE $_{109-132}$ from *C. trachomatis* LGV L3 (Banhart et al. 2017). Using IncE of different chlamydial species is reasonable as the IncE amino acid sequences share 89% identity (Paul et al. 2017). Crystal structures of SNX5 PX:IncE revealed that the C- terminal part of IncE forms a β-hairpin with an N-terminal β- and a C-terminal βB-strand that associates with the hydrophobic groove of SNX5 PX domain (Paul et al. 2017; Elwell et al. 2017; Sun et al. 2017; Banhart et al. 2017). Importantly, regions that distinguish the SNX5 PX $_{20-180}$ structure are distant from the BAR interaction site assuming that the dimerisation of SNX proteins via their BAR domain would not be affected by the interaction complex SNX5:IncE (Elwell et al. 2017). Affinity-purification mass spectrometry revealed the identification of SNX1 when using WT- and mutant SNX5-transiently expressing cells (Elwell et al. 2017). The unimpaired dimerisation of SNX proteins by the SNX5:IncE interaction is in line with our interaction model of SNX-BAR on the inclusion. Moreover, disruption of the small hydrophobic core at SNX5 PX $_{20-180}$ by mutating SNX5 residues Y132 and F136 destabilised the interaction complex SNX5:IncE due to mutations of SNX5 residues Y132 and F136 while endogenous SNX6 remained recruited (Elwell et al. 2017). We aimed to confirm these findings in our infection system at mid-infection time point (24 h p.i.) and mutated SNX5 residues Y132 and F136 to aspartic acid for both residues by quick change mutagenesis (data not shown). eGFP-SNX5 $_{WT}$ localised on the inclusion as expected. eGFP-SNX5 $_{Y132D\ F136D}$ failed to localise on the inclusion (data not shown) consistent with the results of Elwell et al. (Elwell et al. 2017). In sum, targeting specificity requires SNX5 PX $_{Y132\ F136}$ of the hydrophobic groove. Altogether, we postulate the following interaction model on the chlamydial inclusion: SNX5 or SNX6 PX domains directly bind to an inclusion membrane protein, most likely IncE consistent with Mirrashidi et al. and Elwell et al. SNX1 or SNX2, in turn, dimerise with either SNX5 or SNX6 via their BAR domain.

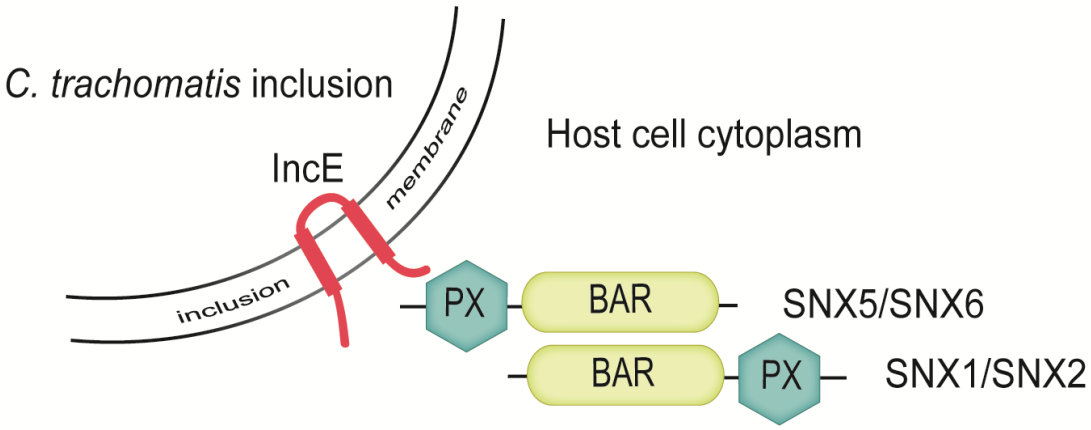

Figure 52. Model of SNX5/6:IncE interaction on the inclusion of *C. trachomatis*.
SNX5 and SNX6 bind to inclusion membrane protein IncE at the cytosolic site. Bar domain of SNX1 and SNX2 dimerise with BAR domain of SNX5 and SNX6. Model of SNX-BAR dimerisation based on van Weering, Verkade and Cullen 2010.

4.2 Characterisation of SNX tubules

Throughout the developmental cycle, we observed tubular structures positive for SNX-BARs. At early infection, these tubules were only positive for SNX-BARs. At mid-infection, these structures were positive not only for SNX-BARs but also for IncA, IncE and possibly other inclusion membrane proteins.

4.2.1 Early SNX tubules

Interestingly, we observed tubular structures positive for endogenous SNX-BARs that were prominent at an early infection time point of 8 h p.i. (Figure 21). SNX tubular structures have been observed in uninfected cells in which GFP-SNX1 fusion protein decorated tubules of early endosomes (Carlton et al. 2004). Overexpression of SNX1 resulted in the formation of an extensive tubular network and high concentration of recombinant SNX1 was capable to induce membrane tubulation demonstrated by an *in vitro* liposome assay (Carlton et al. 2004). Furthermore, cryo-EM revealed enrichment of endogenous SNX1 on tubules of the early endosome (Carlton et al. 2004). As SNX1 possesses a BAR domain that is a dimerisation motif which senses membrane curvature and is capable to drive membrane tubulation, Carlton et al. proposed that SNX proteins containing a BAR domain play a general role in membrane tubulation and trafficking (Takei et al. 1999; Peter et al. 2004; Carlton et al. 2004). In contrast to this hypothesis, Carlton et al. demonstrated later that SNX2 appears only to be able to sense but not to induce membrane curvature concluding that SNX-BARs share the ability to sense membrane curvature while the ability to induce membrane tubulation is not shared (Carlton et al. 2005). The discussion was extended by van Weering et al. in 2012. Membrane remodelling and tubule formation of all 12 human SNX-BARs were analysed in a to date first screen, with the result that SNX-BARs bear an amphipathic helix but display functional diversity (van

Weering et al. 2012). Considering SNX-BARs of the retromer, SNX1 and SNX2 were able to induce membrane tubulation while SNX5 and SNX6 were not, thereby contradicting SNX2 membrane tubulation incapability. Moreover, by defining the dimerisation pattern of SNX-BARs, the study by van Weering et al. revealed that SNX1 and SNX2 are capable of forming homo- and heterodimers while SNX5 and SNX6 are capable of forming heterodimers only. With regard to the retromer, the SNX-BAR dimer occurs in recurring pairs SNX1/5, SNX1/6, SNX2/5 and SNX2/6 (Trousdale and Kim 2015). Eventually, van Weering et al provided a three-step model for SNX-BAR-mediated membrane remodelling: i) BAR domain-mediated dimerisation, ii) membrane association and insertion of an amphipathic helix (present in all SNX-BARs) into the lipid bilayer and iii) formation of higher ordered assemblies through tip-loop contact within the BAR domain (van Weering et al. 2012).

In this thesis, we observed tubules positive for all four SNX-BARs of the retromer complex in *C. trachomatis* infected cells (Figure 14, Figure 17 and Figure 21). Taking the data by van Weering et al. into account, we conclude the following model of early *C. trachomatis* trafficking (Figure 50): During early infection, the inclusion membrane is rapidly remodelled but resembles the endosomal membrane. In the following, SNX-BARs associate with the early inclusion membrane. SNX5 and SNX6 bind to IncE; SNX1 and SNX2, in turn, dimerise with SNX5 and SNX6. Then, membrane tubulation is induced by SNX1 and SNX2. In addition, SNX5 and SNX6 bind to dynein to allow trafficking of the early inclusion towards the MTOC. Concordantly with that, early aligned SNX tubular structures resemble a trafficking route that *C. trachomatis* utilises (Figure 21 A and B). Due to the accumulation of SNX1 at the MTOC and the observation of early SNX1 tubules, we examined *C. trachomatis* trafficking further. Early *C. trachomatis* trafficking was impaired upon disruption of microtubules since nocodazole treatment resulted in strong reduction of SNX1 accumulation at the MTOC at early infection time point but did not inhibit overall SNX1 recruitment at mid-infection time point (Figure 22). In addition, disruption of microtubules resulted in disruption of early (and late) SNX tubules. Taken together, both, early *C. trachomatis* trafficking and formation of SNX tubules are dependent on microtubules. This is consistent with the study by Mirrashidi et al. which demonstrated that nocodazole treatment resulted in disruption of SNX-positive tubules but did not inhibit SNX recruitment (Mirrashidi et al. 2015). Moreover, dependency of *C. trachomatis* trafficking on microtubules is consistent with the model postulating that SNX5 and SNX6 associate with IncE and bind to dynein (Figure 50).

We categorised tubules according to their formed tubular structure phenotype at early infection time point of 8 h p.i. (Figure 21 A). We used confocal microscopy images of *C. trachomatis* infected cells to manually quantify the proportion of cells exhibiting SNX1 tubular structures and to measure SNX1 tubules as being representative for retromer SNX-BARs (Figure 21 C and D). In nearly all *C. trachomatis* infected cells, SNX1 clustered structures were visible (99% of cells) exhibiting a tubule length 0.5 and 1 µm. Singular SNX1 structures were visible in more than 50% of cells with a tubule length between 0.5 and 1 µm and aligned SNX1 structures in almost

20% of cells with a tubule length between 5 and 6 µm in 95% of cases. In uninfected cells, Hunt et al. analysed SNX1 tubules and found that the proportion of control cells showing tubules is between 5% and 10%. Depletion of motor proteins dynein-1 heavy chain, kinesin-1 and dynein containing light chain intermediate chain 2 resulted in an increase of the proportion of tubules (Hunt et al. 2013). Hunt et al. defined dynein-1 and kinesin-1 as motors for SNX1-coated membranes. Tubules of singular SNX1 and SNX1 clustered structures exhibited a length of mainly 0.5 to 1 µm. Aligned SNX1 tubules were 5 to 6 µm in length. Singular SNX1 and SNX1 clustered tubules displayed shorter tubules than observed before in untreated control cells in which SNX1 tubules were on average 2 µm in length (Hunt et al. 2013). Depletion of especially dynein-1 heavy chain, kinesin-1 and dynein containing light chain intermediate chain 2 resulted in an increase of tubule length of 4 to 6 µm. A similar length was observed for aligned SNX1 tubules in untreated *C. trachomatis* infected cells. Hunt et al. correlated specific microtubule motor proteins to motility and tubulation architecture. A possible correlation of *C. trachomatis* and motility is an interesting consideration given that *C. trachomatis* traffics along microtubules. Whether *C. trachomatis* controls motility during trafficking remains to be determined.

In the study by Hunt et al., tubules were counted by hand and their length was determined using the line measurement tool in Volocity 5.4.1 (Perkin Elmer). In this thesis, measurement of the early tubules (proportion of tubules per cells and length of tubules) was also performed by hand. This approach, however, is time-consuming, rate-limiting and more inexact in investigating endosomal tubulation phenotypes (Newton and Reid 2016). Hence, the automated image analysis system to quantify endosomal tubulation proposed by Newton and Reid is a worthwhile tool for future research.

We were not able to identify the ultrastructure of early SNX tubules by using EM. cLEM requires transient expression of SNX fusion proteins. At early infection stage, this technique, however, failed to exhibit distinct phenotypes between uninfected and infected cells as observed for endogenous SNXs.

4.2.2 Mid-infection tubules

At mid-infection, long, occasionally branched tubular structures positive for SNX-BARs but negative for VPS35 were clearly visible (Figure 28 and Figure 29). These structures were also positive for IncA and IncE. Moreover, live-cell imaging revealed highly dynamic tubules (unpublished data). While both examined *C. trachomatis* serovars, *C. trachomatis* D and L2, displayed tubular structures, the number and length of these tubules differed between the serovars (data not shown). In control cells, inclusion tubules displayed tubule length of up to nearly 25 µm (Mirrashidi et al. 2015). Overexpression of IncE in *C. trachomatis* L2 enhanced tubule formation and increased SNX6 recruitment. In contrast, depletion of SNX-BARs decreased both, the number and length of inclusion tubules indicating that recruitment of SNX-BARs enhances inclusion tubulation (Mirrashidi et al. 2015). Given that BAR-bearing proteins are able to induce tubulation, one might think that recruited SNX-BARs induce inclusion

tubules. This is in contrast to the observation in infected SNX5/SNX6 KO cell line in which recruitment of SNX1 and SNX2 was absent but IncE-positive tubules were yet evident (Figure 33).

With this thesis, we provide an ultrastructure of inclusion tubules. By using cLEM, either via chemical fixation according to the protocol from Madela et al. (Madela et al. 2014) or via high-pressure freezing (cryofixation), elongated tubules that emanate from the inclusions were identified as membranous tubular structures (Figure 37). To our knowledge, inclusion tubules have not been investigated by ultrastructure before despite several EM studies on *Chlamydia* spp. EM data rather addressed other chlamydial species or focussed on, for instance, inclusion bodies (EBs, RBs), invasion and replication (e.g. (Matsumoto and Manire 1970; Chang et al. 1982; Prusty et al. 2012; Chang, Leonard, and Zhang 1997; Matsumoto 1981b, 1981a; Lee et al. 2018; Huang et al. 2010; Nans, Saibil, and Hayward 2014). cLEM is advantageous as it combines two techniques and correlates two images. It provides two information of one sample and facilitates the detection of rare events. In combination with TEM, ultrathin sections are generated to optimally visualise intracellular structures though proper registration of positions acquired by different imaging modes is a major problem (Madela et al. 2014). Here, we used µ-dishes with imprinted grids which allow registration of events and seem to be compatible with pre-embedding and post-embedding immunogold labelling but image registration accuracy is not precisely known (Madela et al. 2014). Chemical fixation is well established and easily performed by simply exchanging fluids within the culture dish (Rubbo, Gardner, and Webb 1967; Sabel, Hellman, and McDade 1969). A major drawback of chemical fixation is that it is slow and incomplete which may causes changes in the ultrastructure. When performing live-cell imaging, an additional arrest has to be considered (Madela et al. 2014). To verify our cLEM findings of chemical fixation, we applied HPF (cryofixation) combined with pre-embedding immunogold electron microscopy. Immunogold labelling of thin-sectioned samples is widely used for high-resolution electron microscopy (Hess et al. 2018). Cryofixation immobilises cellular dynamics within milliseconds and is thus the only approach to circumvent artificial ultrastructural deformation (Vanharreveld and Crowell 1964; McDonald 1999; Hess et al. 2018). cLEM in combination with HPF confirmed our findings after chemical fixation. Based on our data, tubular structures can be considered as tubules with some certainty. However, despite the great number of inclusion tubules that we observed in light microscopy, inclusion tubules were rarely detected in EM. In addition, we did not observe conjunctions of the tubules on the inclusion membrane which light microscopic images connote. We are uncertain of whether the highly dynamic tubules collapse during the fixation procedure.

We hypothesised that inclusion tubules may be ER-related structures and examined the localisation of RTN4 in *C. trachomatis* infected cells as *C. trachomatis* has been shown to interact with the ER (Dumoux et al. 2012; Dickinson et al. 2019). RTN4 is an ER membrane-shaping protein and induces ER tubule formation (Voeltz et al. 2006; Diaz and Ahlquist 2012). In infected WT HeLa cells, RTN4 localised along inclusion tubules but weakly localised on the

inclusion membrane (Figure 38). Interestingly, in infected SNX5/SNX6 KO cell line, RTN4 was absent on tubules suggesting that inclusion tubules are not solely ER-related structures. Since SNX1 and SNX2 which in fact drive membrane tubulation were absent on the inclusion in SNX5/SNX6 KO cell line, we can exclude a role of SNXs in tubule formation at this point. Factors driving inclusion tubulation are so far unknown. Future research on inclusion tubules is required to unveil their function and the mechanisms behind.

4.3 Function of SNX-BAR recruitment

4.3.1 Early *C. trachomatis* trafficking is affected in SNX KO

Using CRISPR/Cas9 as a tool to study protein functions

We applied the CRISPR/Cas9 system to knockout SNXs in order to examine the uptake of *C. trachomatis* and early *C. trachomatis* trafficking. Loss of single SNX1 and SNX5 did affect neither *C. trachomatis* uptake nor early *C. trachomatis* trafficking (Figure 24). In human cells, SNX1 and SNX2 do not play a functionally redundant role in controlling EGF and transferrin receptor sorting whereas SNX1 and SNX2 demonstrated redundant roles in retromer association with membranes and, in addition, in mouse development (Schwarz et al. 2002; Carlton et al. 2005; Griffin, Trejo, and Magnuson 2005; Rojas et al. 2007). Redundant roles may also apply to SNX5 and SNX6. Since SNX1 and SNX2, as well as SNX5 and SNX6, may exhibit redundant functions, it is plausible that *C. trachomatis* uptake and trafficking were not affected in SNX1 and SNX5 single KO. Owing to the binding of SNX5 and IncE and the fact that SNX5 and SNX6 bind to dynein, we generated an SNX5/SNX6 double KO cell line to rule out redundant functions of SNX5 and SNX6. Interestingly, loss of both, SNX5 and SNX6 disrupted SNX1 accumulation at the MTOC in *C. trachomatis* infected cells assuming that early SNX1- and likely SNX2-mediated sorting is impaired (Figure 26). Furthermore, KO of SNX5/SNX6 did not affect *C. trachomatis* uptake but resulted in considerably decreased trafficking at 8 h p.i. indicating that *C. trachomatis* trafficking is dependent on retromer's SNX5/SNX6 and that SNX5 and SNX6 may exhibit redundant functions. Taken together, loss of both, SNX5 and SNX6 seems to impair *C. trachomatis* trafficking. This is again in line with our model of early *C. trachomatis* trafficking given that *C. trachomatis* uses the retromer to traffic towards the MTOC as SNX5 and SNX6 bind to dynein.

RNAi and CRISPR/Cas9 are among others two systems to silence and knockout genes, respectively. RNAi involves a dicer enzyme that digests exogenously introduced double-stranded RNA to short interfering RNAs (siRNAs) which further on assemble with an RNA-induced silencing complex (RISC) (Hannon 2002; Doi et al. 2003). Unwound single-stranded siRNAs are used to guide RISC to select target substrates (Elbashir, Lendeckel, and Tuschl 2001; Martinez et al. 2002; Hannon 2002). Finally, RISC silences expression by cleavage of target mRNA (Martinez et al. 2002). CRISPR/Cas system addresses genomic DNA instead of mRNA. The type II CRISPR system derived from *S. pyogenes* encodes Cas9 which is targeted

to genomic DNA by sgRNAs. Cas9 carries out strand-specific cleavage yielding double-strand breaks (DSB) (Jansen et al. 2002; Ran et al. 2013). Upon cleavage, two mayor repair mechanisms occur at the cleaved target DNA locus. On the one hand, the error-prone nonhomologous end-joining (NHEJ) process lacks repair template and re-ligates DSBs thereby producing insertions/deletions (indels) (Perez et al. 2008; Taleei et al. 2013). On the other hand, the homology-directed repair (HDR) process generates defined modifications in the presence of exogenously introduced repair template (Ran et al. 2013). Noteworthily, HDR occurs at lower frequencies than NHEJ and the latter is often utilised when using the CRISPR/Cas9 system as a genome-editing tool to generate targeted genomic DNA mutations, so did we use in this thesis. However, one drawback of the CRISPR/Cas system are off-target activities as nucleases such as Cas9 may cleave off-target DNA sequences due to similar genomic sequences (Hsu et al. 2013; Fu et al. 2013; Jiang et al. 2013). Despite the known potential of off-target activities, we applied CRISPR/Cas9 system to knockout SNXs in order to study function of SNX recruitment during infection with *C. trachomatis*, as suppression of retromer through RNAi may be insufficient.

Loss of SNX5/SNX6 impairs SNX1 and VPS35 accumulation at the MTOC

Loss of SNX5/SNX6 in *C. trachomatis* infected cells revealed disruption of SNX1 accumulation indicating mutual dependence of SNX1 and possibly SNX2 on SNX5/SNX6 (Figure 25). RNAi-mediated suppression of SNX5 and SNX6 resulted in a significant reduction of endogenous SNX1 protein levels (data not shown) arguing that i) the two SNX1/SNX2 and SNX5/SNX6 exist in a stable, endosomally associated complex and that ii) SNX1/SNX2 and SNX5/SNX6 are mutually dependent (Wassmer et al. 2007). The latter supports our observation. Moreover, loss of SNX5/SNX6 caused a decrease in the number of cells displaying VPS35 accumulation at the MTOC compared to CRISPR Ctrl cells indicating that SNX-BARs and VPS35 function together at an early infection time point on the supposition that *C. trachomatis* acts as a cargo and is retrieved by retromer (Figure 27). In uninfected human cells, VPS35 and SNX-BARs were shown to operate independently in CI-MPR trafficking as CI-MPR transport was shown to be depended on direct engagement of heterodimeric combinations of SNX1 and SNX2 with SNX5 and SNX6 without a measurable role for VPS trimer (Kvainickas et al. 2017). In *Caenorhabditis elegans*, on the contrary, SNX-BARs and VPS trimer function together in CED-1 recycling for apoptotic cell clearance (Chen et al. 2010). In conclusion, retromer seems to display functional variability depending on the cargo to be sorted. Whether *C. trachomatis* trafficking is affected in VPS trimer KO cells remains to be determined.

4.3.2 Function of SNX-BARs during mid-infection stage

Using our SNX KO cell lines, we examined *C. trachomatis* primary infection and infectious progeny formation in a more robust system to unveil the function of SNX-BARs during mid-

infection stage (Figure 34 - Figure 36). Primary *C. trachomatis* infection (inclusion formation per nucleus) revealed no distinct difference among single SNX KO cell lines regardless of the examined MOI (Figure 34) suggesting that loss of single SNX does not affect *C. trachomatis* primary infection. This is consistent with the findings by Aeberhard et al. in which they used an MOI of 0.5 (Aeberhard et al. 2015). Interestingly, loss of both, SNX5 and SNX6, resulted in a threefold increase in *C. trachomatis* primary infection at an MOI 0.1 supporting the hypothesis of Aeberhard et al. and Mirrashidi et al. stating that SNX-BARs restrict *C. trachomatis* infection (Aeberhard et al. 2015; Mirrashidi et al. 2015). However, in SNX5/SNX6 KO cell line at an MOI 1, we detected only a difference of a factor 1.4 in primary infection compared to CRISPR Ctrl. Mirrashidi et al. observed no effect in primary infection in SNX5/SNX6 depleted cells but a decrease in primary infection in SNX1/SNX2 and in SNX1/SNX2/SNX5/SNX6 depleted cells (no MOI indicated). The decreased primary infection in SNX1/SNX2/SNX5/SNX6 depleted cells seemed to be the result of SNX1/SNX2 depletion rather than SNX5/SNX6 depletion (Mirrashidi et al. 2015). Mirrashidi et al. suggested that SNX1/SNX2, in particular, may participate in early infection stages which is consistent with our model of early *C. trachomatis* trafficking (see Figure 50). However, effect of loss of both, SNX1 and SNX2 on early *C. trachomatis* trafficking remains to be determined. Based on our findings in primary infection, we suggest that SNX5/SNX6, in particular, may participate in mid-to-late infection stages. This hypothesis is supported by findings of secondary infection. Although *C. trachomatis* replication (genome copy number) was affected in SNX1 single KO, but not in SNX5 KO, chlamydial replication increased in SNX5/SNX6 double KO cell line (Figure 35). We observed a similar trend for infectious progeny formation as loss of SNX5/SNX6 resulted in an increase whereas loss of sole SNX1 or SNX5 revealed only slight differences (Figure 36). Taken together, these data suggest that SNX5/SNX6 restrict *C. trachomatis* infection in mid-to-late infection stages. Increased replication and progeny formation may be explained by an increase in primary infection, thus displaying a correlation. This suggestion, however, is in contrast to Mirrashidi et al. stating no correlation (Mirrashidi et al. 2015). In the study by Aeberhard et al., replication was slightly affected upon depletion of different SNX-BARs with the twofold increase upon SNX5 depletion (Aeberhard et al. 2015). Replication upon depletion of SNX5/SNX6 or SNX1/SNX2 was not examined (Aeberhard et al. 2015). Interestingly, both, the studies by Aeberhard et al. and Mirrashidi et al. revealed enhanced infectious progeny formation upon depletion of SNX-BARs suggesting that these proteins restrict *C. trachomatis* infection. More precisely, Aeberhard et al. and Mirrashidi et al. observed a profound increase of infectious progeny upon SNX5 depletion (by a factor of 5) besides SNX-BARs double depletion (by a factor of 2) and SNX5/SNX6 depletion (by a factor of nearly 10), respectively. We were able to confirm an effect of SNX5/SNX6 double KO on the infectious progeny formation but not for SNX5 single KO. We observed an increase of infectious progeny formation in SNX5/SNX6 KO cell line, though at a lower level. The varying results may lie in the usage of different methodologies to silence SNXs (RNAi versus CRISPR/Cas9-mediated KO) since before, the role of retromer was assessed by

depletion of SNX-BAR mediated by RNAi (Aeberhard et al. 2015; Mirrashidi et al. 2015). Altogether, the results suggest that SNX-BARs may function distinctly and that SNX5 and SNX5/SNX6, in particular, restrict *C. trachomatis* infection during mid-infection consistent with the hypotheses by both, Aeberhard et al. and Mirrashidi et al. SNX5 or SNX5/SNX6 may control processes such as bacterial replication, RB-to-EB transition or EB infectivity (Banhart et al. 2017). We did not examine primary and secondary infection of *C. trachomatis* in SNX2 and SNX6 single, as well as SNX1/SNX2 double KO as these cell lines, have not been generated yet. These cell lines are of future interest as they would round out our understanding of SNX-BAR function in *C. trachomatis* primary and secondary infection.

4.3.3 Distinct roles of the retromer at early and mid-infection time points?

At early infection, the two retromer subcomplexes localised proximal to each other whereas, at mid-infection, signals of each subcomplex were separated (**Fehler! Verweisquelle konnte nicht gefunden werden.**). At mid-infection, SNX-BARs are recruited to the inclusion and localised in a rim-like pattern on the inclusion membrane, consistent with previous findings (Aeberhard et al. 2015; Mirrashidi et al. 2015). In contrast, VPS35 and CI-MPR localised adjacent to the inclusion consistent with previous findings (van Ooij, Apodaca, and Engel 1997; Aeberhard et al. 2015; Mirrashidi et al. 2015). Several findings revealed that SNX5/SNX6 restrict chlamydial infection (Aberhard et al. 2015; Mirrashidi et al. 2015; our unpublished data). Taken together, both, our findings and published results indicate possibly distinct functions of the retromer at different infection time points. Retrograde trafficking along microtubules is enabled trough binding of SNX5 and SNX6 to $p150^{glued}$. During early infection, the retromer may be co-opted by *C. trachomatis* in order to be sorted from endosomes to the MTOC where *Chlamydia* spp. establish their favourable niche as described in section 1.3.1. If so, it is conceivable that the retromer-mediated retrieval favours decoration of the early inclusion with SNX-BARs as *C. trachomatis* acting as retromer cargo intercepts and retains SNX-BARs at early infection and mid-infection, respectively. At mid-infection, the retromer subcomplexes are likely disconnected as SNX-BARs specifically decorate the inclusion in contrast to the VPS trimer. The retromer acts in tubular based endosomal sorting from where it tethers and docks at the inclusion membrane, followed by uncoating and fusion of vesicles and tubules with the recipient membrane. Membrane and vesicle trafficking involves the action of Rab GTPases whose signature is born by cellular organelles in exocytic and endocytic pathways (Zerial and McBride 2001; Stenmark 2009; Bhuin and Roy 2014; Hutagalung and Novick 2011). *Chlamydia* spp. predominantly interact with Rab proteins involved in retrograde and recycling pathways (Rzomp et al. 2003; Rzomp, Moorhead, and Scidmore 2006; Cortes et al. 2007). Some of these interactions were confirmed by proteomic studies (Aeberhard et al. 2015; Mirrashidi et al. 2015). The inclusion membrane of *C. trachomatis* associated with Rab1, Rab6A, Rab8A and Rab11A but not with Rab5 and Rab7 (doctoral thesis from Sophia Edelmann 2016 (Edelmann 2016)). Rab1 regulates ER-Golgi and intra-Golgi traffic (Hutagalung and Novick 2011). Rab8A and

Rab11A regulate endocytic pathways mediated by recycling endosomes (Hackstadt et al. 1996; Grant and Donaldson 2009). Rab6 associates with membranes of the Golgi apparatus/TGN and both, Rab6 and Rab11 sequentially regulate a retrograde transport pathway from recycling endosomes to the Golgi apparatus (Miserey-Lenkei et al. 2007). Rab6-interacting proteins 1 (Rab6 IP1) bind to both, Rab6 and Rab11 and Rab6 IP1 may function in Rab mechanism between these compartments. Rab5 and Rab7 mediate fusion of endocytic vesicles to form early endosomes and late endosomes/endolysosomes, respectively (Hutagalung and Novick 2011). Taken together, the inclusion membrane is positive for Rabs of the retrograde/recycling pathway but negative for Rabs as late endosome/endolysosome markers. *C. trachomatis* may perturb the host cell by either surrogating the TGN supported by the presence of Rab6 and Rab11 or *C. trachomatis* may surrogate endosomal compartments supported by the absence of Rab5 and Rab7. In either way, the inclusion is able to constantly decorate itself with SNX-BARs. Among SNX-BARs, SNX5 and SNX6 directly bind to IncE (Mirrashidi et al. 2015). This interaction likely causes specific recruitment of SNX-BARs but not of the VPS trimer. The latter associates with endosomes through interaction with the GTP loaded form of Rab7 (Rojas et al. 2008; Seaman et al. 2009; Balderhaar et al. 2010). As the inclusion lacks Rab7, *C. trachomatis* may be unable to associate with the VPS trimer. Besides, at mid-infection, SNX-BARs may play a role independent from the VPS trimer as shown by Kvainickas et al. and Simonetti et al. (Kvainickas et al. 2017; Simonetti et al. 2017). Recruitment of SNX-BARs but not of VPS trimer may be supported by PIPs that are originally present in host cellular membranes but are co-opted by *Chlamydia* spp. to remodel the inclusion membrane and that SNX-BARs bind to (Moorhead et al. 2010). Furthermore, *Chlamydia* spp. recruit multiple host proteins such as ARF1 and PI4KIIα which function in PIP metabolism (Moorhead et al. 2010). Further PIP-binding and PIP-metabolising proteins were identified in the host cell-derived proteome of isolated inclusions (Aeberhard et al. 2015). Taken together, *Chlamydia* spp. remodel Rab GTPases and PIP composition of the inclusion membrane to remain undetected within the host cell (Moorhead et al. 2010).

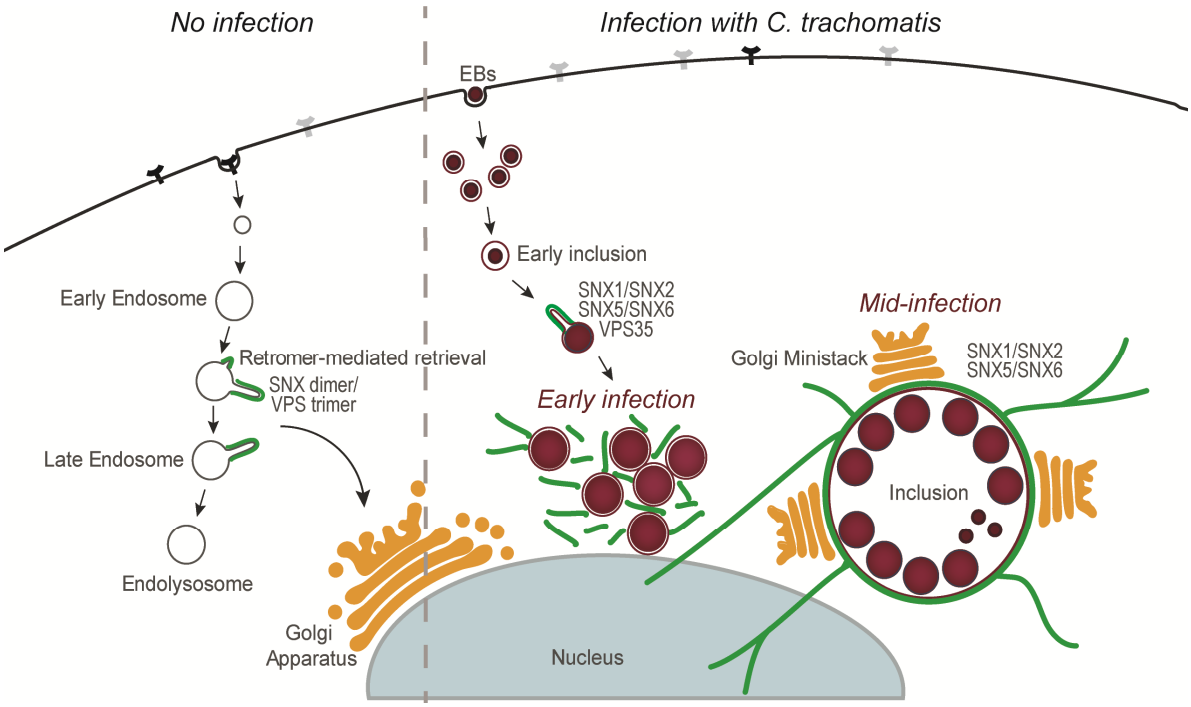

Figure 53. Interaction of *C. trachomatis* with the host cellular retromer at early and mid-infection.
Illustration of the endosomal trafficking system in uninfected cells (left-hand side) and co-option of the endosomal trafficking system by *C. trachomatis* (right-hand side). At early infection stages, the retromer is co-opted by *C. trachomatis* in order to be sorted from endosomes to the MTOC. Both, SNX and VPS subcomplexes are connected. At mid-infection stages, SNX-BARs but not VPS trimer are recruited to the inclusion. SNX and VPS subcomplexes are separated. Adapted from Banhart et al. 2017.

4.4 Intracellular pathogens hijack host's cellular trafficking pathways of the endomembrane system

Intracellular pathogens such as *Chlamydia trachomatis*, *Legionella pneumophila* and *Salmonella enterica* serovar Typhimurium co-opt the endomembrane system to ensure their survival (Canton and Kima 2012; Hilbi and Haas 2012; Personnic et al. 2016). They subvert the endolysosomal system and reside within the pathogen-containing vacuole from where they recruit nutrients including lipids and proteins. Interaction of intracellular pathogens such as the ones named above with the retromer has been described. *Chlamydia* spp. interact with numerous host cellular proteins and the cytoskeleton (Wyrick 2000; Dautry-Varsat, Balana, and Wyplosz 2004; Bastidas et al. 2013; Elwell, Mirrashidi, and Engel 2016). Moreover, host cellular proteins do not only interact with inclusion membrane proteins but were also detected inside the inclusion (Soupene et al. 2012). In this thesis, we showed recruitment of retromer's SNX-BARs to the early and mid-infection inclusion. At early infection time points, SNX-BARs and VPS35 localised in close proximity to *C. trachomatis* and accumulated at the MTOC by 8 h p.i.. Throughout early infection, retromer components co-localised. As we observed co-localisation of bacteria and retromer components, we suggest that *C. trachomatis* hijacks the retromer and

traffics along microtubules. At mid-infection time points, SNX-BARs are localised on the chlamydial inclusion whereas VPS35 is localised adjacent to it. Due to at least a partial separation of the two signals from the two retromer subcomplexes, the subcomplexes may be disconnected and functionally independent. Based on our localisation data of SNX-BARs and VPS35 at mid-infection, we postulate a model in which either SNX5 or SNX6 bind IncE; SNX1 and SNX2 in turn bind to SNX5 and SNX6 independently of the VPS trimer. Recruitment of host cellular SNX-BARs may benefit chlamydial intracellular survival in a way that is not greatly understood. The opportunistic pathogen *L. pneumophila* causes the severe pneumonia Legionnaires' disease. The formation of the pathogen-containing vacuole, for *L. pneumophila* termed *Legionella*-containing vacuole (LCV) is governed by the Icm/Dot type IV secretion system (T4SS). Distinct effector proteins subvert numerous host cellular targets such as PIPs and Rab GTPases Rab5A, Rab7A and Rab21 on the LCV membrane (Bärlocher, Welin, and Hilbi 2017). *L. pneumophila* also interacts with the retromer components SNX1, SNX2 and SNX5 through binding of VPS29 with the effector proteins RidL and blocking of SNX-PI3P binding (Finsel et al. 2013). Finsel et al. concluded that the interaction of SNXs with RidL promotes intracellular replication through blocking of the retrograde transport at endosome exit sites (Finsel et al. 2013; Personnic et al. 2016). Recruitment of the retromer to endosomes requires the interaction of the VPS trimer with activated, GTP-bound Rab7A (Rojas et al. 2008; Seaman et al. 2009; Priya et al. 2015). TBC1D5 is a Rab7 GTPase-activating protein that binds VPS29 and promotes the release of the retromer (Seaman et al. 2009; Priya et al. 2015; Jia et al. 2016). Recent studies demonstrated that a hairpin loop of RidL inserts into a conserved pocket on VPS29 whereby TBC1D5 is outcompeted for binding to VPS29 (Bärlocher et al. 2017; Romano-Moreno et al. 2017; Yao et al. 2018), This displacement resemble the mechanism by the suggested displacement of CI-MPR binding to SNX5 by chlamydial IncE (Elwell et al. 2017). Interaction of RidL and VPS29 did not either preclude retromer dimerisation nor impair localisation of retromer to endosomal membranes suggesting that RidL:VPS29 interaction interferes with lysosome fusion thereby promoting intracellular growth (Bärlocher et al. 2017; Romano-Moreno et al. 2017; Bärlocher, Welin, and Hilbi 2017). *S. enterica* Typhimurium is a facultative intracellular pathogen causing gastroenteritis in humans and inducing typhoid-like systemic disease in mice (Steele-Mortimer 2008). In terms of *Salmonella* infections, the pathogen-containing vacuole is termed *Salmonella*-containing vacuole (SCV). Effector proteins secreted via the T3SS govern the formation of SCV and mediate replication and intracellular survival, similar to other intracellular pathogens (Steele-Mortimer 2008; Brumell and Grinstein 2004). Remodelling of the SCV membrane creates a protected niche and inhibits fusion with lysosomes (Bakowski, Braun, and Brumell 2008; Bakowski et al. 2010). Effector proteins also target numerous host cellular proteins, for instance Rab GTPase Rab5 and PIPs. Moreover, *S.* Typhimurium recruits at least SNX1 and SNX3 (Bujny et al. 2008; Braun et al. 2010). SNX1 depletion resulted in overall delay of bacterial replication indicating that SNX1 plays an important role during maturation of the *Salmonella*-

containing vacuole (Bujny et al. 2008). SNX1 and SNX3 are crucial for tubular-based remodelling of the *Salmonella*-containing vacuole resulting in extensive SNX-positive tubules (Braun et al. 2010). Only SNX1 was detected on the SCV membrane (Bujny et al. 2008). Patrick et al. suggested that generated PI3P on the SCV membrane is recognised by SNX1 and/or SNX3 which then promotes recruitment of the VPS trimer. The *S.* Typhimurium effector SseC engages the retromer promoting recruitment of TBC1D5. This, in turn, stimulates Rab7 activity resulting in retromer release from the SCV (Patrick et al. 2018). One distinct feature to the tubular-based remodelling is the presence of tubular structures that originate from and connect to the *Salmonella*-containing vacuole and include *Salmonella*-induced filaments (Schroeder, Mota, and Meresse 2011). The *S.* Typhimurium effector SifA directs the formation of *Salmonella*-induced filaments (Stein et al. 1996).
Taken together, these examples highlight a role of retrograde trafficking pathways and the human retromer during infection with intracellular pathogens to promote replication.

4.5 *C. trachomatis* playing with ribosomes?

4.5.1 Using BioID assay as a tool to study protein-protein interactions and its limitations

We implemented a proximity-dependent biotin identification assay in our infection system to screen for physiologically relevant protein interactions in (infected) living cells. BioID assay is based on a promiscuous *E.coli* biotin protein ligase that is fused to a targeting protein (Roux et al. 2012; Roux et al. 2018). The fusion protein is expressed in cells where it biotinylates proximal endogenous proteins at targeted sites at the location of the protein of interest (Roux, Kim, and Burke 2013). Biotinylation allows for selective isolation and identification of candidate interactors of a protein of interest with standard biotin-affinity capture followed by MS analysis (streptavidin pulldown). The BioID tool is fundamentally derived from the DamID method in which a prokaryotic Dam methylase is fused to a protein of interest for detection of DNA-protein interactions in eukaryotes (van Steensel and Henikoff 2000). In the BioID system, a prokaryotic biotin ligase BirA carries a R118G mutation at the active site, designated BirA*, to promote promiscuous biotinylation meaning that all proteins in a radius within 10 to 20 nm are non-selectively biotinylated as BirA* has lost its sequence specificity (Choi-Rhee, Schulman, and Cronan 2004; Cronan 2005; Roux et al. 2012; Firat-Karalar and Stearns 2015; Trinkle-Mulcahy 2019). WT BirA catalyses a two-step reaction: i) generation of reactive biotinyl-AMP (biotinoyl-5'-adenylate) from biotin and ATP and ii) attachment of generated biotinyl-AMP to lysine on a subunit of the acetyl-CoA carboxylase. BirA* is capable to generate reactive biotinyl-AMP, albeit with reduced affinity for biotin but also with reduced affinity for the reactive biotinyl-AMP intermediate resulting in a premature release of biotinyl-AMP. Finally, biotinyl-AMP reacts with adjacent primary amines of lysine (Figure 54) (Roux, Kim, and Burke 2013). Diffusion of biotinyl-AMP limits labelling radius that is estimated to be within 10 to 20 nm.

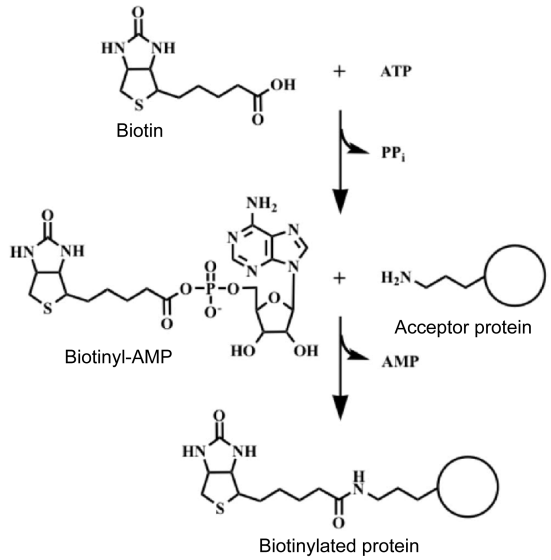

Figure 54. Generation of biotinyl-AMP.
The biotin ligase BirA generates reactive biotinyl-AMP and attaches it to an acceptor protein thereby generating a biotinylated protein. Adapted from Henke and Cronan 2014.

4.5.2 Identification of protein candidates

In this study, BioID was performed to study protein-protein interactions at *C. trachomatis* mid-infection (*C. trachomatis* D, 30 h p.i.). As we positively validated correct myc-BirA*-SNX1 fusion protein expression and localisation, BioID is a valuable tool to identify protein-protein interaction of recruited host cellular SNX1 on the chlamydial inclusion (Figure 40). Cells transiently expressed the fusion protein. Noteworthily, transient expression causes a relative amount of background proteins that would be reduced by generating cells which stably express the fusion protein. We compensated this drawback by using, in parallel, cells expressing BirA* only in parallel to control for background proteins. We fused BirA* N-terminally to SNX1 which might result in biotinylation of proximal proteins before localisation to a specific cellular location (in this thesis: SNX1 localisation on the inclusion membrane). This was circumvented as cells expressed the fusion protein more than 30 h before addition of exogenous biotin; a sufficient period of time of protein expression for SNX1 fusion protein to locate at subcellular target position (inclusion membrane). Besides, biotin excess was present more than 20 h indicating sufficient time for BirA* to biotinylate proximal proteins as biotinylation is saturated within 6 to 24 h (Roux et al. 2012).

Biotinylated proteins were analysed by MS and evaluated by standard transformation and normalisation. Only proteins which were quantified in at least 2/3rd of all preparations were considered and remaining missing values were replaced after normalisation to median intensity for each protein from a normal distribution. BioID significant protein expression differences between samples were identified using FDR-adjusted p-values from an ANOVA statistical test. With that, we identified 40 protein hits as enriched (Figure 41). Among enriched protein hits were the SNX-BARs SNX1, SNX5 and SNX6 (Figure 41). In a non-infectious context, SNX1 dimerises with SNX5 and SNX6 and the analogous pairs are also true for SNX2 (Trousdale and

Kim 2015). We did not detect SNX2 as SNX2 may not be proximal to SNX1 within a radius of 10 to 20 nm or SNX2 does not associate with SNX1. While both, SNX1 and SNX2 were demonstrated to associate with SNX5 and SNX6 in immunoprecipitation experiments, no association between SNX1 and SNX2 was observed supporting our findings (Wassmer et al. 2007). For SNX-BARs that are implicated in retromer biology, SNXs of one group (SNX1/SNX2) interact with SNXs of the other group (SNX5/SNX6) (Wassmer et al. 2007). Interestingly, among enriched proteins, we identified IncE as the only bacterial protein strongly supporting our interaction model on the inclusion membrane postulating binding of SNX1/SNX2 to SNX5/SNX6 which both in turn are able to bind to IncE. This is also in agreement with the findings by Mirrashidi et al. (Mirrashidi et al. 2015). VPS35 was not identified as enriched protein in the BioID assay. Failing to detect VPS35 in BioID using SNX1 fusion protein underlines our localisation data and applies to our interaction model as VPS35 is not recruited but localised adjacent to the inclusion at mid-infection. In addition, the absence of VPS35 among enriched proteins emphasises a separation of the two retromer subcomplexes and possibly two distinct functions of the two subcomplexes at mid-infection. Moreover, we identified several ribosomal proteins, primarily of the large subunit as enriched proteins (RPL13a, RPL15, RPL18, RPL19, RPL27a, RPL28, RPL29, RPL34 and RPL36) (Figure 41). Among enriched proteins, sole ribosomal protein of the small subunit was RPS26. Besides, we identified CCR4-NOT transcription complex subunit 1 (CNOT1), SWI/SNF complex subunit SMARCC1 (SMARCC1) and several splicing factors. CNOT1 is a scaffolding component of the CCR4-NOT complex and linked to cellular processes including miRNA-mediated repression through recruitment of CCR4-NOT complex to miRNA targets and to the RISC complex, thereby acting as transcriptional regulator (Fabian et al. 2011). CNOT1 is also linked to translational repression during translational initiation and general transcription regulation (Albert et al. 2000; Winkler et al. 2006; Ito et al. 2011; Sandler et al. 2011). Chromatin-remodelling enzymes play essential roles in gene expression, DNA replication and repair (Euskirchen, Auerbach, and Snyder 2012; Kadoch and Crabtree 2015). The SWI/SNF family of chromatin-remodelling complexes plays a key role in facilitating the binding of specific transcription factors to nucleosomal DNA in diverse organisms from yeast to humans. Mammalian SWI/SNF regulates transcription from chromatin-assembled genes in a factor-specific manner *in vitro* (Kadam et al. 2000; Phelan et al. 1999). Taken together, the identification of CNOT1, SMARCC1 and splicing factors leads to the assumption that *C. trachomatis* may interfere with the cellular transcriptional and translational machinery. However, we were not able to positively validate association of CNOT1, SMARCC1 and splicing factors by using GFP fusion proteins. The sizes of CNOT1 (266 kD) and SMARCC1 (123 kD) may cause fusion protein instability and loss of functionality as we were not even able to express CNOT1 and SMARCC1 GFP fusion proteins. We also detected filamin A (FLNA) which is considered to be a common false-positive candidate due to the presence in the majority of candidate lists from BioID assays in which fusion proteins were targeted to various subcellular compartments (Roux, Kim, and Burke 2013).

Surprisingly, we detected RPL13a, a ribosomal protein of the large subunit with an extra-ribosomal function in the GAIT complex. The GAIT complex acts as a transcript-selective translation repressor upon IFNγ stimulation in inflammation processes (Mazumder et al. 2003; Chaudhuri et al. 2007; Kapasi et al. 2007; Arif et al. 2012). Considering *C. trachomatis* as an intracellular pathogen that relies on the overall functioning of the host cell while interfering with numerous host's cellular pathways, *C. trachomatis* controlling host cellular translation may be a potential novel survival strategy. Two recent studies analysed host's cellular gene expression including genes coding for ribosomal proteins in *C. trachomatis* infected cells on a global scale (Ohmer et al. 2018; Rother et al. 2018). Ohmer et al. showed a substantial reduction in host cell proteins synthesis during *C. trachomatis* infection. Furthermore, they extracted polysomal and total mRNA from fractionated cell lysates form *C. trachomatis* infected and uninfected cells and analysed gene expression. Genes coding for components of the mitochondrial inner membrane, structural components of the ribosome, translation elongation factors and genes involved in nucleosome and chromatin organisation were most strongly down-regulated suggesting differential regulation of protein expression during *C. trachomatis* infection (Ohmer et al. 2018). However, polysomal and total mRNA exhibited a very different pattern of differentially expressed genes in *C. trachomatis* and uninfected cells. With regard to ribosomal proteins, proteins were down-regulated, though not profoundly. This may be the reason why we did not observe an alteration of RPL13a protein expression in WB analysis. In addition, the detection limit of WB analysis may be limiting in observing protein expression changes. Rother et al. used a genome-wide RNAi screen to identify host factors with pivotal roles in *Chlamydia* infection (Rother et al. 2018). By using a human whole-genome siRNA set targeting nearly 23 000 human genes, 171 essential host factors for *C. trachomatis* infection were identified. Among them, RPS6 was the only ribosomal protein identified to be essential (Rother et al. 2018). Aeberhard et al. detected numerous host-cell derived ribosomal proteins in the inclusion fractions but ribosomal proteins did not pass the enrichment factor (SILAC ratio above 1.5) (Aeberhard et al. 2015). In this thesis, we used iBAQ considering a minimum ratio count of 2, -log(p-value) >1, difference (log2) > 1.8 and a FDR 1% to identify enriched proteins, hence two approaches to identifiy enriched proteins. In addition, Aeberhard et al. isolated inclusions of *C. trachomatis* L2 at 24 h p.i.. In the localisation analysis in this thesis comparing *C. trachomatis* D, *C. trachomatis* L2 and *C. psittaci* DC15, we observed a species-specific recruitment of RPL13a as RPL13a localised on the inclusion of *C. trachomatis* D but mainly localised in a disperse punctutate pattern in the cytosol in *C. trachomatis* L2 and *C. psittaci* DC15 infected cells. This is consistent with the host-derived inclusion proteome of *C. trachomatis* L2 (Aeberhard et al. 2015).

Individual protein candidates were validated by IF and streptavidin pulldown using myc-BirA*-SNX1 fusion protein prior to WB analysis (Figure 42). Of the large subunit, RPL3 (no enriched protein candidate) stained bacteria and did not localise on the inclusion. Two enriched protein candidates revealed opposing results: While RPL13a localised on the inclusion, RPL29 did not.

Of the small subunit, RPS26 was the only ribosomal protein that was identified among enriched proteins but IF revealed only a very weak signal. RPS6 and RPS9, both not enriched in BioID revealed opposing results: While RPS9 localised on the inclusion, RPS6 did not. In conclusion, we detected RPL13a on the inclusion suggesting positive evaluation. RPL29 and RPS26 are evaluated as false-positive or amount of associated ribosomal proteins are lower than the detection limit of IF. Interestingly, RPS9 localised on the inclusion which was not identified as enriched in BioID. RPS9 does not seem to associate with SNX1 as it was not identified in the BioID assay and RPS9 may lie outside of a radius of 10 - 20 nm. However, RPS9 may associate on the inclusion with an unknown protein. We did not detect SNX-BARs, IncE or any of the ribosomal proteins in immunoprecipitation. In immunoprecipitation of eGFP-SNX1 fusion protein (using GFP-Trap® according to manufacturer's protocol), we were not able to detect any of the SNX-BARs enriched in BioID though we enriched GFP fusion protein during immunoprecipitation (data not shown). One possible explanation may be the different detection limits of WB and MS analysis. While the ECL substrate used for WB analyses in this study exhibits a detection limit of approximately 20 pg protein, a mass spectrometers combined with a liquid chromatograph is capable of detecting ionised analytes within ranges of fg thus being a vastly more sensitive detection method than WB analyses (product specifications of Q Exactive mass spectrometer from Thermo Scientific, PS30223-EN-08/16S). Hence, the detection limit of WB analyses may contribute to the failing of detecting SNX1-associated ribosomal proteins. Furthermore, ribosomal proteins such as RPL13a may be rather weakly associated with SNX1 whose binding proteins may be in part washed off during stringent washing steps during streptavidin pulldown. The BioID approach is a complementary alternative to conventional methods such as yeast-2-hybrid system or affinity purifications (e.g. Co-IP using GFP-Trap®) (Roux, Kim, and Burke 2013; Le Sage, Cinti, and Mouland 2016). Yeast-2-hybrid assay, on the one hand, involves exogenously expressed bait and prey fusion proteins in yeast cells. Interaction of bait and prey results in a selectable readout. Advantages are the ability to generate cDNA libraries of prey from diverse cell types and the implication of positive candidates as direct interaction. The main disadvantage is the high rate of false-positive and negative hits (Roux, Kim, and Burke 2013). On the other hand, affinity purification involves isolation of soluble protein complexes that associate with a fusion protein which contains one or more highly specific tags (epitope for antibody-based capture and/or protein domain) prior to MS analysis. The main advantage is the isolation of protein complexes of which inclosed endogenous proteins interact within their natural cellular context. Disadvantages include the potential to lose weak interactions and the difficulty to detect transient interactions (Roux, Kim, and Burke 2013). BioID offers considerable advantages, particularly with regards to the identification of transient or weak interactions due to labelling over a period of time and through its applicability to insoluble subcellular structures (Varnaite and MacNeill 2016; Chen and Perrimon 2017). This advantage may apply to the identification of ribosomal proteins. Besides, labelling of adjacent proteins over a period of time proceeds without interruption in a natural

setting. Labelled proteins are then selectively captured, insensitively to protein solubility or aggregation. In addition, the built-in inducibility through addition of exogenous biotin is controllable. Limitations are the integration of BirA* and false-positive hits which we intended to circumvent by using control cells expressing myc-BirA* only. BirA* is larger than GFP which may impair normal targeting, stability and function. Noteworthily, identification of protein candidates does not necessarily indicate direct or indirect interaction but rather reflects labelling of proximal proteins within the given radius (Roux, Kim, and Burke 2013; Chen and Perrimon 2017). Furthermore, proteins lacking primary amines to be accessible for biotinylation may not be detected. Nonetheless, comparing BioID and immunoprecipitation experiments have demonstrated that both approaches are complementary in identifying protein interactions (Lambert et al. 2015). Combining several tools is thus advisable to gain reliable information.

4.5.3 Recruitment of RPL13a to the inclusion

Localisation of RPL13a on the inclusion of C. trachomatis

IF studies demonstrated localisation of RPL13a on the inclusion of *C. trachomatis* D at mid-infection time points (36 and 48 h p.i.) but not at an earlier infection time point (16 h p.i.) (Figure 43). Moreover, RPL13a localised on *C. trachomatis* D inclusions in nearly 60% of infected cells whereas RPL13a localised on *C. trachomatis* L2 and *C. psittaci* DC15 inclusions in approximately 5% of infected cells (Figure 44). This indicates a species-specific recruitment and RPL13a recruitment to *C. trachomatis* D inclusions may therefore be a specific adaptation of *C. trachomatis* D. Similar to SNX-BARs, RPL13a protein expression did not alter during *C. trachomatis* and *C. psittaci* infection suggesting recruitment but no regulation of RPL13a (Sandra Oehlmann, RKI, unpublished data). Some ribosomal proteins of both, the large and the small subunit, carry out functions often unrelated to protein synthesis of the ribosome (Wool 1996; Lindstrom 2009; Warner and McIntosh 2009; Zhou et al. 2015). These functions beyond classical ribosome function are termed extra-ribosomal functions or ribosome-independent functions. To name but a few, RPL11 and RPL23 regulate proto-oncoprotein HDM2 (human counterpart of MDM2 in mice) activity, a protein that is involved in the regulation of stability and function of p53 protein (Lohrum et al. 2003; Jin et al. 2004). RPL26 regulates p53 protein translation (Takagi et al. 2005). RPS3 has a DNase activity and is also able to bind to NF-kB (Wilson, Deutsch, and Kelley 1994; Wan et al. 2007). RPS6 is involved in liver proliferation but not growth in mice (Volarevic et al. 2000). RPL13a is also a ribosomal protein with an extra-ribosomal function. As it is a component of the GAIT complex, we examined the localisation of other GAIT complex components in IFNγ stimulated cells (Figure 46). As opposed to RPL13a, EPRS and NSAP1 did not localise on the inclusion assuming at least no formation of the GAIT complex on the inclusion site. Whether assembly of GAIT complex occurs in the cytosol was not examined but remains of interest to study possible translation control in the cytosol of *C. trachomatis* infected cells through the GAIT complex. During the GAIT complex assembly

process, EPRS is phosphorylated and assembles with NSAP1 to form the pre-GAIT complex in a first step. In a second step, RPL13a is phosphorylated before it associates with the pre-GAIT complex together with GAPDH (Mazumder et al. 2003; Mukhopadhyay et al. 2009). We did not detect any change of phosphorylation state of RPL13a in HeLa cells assuming no formation of GAIT complex (data not shown). Phosphorylation of EPRS was not analysed but is necessarily of interest to verify GAIT complex formation during *C. trachomatis* infection in more depth. Much more critically, we were in fact not able to detect phosphorylation of RPL13a in human U937 monocytic cells upon IFNγ treatment thus lacking control to examine phosphorylation of GAIT complex components. This is in contrast to the study by Mazumder et al. which demonstrated phosphorylation of RPL13a in U937 monocytic cells (Mazumder et al. 2003). Origins of differences in data outcome need to be further examined.

Function of RPL13a in C. trachomatis infection

RNAi was used to deplete RPL13a in order to assess RPL13a function in *C. trachomatis* infection as the generation of RPL13a KO cell lines failed to study RPL13a function in a more robust system (Figure 47). Upon depletion of RPL13a (depletion efficiency about 70%), replication and infectious progeny formation increased profoundly suggesting that RPL13a restricts *C. trachomatis* infection. Replication was assessed by a *Chlamydia*-specific qPCR targeting the conserved 16S rRNA gene which occurs only once per bacterium (Lienard et al. 2011). This molecular tool detects at least five DNA copies and shows high specificity thus being a reliable tool to analyse *C. trachomatis* replication. Infectious progeny formation was assessed by infectious progeny formation assay which is commonly used within the *Chlamydia* community. The ratio replication : infectious progeny formation exhibited no differences indicating a roughly linear correlation between both parameters: The more RBs replicate, the more infectious EBs are re-differentiated. RPL13a does not seem to affect the process of re-differentiation from RBs to EBs. The distinct difference in absolute numbers of genome copy number and infectious progeny likely lies in freeze-thawing of lysates. While genome copy number is independent of freeze-thawing, infectious progeny is usually reduced by at least one log degree. Furthermore, bacterial Hsp60 protein expression also increased which is in line with increased replication and infectious progeny formation. Concordantly with these findings and with an increased IncA and IncE protein expression, we observed significantly enlarged inclusions. Taken together, our data indicate that RPL13a affects *C. trachomatis* infection. To our knowledge, this is the first finding that links RPL13a with *C. trachomatis* infection and it has just started to shed some light on the potential roles of ribosomal proteins in *C. trachomatis* infections. Further ribosomal proteins need to be screened on a larger scale.

A novel extra-ribosomal function of RPL13a was reported whereby RPL13a acts as an antiviral agent (Mazumder et al. 2014). In macrophages, growth of the RNA virus respiratory syncytial virus (RSV) was highly increased in RPL13a KO cells of various lineages and in RPL13a KO mice macrophages. In these RPL13a-deficient cells, translation of RSV matrix protein was

specifically stimulated while general translation was not affected. Mazumder et al. showed that the recognition of a specific secondary structure in the 3' UTR of the RSV matrix protein mRNA led to a translational arrest of the mRNA in an IFNγ-independent mechanism that is functionally different from the GAIT complex mechanism (Mazumder et al. 2014). Similar to RSV mRNA, a *C. trachomatis* mRNA may harbour such a specific secondary structure in the 3' UTR whose translation is inhibited by RPL13a in an IFNγ-independent mechanism.

4.5.4 Beyond protein synthesis – ribosome heterogeneity

As we observed RPL13a and RPS9 localised on the inclusion, we hypothesised ribosome protein heterogeneity during *C. trachomatis* infection apart from the classical conception of ribosomes. The latter has been challenged as emerging studies have linked ribosome to selectivity for translating sub-pools of transcripts which endows ribosomes with more selective control of gene regulation (Sauert, Temmel, and Moll 2015; Shi and Barna 2015; Preiss 2016; Briggs and Dinman 2017). Though ribosome heterogeneity has been observed in the 1970s, it has been neglected for a long time. However, an increasing number of studies presented evidence that ribosomes can vary in their protein and rRNA complement between different cell types and developmental states (McConkey and Hauber 1975; Sauert, Temmel, and Moll 2015). In addition, a recent study identified translating ribosomes that lacked specific proteins and associated with specific mRNA subsets (Briggs and Dinman 2017; Shi et al. 2017). Altogether, those studies led to resurgence of the conception of ribosomes heterogeneity. It means diversity in composition, function, activity, post-translational modifications of subsets of ribosomal proteins and variations in ribosomal RNA sequences (Xue and Barna 2012a). A simple way to modify a multi-subunit assembly is to vary the relative abundance of individual components (Sauert, Temmel, and Moll 2015). While rRNAs are indispensable for functional active translation, stoichiometry of ribosomal proteins on the ribosome can be adapted (Slavov et al. 2015; Sauert, Temmel, and Moll 2015). Furthermore, ribosomal proteins are encoded by paralogue genes resulting in paralogue or alternative ribosomal proteins whose expression may differ (Xue and Barna 2012a). Altered expression levels of core ribosomal proteins plus ribosomal protein modifications incorporated in the mature and active 80S ribosome constitute additional layers of heterogeneity (Xue and Barna 2012a; Sauert, Temmel, and Moll 2015). In addition to ribosomal proteins, rRNA may contribute to the heterogeneity as incorporation of alternative rRNA molecules and modification of rRNAs have been described (Xue and Barna 2012a; Sauert, Temmel, and Moll 2015). Finally, translation factors such as initiation factors and tRNAs were shown to exhibit modifications and structural diversity, respectively. An emerging hypothesis is that ribosomal proteins may act as 'specificity filters' that allow the ribosome to associate with specific mRNA subset thereby controlling translation. In this context, regulatory elements in mRNAs may help in recognition and translation of mRNA subsets (Mauro and Edelman 2002; Xue and Barna 2012a). Taken together, a whole raft of mechanisms may contribute to the occurrence of heterogeneous ribosomes that through a

regulatory function allow greater specificity in translation in cellular and developmental processes (Xue and Barna 2012a). Ribosome heterogeneity in terms of ribosome protein and/or rRNA composition may be co-opted by *C. trachomatis* in order to control translational processes. Heterogeneous ribosome protein composition with regard to heterogeneous protein expression would be indicated by considerable changes in protein expression of individual ribosomal proteins. Thus, we first examined total ribosome profiles of *C. trachomatis* infected and uninfected cells (Figure 48). The ribosome profile was monitored by absorbance at a wavelength of 254 nm which is the absorption maximum of nucleic acids. The total protein profile was monitored at protein's absorption maximum at a wavelength of 280 nm. We observed an altered ribosome profile of *C. trachomatis* infected cells while the total protein profile of *C. trachomatis* infected cells was similar to uninfected cells suggesting possible heterogeneous ribosomes in *C. trachomatis* infected cells (Figure 48). Second, we deepened our analysis by a proteomic approach using SILAC in order to analyse not total but rather individual ribosomal protein expression of *C. trachomatis* infected and uninfected cells across the sucrose gradient. We hypothesised that changes in protein expression of individual ribosomal proteins may indicate a possible heterogeneous ribosome protein composition (Figure 49). Basically, summed protein expression of ribosomal proteins of the 60S and 40S subunits was not altered but rather exhibited only slight changes. Furthermore, protein expression of individual ribosomal proteins of 60S and 40S subunit did not reveal considerable changes. Finally, BioID significantly enriched protein candidates and among these, ribosomal proteins exhibited a similar protein profile as the proteins of the ribosome subunits. Taken together, our data suggest that the protein expression of individual ribosomal proteins is not altered. Also, BioID significantly enriched ribosomal proteins clustered similar to ribosomal proteins of the 60S subunit suggesting that enriched ribosomal proteins identified in BioID are not differently expressed in *C. trachomatis* infected cells. RPL13a, in particular, did not reveal considerable, altered protein expression and its expression clustered in protein expression of other ribosomal proteins supporting our WB analysis that revealed no regulation in RPL13a expression. This is consistent with findings by Ohmer et al. stating only slight changes in RPL13a gene expression. However, rRNA composition may exhibit heterogeneity. RPL13a is dispensable for canonical ribosome function but required for rRNA methylation within the 90S pre-ribosome during 90S processing (Chaudhuri et al. 2007; Das et al. 2013). In initial experiments, we examined whether *C. trachomatis* interferes in ribosome biogenesis by analysing nuclear ribosomes and ribosomal subunits of *C. trachomatis* infected and uninfected cells using a sucrose gradient followed by analysis of 18S and 5' ETS+18S (5' external transcribed spacer) sequences via qPCR according to Chaudhuri et al. (Sandra Oehlmann, RKI, data not shown). 18S sequence is present in the unprocessed 47S rRNA, the primary constituent of the 90S pre-ribosome and in processed and mature 18S rRNA of the 40S subunit which later assembles to the 80S ribosome while 5' ETS is only present in unprocessed 47S pre-rRNA of the 90S pre-ribosome (Chaudhuri et al. 2007). We detected 3 peaks assuming

successful separation of nuclear 90S pre-ribosome, 66S and 43S pre-ribosomal particles (in the following summarised as pre-ribosomal particles) though spectroscopic monitoring of ribosomal particles may not be sensitive enough. Identification of ribosomal proteins specifically related to each pre-ribosomal particle by WB analysis would validate our assumption of separated pre-ribosomal particles. Nuclear ribosome profile of *C. trachomatis* infected cells did not alter compared to uninfected cells suggesting that *C. trachomatis* does not affect general ribosome biogenesis. Interestingly, unprocessed 47S pre-rRNA increased by a factor of 3 in *C. trachomatis* infected cells suggesting that *C. trachomatis* may interfere in the rRNA composition of pre-ribosomal particles. Future research on possible heterogeneous ribosome RNA composition during *C. trachomatis* infection may unveil a novel mechanism of host-pathogen interactions of intracellular pathogens such as *C. trachomatis*.

4.6 Conclusions and outlook

This thesis revealed that *Chlamydia trachomatis* recruits SNX-BARs at both, early and mid-infection stages. Moreover, VPS35 localised proximally to bacteria at early but not to the inclusion at mid-infection stage. Localisation of CI-MPR being one of retromer cargoes does not seem to be affected by *C. trachomatis* infection. At early infection, SNX-BARs, in particular, SNX5/SNX6 are involved in *C. trachomatis* trafficking as loss of SNX5/SNX6 decreased *C. trachomatis* at the MTOC. At the early infection stage, the retromer may be co-opted by *C. trachomatis* to be sorted from the endosome in which *C. trachomatis* is located after entry into the host cell. The endosomal membrane is then rapidly remodelled towards an inclusion membrane to which the retromer attaches. By use of the retromer, *C. trachomatis* is trafficked to the MTOC where *C. trachomatis* establishes its niche. At mid-infection, the inclusion is specifically decorated with SNX-BARs but not with VPS35. Based on our localisation studies of SNX-BAR functional domains, we conclude that PX domains of SNX5 and SNX6 are sufficient to be recruited to the inclusion while the BAR domains of SNX1 and SNX2 dimerise with either SNX5 or SNX6. In addition, ultrastructure analyses of tubular structures emanating from chlamydial inclusions revealed membrane-bound tubules. These tubules were positive for the ER marker RTN4 but RTN4 was absent along tubules during absence of SNX-BARs on the inclusion. This suggests that the inclusion tubules are in part but not solely ER-related tubules. Further research investigating inclusion tubules is required to unveil their function. At mid-infection, SNX5/SNX6 restrict primary infection, replication and infectious progeny formation. Taken together, we postulate connected retromer subcomplexes at early infection time point but separated subcomplexes at mid-infection time point. The retromer is specifically co-opted by *C. trachomatis* at early infection. At mid-infection in contrast, only SNX-BARs are specifically recruited. This leads us to the conclusion that the retromer may reveal different functions at different time points during the infection with *C. trachomatis*. Analyses of *C. trachomatis* infection in SNX1/SNX2 and VPS KO cell lines are highly of interest to study the function of retromer at early and mid-infection further.

The analysis of SNX1-proximal proteins identified the ribosomal protein of the large ribosome subunit RPL13a suggesting that *C. trachomatis* interferes in host cellular translation processes. RPL13a is recruited to the inclusion at mid-infection and restricts *C. trachomatis* replication and infectious progeny formation. Whether other ribosomal proteins affect *C. trachomatis* infection needs to be determined. Moreover, the total ribosome profile was altered in *C. trachomatis* infected cells. This alteration does not seem to result from altered individual ribosomal protein expressions but might results from a heterogeneous ribosome rRNA composition during the infection with *C. trachomatis*.

Altogether, this thesis contributes to a greater understanding of how *C. trachomatis* intercepts not only host trafficking pathways but possibly host cellular translation. Findings of this thesis may draw conclusions for other host-pathogen interactions such as *L. pneumophila* and *S. enterica* Typhimurium.

Bibliography

Abdelrahman, Y. M., and R. J. Belland. 2005. 'The chlamydial developmental cycle', *FEMS Microbiol Rev*, 29: 949-59.

Abdelsamed, H., J. Peters, and G. I. Byrne. 2013. 'Genetic variation in Chlamydia trachomatis and their hosts: impact on disease severity and tissue tropism', *Future Microbiol*, 8: 1129-46.

Aeberhard, L., S. Banhart, M. Fischer, N. Jehmlich, L. Rose, S. Koch, M. Laue, B. Y. Renard, F. Schmidt, and D. Heuer. 2015. 'The Proteome of the Isolated Chlamydia trachomatis Containing Vacuole Reveals a Complex Trafficking Platform Enriched for Retromer Components', *PLoS Pathog*, 11: e1004883.

Agaisse, H., and I. Derre. 2014. 'Expression of the effector protein IncD in Chlamydia trachomatis mediates recruitment of the lipid transfer protein CERT and the endoplasmic reticulum-resident protein VAPB to the inclusion membrane', *Infect Immun*, 82: 2037-47.

Al-Attar, S., E. R. Westra, J. van der Oost, and S. J. Brouns. 2011. 'Clustered regularly interspaced short palindromic repeats (CRISPRs): the hallmark of an ingenious antiviral defense mechanism in prokaryotes', *Biol Chem*, 392: 277-89.

Al-Zeer, M. A., H. M. Al-Younes, M. Kerr, M. Abu-Lubad, E. Gonzalez, V. Brinkmann, and T. F. Meyer. 2014. 'Chlamydia trachomatis remodels stable microtubules to coordinate Golgi stack recruitment to the chlamydial inclusion surface', *Mol Microbiol*, 94: 1285-97.

Albert, T. K., M. Lemaire, N. L. van Berkum, R. Gentz, M. A. Collart, and H. T. Timmers. 2000. 'Isolation and characterization of human orthologs of yeast CCR4-NOT complex subunits', *Nucleic Acids Res*, 28: 809-17.

Almeida, F., M. P. Luis, I. S. Pereira, S. V. Pais, and L. J. Mota. 2018. 'The Human Centrosomal Protein CCDC146 Binds Chlamydia trachomatis Inclusion Membrane Protein CT288 and Is Recruited to the Periphery of the Chlamydia-Containing Vacuole', *Front Cell Infect Microbiol*, 8: 254.

Andersen, A. A., and D. Vanrompay. 2000. 'Avian chlamydiosis', *Rev Sci Tech*, 19: 396-404.

Arif, A., P. Chatterjee, R. A. Moodt, and P. L. Fox. 2012. 'Heterotrimeric GAIT complex drives transcript-selective translation inhibition in murine macrophages', *Mol Cell Biol*, 32: 5046-55.

Arif, A., P. Yao, F. Terenzi, J. Jia, P. S. Ray, and P. L. Fox. 2018. 'The GAIT translational control system', *Wiley Interdiscip Rev RNA*, 9.

Arighi, C. N., L. M. Hartnell, R. C. Aguilar, C. R. Haft, and J. S. Bonifacino. 2004. 'Role of the mammalian retromer in sorting of the cation-independent mannose 6-phosphate receptor', *J Cell Biol*, 165: 123-33.

Arike, L., K. Valgepea, L. Peil, R. Nahku, K. Adamberg, and R. Vilu. 2012. 'Comparison and applications of label-free absolute proteome quantification methods on Escherichia coli', *J Proteomics*, 75: 5437-48.

Attar, N., and P. J. Cullen. 2010. 'The retromer complex', *Adv Enzyme Regul*, 50: 216-36.

Bachmann, N. L., A. Polkinghorne, and P. Timms. 2014. 'Chlamydia genomics: providing novel insights into chlamydial biology', *Trends Microbiol*, 22: 464-72.

Bakowski, M. A., V. Braun, and J. H. Brumell. 2008. 'Salmonella-containing vacuoles: directing traffic and nesting to grow', *Traffic*, 9: 2022-31.

Bakowski, M. A., V. Braun, G. Y. Lam, T. Yeung, W. D. Heo, T. Meyer, B. B. Finlay, S. Grinstein, and J. H. Brumell. 2010. 'The phosphoinositide phosphatase SopB manipulates membrane surface charge and trafficking of the Salmonella-containing vacuole', *Cell Host Microbe*, 7: 453-62.

Balderhaar, H. J., H. Arlt, C. Ostrowicz, C. Brocker, F. Sundermann, R. Brandt, M. Babst, and C. Ungermann. 2010. 'The Rab GTPase Ypt7 is linked to retromer-mediated receptor recycling and fusion at the yeast late endosome', *J Cell Sci*, 123: 4085-94.

Banhart, S., L. Rose, L. Aeberhard, S. Koch-Edelmann, and D. Heuer. 2017. 'Chlamydia trachomatis and its interaction with the cellular retromer', *Int J Med Microbiol*.

Bannantine, Griffiths, Viratyosin, Brown, and Rockey. 2000. 'A secondary structure motif predictive of protein localization to the chlamydial inclusion membrane', *Cell Microbiol*, 2: 35-47.

Bannantine, J. P., D. D. Rockey, and T. Hackstadt. 1998. 'Tandem genes of Chlamydia psittaci that encode proteins localized to the inclusion membrane', *Mol Microbiol*, 28: 1017-26.

Bannantine, J. P., W. E. Stamm, R. J. Suchland, and D. D. Rockey. 1998. 'Chlamydia trachomatis IncA is localized to the inclusion membrane and is recognized by antisera from infected humans and primates', *Infect Immun*, 66: 6017-21.

Bärlocher, Kevin, Cedric A. J. Hutter, A. Leoni Swart, Bernhard Steiner, Amanda Welin, Michael Hohl, François Letourneur, Markus A. Seeger, and Hubert Hilbi. 2017. 'Structural insights

into Legionella RidL-Vps29 retromer subunit interaction reveal displacement of the regulator TBC1D5', *Nature Communications*, 8: 1543.
Bärlocher, Kevin, Amanda Welin, and Hubert Hilbi. 2017. 'Formation of the Legionella Replicative Compartment at the Crossroads of Retrograde Trafficking', *Front Cell Infect Microbiol*, 7: 482-82.
Barry, C. E., 3rd, S. F. Hayes, and T. Hackstadt. 1992. 'Nucleoid condensation in Escherichia coli that express a chlamydial histone homolog', *Science*, 256: 377-9.
Bassler, J., and E. Hurt. 2018. 'Eukaryotic Ribosome Assembly', *Annu Rev Biochem*.
Bastidas, R. J., C. A. Elwell, J. N. Engel, and R. H. Valdivia. 2013. 'Chlamydial intracellular survival strategies', *Cold Spring Harb Perspect Med*, 3: a010256.
Beatty, W. L. 2006. 'Trafficking from CD63-positive late endocytic multivesicular bodies is essential for intracellular development of Chlamydia trachomatis', *J Cell Sci*, 119: 350-9.
———. 2008. 'Late endocytic multivesicular bodies intersect the chlamydial inclusion in the absence of CD63', *Infect Immun*, 76: 2872-81.
Beatty, W. L., R. P. Morrison, and G. I. Byrne. 1994. 'Persistent chlamydiae: from cell culture to a paradigm for chlamydial pathogenesis', *Microbiol Rev*, 58: 686-99.
Bebear, C., and B. de Barbeyrac. 2009. 'Genital Chlamydia trachomatis infections', *Clin Microbiol Infect*, 15: 4-10.
Belland, R. J., G. Zhong, D. D. Crane, D. Hogan, D. Sturdevant, J. Sharma, W. L. Beatty, and H. D. Caldwell. 2003. 'Genomic transcriptional profiling of the developmental cycle of Chlamydia trachomatis', *Proc Natl Acad Sci USA*, 100: 8478-83.
Ben-Shem, A., N. Garreau de Loubresse, S. Melnikov, L. Jenner, G. Yusupova, and M. Yusupov. 2011. 'The structure of the eukaryotic ribosome at 3.0 A resolution', *Science*, 334: 1524-9.
Bhuin, T., and J. K. Roy. 2014. 'Rab proteins: the key regulators of intracellular vesicle transport', *Exp Cell Res*, 328: 1-19.
Blagoev, B., and M. Mann. 2006. 'Quantitative proteomics to study mitogen-activated protein kinases', *Methods*, 40: 243-50.
Bocker, S., A. Heurich, C. Franke, S. Monajembashi, K. Sachse, H. P. Saluz, and F. Hanel. 2014a. 'Chlamydia psittaci inclusion membrane protein IncB associates with host protein Snapin', *Int J Med Microbiol*.
———. 2014b. 'Chlamydia psittaci inclusion membrane protein IncB associates with host protein Snapin', *Int J Med Microbiol*, 304: 542-53.
Boncompain, G., C. Muller, V. Meas-Yedid, P. Schmitt-Kopplin, P. B. Lazarow, and A. Subtil. 2014. 'The intracellular bacteria Chlamydia hijack peroxisomes and utilize their enzymatic capacity to produce bacteria-specific phospholipids', *PLoS One*, 9: e86196.
Bonifacino, J. S., and B. S. Glick. 2004. 'The mechanisms of vesicle budding and fusion', *Cell*, 116: 153-66.
Bonifacino, J. S., and J. H. Hurley. 2008. 'Retromer', *Curr Opin Cell Biol*, 20: 427-36.
Bonifacino, J. S., and R. Rojas. 2006. 'Retrograde transport from endosomes to the trans-Golgi network', *Nat Rev Mol Cell Biol*, 7: 568-79.
Braun, V., A. Wong, M. Landekic, W. J. Hong, S. Grinstein, and J. H. Brumell. 2010. 'Sorting nexin 3 (SNX3) is a component of a tubular endosomal network induced by Salmonella and involved in maturation of the Salmonella-containing vacuole', *Cell Microbiol*, 12: 1352-67.
Briggs, J. W., and J. D. Dinman. 2017. 'Subtractional Heterogeneity: A Crucial Step toward Defining Specialized Ribosomes', *Mol Cell*, 67: 3-4.
Brumell, J. H., and S. Grinstein. 2004. 'Salmonella redirects phagosomal maturation', *Curr Opin Microbiol*, 7: 78-84.
Brumell, J. H., and M. A. Scidmore. 2007. 'Manipulation of rab GTPase function by intracellular bacterial pathogens', *Microbiol Mol Biol Rev*, 71: 636-52.
Brunham, R. C., and J. Rey-Ladino. 2005. 'Immunology of Chlamydia infection: implications for a Chlamydia trachomatis vaccine', *Nat Rev Immunol*, 5: 149-61.
Bujny, M. V., P. A. Ewels, S. Humphrey, N. Attar, M. A. Jepson, and P. J. Cullen. 2008. 'Sorting nexin-1 defines an early phase of Salmonella-containing vacuole-remodeling during Salmonella infection', *J Cell Sci*, 121: 2027-36.
Burd, C. G. 2011. 'Physiology and pathology of endosome-to-Golgi retrograde sorting', *Traffic*, 12: 948-55.
Bush, R. M., and K. D. Everett. 2001. 'Molecular evolution of the Chlamydiaceae', *Int J Syst Evol Microbiol*, 51: 203-20.
Caldwell, H. D., and R. C. Judd. 1982. 'Structural analysis of chlamydial major outer membrane proteins', *Infect Immun*, 38: 960-8.
Caldwell, H. D., and J. Schachter. 1982. 'Antigenic analysis of the major outer membrane protein of Chlamydia spp', *Infect Immun*, 35: 1024-31.

Canton, J., and P. E. Kima. 2012. 'Interactions of pathogen-containing compartments with the secretory pathway', *Cell Microbiol*, 14: 1676-86.

Capmany, A., and M. T. Damiani. 2010. 'Chlamydia trachomatis intercepts Golgi-derived sphingolipids through a Rab14-mediated transport required for bacterial development and replication', *PLoS One*, 5: e14084.

Cappello, Francesco, Everly Conway de Macario, Valentina Di Felice, Giovanni Zummo, and Alberto J. L. Macario. 2009. 'Chlamydia trachomatis infection and anti-Hsp60 immunity: the two sides of the coin', *PLoS Pathog*, 5: e1000552-e52.

Carabeo, R. A., S. S. Grieshaber, E. Fischer, and T. Hackstadt. 2002. 'Chlamydia trachomatis Induces Remodeling of the Actin Cytoskeleton during Attachment and Entry into HeLa Cells', *Infection and Immunity*, 70: 3793-803.

Carabeo, R. A., S. S. Grieshaber, A. Hasenkrug, C. Dooley, and T. Hackstadt. 2004. 'Requirement for the Rac GTPase in Chlamydia trachomatis invasion of non-phagocytic cells', *Traffic*, 5: 418-25.

Carabeo, R. A., D. J. Mead, and T. Hackstadt. 2003. 'Golgi-dependent transport of cholesterol to the Chlamydia trachomatis inclusion', *Proc Natl Acad Sci U S A*, 100: 6771-6.

Carlton, J., M. Bujny, B. J. Peter, V. M. Oorschot, A. Rutherford, H. Mellor, J. Klumperman, H. T. McMahon, and P. J. Cullen. 2004. 'Sorting nexin-1 mediates tubular endosome-to-TGN transport through coincidence sensing of high- curvature membranes and 3-phosphoinositides', *Curr Biol*, 14: 1791-800.

Carlton, J. G., M. V. Bujny, B. J. Peter, V. M. Oorschot, A. Rutherford, R. S. Arkell, J. Klumperman, H. T. McMahon, and P. J. Cullen. 2005. 'Sorting nexin-2 is associated with tubular elements of the early endosome, but is not essential for retromer-mediated endosome-to-TGN transport', *J Cell Sci*, 118: 4527-39.

Carlton, J. G., and P. J. Cullen. 2005. 'Sorting nexins', *Curr Biol*, 15: R819-20.

Casem, Merri Lynn. 2016. 'Chapter 8 - Exocytosis.' in Merri Lynn Casem (ed.), *Case Studies in Cell Biology* (Academic Press: Boston).

Centers for Disease Control and Prevention, C. 2010. 'Sexually transmitted diseases treatment guidelines, 2010, Department of Health and Human Services, Centers for Disease Control and Prevention.'.

Chamberland, John P., and Brigitte Ritter. 2017. 'Retromer revisited: Evolving roles for retromer in endosomal sorting', *J Cell Biol*.

Chang, J. J., K. R. Leonard, and Y. X. Zhang. 1997. 'Structural studies of the surface projections of Chlamydia trachomatis by electron microscopy', *J Med Microbiol*, 46: 1013-8.

Chang, Jiin-ju, Kevin Leonard, Talmon Arad, Tony Pitt, You-xun Zhang, and Li-hua Zhang. 1982. 'Structural studies of the outer envelope of Chlamydia trachomatis by electron microscopy', *J Mol Biol*, 161: 579-90.

Chaudhuri, S., K. Vyas, P. Kapasi, A. A. Komar, J. D. Dinman, S. Barik, and B. Mazumder. 2007. 'Human ribosomal protein L13a is dispensable for canonical ribosome function but indispensable for efficient rRNA methylation', *Rna*, 13: 2224-37.

Chen, Chiao-Lin, and Norbert Perrimon. 2017. 'Proximity-dependent labeling methods for proteomic profiling in living cells', *Wiley interdisciplinary reviews. Developmental biology*, 6: 10.1002/wdev.272.

Chen, D., H. Xiao, K. Zhang, B. Wang, Z. Gao, Y. Jian, X. Qi, J. Sun, L. Miao, and C. Yang. 2010. 'Retromer is required for apoptotic cell clearance by phagocytic receptor recycling', *Science*, 327: 1261-4.

Choi-Rhee, Eunjoo, Howard Schulman, and John Cronan. 2004. *Promiscuous protein biotinylation by Escherichia coli biotin protein ligase*.

Chua, C. E., Y. S. Lim, M. G. Lee, and B. L. Tang. 2012. 'Non-classical membrane trafficking processes galore', *J Cell Physiol*, 227: 3722-30.

Clausen, J. D., G. Christiansen, H. U. Holst, and S. Birkelund. 1997. 'Chlamydia trachomatis utilizes the host cell microtubule network during early events of infection', *Mol Microbiol*, 25: 441-9.

Cocchiaro, J. L., and R. H. Valdivia. 2009. 'New insights into Chlamydia intracellular survival mechanisms', *Cell Microbiol*, 11: 1571-8.

Collingro, A., P. Tischler, T. Weinmaier, T. Penz, E. Heinz, R. C. Brunham, T. D. Read, P. M. Bavoil, K. Sachse, S. Kahane, M. G. Friedman, T. Rattei, G. S. Myers, and M. Horn. 2011. 'Unity in variety--the pan-genome of the Chlamydiae', *Mol Biol Evol*, 28: 3253-70.

Collins, B. M., S. J. Norwood, M. C. Kerr, D. Mahony, M. N. Seaman, R. D. Teasdale, and D. J. Owen. 2008. 'Structure of Vps26B and mapping of its interaction with the retromer protein complex', *Traffic*, 9: 366-79.

Collins, B. M., C. F. Skinner, P. J. Watson, M. N. Seaman, and D. J. Owen. 2005. 'Vps29 has a phosphoesterase fold that acts as a protein interaction scaffold for retromer assembly', *Nat Struct Mol Biol*, 12: 594-602.

Cortes, C., K. A. Rzomp, A. Tvinnereim, M. A. Scidmore, and B. Wizel. 2007. 'Chlamydia pneumoniae inclusion membrane protein Cpn0585 interacts with multiple Rab GTPases', *Infect Immun*, 75: 5586-96.

Cox, J., I. Matic, M. Hilger, N. Nagaraj, M. Selbach, J. V. Olsen, and M. Mann. 2009. 'A practical guide to the MaxQuant computational platform for SILAC-based quantitative proteomics', *Nat Protoc*, 4: 698-705.

Cox, J., N. Neuhauser, A. Michalski, R. A. Scheltema, J. V. Olsen, and M. Mann. 2011. 'Andromeda: a peptide search engine integrated into the MaxQuant environment', *J Proteome Res*, 10: 1794-805.

Cox, Jürgen, Marco Y. Hein, Christian A. Luber, Igor Paron, Nagarjuna Nagaraj, and Matthias Mann. 2014. 'Accurate Proteome-wide Label-free Quantification by Delayed Normalization and Maximal Peptide Ratio Extraction, Termed MaxLFQ', *Molecular & Cellular Proteomics : MCP*, 13: 2513-26.

Cox, Jürgen, and Matthias Mann. 2008. 'MaxQuant enables high peptide identification rates, individualized p.p.b.-range mass accuracies and proteome-wide protein quantification', *Nat Biotechnol*, 26: 1367-72.

———. 2009. 'Computational principles of determining and improving mass precision and accuracy for proteome measurements in an Orbitrap', *Journal of the American Society for Mass Spectrometry*, 20: 1477-85.

Cozier, G. E., J. Carlton, A. H. McGregor, P. A. Gleeson, R. D. Teasdale, H. Mellor, and P. J. Cullen. 2002. 'The phox homology (PX) domain-dependent, 3-phosphoinositide-mediated association of sorting nexin-1 with an early sorting endosomal compartment is required for its ability to regulate epidermal growth factor receptor degradation', *J Biol Chem*, 277: 48730-6.

Cronan, John. 2005. *Targeted and proximity-dependent promiscuous protein biotinylation by a mutant Escherichia coli biotin protein ligase*.

Cullen, P. J., and H. C. Korswagen. 2012. 'Sorting nexins provide diversity for retromer-dependent trafficking events', *Nat Cell Biol*, 14: 29-37.

Cullen, Peter J. 2008. 'Endosomal sorting and signalling: an emerging role for sorting nexins', *Nat Rev Mol Cell Biol*, 9: 574-82.

Cullen, Peter J., and Florian Steinberg. 2018. 'To degrade or not to degrade: mechanisms and significance of endocytic recycling', *Nature Reviews Molecular Cell Biology*, 19: 679-96.

D'Souza-Schorey, Crislyn, and Philippe Chavrier. 2006. 'ARF proteins: roles in membrane traffic and beyond', *Nat Rev Mol Cell Biol*, 7: 347-58.

Damiani, María Teresa, Julián Gambarte Tudela, and Anahí Capmany. 2014. 'Targeting eukaryotic Rab proteins: a smart strategy for chlamydial survival and replication', *Cell Microbiol*, 16: 1329-38.

Das, P., A. Basu, A. Biswas, D. Poddar, J. Andrews, S. Barik, A. A. Komar, and B. Mazumder. 2013. 'Insights into the mechanism of ribosomal incorporation of mammalian L13a protein during ribosome biogenesis', *Mol Cell Biol*, 33: 2829-42.

Dautry-Varsat, A., M. E. Balana, and B. Wyplosz. 2004. 'Chlamydia--host cell interactions: recent advances on bacterial entry and intracellular development', *Traffic*, 5: 561-70.

Dautry-Varsat, A., A. Subtil, and T. Hackstadt. 2005. 'Recent insights into the mechanisms of Chlamydia entry', *Cell Microbiol*, 7: 1714-22.

Dehoux, Pierre, Rhonda Flores, Catherine Dauga, Guangming Zhong, and Agathe Subtil. 2011. 'Multi-genome identification and characterization of chlamydiae-specific type III secretion substrates: the Inc proteins', *BMC Genomics*, 12: 109.

Derre, I. 2015. 'Chlamydiae interaction with the Endoplasmic Reticulum: contact, function and consequences', *Cell Microbiol*.

———. 2017. 'Hijacking of Membrane Contact Sites by Intracellular Bacterial Pathogens', *Adv Exp Med Biol*, 997: 211-23.

Derre, I., M. Pypaert, A. Dautry-Varsat, and H. Agaisse. 2007. 'RNAi screen in Drosophila cells reveals the involvement of the Tom complex in Chlamydia infection', *PLoS Pathog*, 3: 1446-58.

Derre, I., R. Swiss, and H. Agaisse. 2011. 'The lipid transfer protein CERT interacts with the Chlamydia inclusion protein IncD and participates to ER-Chlamydia inclusion membrane contact sites', *PLoS Pathog*, 7: e1002092.

Di Paolo, G., and P. De Camilli. 2006. 'Phosphoinositides in cell regulation and membrane dynamics', *Nature*, 443: 651-7.

Diaz, Arturo, and Paul Ahlquist. 2012. 'Role of host reticulon proteins in rearranging membranes for positive-strand RNA virus replication', *Curr Opin Microbiol*, 15: 519-24.

Dickinson, M. S., L. N. Anderson, B. M. Webb-Robertson, J. R. Hansen, R. D. Smith, A. T. Wright, and K. Hybiske. 2019. 'Proximity-dependent proteomics of the Chlamydia trachomatis inclusion membrane reveals functional interactions with endoplasmic reticulum exit sites', *PLoS Pathog*, 15: e1007698.

Doi, N., S. Zenno, R. Ueda, H. Ohki-Hamazaki, K. Ui-Tei, and K. Saigo. 2003. 'Short-interfering-RNA-mediated gene silencing in mammalian cells requires Dicer and eIF2C translation initiation factors', *Curr Biol*, 13: 41-6.

Dumoux, M., D. K. Clare, H. R. Saibil, and R. D. Hayward. 2012. 'Chlamydiae assemble a pathogen synapse to hijack the host endoplasmic reticulum', *Traffic*, 13: 1612-27.

Dumoux, M., and R. D. Hayward. 2016. 'Membrane contact sites between pathogen-containing compartments and host organelles', *Biochim Biophys Acta*.

Duncan, Matthew J., Jeoung-Sook Shin, and Soman N. Abraham. 2002. 'Microbial entry through caveolae: variations on a theme', *Cell Microbiol*, 4: 783-91.

Edelmann, Sophia. 2016. 'Human and zoonotic Chlamydia species interact with Golgi-dependent vesicular and non-vesicular trafficking pathways', Inaugural-Dissertation, Freie Universität Berlin.

Elbashir, S. M., W. Lendeckel, and T. Tuschl. 2001. 'RNA interference is mediated by 21- and 22-nucleotide RNAs', *Genes Dev*, 15: 188-200.

Elwell, C. A., N. Czudnochowski, J. von Dollen, J. R. Johnson, R. Nakagawa, K. Mirrashidi, N. J. Krogan, J. N. Engel, and O. S. Rosenberg. 2017. 'Chlamydia interfere with an interaction between the mannose-6-phosphate receptor and sorting nexins to counteract host restriction', *eLife*, 6.

Elwell, C. A., and J. N. Engel. 2012. 'Lipid acquisition by intracellular Chlamydiae', *Cell Microbiol*, 14: 1010-8.

Elwell, C. A., S. Jiang, J. H. Kim, A. Lee, T. Wittmann, K. Hanada, P. Melancon, and J. N. Engel. 2011. 'Chlamydia trachomatis co-opts GBF1 and CERT to acquire host sphingomyelin for distinct roles during intracellular development', *PLoS Pathog*, 7: e1002198.

Elwell, C., K. Mirrashidi, and J. Engel. 2016. 'Chlamydia cell biology and pathogenesis', *Nat Rev Microbiol*, 14: 385-400.

Euskirchen, G., R. K. Auerbach, and M. Snyder. 2012. 'SWI/SNF chromatin-remodeling factors: multiscale analyses and diverse functions', *J Biol Chem*, 287: 30897-905.

Everett, K. D., R. M. Bush, and A. A. Andersen. 1999. 'Emended description of the order Chlamydiales, proposal of Parachlamydiaceae fam. nov. and Simkaniaceae fam. nov., each containing one monotypic genus, revised taxonomy of the family Chlamydiaceae, including a new genus and five new species, and standards for the identification of organisms', *Int J Syst Bacteriol*, 49 Pt 2: 415-40.

Fabian, M. R., M. K. Cieplak, F. Frank, M. Morita, J. Green, T. Srikumar, B. Nagar, T. Yamamoto, B. Raught, T. F. Duchaine, and N. Sonenberg. 2011. 'miRNA-mediated deadenylation is orchestrated by GW182 through two conserved motifs that interact with CCR4-NOT', *Nat Struct Mol Biol*, 18: 1211-7.

Fadel, S., and A. Eley. 2007. 'Chlamydia trachomatis OmcB protein is a surface-exposed glycosaminoglycan-dependent adhesin', *J Med Microbiol*, 56: 15-22.

Faris, R., M. Merling, S. E. Andersen, C. A. Dooley, T. Hackstadt, and M. M. Weber. 2019. 'Chlamydia trachomatis CT229 Subverts Rab GTPase-Dependent CCV Trafficking Pathways to Promote Chlamydial Infection', *Cell Rep*, 26: 3380-90.e5.

Fatica, A., and D. Tollervey. 2002. 'Making ribosomes', *Curr Opin Cell Biol*, 14: 313-8.

Fields, K. A., and T. Hackstadt. 2002. 'The chlamydial inclusion: escape from the endocytic pathway', *Annu Rev Cell Dev Biol*, 18: 221-45.

Finsel, I., C. Ragaz, C. Hoffmann, C. F. Harrison, S. Weber, V. A. van Rahden, L. Johannes, and H. Hilbi. 2013. 'The Legionella effector RidL inhibits retrograde trafficking to promote intracellular replication', *Cell Host Microbe*, 14: 38-50.

Firat-Karalar, E. N., and T. Stearns. 2015. 'Probing mammalian centrosome structure using BioID proximity-dependent biotinylation', *Methods Cell Biol*, 129: 153-70.

Fisher, M. A. 1993. 'Chlamydia trachomatis genital infections', *W V Med J*, 89: 331-4.

Frost, A., R. Perera, A. Roux, K. Spasov, O. Destaing, E. H. Egelman, P. De Camilli, and V. M. Unger. 2008. 'Structural basis of membrane invagination by F-BAR domains', *Cell*, 132: 807-17.

Frost, A., V. M. Unger, and P. De Camilli. 2009a. 'The BAR domain superfamily: membrane-molding macromolecules', *Cell*, 137: 191-6.

Frost, Adam, Vinzenz M. Unger, and Pietro De Camilli. 2009b. 'The BAR domain superfamily: membrane-molding macromolecules', *Cell*, 137: 191-96.

Fu, Y., J. A. Foden, C. Khayter, M. L. Maeder, D. Reyon, J. K. Joung, and J. D. Sander. 2013. 'High-frequency off-target mutagenesis induced by CRISPR-Cas nucleases in human cells', *Nat Biotechnol*, 31: 822-6.

Fucini, R. V., J. L. Chen, C. Sharma, M. M. Kessels, and M. Stamnes. 2002. 'Golgi vesicle proteins are linked to the assembly of an actin complex defined by mAbp1', *Mol Biol Cell*, 13: 621-31.

Fucini, R. V., A. Navarrete, C. Vadakkan, L. Lacomis, H. Erdjument-Bromage, P. Tempst, and M. Stamnes. 2000. 'Activated ADP-ribosylation factor assembles distinct pools of actin on golgi membranes', *J Biol Chem*, 275: 18824-9.

Gallon, M., and P. J. Cullen. 2015. 'Retromer and sorting nexins in endosomal sorting', *Biochem Soc Trans*, 43: 33-47.

Gambarte Tudela, J., A. Capmany, M. Romao, C. Quintero, S. Miserey-Lenkei, G. Raposo, B. Goud, and M. T. Damiani. 2015. 'The late endocytic Rab39a GTPase regulates the interaction between multivesicular bodies and chlamydial inclusions', *J Cell Sci*, 128: 3068-81.

Gambarte Tudela, Julián, Julio Buonfigli, Agustín Luján, Mariano Alonso Bivou, Ignacio Cebrián, Anahí Capmany, and María Teresa Damiani. 2019. 'Rab39a and Rab39b Display Different Intracellular Distribution and Function in Sphingolipids and Phospholipids Transport', *Int J Mol Sci*, 20: 1688.

Geisler, W. M. 2010. 'Duration of untreated, uncomplicated Chlamydia trachomatis genital infection and factors associated with chlamydia resolution: a review of human studies', *J Infect Dis*, 201 Suppl 2: S104-13.

Geisler, W. M., S. Y. Lensing, C. G. Press, and E. W. Hook, 3rd. 2013. 'Spontaneous resolution of genital Chlamydia trachomatis infection in women and protection from reinfection', *J Infect Dis*, 207: 1850-6.

Gershlick, D. C., and M. Lucas. 2017. 'Endosomal Trafficking: Retromer and Retriever Are Relatives in Recycling', *Curr Biol*, 27: R1233-r36.

Ghosh, P., N. M. Dahms, and S. Kornfeld. 2003. 'Mannose 6-phosphate receptors: new twists in the tale', *Nat Rev Mol Cell Biol*, 4: 202-12.

Giles, D. K., and P. B. Wyrick. 2008. 'Trafficking of chlamydial antigens to the endoplasmic reticulum of infected epithelial cells', *Microbes Infect*, 10: 1494-503.

Godi, A., I. Santone, P. Pertile, P. Devarajan, P. R. Stabach, J. S. Morrow, G. Di Tullio, R. Polishchuk, T. C. Petrucci, A. Luini, and M. A. De Matteis. 1998. 'ADP ribosylation factor regulates spectrin binding to the Golgi complex', *Proc Natl Acad Sci U S A*, 95: 8607-12.

Goebel, W., and M. Kuhn. 2000. 'Bacterial replication in the host cell cytosol', *Curr Opin Microbiol*, 3: 49-53.

Grant, B. D., and J. G. Donaldson. 2009. 'Pathways and mechanisms of endocytic recycling', *Nat Rev Mol Cell Biol*, 10: 597-608.

Greub, G., and D. Raoult. 2002. 'Parachlamydiaceae: potential emerging pathogens', *Emerg Infect Dis*, 8: 625-30.

Grieshaber, N. A., E. R. Fischer, D. J. Mead, C. A. Dooley, and T. Hackstadt. 2004. 'Chlamydial histone-DNA interactions are disrupted by a metabolite in the methylerythritol phosphate pathway of isoprenoid biosynthesis', *Proc Natl Acad Sci U S A*, 101: 7451-6.

Grieshaber, S. S., N. A. Grieshaber, N. Miller, and T. Hackstadt. 2006. 'Chlamydia trachomatis causes centrosomal defects resulting in chromosomal segregation abnormalities', *Traffic*, 7: 940-9.

Grieshaber, Scott S., Nicole A. Grieshaber, and Ted Hackstadt. 2003. 'Chlamydia trachomatis uses host cell dynein to traffic to the microtubule-organizing center in a p50 dynamitin-independent process', *J Cell Sci*, 116: 3793-802.

Griffin, C. T., J. Trejo, and T. Magnuson. 2005. 'Genetic evidence for a mammalian retromer complex containing sorting nexins 1 and 2', *Proc Natl Acad Sci U S A*, 102: 15173-7.

Griffiths, E., M. S. Ventresca, and R. S. Gupta. 2006. 'BLAST screening of chlamydial genomes to identify signature proteins that are unique for the Chlamydiales, Chlamydiaceae, Chlamydophila and Chlamydia groups of species', *BMC Genomics*, 7: 14.

Griffiths, G., and K. Simons. 1986. 'The trans Golgi network: sorting at the exit site of the Golgi complex', *Science*, 234: 438-43.

Gullapalli, A., T. A. Garrett, M. M. Paing, C. T. Griffin, Y. Yang, and J. Trejo. 2004. 'A role for sorting nexin 2 in epidermal growth factor receptor down-regulation: evidence for distinct functions of sorting nexin 1 and 2 in protein trafficking', *Mol Biol Cell*, 15: 2143-55.

Gupta, R. S., and E. Griffiths. 2006. 'Chlamydiae-specific proteins and indels: novel tools for studies', *Trends Microbiol*, 14: 527-35.

Gurumurthy, R. K., C. Chumduri, A. Karlas, S. Kimmig, E. Gonzalez, N. Machuy, T. Rudel, and T. F. Meyer. 2014. 'Dynamin-mediated lipid acquisition is essential for Chlamydia trachomatis development', *Mol Microbiol*, 94: 186-201.

Gurumurthy, R. K., A. P. Maurer, N. Machuy, S. Hess, K. P. Pleissner, J. Schuchhardt, T. Rudel, and T. F. Meyer. 2010. 'A loss-of-function screen reveals Ras- and Raf-independent MEK-ERK signaling during Chlamydia trachomatis infection', *Sci Signal*, 3: ra21.

Hackstadt, T., D. D. Rockey, R. A. Heinzen, and M. A. Scidmore. 1996. 'Chlamydia trachomatis interrupts an exocytic pathway to acquire endogenously synthesized sphingomyelin in transit from the Golgi apparatus to the plasma membrane', *Embo j*, 15: 964-77.

Hackstadt, T., M. A. Scidmore-Carlson, E. I. Shaw, and E. R. Fischer. 1999. 'The Chlamydia trachomatis IncA protein is required for homotypic vesicle fusion', *Cell Microbiol*, 1: 119-30.

Hackstadt, Ted. 2000. 'Redirection of Host Vesicle Trafficking Pathways by Intracellular Parasites', *Traffic*, 1: 93-99.

Hafner, L., K. Beagley, and P. Timms. 2008. 'Chlamydia trachomatis infection: host immune responses and potential vaccines', *Mucosal Immunol*, 1: 116-30.

Haft, C. R., M. de la Luz Sierra, R. Bafford, M. A. Lesniak, V. A. Barr, and S. I. Taylor. 2000. 'Human orthologs of yeast vacuolar protein sorting proteins Vps26, 29, and 35: assembly into multimeric complexes', *Mol Biol Cell*, 11: 4105-16.

Halberstädter, L. and von Prowazek, S. 1907a. 'Über Zelleinschlüsse parasitärer Natur beim Trachom." Arbeiten aus dem Kaiserlichen Gesundheitsamte', *Arbeiten aus dem Kaiserlichen Gesundheitsamte*, 26: 4.

———. 1907b. 'Zur Aetiologie des Trachoms.', *Deutsche Medizinische Wochenschrift*, 33: 3.

Hanada, K., K. Kumagai, S. Yasuda, Y. Miura, M. Kawano, M. Fukasawa, and M. Nishijima. 2003. 'Molecular machinery for non-vesicular trafficking of ceramide', *Nature*, 426: 803-9.

Hannon, G. J. 2002. 'RNA interference', *Nature*, 418: 244-51.

Harbour, M. E., S. Y. Breusegem, R. Antrobus, C. Freeman, E. Reid, and M. N. Seaman. 2010. 'The cargo-selective retromer complex is a recruiting hub for protein complexes that regulate endosomal tubule dynamics', *J Cell Sci*, 123: 3703-17.

Harterink, M., F. Port, M. J. Lorenowicz, I. J. McGough, M. Silhankova, M. C. Betist, J. R. T. van Weering, Rghp van Heesbeen, T. C. Middelkoop, K. Basler, P. J. Cullen, and H. C. Korswagen. 2011. 'A SNX3-dependent retromer pathway mediates retrograde transport of the Wnt sorting receptor Wntless and is required for Wnt secretion', *Nat Cell Biol*, 13: 914-23.

Hatch, G. M., and G. McClarty. 1998. 'Phospholipid composition of purified Chlamydia trachomatis mimics that of the eucaryotic host cell', *Infect Immun*, 66: 3727-35.

Hatch, T P, I Allan, and J H Pearce. 1984. 'Structural and polypeptide differences between envelopes of infective and reproductive life cycle forms of Chlamydia spp', *Journal of Bacteriology*, 157: 13-20.

Hatch, T. P. 1996. 'Disulfide cross-linked envelope proteins: the functional equivalent of peptidoglycan in chlamydiae?', *J Bacteriol*, 178: 1-5.

Heinzen, R. A., M. A. Scidmore, D. D. Rockey, and T. Hackstadt. 1996. 'Differential interaction with endocytic and exocytic pathways distinguish parasitophorous vacuoles of Coxiella burnetii and Chlamydia trachomatis', *Infect Immun*, 64: 796-809.

Henke, Sarah, and John Cronan. 2014. *Successful Conversion of the Bacillus subtilis BirA Group II Biotin Protein Ligase into a Group I Ligase*.

Hess, M. W., G. F. Vogel, T. E. Yordanov, B. Witting, K. Gutleben, H. L. Ebner, M. E. G. de Araujo, P. A. Filipek, and L. A. Huber. 2018. 'Combining high-pressure freezing with pre-embedding immunogold electron microscopy and tomography', *Traffic*, 19: 639-49.

Heuer, D., A. Rejman Lipinski, N. Machuy, A. Karlas, A. Wehrens, F. Siedler, V. Brinkmann, and T. F. Meyer. 2009. 'Chlamydia causes fragmentation of the Golgi compartment to ensure reproduction', *Nature*, 457: 731-5.

Hierro, A., A. L. Rojas, R. Rojas, N. Murthy, G. Effantin, A. V. Kajava, A. C. Steven, J. S. Bonifacino, and J. H. Hurley. 2007. 'Functional architecture of the retromer cargo-recognition complex', *Nature*, 449: 1063-7.

Hilbi, H., and A. Haas. 2012. 'Secretive bacterial pathogens and the secretory pathway', *Traffic*, 13: 1187-97.

Hoebeke, J., G. Van Nijen, and M. De Brabander. 1976. 'Interaction of oncodazole (R 17934), a new antitumoral drug, with rat brain tubulin', *Biochem Biophys Res Commun*, 69: 319-24.

Hogan, R. J., S. A. Mathews, S. Mukhopadhyay, J. T. Summersgill, and P. Timms. 2004. 'Chlamydial Persistence: beyond the Biphasic Paradigm', *Infection and Immunity*, 72: 1843-55.

Hong, Z., Y. Yang, C. Zhang, Y. Niu, K. Li, X. Zhao, and J. J. Liu. 2009. 'The retromer component SNX6 interacts with dynactin p150(Glued) and mediates endosome-to-TGN transport', *Cell Res*, 19: 1334-49.

Horvath, P., and R. Barrangou. 2010. 'CRISPR/Cas, the immune system of bacteria and archaea', *Science*, 327: 167-70.

Hower, S., K. Wolf, and K. A. Fields. 2009. 'Evidence that CT694 is a novel Chlamydia trachomatis T3S substrate capable of functioning during invasion or early cycle development', *Mol Microbiol*, 72: 1423-37.

Hsu, P. D., D. A. Scott, J. A. Weinstein, F. A. Ran, S. Konermann, V. Agarwala, Y. Li, E. J. Fine, X. Wu, O. Shalem, T. J. Cradick, L. A. Marraffini, G. Bao, and F. Zhang. 2013. 'DNA targeting specificity of RNA-guided Cas9 nucleases', *Nat Biotechnol*, 31: 827-32.

Huang, Z., M. Chen, K. Li, X. Dong, J. Han, and Q. Zhang. 2010. 'Cryo-electron tomography of Chlamydia trachomatis gives a clue to the mechanism of outer membrane changes', *J Electron Microsc (Tokyo)*, 59: 237-41.

Huitema, K., J. van den Dikkenberg, J. F. Brouwers, and J. C. Holthuis. 2004. 'Identification of a family of animal sphingomyelin synthases', *Embo j*, 23: 33-44.

Hunt, S. D., A. K. Townley, C. M. Danson, P. J. Cullen, and D. J. Stephens. 2013. 'Microtubule motors mediate endosomal sorting by maintaining functional domain organization', *J Cell Sci*, 126: 2493-501.

Huotari, J., and A. Helenius. 2011. 'Endosome maturation', *Embo j*, 30: 3481-500.

Hutagalung, Alex H., and Peter J. Novick. 2011. 'Role of Rab GTPases in membrane traffic and cell physiology', *Physiological reviews*, 91: 119-49.

Hybiske, K., and R. S. Stephens. 2007. 'Mechanisms of host cell exit by the intracellular bacterium Chlamydia', *Proc Natl Acad Sci U S A*, 104: 11430-5.

Ito, K., A. Takahashi, M. Morita, T. Suzuki, and T. Yamamoto. 2011. 'The role of the CNOT1 subunit of the CCR4-NOT complex in mRNA deadenylation and cell viability', *Protein Cell*, 2: 755-63.

Jansen, R., J. D. Embden, W. Gaastra, and L. M. Schouls. 2002. 'Identification of genes that are associated with DNA repeats in prokaryotes', *Mol Microbiol*, 43: 1565-75.

Jewett, T. J., E. R. Fischer, D. J. Mead, and T. Hackstadt. 2006. 'Chlamydial TARP is a bacterial nucleator of actin', *Proc Natl Acad Sci U S A*, 103: 15599-604.

Jia, D., J. S. Zhang, F. Li, J. Wang, Z. Deng, M. A. White, D. G. Osborne, C. Phillips-Krawczak, T. S. Gomez, H. Li, A. Singla, E. Burstein, D. D. Billadeau, and M. K. Rosen. 2016. 'Structural and mechanistic insights into regulation of the retromer coat by TBC1d5', *Nat Commun*, 7: 13305.

Jia, J., A. Arif, B. Willard, J. D. Smith, D. J. Stuehr, S. L. Hazen, and P. L. Fox. 2012. 'Protection of extraribosomal RPL13a by GAPDH and dysregulation by S-nitrosylation', *Mol Cell*, 47: 656-63.

Jiang, W., D. Bikard, D. Cox, F. Zhang, and L. A. Marraffini. 2013. 'RNA-guided editing of bacterial genomes using CRISPR-Cas systems', *Nat Biotechnol*, 31: 233-9.

Jin, A., K. Itahana, K. O'Keefe, and Y. Zhang. 2004. 'Inhibition of HDM2 and activation of p53 by ribosomal protein L23', *Mol Cell Biol*, 24: 7669-80.

Johannes, L., and V. Popoff. 2008. 'Tracing the retrograde route in protein trafficking', *Cell*, 135: 1175-87.

Kadam, S., G. S. McAlpine, M. L. Phelan, R. E. Kingston, K. A. Jones, and B. M. Emerson. 2000. 'Functional selectivity of recombinant mammalian SWI/SNF subunits', *Genes Dev*, 14: 2441-51.

Kadoch, C., and G. R. Crabtree. 2015. 'Mammalian SWI/SNF chromatin remodeling complexes and cancer: Mechanistic insights gained from human genomics', *Sci Adv*, 1: e1500447.

Kapasi, P., S. Chaudhuri, K. Vyas, D. Baus, A. A. Komar, P. L. Fox, W. C. Merrick, and B. Mazumder. 2007. 'L13a blocks 48S assembly: role of a general initiation factor in mRNA-specific translational control', *Mol Cell*, 25: 113-26.

Kerr, M. C., J. S. Bennetts, F. Simpson, E. C. Thomas, C. Flegg, P. A. Gleeson, C. Wicking, and R. D. Teasdale. 2005. 'A novel mammalian retromer component, Vps26B', *Traffic*, 6: 991-1001.

Khatter, H., A. G. Myasnikov, S. K. Natchiar, and B. P. Klaholz. 2015. 'Structure of the human 80S ribosome', *Nature*, 520: 640-5.

Klinger, S. C., P. Siupka, and M. S. Nielsen. 2015. 'Retromer-Mediated Trafficking of Transmembrane Receptors and Transporters', *Membranes (Basel)*, 5: 288-306.

Koch-Edelmann, S., S. Banhart, E. M. Saied, L. Rose, L. Aeberhard, M. Laue, J. Doellinger, C. Arenz, and D. Heuer. 2017. 'The cellular ceramide transport protein CERT promotes Chlamydia psittaci infection and controls bacterial sphingolipid uptake', *Cell Microbiol*.

Koch-Institute, Robert. 2013. 'Chlamydia trachomatis - Laborsentinel', *Epidemiologisches Bulletin*, 46.

Koharudin, L. M., W. Furey, H. Liu, Y. J. Liu, and A. M. Gronenborn. 2009. 'The phox domain of sorting nexin 5 lacks phosphatidylinositol 3-phosphate (PtdIns(3)P) specificity and preferentially binds to phosphatidylinositol 4,5-bisphosphate (PtdIns(4,5)P2)', *J Biol Chem*, 284: 23697-707.

Kokes, M., J. D. Dunn, J. A. Granek, B. D. Nguyen, J. R. Barker, R. H. Valdivia, and R. J. Bastidas. 2015. 'Integrating Chemical Mutagenesis and Whole-Genome Sequencing as a Platform for Forward and Reverse Genetic Analysis of Chlamydia', *Cell Host Microbe*.

Kressler, D., E. Hurt, and J. Bassler. 2017. 'A Puzzle of Life: Crafting Ribosomal Subunits', *Trends Biochem Sci*, 42: 640-54.

Kumar, Y., and R. H. Valdivia. 2008a. 'Actin and intermediate filaments stabilize the Chlamydia trachomatis vacuole by forming dynamic structural scaffolds', *Cell Host Microbe*, 4: 159-69.

———. 2008b. 'Reorganization of the host cytoskeleton by the intracellular pathogen Chlamydia trachomatis', *Commun Integr Biol*, 1: 175-7.

Kvainickas, Arunas, Ana Jimenez-Orgaz, Heike Nägele, Zehan Hu, Jörn Dengjel, and Florian Steinberg. 2017. 'Cargo-selective SNX-BAR proteins mediate retromer trimer independent retrograde transport', *J Cell Biol*.

Laemmli, U. K. 1970. 'Cleavage of structural proteins during the assembly of the head of bacteriophage T4', *Nature*, 227: 680-5.

Lambert, J. P., M. Tucholska, C. Go, J. D. Knight, and A. C. Gingras. 2015. 'Proximity biotinylation and affinity purification are complementary approaches for the interactome mapping of chromatin-associated protein complexes', *J Proteomics*, 118: 81-94.

Lauffer, B. E., C. Melero, P. Temkin, C. Lei, W. Hong, T. Kortemme, and M. von Zastrow. 2010. 'SNX27 mediates PDZ-directed sorting from endosomes to the plasma membrane', *J Cell Biol*, 190: 565-74.

Le Sage, V., A. Cinti, and A. J. Mouland. 2016. 'Proximity-Dependent Biotinylation for Identification of Interacting Proteins', *Curr Protoc Cell Biol*, 73: 17.19.1-17.19.12.

Lee, J. K., G. A. Enciso, D. Boassa, C. N. Chander, T. H. Lou, S. S. Pairawan, M. C. Guo, F. Y. M. Wan, M. H. Ellisman, C. Sutterlin, and M. Tan. 2018. 'Replication-dependent size reduction precedes differentiation in Chlamydia trachomatis', *Nat Commun*, 9: 45.

Liang, P., M. Rosas-Lemus, D. Patel, X. Fang, K. Tuz, and O. Juarez. 2018. 'Dynamic energy dependency of Chlamydia trachomatis on host cell metabolism during intracellular growth: Role of sodium-based energetics in chlamydial ATP generation', *J Biol Chem*, 293: 510-22.

Lienard, J., A. Croxatto, S. Aeby, K. Jaton, K. Posfay-Barbe, A. Gervaix, and G. Greub. 2011. 'Development of a new chlamydiales-specific real-time PCR and its application to respiratory clinical samples', *J Clin Microbiol*, 49: 2637-42.

Lindstrom, M. S. 2009. 'Emerging functions of ribosomal proteins in gene-specific transcription and translation', *Biochem Biophys Res Commun*, 379: 167-70.

Lodish, H. F., Berk, A., Kaiser, C., Krieger, M., Scott, M. P., Bretscher, A., Ploegh, H. L., Matsudaira, P. T. 2008. *Molecular Cell Biology 6th Ed* (New York: W. H. Freeman and Company).

Lohrum, M. A., R. L. Ludwig, M. H. Kubbutat, M. Hanlon, and K. H. Vousden. 2003. 'Regulation of HDM2 activity by the ribosomal protein L11', *Cancer Cell*, 3: 577-87.

Longbottom, D., and L. J. Coulter. 2003. 'Animal chlamydioses and zoonotic implications', *J Comp Pathol*, 128: 217-44.

Lu, L., and W. Hong. 2014. 'From endosomes to the trans-Golgi network', *Semin Cell Dev Biol*, 31: 30-9.

Lutter, Erika I., Craig Martens, and Ted Hackstadt. 2012. 'Evolution and Conservation of Predicted Inclusion Membrane Proteins in Chlamydiae', *Comp Funct Genomics*, 2012: 1-13.

Madela, K., S. Banhart, A. Zimmermann, J. Piesker, N. Bannert, and M. Laue. 2014. 'A simple procedure to analyze positions of interest in infectious cell cultures by correlative light and electron microscopy', *Methods Cell Biol*, 124: 93-110.

Malhotra, M., S. Sood, A. Mukherjee, S. Muralidhar, and M. Bala. 2013. 'Genital Chlamydia trachomatis: an update', *Indian J Med Res*, 138: 303-16.

Martinez, J., A. Patkaniowska, H. Urlaub, R. Luhrmann, and T. Tuschl. 2002. 'Single-stranded antisense siRNAs guide target RNA cleavage in RNAi', *Cell*, 110: 563-74.

Matsumoto, A. 1981a. 'Electron microscopic observations of surface projections and related intracellular structures of Chlamydia organisms', *J Electron Microsc (Tokyo)*, 30: 315-20.

———. 1981b. 'Isolation and electron microscopic observations of intracytoplasmic inclusions containing Chlamydia psittaci', *J Bacteriol*, 145: 605-12.

Matsumoto, A., H. Bessho, K. Uehira, and T. Suda. 1991. 'Morphological studies of the association of mitochondria with chlamydial inclusions and the fusion of chlamydial inclusions', *J Electron Microsc (Tokyo)*, 40: 356-63.

Matsumoto, A., and G. P. Manire. 1970. 'Electron microscopic observations on the effects of penicillin on the morphology of Chlamydia psittaci', *J Bacteriol*, 101: 278-85.

Mauro, V. P., and G. M. Edelman. 2002. 'The ribosome filter hypothesis', *Proc Natl Acad Sci U S A*, 99: 12031-6.

Maxfield, F. R., and T. E. McGraw. 2004. 'Endocytic recycling', *Nat Rev Mol Cell Biol*, 5: 121-32.

Mayinger, P. 2012. 'Phosphoinositides and vesicular membrane traffic', *Biochim Biophys Acta*, 1821: 1104-13.

Mazumder, B., D. Poddar, A. Basu, R. Kour, V. Verbovetskaya, and S. Barik. 2014. 'Extraribosomal l13a is a specific innate immune factor for antiviral defense', *J Virol*, 88: 9100-10.

Mazumder, B., P. Sampath, V. Seshadri, R. K. Maitra, P. E. DiCorleto, and P. L. Fox. 2003. 'Regulated release of L13a from the 60S ribosomal subunit as a mechanism of transcript-specific translational control', *Cell*, 115: 187-98.

McConkey, E. H., and E. J. Hauber. 1975. 'Evidence for heterogeneity of ribosomes within the HeLa cell', *J Biol Chem*, 250: 1311-8.

McDonald, K. 1999. 'High-pressure freezing for preservation of high resolution fine structure and antigenicity for immunolabeling', *Methods Mol Biol*, 117: 77-97.

McGough, I. J., and P. J. Cullen. 2011. 'Recent advances in retromer biology', *Traffic*, 12: 963-71.

McMahon, Harvey T., and Jennifer L. Gallop. 2005. 'Membrane curvature and mechanisms of dynamic cell membrane remodelling', *Nature*, 438: 590-96.

McNally, K. E., and P. J. Cullen. 2018. 'Endosomal Retrieval of Cargo: Retromer Is Not Alone', *Trends Cell Biol*, 28: 807-22.

McNally, K. E., R. Faulkner, F. Steinberg, M. Gallon, R. Ghai, D. Pim, P. Langton, N. Pearson, C. M. Danson, H. Nagele, L. L. Morris, A. Singla, B. L. Overlee, K. J. Heesom, R. Sessions, L. Banks, B. M. Collins, I. Berger, D. D. Billadeau, E. Burstein, and P. J. Cullen. 2017. 'Retriever is a multiprotein complex for retromer-independent endosomal cargo recycling', *Nat Cell Biol*.

Mehlitz, A., S. Banhart, A. P. Maurer, A. Kaushansky, A. G. Gordus, J. Zielecki, G. Macbeath, and T. F. Meyer. 2010. 'Tarp regulates early Chlamydia-induced host cell survival through interactions with the human adaptor protein SHC1', *J Cell Biol*, 190: 143-57.

Menozzi, F. D., K. Pethe, P. Bifani, F. Soncin, M. J. Brennan, and C. Locht. 2002. 'Enhanced bacterial virulence through exploitation of host glycosaminoglycans', *Mol Microbiol*, 43: 1379-86.

Mirrashidi, K. M., C. A. Elwell, E. Verschueren, J. R. Johnson, A. Frando, J. Von Dollen, O. Rosenberg, N. Gulbahce, G. Jang, T. Johnson, S. Jager, A. M. Gopalakrishnan, J. Sherry, J. D. Dunn, A. Olive, B. Penn, M. Shales, J. S. Cox, M. N. Starnbach, I. Derre, R. Valdivia, N. J. Krogan, and J. Engel. 2015. 'Global Mapping of the Inc-Human Interactome Reveals that Retromer Restricts Chlamydia Infection', *Cell Host Microbe*.

Miserey-Lenkei, S., F. Waharte, A. Boulet, M. H. Cuif, D. Tenza, A. El Marjou, G. Raposo, J. Salamero, L. Heliot, B. Goud, and S. Monier. 2007. 'Rab6-interacting protein 1 links Rab6 and Rab11 function', *Traffic*, 8: 1385-403.

Mital, J., E. I. Lutter, A. C. Barger, C. A. Dooley, and T. Hackstadt. 2015. 'Chlamydia trachomatis inclusion membrane protein CT850 interacts with the dynein light chain DYNLT1 (Tctex1)', *Biochem Biophys Res Commun*.

Mital, J., N. J. Miller, D. W. Dorward, C. A. Dooley, and T. Hackstadt. 2013. 'Role for chlamydial inclusion membrane proteins in inclusion membrane structure and biogenesis', *PLoS One*, 8: e63426.

Mital, J., N. J. Miller, E. R. Fischer, and T. Hackstadt. 2010. 'Specific chlamydial inclusion membrane proteins associate with active Src family kinases in microdomains that interact with the host microtubule network', *Cell Microbiol*, 12: 1235-49.

Monden, K., and H. Kumon. 2009. '[Genital chlamydial infection]', *Nihon Rinsho*, 67: 125-8.

Moore, E. R., E. R. Fischer, D. J. Mead, and T. Hackstadt. 2008. 'The chlamydial inclusion preferentially intercepts basolaterally directed sphingomyelin-containing exocytic vacuoles', *Traffic*, 9: 2130-40.

Moore, Elizabeth R., and Scot P. Ouellette. 2014. 'Reconceptualizing the chlamydial inclusion as a pathogen-specified parasitic organelle: an expanded role for Inc proteins', *Front Cell Infect Microbiol*, 4.

Moorhead, A. M., J. Y. Jung, A. Smirnov, S. Kaufer, and M. A. Scidmore. 2010. 'Multiple host proteins that function in phosphatidylinositol-4-phosphate metabolism are recruited to the chlamydial inclusion', *Infect Immun*, 78: 1990-2007.

Moorhead, A. R., K. A. Rzomp, and M. A. Scidmore. 2007. 'The Rab6 effector Bicaudal D1 associates with Chlamydia trachomatis inclusions in a biovar-specific manner', *Infect Immun*, 75: 781-91.

Moulder, J. W. 1966. 'The relation of the psittacosis group (Chlamydiae) to bacteria and viruses', *Annu Rev Microbiol*, 20: 107-30.

———. 1991. 'Interaction of chlamydiae and host cells in vitro', *Microbiol Rev*, 55: 143-90.

Mpiga, P., and M. Ravaoarinoro. 2006. 'Chlamydia trachomatis persistence: an update', *Microbiol Res*, 161: 9-19.

Mukhopadhyay, R., J. Jia, A. Arif, P. S. Ray, and P. L. Fox. 2009. 'The GAIT system: a gatekeeper of inflammatory gene expression', *Trends Biochem Sci*, 34: 324-31.

Munier-Lehmann, H., F. Mauxion, and B. Hoflack. 1996. 'Function of the two mannose 6-phosphate receptors in lysosomal enzyme transport', *Biochem Soc Trans*, 24: 133-6.

Nans, A., H. R. Saibil, and R. D. Hayward. 2014. 'Pathogen-host reorganization during Chlamydia invasion revealed by cryo-electron tomography', *Cell Microbiol*, 16: 1457-72.

Nelson, DE. 2012. 'The Chlamydial Cell Envelope.' in Bavoil PM Tan M (ed.), *Intracellular Pathogens 1: Chlamydiales* (ASM Press).

Newman, L., J. Rowley, S. Vander Hoorn, N. S. Wijesooriya, M. Unemo, N. Low, G. Stevens, S. Gottlieb, J. Kiarie, and M. Temmerman. 2015. 'Global Estimates of the Prevalence and Incidence of Four Curable Sexually Transmitted Infections in 2012 Based on Systematic Review and Global Reporting', *PLoS One*, 10: e0143304.

Newton, Timothy M., and Evan Reid. 2016. 'An Automated Image Analysis System to Quantify Endosomal Tubulation', *PLoS One*, 11: e0168294.

Nielsen, M. S., P. Madsen, E. I. Christensen, A. Nykjaer, J. Gliemann, D. Kasper, R. Pohlmann, and C. M. Petersen. 2001. 'The sortilin cytoplasmic tail conveys Golgi-endosome transport and binds the VHS domain of the GGA2 sorting protein', *Embo j*, 20: 2180-90.

Nisar, S., E. Kelly, P. J. Cullen, and S. J. Mundell. 2010. 'Regulation of P2Y1 receptor traffic by sorting Nexin 1 is retromer independent', *Traffic*, 11: 508-19.

Niu, Y., C. Zhang, Z. Sun, Z. Hong, K. Li, D. Sun, Y. Yang, C. Tian, W. Gong, and J. J. Liu. 2013. 'PtdIns(4)P regulates retromer-motor interaction to facilitate dynein-cargo dissociation at the trans-Golgi network', *Nat Cell Biol*, 15: 417-29.

Norwood, S. J., D. J. Shaw, N. P. Cowieson, D. J. Owen, R. D. Teasdale, and B. M. Collins. 2011. 'Assembly and solution structure of the core retromer protein complex', *Traffic*, 12: 56-71.

Nunes, A., and J. P. Gomes. 2014. 'Evolution, phylogeny, and molecular epidemiology of Chlamydia', *Infect Genet Evol*, 23: 49-64.

Ohmer, M., T. Tzivelekidis, N. Niedenfuhr, L. Volceanov-Hahn, S. Barth, J. Vier, M. Borries, H. Busch, L. Kook, M. L. Biniossek, O. Schilling, S. Kirschnek, and G. Hacker. 2018. 'Infection of HeLa cells with Chlamydia trachomatis inhibits protein synthesis and causes multiple changes to host cell pathways', *Cell Microbiol*: e12993.

Ong, S. E., B. Blagoev, I. Kratchmarova, D. B. Kristensen, H. Steen, A. Pandey, and M. Mann. 2002. 'Stable isotope labeling by amino acids in cell culture, SILAC, as a simple and accurate approach to expression proteomics', *Mol Cell Proteomics*, 1: 376-86.

Ong, Shao-En, and Matthias Mann. 2007. 'A practical recipe for stable isotope labeling by amino acids in cell culture (SILAC)', *Nat. Protocols*, 1: 2650-60.

Ouellette, S. P., and R. A. Carabeo. 2010. 'A Functional Slow Recycling Pathway of Transferrin is Required for Growth of Chlamydia', *Front Microbiol*, 1: 112.

Ouellette, S. P., F. C. Dorsey, S. Moshiach, J. L. Cleveland, and R. A. Carabeo. 2011. 'Chlamydia species-dependent differences in the growth requirement for lysosomes', *PLoS One*, 6: e16783.

Patrick, K. L., J. A. Wojcechowskyj, S. L. Bell, M. N. Riba, T. Jing, S. Talmage, P. Xu, A. L. Cabello, J. Xu, M. Shales, D. Jimenez-Morales, T. A. Ficht, P. de Figueiredo, J. E. Samuel, P. Li, N. J. Krogan, and R. O. Watson. 2018. 'Quantitative Yeast Genetic Interaction Profiling of Bacterial Effector Proteins Uncovers a Role for the Human Retromer in Salmonella Infection', *Cell Syst*, 7: 323-38.e6.

Paul, Blessy, Hyun Sung Kim, Markus C. Kerr, Wilhelmina M. Huston, Rohan D. Teasdale, and Brett M. Collins. 2017. 'Structural basis for the hijacking of endosomal sorting nexin proteins by Chlamydia trachomatis', *eLife*, 6: e22311.

Pechmann, S., F. Willmund, and J. Frydman. 2013. 'The ribosome as a hub for protein quality control', *Mol Cell*, 49: 411-21.

Peeling, R. W., and R. C. Brunham. 1996. 'Chlamydiae as pathogens: new species and new issues', *Emerg Infect Dis*, 2: 307-19.

Perara, E., D. Ganem, and J. N. Engel. 1992. 'A developmentally regulated chlamydial gene with apparent homology to eukaryotic histone H1', *Proc Natl Acad Sci U S A*, 89: 2125-9.

Perez, E. E., J. Wang, J. C. Miller, Y. Jouvenot, K. A. Kim, O. Liu, N. Wang, G. Lee, V. V. Bartsevich, Y. L. Lee, D. Y. Guschin, I. Rupniewski, A. J. Waite, C. Carpenito, R. G. Carroll, J. S. Orange, F. D. Urnov, E. J. Rebar, D. Ando, P. D. Gregory, J. L. Riley, M. C. Holmes, and C. H. June. 2008. 'Establishment of HIV-1 resistance in CD4+ T cells by genome editing using zinc-finger nucleases', *Nat Biotechnol*, 26: 808-16.

Personnic, N., K. Barlocher, I. Finsel, and H. Hilbi. 2016. 'Subversion of Retrograde Trafficking by Translocated Pathogen Effectors', *Trends Microbiol*.

Peter, B. J., H. M. Kent, I. G. Mills, Y. Vallis, P. J. Butler, P. R. Evans, and H. T. McMahon. 2004. 'BAR domains as sensors of membrane curvature: the amphiphysin BAR structure', *Science*, 303: 495-9.

Phelan, M. L., S. Sif, G. J. Narlikar, and R. E. Kingston. 1999. 'Reconstitution of a core chromatin remodeling complex from SWI/SNF subunits', *Mol Cell*, 3: 247-53.

Preiss, T. 2016. 'All Ribosomes Are Created Equal. Really?', *Trends Biochem Sci*, 41: 121-23.

Priya, A., I. V. Kalaidzidis, Y. Kalaidzidis, D. Lambright, and S. Datta. 2015. 'Molecular insights into Rab7-mediated endosomal recruitment of core retromer: deciphering the role of Vps26 and Vps35', *Traffic*, 16: 68-84.

Prosser, D. C., D. Tran, A. Schooley, B. Wendland, and J. K. Ngsee. 2010. 'A novel, retromer-independent role for sorting nexins 1 and 2 in RhoG-dependent membrane remodeling', *Traffic*, 11: 1347-62.

Prusty, Bhupesh, Linda Bö Hme, Birgit Bergmann, Christine Siegl, Eva Krause, Adrian Mehlitz, and Thomas Rudel. 2012. *Imbalanced Oxidative Stress Causes Chlamydial Persistence during Non-Productive Human Herpes Virus Co-Infection*.

Ramakrishnan, V. 2002. 'Ribosome structure and the mechanism of translation', *Cell*, 108: 557-72.

Ran, F. Ann, Patrick D. Hsu, Jason Wright, Vineeta Agarwala, David A. Scott, and Feng Zhang. 2013. 'Genome engineering using the CRISPR-Cas9 system', *Nat. Protocols*, 8: 2281-308.

Rappsilber, J., Y. Ishihama, and M. Mann. 2003. 'Stop and go extraction tips for matrix-assisted laser desorption/ionization, nanoelectrospray, and LC/MS sample pretreatment in proteomics', *Anal Chem*, 75: 663-70.

Rappsilber, J., M. Mann, and Y. Ishihama. 2007. 'Protocol for micro-purification, enrichment, pre-fractionation and storage of peptides for proteomics using StageTips', *Nat Protoc*, 2: 1896-906.

Rejman Lipinski, A., J. Heymann, C. Meissner, A. Karlas, V. Brinkmann, T. F. Meyer, and D. Heuer. 2009. 'Rab6 and Rab11 regulate Chlamydia trachomatis development and golgin-84-dependent Golgi fragmentation', *PLoS Pathog*, 5: e1000615.

Resnikoff, S., D. Pascolini, D. Etya'ale, I. Kocur, R. Pararajasegaram, G. P. Pokharel, and S. P. Mariotti. 2004. 'Global data on visual impairment in the year 2002', *Bull World Health Organ*, 82: 844-51.

Robertson, D. K., L. Gu, R. K. Rowe, and W. L. Beatty. 2009. 'Inclusion biogenesis and reactivation of persistent Chlamydia trachomatis requires host cell sphingolipid biosynthesis', *PLoS Pathog*, 5: e1000664.

Rockey, D. D., D. Grosenbach, D. E. Hruby, M. G. Peacock, R. A. Heinzen, and T. Hackstadt. 1997. 'Chlamydia psittaci IncA is phosphorylated by the host cell and is exposed on the cytoplasmic face of the developing inclusion', *Mol Microbiol*, 24: 217-28.

Rockey, D. D., R. A. Heinzen, and T. Hackstadt. 1995. 'Cloning and characterization of a Chlamydia psittaci gene coding for a protein localized in the inclusion membrane of infected cells', *Mol Microbiol*, 15: 617-26.

Rockey, D. D., and J. L. Rosquist. 1994. 'Protein antigens of Chlamydia psittaci present in infected cells but not detected in the infectious elementary body', *Infect Immun*, 62: 106-12.

Rockey, D. D., M. A. Scidmore, J. P. Bannantine, and W. J. Brown. 2002. 'Proteins in the chlamydial inclusion membrane', *Microbes Infect*, 4: 333-40.

Rohde, Gernot, Eberhard Straube, Andreas Essig, Petra Reinhold, and Konrad Sachse. 2010. 'Chlamydial zoonoses', *Deutsches Arzteblatt international*, 107: 174-80.

Rojas, R., S. Kametaka, C. R. Haft, and J. S. Bonifacino. 2007. 'Interchangeable but essential functions of SNX1 and SNX2 in the association of retromer with endosomes and the trafficking of mannose 6-phosphate receptors', *Mol Cell Biol*, 27: 1112-24.

Rojas, R., T. van Vlijmen, G. A. Mardones, Y. Prabhu, A. L. Rojas, S. Mohammed, A. J. Heck, G. Raposo, P. van der Sluijs, and J. S. Bonifacino. 2008. 'Regulation of retromer recruitment to endosomes by sequential action of Rab5 and Rab7', *J Cell Biol*, 183: 513-26.

Romano-Moreno, M., A. L. Rojas, C. D. Williamson, D. C. Gershlick, M. Lucas, M. N. Isupov, J. S. Bonifacino, M. P. Machner, and A. Hierro. 2017. 'Molecular mechanism for the subversion of the retromer coat by the Legionella effector RidL', *Proc Natl Acad Sci U S A*, 114: E11151-e60.

Rother, Marion, Erik Gonzalez, Ana Rita Teixeira da Costa, Lea Wask, Isabella Gravenstein, Matteo Pardo, Matthias Pietzke, Rajendra Kumar Gurumurthy, Jörg Angermann, Robert Laudeley, Silke Glage, Michael Meyer, Cindrilla Chumduri, Stefan Kempa, Klaus Dinkel, Anke Unger, Bert Klebl, Andreas Klos, and Thomas F. Meyer. 2018. 'Combined Human Genome-wide RNAi and Metabolite Analyses Identify IMPDH as a Host-Directed Target against Chlamydia Infection', *Cell Host Microbe*, 23: 661-71.e8.

Roux, K. J., D. I. Kim, and B. Burke. 2013. 'BioID: a screen for protein-protein interactions', *Curr Protoc Protein Sci*, 74: Unit 19.23.

Roux, K. J., D. I. Kim, M. Raida, and B. Burke. 2012. 'A promiscuous biotin ligase fusion protein identifies proximal and interacting proteins in mammalian cells', *J Cell Biol*, 196: 801-10.

Roux, Kyle J., Dae In Kim, Brian Burke, and Danielle G. May. 2018. 'BioID: A Screen for Protein-Protein Interactions', *Current protocols in protein science*, 91: 19.23.1-19.23.15.

Rubbo, S. D., J. F. Gardner, and R. L. Webb. 1967. 'Biocidal activities of glutaraldehyde and related compounds', *J Appl Bacteriol*, 30: 78-87.

Rzomp, K. A., A. R. Moorhead, and M. A. Scidmore. 2006. 'The GTPase Rab4 interacts with Chlamydia trachomatis inclusion membrane protein CT229', *Infect Immun*, 74: 5362-73.

Rzomp, K. A., L. D. Scholtes, B. J. Briggs, G. R. Whittaker, and M. A. Scidmore. 2003. 'Rab GTPases are recruited to chlamydial inclusions in both a species-dependent and species-independent manner', *Infect Immun*, 71: 5855-70.

Sabel, F. L., A. Hellman, and J. J. McDade. 1969. 'Glutaraldehyde inactivation of virus in tissue', *Appl Microbiol*, 17: 645-6.

Sachse, K., P. M. Bavoil, B. Kaltenboeck, R. S. Stephens, C. C. Kuo, R. Rossello-Mora, and M. Horn. 2015. 'Emendation of the family Chlamydiaceae: proposal of a single genus, Chlamydia, to include all currently recognized species', *Syst Appl Microbiol*, 38: 99-103.

Sampath, P., B. Mazumder, V. Seshadri, and P. L. Fox. 2003. 'Transcript-selective translational silencing by gamma interferon is directed by a novel structural element in the ceruloplasmin mRNA 3' untranslated region', *Mol Cell Biol*, 23: 1509-19.

Sandler, H., J. Kreth, H. T. Timmers, and G. Stoecklin. 2011. 'Not1 mediates recruitment of the deadenylase Caf1 to mRNAs targeted for degradation by tristetraprolin', *Nucleic Acids Res*, 39: 4373-86.

Sauert, M., H. Temmel, and I. Moll. 2015. 'Heterogeneity of the translational machinery: Variations on a common theme', *Biochimie*, 114: 39-47.

Savitski, Mikhail M., Mathias Wilhelm, Hannes Hahne, Bernhard Kuster, and Marcus Bantscheff. 2015. 'A Scalable Approach for Protein False Discovery Rate Estimation in Large Proteomic Data Sets', *Molecular & Cellular Proteomics : MCP*, 14: 2394-404.

Schaab, Christoph, Tamar Geiger, Gabriele Stoehr, Juergen Cox, and Matthias Mann. 2012. 'Analysis of High Accuracy, Quantitative Proteomics Data in the MaxQB Database', *Molecular & Cellular Proteomics : MCP*, 11: M111.014068.

Schachter, J. 1978. 'Chlamydial infections (first of three parts)', *N Engl J Med*, 298: 428-35.

———. 1999. 'Infection and disease epidemiology. In Chlamydia: Intracellular biology, pathogenesis, and immunity (ed. Stephens RS).' in (American Society for Microbiology, Washington, DC).

Schachter, J., R. S. Stephens, P. Timms, C. Kuo, P. M. Bavoil, S. Birkelund, J. Boman, H. Caldwell, L. A. Campbell, M. Chernesky, G. Christiansen, I. N. Clarke, C. Gaydos, J. T. Grayston, T. Hackstadt, R. Hsia, B. Kaltenboeck, M. Leinonnen, D. Ojcius, G. McClarty, J. Orfila, R. Peeling, M. Puolakkainen, T. C. Quinn, R. G. Rank, J. Raulston, G. L. Ridgeway, P. Saikku, W. E. Stamm, D. T. Taylor-Robinson, S. P. Wang, and P. B. Wyrick. 2001. 'Radical changes to chlamydial taxonomy are not necessary just yet', *Int J Syst Evol Microbiol*, 51: 249; author reply 51-3.

Schmeing, T. M., and V. Ramakrishnan. 2009. 'What recent ribosome structures have revealed about the mechanism of translation', *Nature*, 461: 1234-42.

Schofl, G., A. Voigt, K. Litsche, K. Sachse, and H. P. Saluz. 2011. 'Complete genome sequences of four mammalian isolates of Chlamydophila psittaci', *J Bacteriol*, 193: 4258.

Schramm, N., C. R. Bagnell, and P. B. Wyrick. 1996. 'Vesicles containing Chlamydia trachomatis serovar L2 remain above pH 6 within HEC-1B cells', *Infect Immun*, 64: 1208-14.

Schroeder, N., L. J. Mota, and S. Meresse. 2011. 'Salmonella-induced tubular networks', *Trends Microbiol*, 19: 268-77.

Schwartz, W. 1966. 'J. W. Moulder, The Psittacosis Group as Bacteria. Ciba Lectures in Microbial Biochemistry. 95 S., 30 Abb., 15 Tab. New York, London, Sydney 1964: John Wiley and Sons Inc. sh 30.—', *Zeitschrift für allgemeine Mikrobiologie*, 6: 136-36.

Schwarz, D. G., C. T. Griffin, E. A. Schneider, D. Yee, and T. Magnuson. 2002. 'Genetic analysis of sorting nexins 1 and 2 reveals a redundant and essential function in mice', *Mol Biol Cell*, 13: 3588-600.

Scidmore-Carlson, M. A., E. I. Shaw, C. A. Dooley, E. R. Fischer, and T. Hackstadt. 1999. 'Identification and characterization of a Chlamydia trachomatis early operon encoding four novel inclusion membrane proteins', *Mol Microbiol*, 33: 753-65.

Scidmore, M. A., E. R. Fischer, and T. Hackstadt. 2003. 'Restricted Fusion of Chlamydia trachomatis Vesicles with Endocytic Compartments during the Initial Stages of Infection', *Infect Immun*, 71: 973-84.

Scidmore, M. A., and T. Hackstadt. 2001. 'Mammalian 14-3-3beta associates with the Chlamydia trachomatis inclusion membrane via its interaction with IncG', *Mol Microbiol*, 39: 1638-50.

Scidmore, M. A., D. D. Rockey, E. R. Fischer, R. A. Heinzen, and T. Hackstadt. 1996. 'Vesicular interactions of the Chlamydia trachomatis inclusion are determined by chlamydial early protein synthesis rather than route of entry', *Infect Immun*, 64: 5366-72.

Seaman, M. N. 2004. 'Cargo-selective endosomal sorting for retrieval to the Golgi requires retromer', *J Cell Biol*, 165: 111-22.

———. 2012. 'The retromer complex - endosomal protein recycling and beyond', *J Cell Sci*, 125: 4693-702.

Seaman, M. N., M. E. Harbour, D. Tattersall, E. Read, and N. Bright. 2009. 'Membrane recruitment of the cargo-selective retromer subcomplex is catalysed by the small GTPase Rab7 and inhibited by the Rab-GAP TBC1D5', *J Cell Sci*, 122: 2371-82.

Seaman, M. N., E. G. Marcusson, J. L. Cereghino, and S. D. Emr. 1997. 'Endosome to Golgi retrieval of the vacuolar protein sorting receptor, Vps10p, requires the function of the VPS29, VPS30, and VPS35 gene products', *J Cell Biol*, 137: 79-92.

Seaman, M. N., J. M. McCaffery, and S. D. Emr. 1998. 'A membrane coat complex essential for endosome-to-Golgi retrograde transport in yeast', *J Cell Biol*, 142: 665-81.

Seet, L. F., and W. Hong. 2006. 'The Phox (PX) domain proteins and membrane traffic', *Biochim Biophys Acta*, 1761: 878-96.

Seto, S., K. Sugaya, K. Tsujimura, T. Nagata, T. Horii, and Y. Koide. 2013. 'Rab39a interacts with phosphatidylinositol 3-kinase and negatively regulates autophagy induced by lipopolysaccharide stimulation in macrophages', *PLoS One*, 8: e83324.

Sharma, M., M. A. Recuero-Checa, F. Y. Fan, and D. Dean. 2018. 'Chlamydia trachomatis regulates growth and development in response to host cell fatty acid availability in the absence of lipid droplets', *Cell Microbiol*, 20.

Shaw, E. I., C. A. Dooley, E. R. Fischer, M. A. Scidmore, K. A. Fields, and T. Hackstadt. 2000. 'Three temporal classes of gene expression during the Chlamydia trachomatis developmental cycle', *Mol Microbiol*, 37: 913-25.

Shewan, A. M., E. M. van Dam, S. Martin, T. B. Luen, W. Hong, N. J. Bryant, and D. E. James. 2003. 'GLUT4 recycles via a trans-Golgi network (TGN) subdomain enriched in Syntaxins 6 and 16 but not TGN38: involvement of an acidic targeting motif', *Mol Biol Cell*, 14: 973-86.

Shi, H., R. Rojas, J. S. Bonifacino, and J. H. Hurley. 2006. 'The retromer subunit Vps26 has an arrestin fold and binds Vps35 through its C-terminal domain', *Nat Struct Mol Biol*, 13: 540-8.

Shi, Z., and M. Barna. 2015. 'Translating the genome in time and space: specialized ribosomes, RNA regulons, and RNA-binding proteins', *Annu Rev Cell Dev Biol*, 31: 31-54.

Shi, Z., K. Fujii, K. M. Kovary, N. R. Genuth, H. L. Rost, M. N. Teruel, and M. Barna. 2017. 'Heterogeneous Ribosomes Preferentially Translate Distinct Subpools of mRNAs Genome-wide', *Mol Cell*, 67: 71-83.e7.

Simonetti, B., and P. J. Cullen. 2018. 'Actin-dependent endosomal receptor recycling', *Curr Opin Cell Biol*, 56: 22-33.

Simonetti, B., C. M. Danson, K. J. Heesom, and P. J. Cullen. 2017. 'Sequence-dependent cargo recognition by SNX-BARs mediates retromer-independent transport of CI-MPR', *J Cell Biol*.

Slavov, N., S. Semrau, E. Airoldi, B. Budnik, and A. van Oudenaarden. 2015. 'Differential Stoichiometry among Core Ribosomal Proteins', *Cell Rep*, 13: 865-73.

Smythe, E., and K. R. Ayscough. 2006. 'Actin regulation in endocytosis', *J Cell Sci*, 119: 4589-98.

Solomon, A. W., A. Foster, and D. C. Mabey. 2006. 'Clinical examination versus Chlamydia trachomatis assays to guide antibiotic use in trachoma control programmes', *Lancet Infect Dis*, 6: 5-6; author reply 7-8.

Soupene, E., J. Rothschild, F. A. Kuypers, and D. Dean. 2012. 'Eukaryotic protein recruitment into the Chlamydia inclusion: implications for survival and growth', *PLoS One*, 7: e36843.

Stanhope, Rebecca, Elizabeth Flora, Charlie Bayne, and Isabelle Derré. 2017. 'IncV, a FFAT motif-containing Chlamydia protein, tethers the endoplasmic reticulum to the pathogen-containing vacuole', *Proceedings of the National Academy of Sciences*, 114: 12039.

Steele-Mortimer, Olivia. 2008. 'The Salmonella-containing vacuole: moving with the times', *Curr Opin Microbiol*, 11: 38-45.

Stein, M. A., K. Y. Leung, M. Zwick, F. Garcia-del Portillo, and B. B. Finlay. 1996. 'Identification of a Salmonella virulence gene required for formation of filamentous structures containing lysosomal membrane glycoproteins within epithelial cells', *Mol Microbiol*, 20: 151-64.

Stenmark, Harald. 2009. 'Rab GTPases as coordinators of vesicle traffic', *Nature Reviews Molecular Cell Biology*, 10: 513.

Stephens, R. S., S. Kalman, C. Lammel, J. Fan, R. Marathe, L. Aravind, W. Mitchell, L. Olinger, R. L. Tatusov, Q. Zhao, E. V. Koonin, and R. W. Davis. 1998. 'Genome sequence of an obligate intracellular pathogen of humans: Chlamydia trachomatis', *Science*, 282: 754-9.

Stephens, R. S., G. Myers, M. Eppinger, and P. M. Bavoil. 2009. 'Divergence without difference: phylogenetics and taxonomy of Chlamydia resolved', *FEMS Immunol Med Microbiol*, 55: 115-9.

Su, H, L Raymond, D D Rockey, E Fischer, T Hackstadt, and H D Caldwell. 1996. 'A recombinant Chlamydia trachomatis major outer membrane protein binds to heparan sulfate receptors on epithelial cells', *Proceedings of the National Academy of Sciences*, 93: 11143-48.

Su, H., G. McClarty, F. Dong, G. M. Hatch, Z. K. Pan, and G. Zhong. 2004. 'Activation of Raf/MEK/ERK/cPLA2 signaling pathway is essential for chlamydial acquisition of host glycerophospholipids', *J Biol Chem*, 279: 9409-16.

Subtil, A., and A. Dautry-Varsat. 2004. 'Chlamydia: five years A.G. (after genome)', *Curr Opin Microbiol*, 7: 85-92.

Subtil, A., C. Parsot, and A. Dautry-Varsat. 2001. 'Secretion of predicted Inc proteins of Chlamydia pneumoniae by a heterologous type III machinery', *Mol Microbiol*, 39: 792-800.

Suchland, Robert J., Daniel D. Rockey, John P. Bannantine, and Walter E. Stamm. 2000. 'Isolates of Chlamydia trachomatis That Occupy Nonfusogenic Inclusions Lack IncA, a Protein Localized to the Inclusion Membrane', *Infection and Immunity*, 68: 360-67.

Sudhof, T. C., and J. E. Rothman. 2009. 'Membrane fusion: grappling with SNARE and SM proteins', *Science*, 323: 474-7.

Sun, Q., X. Yong, X. Sun, F. Yang, Z. Dai, Y. Gong, L. Zhou, X. Zhang, D. Niu, L. Dai, J. J. Liu, and D. Jia. 2017. 'Structural and functional insights into sorting nexin 5/6 interaction with bacterial effector IncE', *Signal Transduct Target Ther*, 2: 17030.

Swarbrick, J. D., D. J. Shaw, S. Chhabra, R. Ghai, E. Valkov, S. J. Norwood, M. N. Seaman, and B. M. Collins. 2011. 'VPS29 is not an active metallo-phosphatase but is a rigid scaffold required for retromer interaction with accessory proteins', *PLoS One*, 6: e20420.

Takagi, M., M. J. Absalon, K. G. McLure, and M. B. Kastan. 2005. 'Regulation of p53 translation and induction after DNA damage by ribosomal protein L26 and nucleolin', *Cell*, 123: 49-63.

Takei, K., V. I. Slepnev, V. Haucke, and P. De Camilli. 1999. 'Functional partnership between amphiphysin and dynamin in clathrin-mediated endocytosis', *Nat Cell Biol*, 1: 33-9.

Taleei, R., P. M. Girard, K. Sankaranarayanan, and H. Nikjoo. 2013. 'The non-homologous end-joining (NHEJ) mathematical model for the repair of double-strand breaks: II. Application to damage induced by ultrasoft X rays and low-energy electrons', *Radiat Res*, 179: 540-8.

Teasdale, R. D., and B. M. Collins. 2012. 'Insights into the PX (phox-homology) domain and SNX (sorting nexin) protein families: structures, functions and roles in disease', *Biochem J*, 441: 39-59.

Teasdale, R. D., D. Loci, F. Houghton, L. Karlsson, and P. A. Gleeson. 2001. 'A large family of endosome-localized proteins related to sorting nexin 1', *Biochem J*, 358: 7-16.

Temkin, P., B. Lauffer, S. Jager, P. Cimermancic, N. J. Krogan, and M. von Zastrow. 2011. 'SNX27 mediates retromer tubule entry and endosome-to-plasma membrane trafficking of signalling receptors', *Nat Cell Biol*, 13: 715-21.

Tjaden, J., H. H. Winkler, C. Schwöppe, M. Van Der Laan, T. Möhlmann, and H. E. Neuhaus. 1999. 'Two nucleotide transport proteins in Chlamydia trachomatis, one for net nucleoside triphosphate uptake and the other for transport of energy', *Journal of Bacteriology*, 181: 1196-202.

Trinkle-Mulcahy, Laura. 2019. 'Recent advances in proximity-based labeling methods for interactome mapping', *F1000Research*, 8: F1000 Faculty Rev-135.

Trousdale, Christopher, and Kyoungtae Kim. 2015. 'Retromer: Structure, function, and roles in mammalian disease', *European Journal of Cell Biology*.

Tschochner, H., and E. Hurt. 2003. 'Pre-ribosomes on the road from the nucleolus to the cytoplasm', *Trends Cell Biol*, 13: 255-63.

van Ooij, C., G. Apodaca, and J. Engel. 1997. 'Characterization of the Chlamydia trachomatis vacuole and its interaction with the host endocytic pathway in HeLa cells', *Infect Immun*, 65: 758-66.

Van Ooij, Christiaan, Lisa Kalman, Sven Van Ijzendoorn, Masahiro Nishijima, Kentaro Hanada, Keith Mostov, and Joanne N. Engel. 2000. 'Host cell-derived sphingolipids are required for the intracellular growth of Chlamydia trachomatis', *Cell Microbiol*, 2: 627-37.

van Steensel, B., and S. Henikoff. 2000. 'Identification of in vivo DNA targets of chromatin proteins using tethered dam methyltransferase', *Nat Biotechnol*, 18: 424-8.

van Weering, J. R., R. B. Sessions, C. J. Traer, D. P. Kloer, V. K. Bhatia, D. Stamou, S. R. Carlsson, J. H. Hurley, and P. J. Cullen. 2012. 'Molecular basis for SNX-BAR-mediated assembly of distinct endosomal sorting tubules', *Embo j*, 31: 4466-80.

van Weering, J. R., P. Verkade, and P. J. Cullen. 2010. 'SNX-BAR proteins in phosphoinositide-mediated, tubular-based endosomal sorting', *Semin Cell Dev Biol*, 21: 371-80.

———. 2012. 'SNX-BAR-mediated endosome tubulation is co-ordinated with endosome maturation', *Traffic*, 13: 94-107.

Vanharreveld, A., and J. Crowell. 1964. 'ELECTRON MICROSCOPY AFTER RAPID FREEZING ON A METAL SURFACE AND SUBSTITUTION FIXATION', *Anat Rec*, 149: 381-5.

Varnaite, R., and S. A. MacNeill. 2016. 'Meet the neighbors: Mapping local protein interactomes by proximity-dependent labeling with BioID', *Proteomics*, 16: 2503-18.

Vasilevsky, S., G. Greub, D. Nardelli-Haefliger, and D. Baud. 2014. 'Genital Chlamydia trachomatis: understanding the roles of innate and adaptive immunity in vaccine research', *Clin Microbiol Rev*, 27: 346-70.

Voeltz, Gia K., William A. Prinz, Yoko Shibata, Julia M. Rist, and Tom A. Rapoport. 2006. 'A Class of Membrane Proteins Shaping the Tubular Endoplasmic Reticulum', *Cell*, 124: 573-86.

Volarevic, S., M. J. Stewart, B. Ledermann, F. Zilberman, L. Terracciano, E. Montini, M. Grompe, S. C. Kozma, and G. Thomas. 2000. 'Proliferation, but not growth, blocked by conditional deletion of 40S ribosomal protein S6', *Science*, 288: 2045-7.

Vyas, K., S. Chaudhuri, D. W. Leaman, A. A. Komar, A. Musiyenko, S. Barik, and B. Mazumder. 2009. 'Genome-wide polysome profiling reveals an inflammation-responsive posttranscriptional operon in gamma interferon-activated monocytes', *Mol Cell Biol*, 29: 458-70.

Wan, F., D. E. Anderson, R. A. Barnitz, A. Snow, N. Bidere, L. Zheng, V. Hegde, L. T. Lam, L. M. Staudt, D. Levens, W. A. Deutsch, and M. J. Lenardo. 2007. 'Ribosomal protein S3: a KH domain subunit in NF-kappaB complexes that mediates selective gene regulation', *Cell*, 131: 927-39.

Wang, J., A. Fedoseienko, B. Chen, E. Burstein, D. Jia, and D. D. Billadeau. 2018. 'Endosomal receptor trafficking: Retromer and beyond', *Traffic*.

Wang, J., Y. Zhang, C. Lu, L. Lei, P. Yu, and G. Zhong. 2010. 'A genome-wide profiling of the humoral immune response to Chlamydia trachomatis infection reveals vaccine candidate antigens expressed in humans', *J Immunol*, 185: 1670-80.

Wang, Y. 1999. 'Etiology of trachoma: a great success in isolating and cultivating Chlamydia trachomatis', *Chin Med J (Engl)*, 112: 938-41.

Warner, Jonathan R., and Kerri B. McIntosh. 2009. 'How Common Are Extraribosomal Functions of Ribosomal Proteins?', *Molecular Cell*, 34: 3-11.

Wassmer, T., N. Attar, M. V. Bujny, J. Oakley, C. J. Traer, and P. J. Cullen. 2007. 'A loss-of-function screen reveals SNX5 and SNX6 as potential components of the mammalian retromer', *J Cell Sci*, 120: 45-54.

Wassmer, Thomas, Naomi Attar, Martin Harterink, Jan R. T. van Weering, Colin J. Traer, Jacqueline Oakley, Bruno Goud, David J. Stephens, Paul Verkade, Hendrik C. Korswagen, and Peter J. Cullen. 2009. 'The Retromer Coat Complex Coordinates Endosomal Sorting and Dynein-Mediated Transport, with Carrier Recognition by the trans-Golgi Network', *Developmental Cell*, 17: 110-22.

Wehrl, W., V. Brinkmann, P. R. Jungblut, T. F. Meyer, and A. J. Szczepek. 2004. 'From the inside out--processing of the Chlamydial autotransporter PmpD and its role in bacterial adhesion and activation of human host cells', *Mol Microbiol*, 51: 319-34.

Wilson, D. M., 3rd, W. A. Deutsch, and M. R. Kelley. 1994. 'Drosophila ribosomal protein S3 contains an activity that cleaves DNA at apurinic/apyrimidinic sites', *J Biol Chem*, 269: 25359-64.

Wilson, Daniel N., and Jamie H. Doudna Cate. 2012. 'The structure and function of the eukaryotic ribosome', *Cold Spring Harb Perspect Biol*, 4: a011536.

Wilson, Daniel N., and Knud H. Nierhaus. 2005. 'Ribosomal Proteins in the Spotlight', *Critical Reviews in Biochemistry and Molecular Biology*, 40: 243-67.

Winkler, G. S., K. W. Mulder, V. J. Bardwell, E. Kalkhoven, and H. T. Timmers. 2006. 'Human Ccr4-Not complex is a ligand-dependent repressor of nuclear receptor-mediated transcription', *Embo j*, 25: 3089-99.

Wool, I. G. 1996. 'Extraribosomal functions of ribosomal proteins', *Trends Biochem Sci*, 21: 164-5.
World Health Organization, D. o. R. H. a. R. 2012. 'Global incidence and prevalence of selected curable sexually transmitted infections - 2008, WHO'.
World Health Organization, Dept. of Reproductive Health and Research. 2010. 'WHO Global strategy for the prevention and control of sexually transmitted infections: 2006–2015: breaking the chain of transmission 2007', *Geneva, Switzerland*.
Wylie, J. L., G. M. Hatch, and G. McClarty. 1997. 'Host cell phospholipids are trafficked to and then modified by Chlamydia trachomatis', *J Bacteriol*, 179: 7233-42.
Wyrick, P. B. 2000. 'Intracellular survival by Chlamydia', *Cell Microbiol*, 2: 275-82.
Xue, S., and M. Barna. 2012a. 'Specialized ribosomes: a new frontier in gene regulation and organismal biology', *Nat Rev Mol Cell Biol*, 13: 355-69.
Xue, Shifeng, and Maria Barna. 2012b. 'Specialized ribosomes: a new frontier in gene regulation and organismal biology', *Nat Rev Mol Cell Biol*, 13: 355-69.
Yao, J., F. Yang, X. Sun, S. Wang, N. Gan, Q. Liu, D. Liu, X. Zhang, D. Niu, Y. Wei, C. Ma, Z. Q. Luo, Q. Sun, and D. Jia. 2018. 'Mechanism of inhibition of retromer transport by the bacterial effector RidL', *Proc Natl Acad Sci U S A*, 115: E1446-e54.
Zauber, Henrik, Marieluise Kirchner, and Matthias Selbach. 2018. 'Picky: a simple online PRM and SRM method designer for targeted proteomics', *Nature Methods*, 15: 156.
Zerial, M., and H. McBride. 2001. 'Rab proteins as membrane organizers', *Nat Rev Mol Cell Biol*, 2: 107-17.
Zheng, L., U. Baumann, and J. L. Reymond. 2004. 'An efficient one-step site-directed and site-saturation mutagenesis protocol', *Nucleic Acids Res*, 32: e115.
Zhong, G., P. Fan, H. Ji, F. Dong, and Y. Huang. 2001. 'Identification of a chlamydial protease-like activity factor responsible for the degradation of host transcription factors', *J Exp Med*, 193: 935-42.
Zhong, G., T. Fan, and L. Liu. 1999. 'Chlamydia inhibits interferon gamma-inducible major histocompatibility complex class II expression by degradation of upstream stimulatory factor 1', *J Exp Med*, 189: 1931-8.
Zhong, G., L. Liu, T. Fan, P. Fan, and H. Ji. 2000. 'Degradation of transcription factor RFX5 during the inhibition of both constitutive and interferon gamma-inducible major histocompatibility complex class I expression in chlamydia-infected cells', *J Exp Med*, 191: 1525-34.
Zhong, Q., M. J. Watson, C. S. Lazar, A. M. Hounslow, J. P. Waltho, and G. N. Gill. 2005. 'Determinants of the endosomal localization of sorting nexin 1', *Mol Biol Cell*, 16: 2049-57.
Zhou, Xiang, Wen-Juan Liao, Jun-Ming Liao, Peng Liao, and Hua Lu. 2015. 'Ribosomal proteins: functions beyond the ribosome', *Journal of molecular cell biology*, 7: 92-104.
Zuck, M., A. Sherrid, R. Suchland, T. Ellis, and K. Hybiske. 2016. 'Conservation of extrusion as an exit mechanism for Chlamydia', *Pathog Dis*, 74.

Appendix

Analysis of *C. trachomatis* primary infection in SNX KO cell lines using ImageJ

HeLa, CRISPR Ctrl and SNX KO cell lines were infected with *C. trachomatis* for 36 h and stained for chlamydial Hsp60. Epifluorescence images were randomly taken of 8 fields of view using a Zeiss Axiovert 200 microscope. Scripts were used to count inclusions and nuclei using ImageJ.

Script to count nuclei:

```
run("Set Scale...", "distance=150 known=1 pixel=1 unit=pixel");
run("8-bit");
run("Gaussian Blur...", "sigma=3");
//setThreshold(13, 100);
run("Convert to Mask");
setAutoThreshold("Triangle");
//run("Threshold...");
run("Watershed");
run("Analyze Particles...", "size=3000-Infinity pixel circularity=0.50-1.00 show=Outlines display exclude clear summarize add in_situ")
```

Script to count inclusions of SNX single KO cell line including HeLa and CRISPR Ctrl cell lines:

```
run("Set Scale...", "distance=150 known=1 pixel=1 unit=pixel");
run("8-bit");
run("Gaussian Blur...", "sigma=3");
run("Enhance Contrast...", "saturated=0.01");
setAutoThreshold("Triangle");
//run("Threshold...");
setThreshold(16, 85);
setOption("BlackBackground", true);
run("Convert to Mask");
run("Watershed");
run("Analyze Particles...", "size=300-Infinity circularity=0.50-1.00 show=Outlines display exclude clear summarize add in_situ")
```

Inclusions of SNX5/SNX6 double KO cell line were counted manually.

List of identified proteins in BioID

Table 32. Identified protein hits in BioID.
List of total protein hits identified by nLC-MS/MS after streptavidin pulldown of biotinylated proteins of *C. trachomatis* infected HeLa cells (MOI 2). n=3.

See Table 32 of in total identified protein hits on compact disc.

List of identified enriched proteins in BioID

Table 33. Enriched proteins identified in BioID using myc-BirA*-SNX1 fusion protein.
List of enriched protein hits identified by nLC-MS/MS after streptavidin pulldown of biotinylated proteins of *C. trachomatis* infected HeLa cells (MOI 2). Enrichment of proteins was calculated based on intensity based absolute quantification (iBAQ), minimum ratio count of 2, -log(p-value) >1, difference (log2) > 1.8, FDR 1%, no missing values; Q-value: adjusted p-value using an optimised FDR approach (Savitski et al. 2015), Score: peptide score resulting from peptides and fragment masses searched in an organisms specific database that are then scored by a probability-based approach (Cox and Mann 2008, 2009; Schaab et al. 2012; Cox et al. 2014); Protein ID: Uniprot ID of the first protein of the Majority protein column of a protein group. n=3.

Significant (FDR 1 %, s0 = 1)	-LOG(P-value)	Difference (log2)	Protein IDs	Protein names	Gene names
+	4.833300247	10.99228827	Q13596;Q13596-3;Q13596-2;H0YK42;J3KPH4;H0YKD5;H0YK58;H0YKT3;H0YKL5;H0YK43	Sorting nexin-1	SNX1
+	3.126437851	8.092104276	Q9Y5X3;Q5QPE4;Q5QPE5;A0A087WUY5;U3KQL0;U3KQP5;Q9Y5X3-2	Sorting nexin-5	SNX5
+	3.5392764	7.317339261	A5YKK6-3;A5YKK6-2;A5YKK6;A5YKK6-4;B5MDN3;H3BMZ2;H3BVC9	CCR4-NOT transcription complex subunit 1	CNOT1
+	2.956766351	4.216799736	Q92922;Q5SYV2;A0A0A0MT55;O9UL12-2;O9UL12	SWI/SNF complex subunit SMARCC1	SMARCC1
+	2.628047048	3.982415835	Q5VTL8;Q5VTL8-2;A0A0A0MRN0	Pre-mRNA-splicing factor 38B	PRPF38B
+	2.088446374	3.804832141	P0DJI4	INCE_CHLTR Inclusion membrane protein E	IncE
+	3.99404393	3.649139086	A0A0A0MRI2;Q9UNH7-2;Q9UNH7;H0YJF8;G3V4Z5;G3V2U1;G3V5U2	Sorting nexin-6;Sorting nexin-6, N-terminally processed	SNX6
+	3.192154187	3.328785261	P47914	60S ribosomal protein L29	RPL29
+	1.276627022	3.220507622	A0A0B4J1Z1;C9JAB2;Q16629-3;Q16629-2;Q16629-4;Q16629;F8WEA1	Serine/arginine-rich splicing factor 7	SRSF7
+	2.630554555	3.201745669	P16403;P10412;P16402;P22492;Q0D539	Histone H1.2;Histone H1.4;Histone H1.3	HIST1H1C; HIST1H1E; HIST1H1D
+	4.299511063	3.118323962	O75165;H0Y8Q2;H0YA63	Dnaj homolog subfamily C member 13	DNAJC13
+	2.75938635	2.91584301	A0A0A0MR02;P45880-2;P45880;P45880-1;Q5JSD2;Q5JSD1	Voltage-dependent anion-selective channel protein 2	VDAC2
+	2.055524127	2.904496829	J3KTL2;Q07955;Q07955-3;Q07955-2;J3KSR8;J3QQV5;J3KSW7	Serine/arginine-rich splicing factor 1	SRSF1
+	1.183710155	2.894100507	P60709;P62367;P68133;P68032;P62736;G5E9R0;E7EVS6;A6NL76;C9JTX5;C9JZR7;P63267-2;C9JUM1;F8WB63;B8ZZJ2;C9JFL5;F6UVO4;F6QUT6;Q6S8J3;A5A3E0;P0CG38;F8WCH0;Q9BYX7;P0CG39	Actin, cytoplasmic 1;Actin, cytoplasmic 1, N-terminally processed;Actin, gamma-enteric smooth muscle;Actin, alpha skeletal muscle;Actin, alpha cardiac muscle 1;Actin, aortic smooth muscle	ACTB;ACTG2;ACTA1;ACTC1;ACTA2
+	1,75024466	2,752367973	P40429;M0QYS1;Q8J015;M0QZU1;A0A096LPE0;Q6NVV1	60S ribosomal protein L13a	RPL13A;RPL13a
+	2,396450292	2,681356748	P46779;H0YKD8;P46779-2;P46779-3;H0YLP6;H0YMF4;P46779-4;P46779-5	60S ribosomal protein L28	RPL28
+	1,93576691	2,657863935	P38646;D6RAJ3;D6RJI2;H0YBG6 Q13085;Q13085-4;Q13085-3;Q13085-2;Q59FY4;A0A087X0W4;S4R3S7;A0A087WWN5;A0A0C4DGT1;A0A087WVR6;A0A087X2F8;A0A087X1Z6;A0A087WYK6	Stress-70 protein, mitochondrial	HSPA9
+	1,499034192	2,651949247		Acetyl-CoA carboxylase 1;Biotin carboxylase	ACACA
+	1,588390358	2,616516431	P84103-2;P84103;A0A087X2D0	Serine/arginine-rich splicing factor 3	SRSF3
+	1,666601146	2,594865481	J3QSB5;O9Y3U8;J3KTD3	60S ribosomal protein L36	RPL36
+	1,867289456	2,529655774	Q8WUH6	Transmembrane protein 263	TMEM263
+	1,416319037	2,469510714	E9PHF7;Q96RQ3;F5GYT8;E9PG35;G5E9X5	Methylcrotonoyl-CoA carboxylase subunit alpha, mitochondrial	MCCC1
+	3,186753953	2,43181324	Q9ULH7;Q9ULH7-4;Q9ULH7;Q9ULH7-5;I3L2S3;O9ULH7-2;Q9ULH7;3;E7ER32;A0A087X287;B0QY83;A0A087WU73;W0Z7M9;Q969V6;B0QY84;Q8IZQ8-2;Q8IZQ8;Q8IZQ8-3	MKL/myocardin-like protein 2	MKL2
+	2,923632825	2,386032422	P11021	78 kDa glucose-regulated protein	HSPA5
+	2,756524467	2,365866661	Q9NWB6;Q9NWB6-3;Q9NWB6-2;X6R9F1	Arginine and glutamate-rich protein 1	ARGLU1
+	1,479242802	2,289024035	Q13247-3;Q13247;Q13247-2	Serine/arginine-rich splicing factor 6	SRSF6
+	1,605801219	2,277795474	Q5JNZ5;P62854	Putative 40S ribosomal protein S26-like 1;40S ribosomal protein S26	RPS26P11;RPS26
+	1,581754336	2,244218508	E7EX53;E7EQV9;P61313;E7ENU7;P61313-2;E7ERA2	Ribosomal protein L15;60S ribosomal protein L15	RPL15
+	2,505366114	2,201408068	J3QR09;J3KTE4;P84098;J3QL15	Ribosomal protein L19;60S ribosomal protein L19	RPL19
+	4,472678321	2,196694547	Q9Y383;A0A0A6YYC3;O96HJ9-2;A0A0A6YYJ8;O9Y383-3;O9Y383-2;A8MYV2;O9NQ29-2;O9NQ29	Putative RNA-binding protein Luc7-like 2	LUC7L2
+	1,965900341	2,122344653	G3V203;H0YHA7;J3QQ67;Q07020-2;Q07020;F8VUA6;F8VYV2;A0A075B7A0	60S ribosomal protein L18	RPL18
+	3,030804269	2,108804385	Q7L4I2;Q7L4I2-2;H0YGP9;E1B6W4;E9PI52	Arginine/serine-rich coiled-coil protein 2	RSRC2
+	1,782928955	2,098395348	P49207	60S ribosomal protein L34	RPL34
+	2,655356859	2,022831917	I3L2N2;O14641;I3L0Z8;I3L0M7;I3L2W9;C9K0P9	Segment polarity protein dishevelled homolog DVL-2	DVL2
+	2,40740205	2,000842094	P46776;E9PJD9;E9PLL6;E9PLX7	60S ribosomal protein L27a	RPL27A
+	2,028503895	1,955756823	Q8WXA9-2;Q8WXA9;A0A087WY03;E5RFV3	Splicing regulatory glutamine/lysine-rich protein 1	SREK1
+	2,910695396	1,865926425	O14684	Prostaglandin E synthase	PTGES
+	2,716061168	1,855198224	P23528;G3V1A4;E9PP50;E9PK25;E9PLJ3;E9PS23;E9PQB7;O9Y281-3;O9Y281	Cofilin-1	CFL1
+	2,194705606	1,686023394	Q5HY54;P21333-2;P21333;F8WE98;H0Y6C6;H7C2E7	Filamin-A	FLNA
+	3,497174821	1,683740298	P11142;E9PKE3;E9PNE6;P11142-2;A8K7Q2;E9PLF4;E9PQC4;E9POK7;E9PKK5;P54652;E9PPY6;E9PN25;E9PM13;E9PI65	Heat shock cognate 71 kDa protein	HSPA8

Immunoblot analysis indicating enrichment of ribosomal subunits

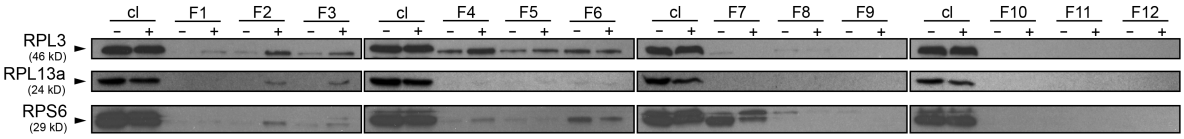

Figure 55. Enrichment of ribosomes and ribosomal subunits after gradient centrifugation using a sucrose gradient.
Immunoblot of ribosomal proteins in *C. trachomatis* D (MOI 5) and uninfected HeLa cells after fractionation of ribosomes and ribosomal subunits by density gradient centrifugation using a sucrose gradient. Representative immunoblot shown for n=2. cl: cleared lysate; F: fraction; -: uninfected HeLa cells; +: *C. trachomatis* D infected HeLa cells.

We used an antibody against RPL3 as a marker for the large ribosomal subunit. This antibody has been tested in WB before to exclude a cross reaction as it was observed in IF analysis.

Ribosomal protein profiles of *C. trachomatis* infected cells

Table 34. Ribosomal protein profiling.
List of ribosomal protein hits identified by nLC-MS/MS after fractionation of ribosomes and ribosomal subunits using a sucrose density gradient of *C. trachomatis* infected (L, light labelled) (MOI 5) and uninfected (H, heavy labelled) HeLa cells. n=3. Ratio H/L: SILAC ratio 'uninfected cells/infected cells' per fraction; Q-value: adjusted p-value using an optimised FDR approach (Savitski et al. 2015), Score: peptide score resulting from peptides and fragment masses searched in an organisms specific database that are then scored by a probability-based approach (Cox and Mann 2008, 2009; Schaab et al. 2012; Cox et al. 2014); Protein ID: Uniprot ID of the first protein of the Majority protein column of a protein group.

See Table 34 showing results matrix on compact disc.

Abbreviations and Symbols

Abbreviations

Abbreviation	Name
(M)OMP	(major) outer membrane protein
aa	amino acid
AB	aberrant body
ABC	ATP-binding cassette
ACN	acetonitrile
ACTB	beta Actin
AHNAK	actin-binding protein
AMP	adenosine monophosphate
APS	ammonium persulfate
Arf	ADP-ribosylation
ATCC	American Type Culture Collection
ATP	adenosine triphosphate
BAR	Bin/amphiphysin/Rvs
BioID	proximity-dependent biotinylation assay
BLAST	Basic Local Alignment Search Tool
bp	base pairs
BS3	Suberic acid-bis-(3-sulfo-N-hydroxysuccinimide ester
BSA	bovine serum albumin
C. psittaci	*Chlamydia psittaci*
C. trachomatis	*Chlamydia trachomatis*
CDC	Centers for Disease Control and Prevention
cDNA	complementary DNA
CERT	ceramide endoplasmic reticulum transport protein
CHX	cycloheximide
CI *(in figure legends)*	confidence interval
CI-MPR	cation-independent mannose phosphate receptor
cLSM	confocal laser scanning microcope
CO_2	carbon dioxide
CPAF	chlamydial protease-like activation factor
CRISPR	clustered regularly interspaced short palindromic repeats
Ctrl	control
DAPI	4',6-diamidino-2-phenylindole
dd	double distilled
DFA	direct fluorescent staining with monoclonal antibodies
dFCS	dialysed FCS
DMEM	Dulbecco’s modified eagle medium
DMSO	dimethyl sulfoxide
DNA	deoxyribonucleic acid
DTT	dithiothreitol
e.g.	*exempli gratia*
EB	elementary body

ECL	enhanced chemiluminescence
EDTA	ethylene diamine tetraacetic acid
eGFP	(enhanced) green fluorescent protein
EGTA	ethylene glycol tetraacetic acid
EIA	enzyme immunoassay
EM	electron microscopy
ER	endoplasmic reticulum
ERGIC	ER-Golgi intermediate compartment
et al.	*et alii*
FA	formic acid
FCS	fetal calf serum
FDR	false discovery rate
for	forward
GA	Golgi apparatus
GAIT	gamma interferon inhibitor of translation
GAPDH	glyceraldehyde 3-phosphate dehydrogenase
GCN	genome copy number
GST	glutathione S-transferase
GTP	guanosine triphosphate
h p.i.	hours post infection (word of Latin origin hours *post infectionem*)
H_2O	water
HCl	hydrochloric acid
HeLa	Henrietta Lacks
HKI	Hans Knöll Institute
HPF	high-pressure freezing
HRP	horse-radish peroxidase
HSP	heat shock protein
IAA	iodoacetamide
iBAQ	intensity based absolute quantification
IF	immunofluorescence
IFNγ	interferon gamma
IFU	inclusion forming units
Inc	inclusion membrane protein
indel	insertion/deletion
IPTG	isopropyl β-D-1-thiogalactopyranoside
IUPAC	International Union of Pure and Applied Chemistry
kb	kilobase
KCl	potassium chloride
kD	kilo Dalton
KO	knockout
LB	Luria-Bertani
LC-MS/MS	liquid chromatography coupled to tandem mass spectrometry
LGV	lymphogranuloma venereum
LM	light microscopy
log	logarithm
LPS	lipopolysaccharide

Mb	mega base (equal to mega base pairs)
MCS	membrane contact sites
MeOH	methanol
$MgCl_2$	magnesium chloride
MHC	major histocompatibility complex
MIP	maximum intensity projection
MOI	multiplicity of infection
MPR	mannose phosphate receptors
mRNA	messenger RNA
MS	mass spectrometry
MTOC	microtubule-organising centre
n.d.	not detected
NAAT	nucleic acid amplification test
NaCl	sodium chloride
NCBI	National Center for Biotechnology Information
nLC-MS/MS	nano liquid chromatography coupled to tandem mass spectrometry
Noc	nocodazole
OD	optical density
OmcA	small cysteine-rich outer membrane protein A
OmcB	small cysteine-rich outer membrane protein B
PAMP	pathogen-associated molecular pattern
PBS	phosphate-buffered saline
PCR	polymerase chain reaction
PD	pulldown
PFA	paraformaldehyde
PI	phosphatidylinositol
PI4K	phosphatidylinositol 4-kinase
PIP	phosphatidylinositol phosphate
PM	plasma membrane
PNK	polynucleotide kinase
ppm	parts per million
PRM	parallel reaction monitoring
PVDF	polyvinylidene difluoride
PX	phox-homology
qPCR	quantitative PCR
Rab	Ras-related protein in brain (member ras oncogene family)
RB	reticulate body
rev	reverse
RhoA	Ras homolog gene family, member A
RISC	RNA-induced silencing complex
RKI	Robert Koch institute
RNA	ribonucleic acid
RNAi	RNA interference
ROI	region of interest
RPL	ribosomal protein of the large subunit
rpm	revolutions per minute
RPMI	Roswell Park Memorial Institute medium

RPP	pattern recognition receptors
RPS	ribosomal protein of the small subunit
rRNA	ribosomal RNA
RT	room temperature
RT-PCR	reverse-transcriptase-PCR
SD	standard deviation
SDS	sodium dodecyl sulfate
SDS-PAGE	SDS- polyacrylamide gel electrophoresis
sgRNA	single guide RNA
SILAC	stable isotope labelling by amino acids in cell culture
siRNA	small interfering RNA
SMS	sphingomyelin synthase
SNARE	soluble N-ethylmaleimide-sensitive-factor attachment receptor
snoRNA	small nucleolar ribonucleoproteins
SNX	sorting nexin protein
spp	species
STAGE	stop and go extraction
STX	syntaxin protein
T3SS	type III secretion system
TARP	translocated actin-recruiting phosphoprotein
TBS	Tris-buffered saline
TBS-T	Tris-buffered saline supplemented with Tween® 20
TCA	trichloroacetic acid
TEM	transmission electron microscopy
TEMED	N,N,N´,N´,-tetramethylendiamine
TFA	trifluoroacetic acid
TGN	*trans*-Golgi network
TLR	Toll-like receptor
tRNA	transfer-RNA
UA	urea buffer
UTR	untranslated region
UV/Vis	ultraviolet/visible
VAMP	vesicle-associated membrane protein
VPS	vacuolar protein sorting protein
WASH	Wiskott–Aldrich syndrome protein and SCAR homologue
WB	Western Blot
WCL	whole-cell lysate
WHO	World Health Organization
WT	wild type
β	beta

Symbols

Symbol	Name	Unit
°C	degree Celsius	SI unit
µg	microgram	10^{-6} g
µL	microlitre	10^{-6} l
µm	micrometre	10^{-6} m
µM	micro Molar	mol/m^6
A	Absorbance	relative unit
Å	Ångström	10^{-10} m
Da	Dalton	$1.660538921(73)\times10^{-27}$ kg
h	hour(s)	3600 s
kg	kilogram	1 kg
mA	milliampere	SI unit
mg	milligram	10^{-6} kg
min	minute(s)	60 seconds
mL	millilitre	10^{-6} m^3
mM	milli Molar	mol/m^3
ng	nanogram	10^{-9} g
nm	nanometre	10^{-9} m
pH	*pondus Hydrogenii*	$-\log_{10}([H^+])$
pmol	pikomol	10^{-12} m
RT	room temperature	25 °C (as defined by IUPAC)
S	Svedberg	10^{-13}
s	second	SI unit
V	Volt	SI unit
x *g*	times gravity (relative centrifugal force)	9.81 m/s^2

List of Figures

List of Tables

Acknowledgements

I am sincerely grateful to my supervisor Dr. Dagmar Heuer for the challenging and exciting project in which I worked autonomously and was able to realise own ideas. This project exalted my fascination for biology even more. Dagmar Heuer's precedent-setting and scientific support was not only infectious but also conducive to the project's output.

Special thanks to Prof. Dr. Helge Ewers for his time to review my doctoral thesis and for being a member of my thesis advisory committee. I also thank Prof. Dr. Leif Erik Sander who was a further member of my thesis advisory committee. This committee was a great opportunity to regularly discuss the state of the project and future ideas.

Dr. Sebastian Banhart deserves special credits for being a fantastic PostDoc and colleague. He has companioned me from the first day in the lab as a Master student to the end of my doctoral thesis. Sebastian Banhart has supported me in any scientific concerns, whether inducting me in confocal microscopy, reading bits and pieces of texts, discussing the project out of the box or encouraging me in successful as well as tedious times. Cordial thanks for having a sympathetic ear at any time, delving in the rectangular world and for sharing a sense of i-rony.

Many thanks to the very talented and motivated Master students Stefanie Lüth and Sandra Oehlmann who have contributed greatly to this thesis. I cannot emphasise enough my thanks to Sandra Oehlmann who was a diligent, efficient and autonomous student worker and who was always on hand with help.
I thank all former and current colleagues of Unit 19 at RKI for their continuous and strenuous efforts in the lab and for spicing up everyday lab work with numerous small-talks and tittle-tattles. I thank my former labmates Sophia Edelmann (née Koch) and Lukas Aeberhard for critical discussions, inspiring ideas and office chats during sunsets. I thank Andrea Martini, Tanja Pilz, Henning Krüger, Jean-Marc Gensch and Petra Baer for any help and the daily doses of wee jokes in the lab. All colleagues have created a tremendous atmosphere to work in.

I owe special thanks to Dr. Michael Laue (head of Advanced Light and Electron Microscopy, RKI) for providing the core facility of light and electron microscopy that enabled me to spend hours in the dark with the confocal laser scanning microscope. Many thanks for the cooperation to shed light on the ultrastructure of inclusion tubules. I am grateful to Dr. Kazimierz Madela (Advanced Light and Electron Microscopy, RKI) for the fiery introduction to the laser scanning microscope and cLEM technique and Dr. Jörg Döllinger (Proteomics and Spectroscopy, RKI) for the introduction to mass spectrometry, his helping hands in analysing our mass spectrometry data and his long wind for discussing the x^{th} graph and answering my countless questions.

My sincere thanks to the Center of Infection Biology and Immunity (ZIBI) and the ZIBI graduate school for the great opportunity to be part of a unique interdisciplinary framework for young scientists. The ZIBI affords an excellent network of researchers and training within infection biology, immunity and beyond.

I cannot thank Frank, Birgit and Sophia enough for their continuous and absolute support, confidence and patience. I would not have come this far without them.
I deeply thank my friends who have always encouraged me and who have given me the best daily settlement I can imagine.
Deep gratitude to Axel for his sympathy, encouragement and open arms.
Thank you!

Publications

Articles

Exchange of core chromosomes and horizontal transfer of lineage-specific chromosomes in Fusarium oxysporum.
Vlaardingerbroek, I., B. Beerens, **L. Rose**, L. Fokkens, B. J. Cornelissen, and M. Rep. Environ Microbiol. 2016

The Proteome of the Isolated Chlamydia trachomatis Containing Vacuole Reveals a Complex Trafficking Platform Enriched for Retromer Components.
Aeberhard, L., S. Banhart, M. Fischer, N. Jehmlich, **L. Rose**, S. Koch, M. Laue, B. Y. Renard, F. Schmidt, and D. Heuer. PLoS Pathog. 2015, 11: e1004883

The cellular ceramide transport protein CERT promotes Chlamydia psittaci infection and controls bacterial sphingolipid uptake.
Koch-Edelmann, S., S. Banhart, E. M. Saied, **L. Rose**, L. Aeberhard, M. Laue, J. Doellinger, C. Arenz, and D. Heuer. Cell Microbiol. 2017

Chlamydia trachomatis and its interaction with the cellular retromer.
Banhart, S., **L. Rose**, L. Aeberhard, S. Koch-Edelmann, and D. Heuer. Int J Med Microbiol. 2017

The ribosomal protein RPL13a promotes C. trachomatis infection.
Rose L, S. Oehlmann, S. Banhart, J. Doellinger and D. Heuer.
Cell Microbiol., In preparation

SNX5 and SNX6 restrict trafficking of C. trachomatis towards the MTOC during early infection.
Rose L, … and D. Heuer.
Cell Microbiol., In preparation

Talks

Interactions of Chlamydia trachomatis with the retromer complex during acute infections.
Laura Rose, Sebastian Banhart, Lukas Aeberhard, Sophia Edelmann and Dagmar Heuer
14th German Chlamydia Workshop 2016, Freiburg, Germany

Poster presentations

Establishment of an in vitro persistence model in Chlamydia trachomatis serovar D to characterize host-pathogen interactions.
Laura Rose, Sebastian Banhart, Lukas Aeberhard, Sophia Edelmann and Dagmar Heuer
13th German Chlamydia Workshop, Vienna, Austria

Interactions of Chlamydia trachomatis with the retromer complex during acute infections.
Laura Rose, Sebastian Banhart, Lukas Aeberhard, Sophia Edelmann and Dagmar Heuer
8th MaxQuant Summer School 2016, Oxford, United Kingdom

Chlamydia interacts with retrograde trafficking pathways - understanding the underlying mechanisms.
Laura Rose, Sebastian Banhart, Lukas Aeberhard, Sophia Edelmann and Dagmar Heuer
SPP1580 Internal Meeting 2015, Bonn, Germany

Sorting the role of human retromer complex in Chlamydia trachomatis infections.
Laura Rose, Stefanie Lüth, Sebastian Banhart, Sophia Edelmann, Lukas Aeberhard, Bernard Y. Renard, Frank Schmidt and Dagmar Heuer
SPP1580 International Meeting 2017, Glashütten, Germany

Identification of sorting nexin 1-associated proteins during C. trachomatis infection using proximity-dependent biotinylation.
Laura Rose, Sebastian Banhart and Dagmar Heuer
Gordon Research Conference, Andover, NH, United States

Selbstständigkeitserklärung

Ich erkläre, dass ich die vorliegende Arbeit selbstständig und nur unter Verwendung der angegebenen Literatur und Hilfsmittel angefertigt habe. Wurden Ergebnisse in Kooperation produziert, ist dies entsprechend angegeben.

Berlin, September 2019 Laura Rose